https://ntrs.nasa.gov/search.jsp?R=19660016287 2020-03-16T19:54:47+00:00Z

CR 65341

RE-242

INVESTIGATION OF LUNAR SURFACE CHEMICAL CONTAMINATION BY LEM DESCENT ENGINE AND ASSOCIATED EQUIPMENT

March 1966

GPO PRICE $ _____

CFSTI PRICE(S) $ _____

Hard copy (HC) $ 6.00

Microfiche (MF) 1.25

653 July 65

Grumman RESEARCH DEPARTMENT

LIBRARY COPY

MAR 28 1966

MANNED SPACECRAFT CENTER
HOUSTON, TEXAS

N66 25576 (ACCESSION NUMBER)
215 (PAGES)
CR-65341 (NASA CR OR TMX OR AD NUMBER)
(THRU) 1
(CODE) 30
(CATEGORY)
FACILITY FORM 602

GRUMMAN AIRCRAFT ENGINEERING CORPORATION
BETHPAGE, NEW YORK

Grumman Research Department Report RE-242

INVESTIGATION OF LUNAR SURFACE CHEMICAL CONTAMINATION BY LEM DESCENT ENGINE AND ASSOCIATED EQUIPMENT[†]

by

L. Aronowitz
N. Milford
S. Penn
F. Pomilla
J. Scanlon
M. Sidran

Geo-Astrophysics Section

C. Baulknight
F. Koch
T. Luzzi
D. Weiss

Fluid Mechanics Section

and

J. Berkowitz-Mattuck
A. Buchler
P. Glaser
A. Wechsler

Arthur D. Little, Inc.

March 1966

[†]Final Report on Contract NAS 9-4860

Approved by: Charles E. Mack, Jr.
Charles E. Mack, Jr.
Director of Research

ACKNOWLEDGEMENTS

The authors of this report wish to acknowledge a debt of gratitude to the many people at Grumman Aircraft Engineering Corporation who devoted their time and skills to the solution of equations, in the selection of realistic lunar environmental parameters, in computer programming, in providing necessary information about the LEM and the Apollo mission, and other essential parts of the study. The following list is far from complete and the authors sincerely regret unintentional omissions: Eleanor Damasco, Arnold Goldford, Paul Kalben, Dr. G. McCoyd, Eugene McDonald, Paul Munter, Dr. R. Oman, Caryl Quint, Joseph Reichman, Martin Solon, Dr. M. Spergel, Eloise M. Turner, Mike Urkowitz, and M. R. Wohlers.

The Bibliography (Sec. III.C) was prepared by Mr. S. Penn.

Many helpful suggestions concerning the relative importance of various contaminant species, and suggestions on sampling techniques were supplied by James E. Townsend of the National Aeronautics and Space Administration's Manned Spacecraft Center.

We particularly wish to thank the following Grumman Biologists and Physiologists (see Sec. II.B.3) for their valuable contributions to the study of bacterial contamination: Ray Davis, Robert J. Delvecchio, William Kunz, Joseph Lisa, Robert Madey, Lawrence Slote, Ray Stern, and Wong Wai.

TABLE OF CONTENTS

LIST OF ILLUSTRATIONS

LIST OF TABLES

I. INTRODUCTION AND SUMMARY

The Apollo mission will bring to earth the first samples ever taken on a world other than our own. Scientists eagerly await the opportunity to study these specimens by the most refined techniques available. To gain maximum knowledge from the analyses, it is necessary to know if these samples have suffered physical or chemical changes or contamination during the mission. This Final Report describes an investigation of sample contamination that may be produced by the Lunar Excursion Module (LEM) descent engine and other Apollo mission equipment. The study was conducted by the Grumman Aircraft Engineering Corporation, as prime contractor, and Arthur D. Little, Inc., as subcontractor.

The work accomplished is described in a series of separate notes that have been collected into this Final Report. In Section II, a brief discussion of these notes is given to guide those seeking detailed treatments of particular topics to the appropriate notes.

During the contract period, a written report (Ref. 1) was prepared of an oral presentation given at NASA's Manned Spacecraft Center, Houston, Texas on November 2, 1965. This Interim Report, which summarized the work done on the contract to November 1965, was detailed and included much pertinent background material. To facilitate preparation of this Final Report, and to avoid unnecessary duplications, the Final Report will, in several sections, present a summary of sections of Ref. 1. Those desiring additional information are referred to Ref. 1.

A useful description of the Apollo mission is found in Ref. 2. This reference has become obsolete in part and the descriptions of landing sites, trajectories, lunar stay, and other parts of the mission do not represent current thinking on these subjects. A revised version of Ref. 2 is scheduled to be issued during 1966. Values of parameters used in calculating contamination distributions, in determining the maximum excursion of the astronauts from the LEM, and other factors in the present study are taken from material that was prepared for the revised version (see Ref. 3).

Under the present contract, a study was made of the composition of inorganic and organic contaminants from the LEM descent engine exhaust and from gas vented from the ascent stage

or leaked from the space suits. Transient temperatures distributions produced on and below the lunar surface by the impinging rocket plume were computed. Means for minimizing and compensating for contamination in samples were surveyed.

The study has examined the composition of the contaminants coming from the LEM. The propellant combustion products were calculated by a computer program. The calculation is sufficiently accurate for the principal species, but concentrations of some minor constituents that are present in trace amounts may differ appreciably from the computer values. These trace species could be of importance in biological experiments on samples and their concentrations should be determined experimentally. Over a third of the descent engine exhaust is H_2O, and almost a third is N_2, with H_2, CO, CO_2, H, and O accounting for most of the remainder. The composition of the Refrasil in the engine's ablative material has been determined.

Contaminants arising from the astronauts' biological and physiological processes include H_2S, CH_4, and possibly O_3 and NH_3.

Contamination due to bacteria and biological debris was examined. It was concluded that unless specific measures are taken to prevent it, the probability of bacteriological sample contamination approaches 100 percent. There is an urgent need for further experimental data on the amount and composition of the bacterial contaminants that can be expected on the Apollo mission. A bibliography on bacteriological contaminants has been prepared.

An investigation of photochemical synthesis on carbohydrates or amino acids in the lunar radiation environment showed that rates of production of such contaminants, which are particularly undesirable in exobiological experiments, are negligible. Some photochemical production of H_2O_2 may occur. The lunar particle radiation environment may produce chemically catalytic sites on the lunar surface. Such sites could promote chemical reactions between contaminant species. Catalytic production of amino acids appears to be unlikely. Existing experimental data on the effects of simulated lunar environmental conditions on catalytic reactions are inadequate, and more data would be useful.

Sources of contamination not considered in this study include the Reaction Control System rocket exhausts, the Radiothermal

Generator, radioactive sources in the LEM Propellant Quantity Gauging System, contamination from Pre-Apollo missions, and radioactivity induced in atoms of LEM materials by high energy particle radiation. The last two items have possible importance. The last item might have significance to a particularly sensitive radioactivity experiment. Pre-Apollo contamination deserves investigation because it is not certain that all such contamination effects on the lunar samples will be negligible.

Probably the most useful tools for compensating for the effects of contamination in samples are maps showing the distributions in space and time of contamination on the lunar surface and in the atmosphere during the period when the samples are collected. A computer program was developed to calculate the "Far Field" flux of rocket exhaust contaminant molecules to the lunar surface. (The term "Far Field" denotes that the LEM is sufficiently far from the lunar surface so that interactions between exhaust molecules and the surface can be studied by free molecular flow dynamics.) The calculations show that the density of Far Field contamination impinging on the lunar surface at the touchdown point is of the order of a few tenths of a g/m^2. Samples collected in the downrange direction from the touchdown site will contain the greatest Far Field contamination. Density decreases with increasing distance from the touchdown point.

Molecules striking the surface may either rebound or be adsorbed. Adsorbed molecules may subsequently be desorbed. Unfortunately, existing data on adsorption and desorption under lunar environmental conditions are inadequate to make realistic estimates of the distributions of adsorbed surface contamination resulting from the Far Field molecular flux. More reliable data on adsorption and desorption are essential to this and several other aspects of the study of lunar contamination.

The problems of "Near Field" contamination are more complex than those of the Far Field. ("Near Field" denotes that the LEM altitude is low enough so that the continuum gas dynamic interactions between the rocket plume and the surface occur.) Erosion of the lunar surface and transient temperature changes produced by the impinging rocket plume have been examined, and adsorption of Near Field exhaust gas has been studied.

Distributions of adsorbed Near Field exhaust gas on a solid lunar surface model with a composition similar to meteorites

were computed. An analysis was made to determine suitable values for adsorption and desorption coefficients on the surface for the principal gas species. Results indicate that H, H_2, CO, and CO_2, will desorb so rapidly that they will not be present in surface samples. Other species, H_2O, N_2, NO, O, O_2, and OH, may be present in the samples if the gases are chemically adsorbed on the surface. If chemical adsorption occurs, the order of magnitude of the contamination density at a distance of 20m from the touchdown point will be 0.2 g/m^2 for H_2O, 0.01 g/m^2 for OH, and 1 mg/m^2 for OH, NO, O, and O_2. Contamination density decreases rapidly with distance, falling below a $\mu\mu$ g/m^2 at a distance of about 1/2 kilometer from the touchdown point.

The validity of these estimates is questionable because of the previously mentioned lack of reliable data on adsorption and desorption under lunar conditions. Values of contamination densities calculated for distances closer than 15 m from the touchdown point were disregarded. The lunar surface in this region will experience temperature transients due to the impinging rocket plume. Desorption rates depend sensitively on temperature, and it was not considered useful to attempt to estimate contamination density at less than 15 m until better data are available.

Material eroded from the lunar surface by the rocket plume is expected to be heavily contaminated by direct contact with the exhaust gas. Eroded material that is redeposited on the lunar surface may form an important source of sample contamination. The distribution of lunar surface material eroded by the rocket plume and redeposited on the surface was investigated using a theoretical lunar surface model consisting of a smooth layer of spherical particles of 1, 0.1, and 0.01 mm diameter. Results show that the density of redeposited particles decreases sharply with increasing particle diameter and with distance from the touchdown point. For 1 mm particles, the density has a maximum value near the LEM of less than 10^5 particles/m^2 (10 particles/cm^2) and the density decreases to less than 10^4 particles/m^2 at a distance of 60 m from the LEM. By contrast, the 0.01 mm particles have a maximum density greater than 10^{10} particles/m^2 and the density decreases to 10^4 particles/m^2 (1 particle/cm^2) at a distance greater than 100 m from the LEM.

A computer program has been developed to trace the temperature histories of the eroded particles. Calculations show that small

particles (less than 0.1 mm radius) may reach temperatures in excess of 1100°K. When adequate data on adsorption and desorption rates become available, the temperature histories can be used to calculate the amount and composition of the contamination on the surfaces of the particles.

The transient temperature distribution produced on and below the lunar surface by the Near Field impingement of the descent rocket plume will play an important role in determining adsorption and desorption rates for rocket exhaust gas, and in possible chemical or phase changes in surface materials. It is also desirable to know the thermal history of samples gathered in the vicinity of the LEM. A computer program was used to calculate temperature distributions in eight model lunar surfaces including solid, particulate, vesicular, and rubble surfaces. Surface erosion was not considered in these calculations. Results show that the maximum surface temperature of over 1500°K occurs at the touchdown point. The transient temperature variation decreases rapidly in amplitude with increasing distance from the LEM, becoming negligible about 30 ft. from the touchdown point. Because of the low thermal conductivity of lunar material the transient temperature variations penetrate only a few centimeters into the surface.

The recent Luna 9 photographs provide an excellent opportunity for improving the calculated Near Field distributions. While it is certainly premature to conclude that all areas of the moon resemble the one in the photographs, it would be desirable to recalculate the distributions using parameters suggested by the photographs. Thus, the distribution of eroded material could be calculated using an appropriate value for the resistance of the surface to the shearing stress of a rocket exhaust. The variations of transient temperature with depth could be recalculated taking account of the penetration of hot exhaust gas into a porous surface. The effects of gas penetration might cause temperature transients to penetrate more deeply below the lunar surface than is indicated by the present calculations.

The depth of penetration of exhaust gas into porous surfaces should be examined. Several suggested schemes for obtaining contamination-free samples involve drilling to a sufficient depth to avoid surface contamination. If exhaust contaminants can penetrate deeply into a porous lunar surface such schemes might require drilling to an impractical depth.

Because the weight of propellant for the descent stage is a sizable fraction of the estimated total weight of the lunar atmosphere, contamination of the lunar atmosphere by the descent engine exhaust gas has been investigated. Computer programs were developed to calculate the density distributions of the contaminant species as a function of time and of position on the lunar surface. Dissipation of contamination by the solar wind, thermal, and other loss mechanisms are included in the programs.

The results show that the density of contaminant gases in the atmosphere is a maximum in the region of LEM touchdown. There is no significant variation within 300 meters of this point after the initial stages of the mission. The light molecules H and H_2 are uniformly distributed over the moon's surface in a couple of hours, while the heavier contaminants require up to six days to attain a uniform distribution. For those contaminant gas species that do not stick to the surface, the number densities remain sufficiently large for significantly long times that they will be readily detectable by standard instruments.

Methods for minimizing, detecting, and compensating for contamination have been explored. It has already been pointed out that probably, the most important tools in identifying and compensating for contamination are maps and time histories of the contaminant species. The location and time at which every lunar sample is collected should be recorded. This will permit a statistical comparison between the relative smounts of various species of constitutents in the samples and the predicted contaminant distributions. Such a comparison will help distinguish naturally occurring lunar substances from contaminants. It is important, therefore, that contaminant distribution maps be made as accurate as possible. The statistical comparison should utilize the results of studies of possible synthesis of new contaminant species by chemical reactions in the lunar radiation environment.

A possible method for minimizing contamination in samples is to collect them from regions that are partially or totally shielded from rocket exhaust gas. The Luna 9 photographs suggest that such regions may exist under rocks or inside cavities that are distant from the LEM touchdown point.

Several devices are suggested for minimizing contamination in samples. These include a sampling probe to be dropped from

the LEM before or immediately after touchdown, and an instrument to be used by the astronaut that will decontaminate a portion of the lunar surface and then take a sample at a sufficient depth below the surface to avoid surface contamination.

II. DISCUSSION

A. The Lunar Environment

The lunar environment will determine the relative importance of many contaminant processes. For example, the rate of decay of atmospheric contamination depends on the intensity of the solar wind (Sec. IV.E), erosion of material from the lunar surface by the plume of the descent stage rocket depends on the resistance of the surface to the shearing stress produced on the surface by the exhaust gas flow (Sec. IV.B., and Sec. IV.G), absorption of the rocket exhaust gas by lunar surface materials depends on the chemical composition of the surface (Sec. IV.D, and Sec. IV.F), etc. A brief discussion of the lunar atmosphere, surface, meteoroid environment, thermal environment, and other environmental factors affecting contamination are given in Sec. II of Ref. 1.

1. Surface Models

A set of surface models was chosen that was sufficiently extensive so that it could include most of the suggested details of the lunar surface, e.g., electrostatic effects, sintering by the solar wind, dendritic structure, etc. The models are listed in Table 1, which is reproduced from page 5 of Ref. 1. The choice of models is briefly discussed on page 3 of Ref. 1. All the models were used in calculating temperature distributions in the lunar surface (Secs. II.D.6, and IV.H). Model 1 was used in computing the distributions of redeposited material eroded by rocket plume impingement (Secs. II.D.3, IV.B, and IV.C). Model 3 was used to calculate absorption of exhaust gas on the lunar surface (Secs. II.D.3, and IV.D).

Table 1

LUNAR SURFACE MODELS

1. Homogeneous particulate	5. Two-layer particulate-rock
2. Homogeneous vesicular	6. Two-layer vesicular-rock
3. Homogeneous solid	7. Rubble
4. Two-layer particulate-vesicular	8. Particulate and rubble

2. Surface Temperature

Ambient lunar surface temperature is discussed on page 5 of Ref. 1. Figure 1, reproduced from page 41 of Ref. 1, shows the temperature in the vicinity of the anticipated latitude of the touchdown site during one lunation. The short horizontal line located at the right-hand bottom of the graph indicates touchdown at a longitude of 45° with respect to the terminator and a stay of up to 44 hours. (See discussion on page 5 of Ref. 1.)

B. Nature of the Organic and Inorganic Specific Chemical and/or Elemental Contaminants Produced by the LEM Descent Engine, the Depressurization of the Ascent Stage, and the Exhaust from the Space Suits

The sources of contamination considered in the present study are the inorganic, organic, and bacterial products in the descent rocket exhaust, and the gas vented from ascent stage cabin and space suit leakage. Composition of contaminants from these sources is discussed in Sec. IV of Ref. 1.

1. The Descent Engine

a. Combustion Products: The descent engine is the largest source of contaminants. Composition of the propellants and propellant combustion products is given in Sec. IV.A.1 of Ref. 1. The composition of the combustion products is shown in Table 2, which is reproduced from page 10 of Ref. 1. This composition was calculated using a Grumman computer program and assumes that the chemical composition is frozen near the throat of the nozzle. As noted in Ref. 1, these results are sufficiently accurate for the principal constituents. However, some of the minor constituents may be present in amounts appreciably different from those computed. It would be impractical to compute the amounts of these trace compounds more accurately. If a constituent of the exhaust is suspected as being potentially troublesome for a particular type of scientific analysis, it would be logical to measure experimentally its concentration in the exhaust.

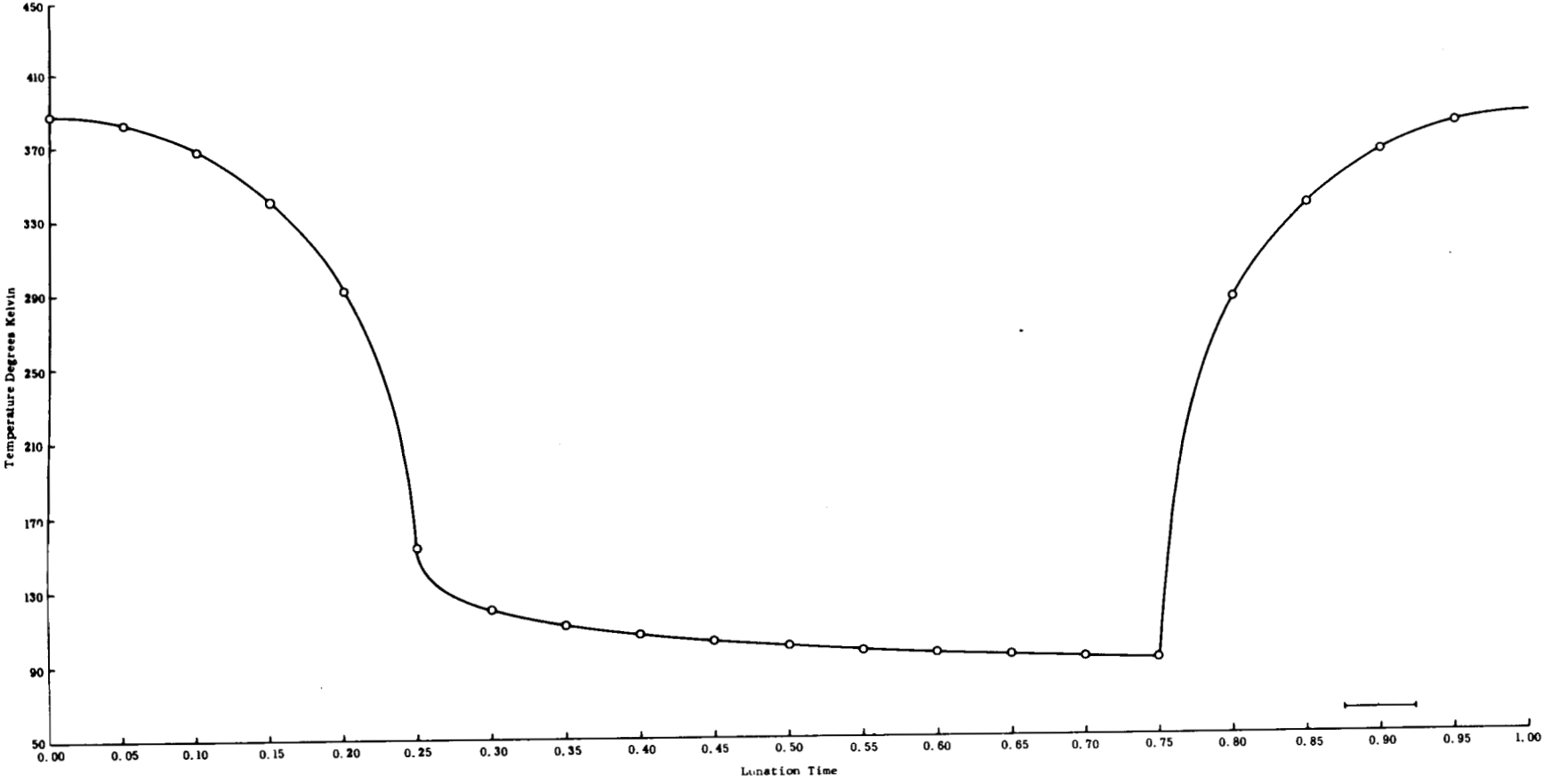

Fig. 1 Lunar Surface Temperature

Table 2

COMBUSTION PRODUCTS IN LEM DESCENT ROCKET EXHAUST

Exhaust Composition	Mole Percent
H_2O	36
N_2	32
H_2	13
CO	9.6
CO_2	3.7
H	1.9
OH	1.6
NO	0.24
O_2	0.15
O	0.14

Trace amounts of N, CHO, NH (10^{-4}); NH_2, H_2O_2, NH_3, NO_2, N_2O, HNO (10^{-5}); HCN, HNCO, CH_2O, HNO_2 cis and trans (10^{-6}); e^-, NO^+ (10^{-7}); OH^-, CN (10^{-8}); C (10^{-10}).

b. Ablative Material: Composition of the Refrasil used in the ablative material is shown in Table 3, reproduced from page 11 of Ref. 1. Much of the material ablated near the throat resolidifies along the nozzle and only a fraction of it appears in the exhaust.

Little data are available on the products that will appear in the exhaust from the phenolic resin. Best estimates indicate that there will be little ash, and the phenolic will decompose mainly into products that are already present from combustion of the propellants. Thus, the phenolic resin is probably not an important source of contaminants. Experimental investigation would be required to determine the exhaust products arising from this source.

Table 3

COMPOSITION OF 99.4% PURE REFRASIL

SiO_2	99.4%
Al_2O_3	.11
TiO_2	.33
ZiO_2	.017
B_2O_3	.081
K_2O	.0005
Na_2O	.0014
MgO	.0027
CaO	.0042
Fe_2O_3, CuO, Cr_2O_3, MnO	nil

2. Contaminants from Biological and Metabolic Processes

The composition of contaminants from these sources is discussed in Sec. IV.B of Ref. 1.

Estimated production rates for various gases and currently accepted levels for maximum allowable concentrations consistent with the astronauts' environmental requirements are shown in Table 4, reproduced from page 12 of Ref. 1. Upon decompression of the space capsule preliminary to the exit of the astronauts, the gases will be expelled. Because biological and metabolic processes are variable and depend upon many human factors as well as temperature, pressure, and other environmental conditions, quantitative estimates are only approximations.

Reference 1 also discusses the possible synthesis of ozone and ammonia in the LEM ascent stage by photochemical reactions between contaminants. Reference 1 notes that the astronauts' life support system can add water as a contaminant to the lunar environment. However, as indicated in Table 2, water is so large a fraction of the rocket exhaust that the additional water from the life support system probably will not be significant.

Table 4

BIOLOGICALLY PRODUCED CONTAMINANTS

Gas	Maximum Allowable Concentration (lb/lb mixture)	Production Rate (lb/man-hour)
H	2.57×10^{-3}	1.3×10^{-5}
H_2S	6.18×10^{-5}	2.8×10^{-9}
CH_4	2.65×10^{-2}	3.33×10^{-5}
CO	6.45×10^{-5}	1.9×10^{-6}
O_3	2.21×10^{-7}	This depends upon the kinetics of the reaction Peak: 4.4×10^{-5} Ave: 1.5×10^{-5}
NH_3	3.91×10^{-3}	

A brief note on the space suit life support system is given in Sec. III.A.

3. Bacteriological Contamination

As indicated in Sec. IV.C of Ref. 1, a panel of Grumman biologists and physiologists assembled several times to consider problems of bacteriological contamination of lunar samples. The panel concluded that, unless specific measures are taken to prevent it, the probability of contamination of lunar samples by live or dead organisms approaches 100 percent. The panel indicated that the sensitivity of bacteriological analyses is such that a contamination level of one viable bacteria/cm^2 may provide detectable contamination. Also, the sensitivity of methods of analysis now being developed is such that a contamination level approaching one nonviable organism/cm^2 may be detectable. This extreme sensitivity emphasizes the importance of bacteriological contamination, particularly in the field of exobiological experiments.

Several possible approaches to the prevention or minimization of biological contamination in samples were suggested by the panel. These suggestions, and several others are presented in Sec. IV.I of this report.

Bacterial contamination from vented gas and suit leakage will depend on the type and amounts of contaminants present in those sources. A brief summary was made of the literature concerning bacteriological testing of subjects sealed in chambers with simulated space vehicle environments. Results of this survey appear in Sec. III.C. That section makes it clear that existing data are inadequate to determine the nature and quantity of bacterial contaminants to be expected on the Apollo mission. Much additional testing in this area is required.

4. Chemical Reactions

Sections II.B.1, II.B.2, and II.B.3 treated the composition of contaminants from the Apollo mission sources. The problem of contaminant composition is complicated by the lunar radiation environment that, in the absence of a shielding atmosphere, may cause chemical reactions resulting in the synthesis of new species of contaminants. In Sec. III.B, possible photochemical and radiation-damage induced reactions with exhaust gas constituents in the lunar environment are examined. It is shown that the radiation environment of the moon can influence the nature of the chemical contamination of the lunar surface in two ways. First, in the absence of an atmosphere, the entire solar spectrum, including the photochemically active vacuum ultraviolet, can reach the engine exhaust producing possible photochemical reactions. Some photochemical production of H_2O_2 may occur. Second, the constant bombardment of the moon by high-energy radiation and solar wind over the billion years of lunar history may have created a large number of surface sites in highly excited and, hence, chemically reactive states that may catalyze reactions between contaminant species.

The photochemistry of water vapor, nitrogen, CO_2, and NO are discussed, and their calculated rates of photochemical decomposition are given in Table 7. Photochemical reactions between adsorbed gases on the lunar surface will be of greater importance. Maximum rates of formation and the times required to form microgram/cm^2 quantities of formaldehyde, ammonia, hydrogen peroxide, and a number of atomic species were calculated. The data are summarized in Table 8. Further reactions among the radicals produced are possible but cannot be predicted quantitatively.

It should be noted that photochemical reactions may take place in the ascent stage as well as on the surface. In Sec. IV.B of Ref. 1 it is suggested that ammonia and ozone may be synthesized by photochemical reactions between metabolically produced contaminants.

A number of experiments in which amino acids were synthesized from mixtures of simple inorganic gases were evaluated with respect to the LEM contamination problem. Unless the lunar surface is highly catalytic, amino acids are not expected to be synthesized in detectable concentration.

Section III.B also considers the possible formation of chemically catalytic sites on the lunar surface due to radiation damage. Such sites could catalyze particular chemical reactions. Due to the high vacuum and radiation environment of the moon, the lunar surface should have maximum catalytic activity for the particular materials involved. However, it is impossible to predict the reactions that might be catalyzed or to calculate even the order of magnitude of the reaction rates.

As shown in Sec. II.B.1, a large amount of water vapor will be produced in the engine exhaust. Possible chemical reactions between the water vapor and silicates that may be present in lunar surface material were examined in Sec. VII of Ref. 1. Table 5, which is reproduced from page 27 of Ref. 1, shows the reactions considered. It was concluded that hydrolysis of the silicates is unlikely to occur.

Table 5

REACTION OF WATER VAPOR AND SILICATES

FREE ENERGY OF REACTION AT 1300°K

	ΔF, kcal
$Na_2SiO_3(c) + H_2O(g) \rightarrow 2NaOH(g) + SiO_2(c)$	+29.8
$Na_2SiO_3(c) + H_2O(g) \rightarrow 2NaOH(\ell) + SiO_2(c)$	+23.6
$MgSiO_3(c) + H_2O(g) \rightarrow Mg(OH)_2(c) + SiO_2(c)$	+23.0
$Fe_2SiO_4(c) + H_2O(g) \rightarrow Fe_2O_3(c) + SiO_2(c) + H_2(g)$	+ 5.6

c = crystal g = gas ℓ = liquid

C. Sources of Contamination Not Considered

Sources of contamination not considered in the present study are discussed in Sec. III of Ref. 1. These include:

- Reaction Control System Rocket Exhaust
- Radioactivity induced in atoms of some LEM materials by high energy particle radiation

- Radioactive sources in the Propellant Quantity Gauging System
- The Radiothermal Generator
- Contamination from pre-Apollo missions

Of these, the last should be investigated (see Sec. V.B). The second source listed above might be of importance, but only if a type of sample analysis was being considered that showed unusual sensitivity to radioactive contamination. Reasons for neglect of these five items are discussed in Sec. III of Ref. 1.

D. Concentration of Contamination on the Lunar Surface and in the Lunar Atmosphere

1. The Degree of Contamination

It was emphasized in Sec. V.A of Ref. 1 that the degree of contamination of a given sample should be judged in terms of the analyses that will be performed on it. Thus, a sample that might be considered hopelessly contaminated by a biologist planning an exobiological experiment could be rated as being free from contamination by a geologist. Distribution of contaminants from the descent engine plume on the lunar surface will be widespread. However, the total mass of the Apollo contaminants is insufficient to form a coating one monolayer thick if uniformly distributed over the surface of the moon. Even if the surface of the moon were perfectly smooth, a rough estimate (see Fig. 2 of Ref. 1) shows that it would require an amount of water on the order of 10^4 tons to form a monolayer on the entire surface. The total mass of the propellant combustion products is only a tiny fraction of this amount. Thus, the concentration of contamination can be expected to decrease to very small levels with increasing distance from the touchdown point.

Maps of the distribution of contaminants on the surface, therefore, will be an important tool in compensating for contamination. For certain types of analyses, such maps may indicate that the astronaut need to collect samples at distances of only 1000 or less feet from the LEM so that they can be considered relatively uncontaminated. Such distances are within the astronauts' range. The maps may also indicate that, to secure samples with tolerable contamination levels for more sensitive types of analyses, the astronaut would have to travel prohibitively large distances from the LEM. In this case, means must be developed to reduce or compensate

for the contamination in the collected samples. The 1000-foot maximum range was taken from the AMPTF Design Reference Mission (Ref. 2), portions of which have become obsolete. A revised version is scheduled for 1966. Recent calculations of maximum range based on faster walking rates may increase the above value by a factor of two or three. However, on the initial manned mission, the astronauts may limit their excursions to less than the maximum attainable range.

To facilitate analysis of the distribution of exhaust plume contaminants, the study of distribution has been divided into two main categories. The first, which we term "Far Field Contamination," occurs when the LEM is sufficiently distant from the lunar surface so that gas dynamic interactions between the plume and the surface may be neglected. In the second, "Near Field Contamination," complicated interaction processes between the plume and the surface must be considered.

2. The Far Field Distribution

The gas plume issuing from the LEM descent engine deposits contaminants on the lunar surface. The plume has two major flow regimes. Adjacent to the nozzle exit there is a compressible continuum fluid flow regime. As the gas expands outward from the nozzle, the density decreases and a far field free molecular flow regime develops. The Far Field Distribution considers the intersection of the plume with the lunar surface when the LEM is sufficiently distant from the moon so that only the far field flow regime of the plume intersects the surface.

A computer program has been prepared that determines the total flux of far field contaminant molecules at each point on the lunar surface. The model used for the computer program is discussed in Sec. IV.A. The moon is treated as a smooth sphere. The exhaust is treated as a point source of molecules, all of which move with the same speed. The assumption of a point source is justified by the relatively large distance of the LEM from the surface. The uniform speed assumption is justified because in the continuum regime the average macroscopic velocity of molecules is relatively independent of molecular weight, and at the boundary of the regime the Mach number is sufficiently high so that the random thermal velocities of the molecules are small compared to the macroscopic velocity. The assumption of an axisymmetric molecular flux density distribution from the point source is a good representation of the actual plume density distribution.

The computer program is designed to be versatile. Any LEM trajectory can be included in the program. Any orientation of the LEM at each point along the trajectory can be included. The exhaust speed (speed of the molecules) is an input parameter. The axisymmetric point source molecular flux distribution can be taken from a theoretically or empirically derived analytic function or from a table of experimentally determined values. A method of characteristics is being used to determine the density distribution.

As described in Sec. IV.A, the total number of molecules incident on each point on the lunar surface can be calculated. The velocity and angle of incidence of the impacting molecules are also calculated because they play a role in determining sticking probabilities. To facilitate drawing distribution maps, the program gives the location points on the lunar surface in a spherical coordinate system with its origin at the center of the moon. Latitude, θ_n, is measured from a polar axis passing through the LEM touchdown point. Longitude, δ, is measured from a reference plane tangent to the LEM trajectory at touchdown.

Computed values for the far field distribution are given in Table 11. A detailed plot of the distribution in the vicinity of the touchdown point is shown in Fig. 6. The results are for a simplified LEM trajectory, discussed in that section, and may be used as indicative of the variation of contamination level with position on the surface. Results for other trajectories are presented elsewhere (Ref. 3).

It should be clearly understood that the results discussed above are the distribution of the total number of molecules impacting on a region. The distribution of far field contamination is also determined by the degree to which this flux is adsorbed on the surface and on the rate at which it is subsequently desorbed (note that far field contamination forms part of the N_{io} term defined in Sec. IV.D. If the probability that a given species of molecule will stick to the lunar surface when it impinges is unity, and if its subsequent rate of desorption is so slow that only minor desorption takes place during the lunar stay, then the total number of impacting molecules for that species will correspond closely to far field contamination distribution. Otherwise, the impinging flux of molecules may "bounce" several times before sticking or may become part of the atmosphere (cf., Sec. IV.D). As discussed in Sec. IV.G, existing data on adsorption and desorption rates under lunar environmental conditions allow little more than a rough estimate of orders of magnitude for these quantities. From the results of Sec. IV.F and IV.G, it can be said that species of molecules incident on regions of the lunar surface

where they undergo chemical reactions with surface materials have probability of sticking close to unity and very low desorption rates. Thus, for these regions, the far field distribution of these species, or rather of their reaction products, will be given by the far field flux. Conversely, species that are physically adsorbed on the surface may desorb so rapidly that negligible amounts will remain by the time the samples are collected.

In any event, the far field flux computation is independent of either adsorption or desorption. The flux results can be used to calculate the distribution of far field contamination whenever better adsorption and desorption data are available.

An interesting result has been found. In Ref. 1 it was suggested that because of the widespread distribution of far field contamination, almost all of the lunar surface might be contaminated. It is now apparent that only those regions of the surface that are in line of sight of the LEM while its rocket is firing will receive appreciable far field contamination. This finding is not significant for the Apollo mission because of the limited distance that the astronauts can move from the touchdown site. However, it is encouraging that astronauts on a future manned mission in which a lunar vehicle is used can hope to travel to areas of the lunar surface that will be relatively uncontaminated by their own or earlier missions.

3. Near Field Contamination

a. Erosion: The near field distribution considers the contamination of the lunar surface that occurs when the continuum region of the descent engine rocket plume contacts the lunar surface. Shock waves in the plume, erosion of surface material, and heating of the surface are factors in determining the composition and distribution of contamination of the surface and in the atmosphere (see Sec. IV.B).

Material eroded from the lunar surface by the rocket plume is expected to be heavily contaminated by direct contact with the exhaust gas. Eroded material that is redeposited on the lunar surface may form an important source of sample contamination. Therefore, the distribution of redeposited material was investigated using a theoretical lunar surface model consisting of a smooth layer of spherical particles of uniform but arbitrary radius. A computer program was developed to calculate the distribution of the density of redeposited particles on the lunar surface.

Eroded particles can be transported by the gas by three processes (see Sec. V.C of Ref. 1 and also Sec. IV.B of this report). Small particles are entrained (suspended) in the gas and carried along by it. Massive particles, too heavy to be picked up by the gas, may "creep" along the surface. Creep is not expected to result in wide distribution of eroded material and has not been investigated. Particles of intermediate size, too large to be completely suspended in the gas, can be picked up into the gas stream; they will then fall to the surface and bounce back again into the gas stream. Because such particles move in a series of hops, the process is termed "saltation."

Particles transported by the gas stream will be carried by it to the edge of the continuum regime of flow. It is assumed the particles then follow ballistic trajectories until they collide with the lunar surface. A model for the saltation process has been programmed (see Sec. IV.B).

The characteristics of the gas flow field and the rate of erosion were calculated utilizing the erosion studies of Roberts. Roberts' erosion studies were also used for the "Suspension Model" (Sec. IV.C).

Eroded particle density distributions have been computed for three particle sizes. The results are shown elsewhere (Ref. 3). Distributions were calculated for 1, 0.1, and 0.01 mm diameter particles. Results showed that particle density decreased sharply with increasing diameter. The maximum value of the density of redeposited 1 mm particles was less than 10^5 particles/m^2 while the value was greater than 10^{10} particles/m^2 for the 0.01 mm particles. The density decreased to 10^4 particles/m^2 (1 particle/cm^2) at a distance of about 60 m from the LEM in the case of the 1 mm particles and at a distance of 110m for the 0.01 mm particles.

The results indicate that the saltation model is valid over a wide range of particle sizes since most of the particles make many hops before leaving the continuum regime. Examination of the program and the results indicate that the calculated values are correct to within an order of magnitude.

Results for the saltation model and for the suspension model (Secs. IV.B and C) are representative of an uncompacted "dust" surface model composed of particles that do not cohere. The choice was considered a conservative one since it has frequently been suggested that the lunar surface is covered by a layer of dust of finite, though possibly small, depth. The Luna 9 photographs indicate a surface that is vesicular or semicompacted. The computer

programs are capable of calculating the distribution of erosion from such surfaces provided that data on the resistance of the surface to the shearing forces of a rocket exhaust are available. The Luna 9 photographs may not be characteristic of surface conditions in suitable LEM touchdown sites. However, it would be useful to calculate erosion distributions for model surfaces with parameters matching those indicated by Luna 9.

Lunar material eroded by the descent engine rocket plume and redeposited on the lunar surface is expected to be a significant contaminant in samples gathered in the vicinity of the LEM. The temperature history of the eroded material as it is transported by the hot exhaust gas and subsequently cools will play a determining role in the amount and composition of contaminants adsorbed on its surface. Therefore, a study has been made resulting in a computer program for calculating the distribution of redeposited material on the lunar surface and the temperature history of the material deposited at any location. The surface model used was a layer of spherical particles that were transported by suspension.

A solution for the heat transfer equation was derived to determine heat transfer to the particles by convection under the combined boundary conditions of nonzero surface temperature and gas temperature. Radiation cooling of the particles was included. The temperature history of eroded particles was computed (Sec. IV.C). Results shown in Fig. 12 indicate that the surfaces of small particles (less than 0.1 mm in radius) may reach temperatures in excess of 1100°K.

b. Adsorption on Solid Surface: Distribution of contamination on the lunar surface by rocket plume erosion has been discussed in Sec. II.D.3.a. We here consider contamination of the lunar surface in the absence of erosion due to adsorption of the various constituents of the rocket exhaust gas. This process will occur at a distance sufficiently far from the touchdown point so that erosion is negligible. If the lunar surface around the touchdown site has high resistance to erosion this distance may be small. The distance will be larger if an easily eroded layer of uncompacted or loosely compacted dust exists at the touchdown site.

Section IV.D presents a study of the adsorption of species of exhaust gas on a plane, noneroding, surface model whose chemical composition was chosen to resemble that of certain meteorites. An equation for the number, N_i, of molecules of the i^{th} species of gas that are adsorbed on a unit area of surface at time t was found. The rate at which these molecules are adsorbed is given by fS, where f is the flux of the species of molecule from the gas to a unit area of the surface per unit time, and S, the "sticking" coefficient, depends on the molecular species, on the average energy with which they strike the surface, and on the chemical composition of the surface (see Sec. IV.G).

The rate of desorption of molecules is given by DN where D, the "desorption" coefficient, is related to the heat of adsorption, Q, for the species and to the lunar surface temperature, T, by the expression $D = (1/\tau_o)\, e^{-Q/(RT)}$, where τ_o is a constant characteristic of the surface composition, and R is the gas constant.

A computer program to evaluate N(t) was constructed. The program includes effects of variation in D with changing values of T as a result of surface heating by the impinging rocket plume and subsequent surface cooling after engine shut down.

It was concluded, using the rates of desorption for various contaminant species given in Table 14, that H, H_2, CO, and CO_2 will desorb so rapidly that they will not be present in the collected samples. Other species, H_2O, N_2, NO, O, O_2, and OH can be present, but only if the composition of the lunar surface is such that these species are chemically adsorbed. The computed concentrations of these species in units of kg/m^2 on surface areas where they are chemically adsorbed is given in Fig. 13 for areas at various distances from the LEM. In computing these results it was assumed that the lunar surface temperature is constant. This is a valid assumption at distances greater than about 30 ft. from the touchdown point where heating of the surface by the impinging rocket plume is small enough so that its effects on desorption can be neglected (see Tables 24 and 27). Because of the present lack of data on the values of S and D in the lunar environment, these results at best can be used only as qualitative guides. Experimental studies should be made on the parameters determining N(t) and the calculations should be repeated when better data are available. Variations of D with T, which are of importance at distances from the LEM of less than 30 ft. also require experimental investigation.

4. Atmospheric Contamination

Computer programs were developed to trace the history afte touchdown of the concentrations of CO, CO_2, H, H_2, H_2O, N_2, NO, O, O_2, and OH in the lunar atmosphere (Sec. IV.E). Adopting as source function for the atmospheric contaminants the appropriate fraction of the space and time distribution of the LEM gases striking the lunar surface, calculations have been made of two models of lunar atmosphere contamination. Model I, valid for later times, gives

the average over the moon of the contaminant gas density as a function of solar wind velocity and time after the LEM landing.

In this simplified model of the lunar atmosphere, the exhaust gases from the LEM are assumed to spread uniformly over the lunar surface, attain the temperature of the surface and then be re-emitted into the ambient lunar atmosphere at a uniform time rate. In turn, these exhaust gases are assumed lost from the atmosphere through the mechanisms of: a) collisions (elastic and charge exchange) with the solar wind; b) interactions with solar photons producing photoionization and photodissociation; c) thermal evaporation from the top of the atmosphere; and d) sticking to the lunar surface.

Because the ambient lunar atmosphere is extremely rarefied ($< 10^{-9}$ of the earth's atmosphere), the mean free path of the exhaust gases is very large so that the assumption of a uniform distribution over the lunar surface is reasonable for long times after rocket shutoff. This model then should give the asymptotic values of the gas densities approached by space dependent distribution models.

Model II uses a more realistic initial distribution of contaminants. In this model the initial space distribution of the LEM exhaust gas as it impinges on the lunar surface is taken as known input from the far field and near field gas dynamics calculations (cf., Secs. II.D.2 and II.D.3). The gas particles in this initial distribution subsequently undergo a three dimensional diffusion into the thin lunar atmosphere. It is assumed that this can be adequately represented by a diffusion of the particles in two dimensions across the lunar surface with concurrent loss mechanisms occurring in the vertical column of gas of scale height, h, for each species. As in Model I, the atmospheric number density, n, for each species is assumed uniform over the scale height, h, and the particles are assumed to be thermalized upon striking the lunar surface. In addition to the loss mechanisms used in Model I, Model II considers in some detail the adsorption and desorption occurring at the lunar surface for each gas species.

Results for Model I are shown in Figs. 14-33 of Sec. IV.E. The number density, $n(t)$, of contaminant molecules in the atmosphere are given for t in the range $0 \leq t \leq 10^7$ sec. The zero value of t corresponds to the initial ignition of the LEM descent engine. Note that $n(t)$ is the total of the ambient atmosphere plus the LEM exhaust for each particular species. The results are

for a solar wind flux = 10^9 cm^{-2} sec^{-1} and a lunar surface temperature T = 300°K. Results for additional values of the parameters were calculated at Grumman and appear elsewhere (see Sec. IV.E).

Results for Model II are shown in Figs. 34-65 of Sec. IV.E. Here, the number density, n(t), is that for the LEM exhaust gas products only; the ambient atmosphere density is neglected. The results in Figs. 34-65 assume a lunar surface temperature T = 300°K and a solar wind flux 10^9 cm^{-2} sec^{-1}. Results were calculated for the case of no sticking of contaminant molecules to the lunar surface ($f_1 = f_2 = 0$), and for the case in which the sticking coefficients have the values given in Table 20. Results for additional values of the parameters were calculated at Grumman and appear elsewhere (see Sec. IV.E).

5. Interactions of Contaminant Molecules with the Lunar Surface

The probability that a contaminant molecule that strikes the lunar surface will stick, and the rate at which gas adsorbed on the surface will desorb are necessary data for calculating distributions of exhaust gas adsorbed on the surface and of atmospheric contamination (cf., Secs. II.D.2 and II.D.4). Sticking coefficients for 10 species of exhaust gas were calculated and the results presented in Tables 20 and 22. The surface model used was a rough surface having a chemical composition similar to that of meteoroids. The calculations utilized a study of accommodation coefficients that was conducted at Grumman (Ref. 4) and the results of a computer program developed by that study.

Rates of desorption of the 10 species of gas were studied and the calculated desorption lifetimes are shown in Tables 17 and 18. Thermal desorption, solar wind produced desorption, and desorption by meteoroid impact are discussed in Sec. IV.F.

Unfortunately, lack of data on adsorption and desorption processes under lunar environmental conditions is so severe that calculated values in Secs. IV.F and IV.G, so important for determining contaminant distributions, are only approximations of the order of magnitude. Better data are urgently needed.

6. Thermal Distributions

The transient temperature distribution produced on and below the lunar surface by the impingement of the descent rocket plume will play an important role in determining adsorption and desorption

rates for rocket exhaust gas (Secs. IV.G, IV.F, and IV.G), and in possible chemical or phase changes in surface materials (see Sec. V.E of Ref. 1). It is also desirable to know the thermal history of samples gathered in the vicinity of the LEM.

Section IV.H herein discusses temperature distributions calculated by means of a computer program. The heat flux to the lunar surface was obtained from data supplied by Grumman. Values of the lunar thermal parameters used in the calculations are listed in Table 23. The calculated maximum temperatures reached at various depths and various distances from the touchdown point are given in Table 27. The temperature distributions at various depths below the lunar surface are shown in Fig. 71. For the parameters of Table 23 the temperature transients do not penetrate beyond the first few centimeters.

It should be noted that the computer program used to calculate these distributions can incorporate thermal parameters corresponding to vesicular or porous surface, but the program does not allow for penetration of hot exhaust gas into the lunar surface. Since the Luna 9 photographs indicate that considerable penetration of gas into the surface can occur, it would be desirable to recalculate the temperature distributions taking note of penetration effects. Gas penetration may produce temperature transients at greater depths than predicted by the present results.

7. Distributions of Space Suit Leakage and Vented Gas

The metabolic and bacterial contaminants discussed in Secs. II.B.2 and II.B.3 are distributed by gas leaked from the space suits and vented from the ascent stage. The importance of space suit leakage is apparent since the astronaut will closely approach, and may possibly even come in contact with, the samples he is collecting. Therefore, every sample collected by an astronaut will have had space suit leakage squirted at it.

The distribution and the rate of leakage from a space suit, which is of the order of several hundred cc per minute, will be influenced by the astronauts' activities. Tests should be made of the rate and location of suit leakage while the astronaut is engaged in activities simulating sample collection procedures on the Apollo mission.

When leakage rates and locations are determined, the distribution of contamination that they will produce can be calculated in a relatively simple manner. However, in view of the limited time period and size of the present contract, it was decided not to pursue this question. Instead, efforts have been directed toward the

investigation of the probable composition and amount of bacteriological contamination (Sec. II.B.3, III.A, and III.C)and toward the establishment of appropriate methods of reducing or compensating for space suit and ascent stage leakage contamination (Secs. II.E and IV.I).

E. Minimizing, Detecting, and Compensating for Contamination

Appreciable contamination will exist in the lunar regions that the Apollo astronauts can explore. It is advisable therefore, to attempt to minimize and identify contaminants (cf., Sec. IX of Ref. 1). Probably, the most important tools in identifying and compensating for contamination are maps and time histories of the contaminant species (Secs. II.D, IV.A, B, C, D, and E). The location and time at which every lunar sample is collected should be recorded. This will allow a statistical comparison between the relative amounts of various species of constituents in the samples and the predicted contaminant distributions. Such a comparison will help distinguish naturally occurring lunar substances from contaminants. It is important, therefore, that contaminant distribution maps be made as accurate as possible. The statistical comparison will utilize the results of studies of possible synthesis of new contaminant species by chemical reactions in the lunar environment (Secs. II.B.4, III.B).

A possible method of minimizing contamination in samples is to collect them from regions that are partially or totally shielded from rocket exhaust gas. Such regions may exist under rocks or inside cavities that are distant from the LEM touchdown point. The Luna 9 photographs suggest that such surface features exist. It should be noted, however, that back contamination problems may occur in connection with samples taken from locations shielded from the lunar radiation environment.

In Sec. IV.I, various devices for minimizing contamination are suggested. While these are presented as methods for minimizing bacteriological contamination, the suggestions are applicable to chemical contamination. Section IV.I suggests the possibility of dropping a sampling probe from the LEM prior to or immediately after touchdown. The probe would be designed to take a surface and near surface sample and seal it against further contamination. The sample would subsequently be retrieved by an astronaut. Another suggestion involves the dropping of a container of a substance from the LEM prior to touchdown. When it hits the surface the substance would spread over a region and form a close-fitting impenetrable shield against contamination.

The use of tracers to detect the presence of contaminants that have come from the LEM is also suggested. Problems arise in the selection of a tracer substance that is readily identifiable, nontoxic, noninjurious, and compatible with all phases of the scientific mission.

Another suggestion is for an instrument to be used by the astronaut. The instrument would sterilize a small area of the lunar surface and would then take a sample with a sterilized tool at sufficient depth to avoid the surface contamination. The sample would be sealed in such a way that it could be extracted without suffering contamination from spacesuit leakage. The sample would be free of both bacterial and chemical contamination. In connection with using a tool to take a sample at a depth below the surface, the Luna 9 photographs indicate a porous surface into which contaminants may penetrate. It is apparent that the depth of penetration of contaminants into porous surfaces should be investigated (see Sec. V.B).

III. CONTAMINANT COMPOSITION

A. Metabolic and Biological Contaminants [C. Baulknight]

1. Portable Life Support System and Space Suit

The leakage rate of CO_2, O_2, H_2O vapor, and flatus gases from the Portable Life Support System (PLSS) and the Space Suit constitutes additional sources of chemical contaminants. As far as is presently known, however, no actual tests have been made on such systems. This problem is now being investigated by scientists at Hamilton Standard (Ref. 5) who have made a series of experimental studies on an 'assimulated' PLSS – space suit configuration to determine the effectiveness of lithium hydroxide (LiOH) in the removal of CO_2 in a flow system. These experiments were performed to correspond to varying mission profiles and to several metabolic work loads. The mission profiles correspond, for instance to total inlet weight flow rate, CO_2 inlet weight flow (lbs/hr), dewpoint (°F), etc., and the work loads vary from 1200 BTU to 2000 BTU.

Although these tests were not performed on the space suit and PLSS directly, the information may be directly related. Some of the conclusions and recommendations deducible from their investigations are:

- Cartridge efficiency is inversely proportional to the production rate of CO_2, the contact time of the gas with the LiOH bed and the partial pressure of the entering H_2O vapor.
- The efficiency of the LiOH in the removal of CO_2 appears to be related to its particle size.
- Other CO_2 absorbing material should be tested and compared with LiOH. Lithium peroxide has been suggested, because during its interaction with CO_2, $\frac{1}{2}$ mole of oxygen is generated for each mole of absorbent.
- The experimental test facility should include a capability of investigating the leakage from all the reservoir components, i.e., the CO_2 and oxygen.
- Leak rate test on a space suit and the PLSS system should be conducted with a human performing an activity equivalent to some prescribed metabolic workload.

The presently accepted leak-rate for the PLSS is 20.0 std. cc/min; for the suit it is 200 Std. cc/min. These rates refer to the total gas mixture and not to any particular specie. One would expect, on the basis of the tests run thus far, that the major species of "leaked" gases would be CO_2, O_2, H_2O vapor and flatus gases. No realistic estimates of the percentage of these gases can be made on the basis of presently available information.

B. Photochemical and Radiation-Damage Induced Reactions

[A. Buchler, J. Berkowitz-Mattuck and P. Glaser]

1. General

The radiation environment of the moon can influence the nature of the chemical contamination of the lunar surface in two ways. First, in the absence of an atmosphere, the entire solar spectrum, including the photochemically active vacuum ultraviolet, can reach the engine exhaust products and the contaminants adsorbed on the lunar surface. Second, the constant bombardment of the moon by high-energy radiation and solar wind over the billion years of lunar history may have created a large number of surface sites in highly excited and hence chemically reactive states.

References to the hover period in this Section are from portions of Ref. 2 that are now obsolete. As sufficiently similar conditions exist during the Lo-Gate to Pre-Touchdown phases of currently planned trajectories, the hover terminology in this Section has not been changed, so as to avoid unnecessary references to classified documents (Ref. 3).

2. Photochemical Reactions

a. The Solar Spectrum: Most of the energy from the sun is in the visible range. Out of a total solar radiation of about 1.4×10^6 ergs/cm^2 -sec, a very small fraction, about 400 ergs/cm^2 -sec, lies at wavelengths less than 2000 A. Since the primary process in any photochemical reaction is the absorption of energy, it is only the short wavelength, high energy radiation which exceeds a minimum threshold energy that can lead to such reaction among the simple molecules that compose the LEM exhaust. The photon flux from the sun in the ultraviolet region is plotted in Fig. 2 (Ref. 6); the number of particles/cm^2 -sec with energy greater than E ev is plotted against E.

b. Absorption Processes in the LEM Exhaust: A list of the most abundant combustion and a few selected minor products of the LEM exhaust and their corresponding concentrations in mole-percent is given in Table 6. For each species, the maximum wavelength at which significant absorption occurs is listed. We see that only that portion of the solar spectrum with wave-

lengths less than 1800 Å or energies greater than 7 ev can initiate photochemical reactions. The number of photons available in this region is less than $10^{13}/cm^2$ -sec. Photochemically excited molecules produced by absorption of photons may lose energy in chemical reaction or may dissociate to free radials or ions that in turn can initiate more extensive reactions. From the point of view of chemical contamination of the lunar surface, the reactions of greatest interest are those that lead to the formation of organic compounds.

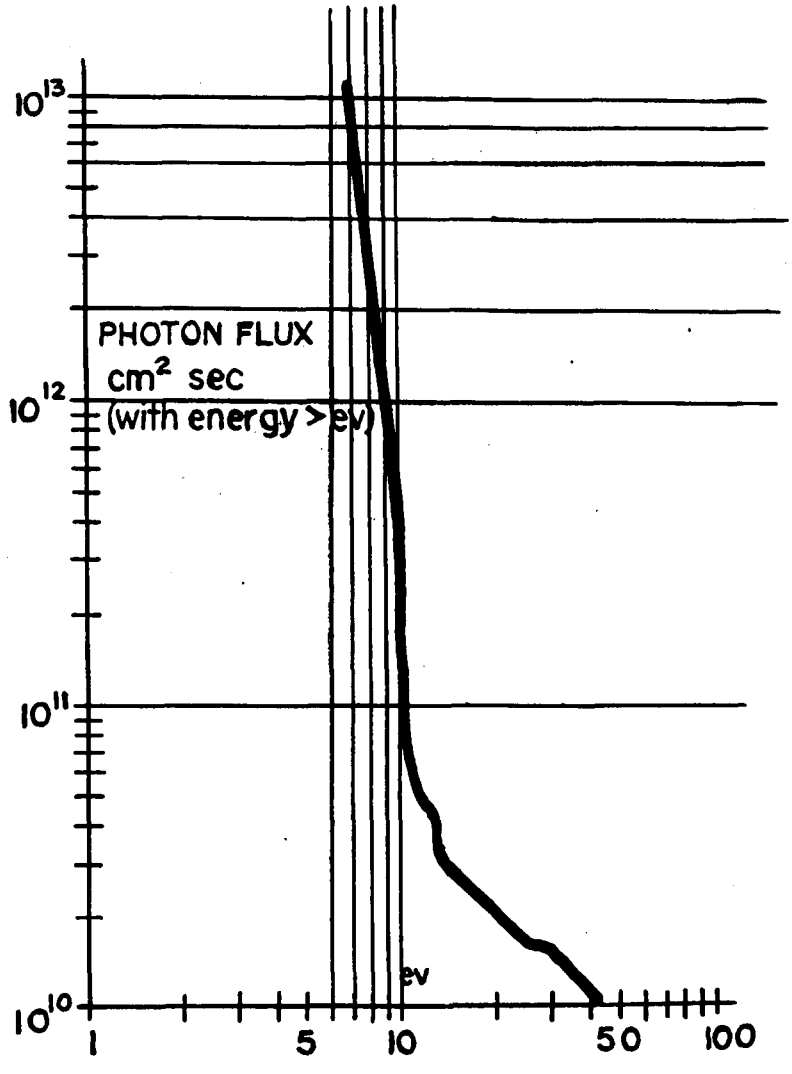

Fig. 2 The Integrated Solar Photon Flux Is Shown Plotted against the Energy of the Photons. The Ordinate Gives the Total Number of Photons per cm^2 sec with Energy Equal or Greater than that Given on the Abscissa.

Table 6

COMBUSTION – MINOR PRODUCTS OF LEM EXHAUST

Species	Mole %	Absorption is Detectable at Wavelengths Less Than
H_2O	36	1800 Å
N_2	32	1450
H_2	13	1200
CO	9.6	1600
CO_2	3.7	1600
H	1.9	-
OH	1.6	3080
NO	0.24	1800
CHO	$\sim 10^{-2}$	-
NH	$\sim 10^{-2}$	~4500

c. Reactions in the Gas Phase during Hover: Because there essentially are no intermolecular collisions in the exhaust gas prior to deposition on the lunar surface, the only photochemical reactions that can occur in the gas phase during hover are those that involve photon absorption and possible subsequent decomposition to radicals or ions.

The absorption of light of intensity, I_o, by a layer of gas of thickness x and pressure P is described by the Beer-Lambert Law:

$$I = I_o e^{-\epsilon P x} , \qquad (1)$$

where ϵ is related to the absorption cross section σ by:

$$\sigma(cm^2) = \epsilon(atm^{-1}\ cm^{-1})/n_o \quad ,$$

where

$$n_o = 2.687 \times 10^{19}\ cm^{-3}\ atm^{-1} \quad ,$$

the Loschmidt number, During hover, gas is released from about 200 feet [hence $x \simeq 6100$ cm] and the pressure of water, the most abundant species, is of the order of 0.01 torr. The pressure of other species can be calculated from Table 6.

Water shows significant absorption only at wavelengths less than 1800 Å or energies greater than 7 ev. From Fig. 2, the number of photons in the solar spectrum with energy greater than 7 ev is $I_o \simeq 9 \times 10^{12}/cm^2$ - sec. During the hover period, the pressure of water vapor is of the order of 0.01 torr. The absorption cross section varies considerably with wavelength (Refs. 7 and 8), but for order of magnitude calculations, we may use an average value of $\epsilon \simeq 30\ atm^{-1}\ cm^{-1}$. The primary decomposition processes of photochemically excited water molecules are as follows:

$$H_2O + h\nu \rightarrow H(^2S) + OH^* \qquad (2)$$

$$H_2O + h\nu \rightarrow H_2 + O^*(^1D) \quad . \qquad (3)$$

The hydrogen atoms are produced in the ^2S ground state. The OH radicals are produced in the $X^2\Pi$ state at wavelengths between 1430 and 1800 Å, but in an excited $A^2\Sigma^+$ state at wavelengths below 1400 Å. The oxygen atoms are produced in the metastable ^1D state. From Eq. (1), the maximum amount of water vapor in the exhaust that could be photochemically dissociated during hover is 8×10^{12} molecules/cm^2 -sec. This is to be compared with the total amount of water released that is of the order of 10^{18} molecules/cm^2 -sec.

The most important photochemical reaction of N_2 is photoionization, which becomes significant in the spectral region below 800 Å ($E > 15$ ev). The cross section for the process,

$$N_2 + h\nu \rightarrow N_2^+ + e^- \quad , \tag{4}$$

is of the order of 2×10^{-17} cm^2. From Fig. 2, $I_o \simeq 3 \times 10^{10}$ photons/cm^2 -sec for $E > 15$ ev. As the pressure of N_2 in the LEM exhaust is of the order of 0.009 torr, the maximum rate of formation of N_2^+ during a 40 second hover period would be 2×10^8 ions/cm^2 -sec.

For CO_2 the primary photolytic reaction is decomposition to CO and metastable oxygen atoms:

$$CO_2 + h\nu \rightarrow CO(X^1\Sigma) + O(^1D) \quad . \tag{5}$$

Reaction occurs at wavelengths below 1600 Å or energies greater than 8 ev. With $I_o \simeq 2.8 \times 10^{12}$ photons/cm^2 -sec, $\epsilon \simeq 10$ cm^{-1} atm^{-1}, pressure of CO_2 - 10^{-3} torr, and quantum yield of 1, we find that about 4.8×10^{-11} CO_2 molecules/cm^2-sec are photolytically decomposed.

For NO the strong absorption is below 1800 Å ($E > 7$ ev) and the primary reaction is decomposition:

$$NO \xrightarrow{h\nu} N(^4S) + O(^3P) \tag{6}$$

Although the absorption coefficient is quite high, $\epsilon \simeq 60$ atm^{-1}cm^{-1}, the pressure of NO in the exhaust is so low, 6.7×10^{-5} torr, that $I/I_o \simeq 0.966$. Because $I_o \simeq 9 \times 10^{12}$ photons/cm^2 -sec, the maximum number of NO molecules that can dissociate is 3.1×10^{11}/cm^2 -sec. At wavelengths below 1236 Å ($E > 10$ ev), the primary photochemical reaction of NO becomes ionization:

$$NO \xrightarrow{h\nu} NO^+ + e^- \quad .$$

The photon flux for $E > 10$ ev is about 2.5×10^{11}photons/cm^2 -sec. With $\epsilon \simeq 60$ atm^{-1}cm^{-1} the number of NO^+ ions formed will be less than 9.5×10^{-9} per cm^2 -sec.

d. Reactions Between Adsorbed Species on the Lunar Surface: It is clear from the above discussion that the number of radicals and ions produced in the exhaust gas due to photon absorption

during the hover period is exceedingly small and would not alter the exhaust gas composition detectably. Reactions involving collisions between photochemically produced species are extremely unlikely in the exhaust gas during hover but may become important with respect to reactions between adsorbed molecules on the lunar surface.

We consider first a number of photochemical reactions that could lead to the formation of organic molecules and about which enough is known for at least order-of-magnitude calculations of the amounts of product to be expected. It should be emphasized that most of the experimental data available on photochemical reactions have been obtained for homogeneous gas phase reactions. If similar reactions take place on the lunar surface, the influence of the surface itself on the reaction kinetics could be very large, although, as discussed below, this effect will be almost impossible to calculate beforehand. In the extreme case of a highly catalytic surface, reaction could be so extensive and rapid that none of the exhaust products would retain its original identity.

Carbon monoxide photochemically excited at wavelengths less than 1550 Å can react with hydrogen to produce formaldehyde. The reaction has been described by the following steps:

$$CO \xrightarrow{h\nu} CO^* \qquad (7)$$

$$CO^* + H_2 \longrightarrow CO + 2H \qquad (8)$$

$$M + H + CO \longrightarrow HCO + M \qquad (9)$$

$$2HCO \longrightarrow (CHO)_2 \qquad (10)$$

$$2HCO \longrightarrow CH_2O + CO \quad . \qquad (11)$$

The strongest absorption band of CO is around 8 ev (λ = 1550 Å) corresponding to the transition $A'\pi \leftarrow X'\Sigma^+$. On the lunar surface, we will assume that the rate of formation of photochemically excited CO* , R_{CO^*}(molecules/cm^2 -sec) is given by:

$$R_{CO^*} = n_{CO}\sigma I_o \quad , \qquad (12)$$

where n_{CO}(molecules/cm^2) is the surface concentration of CO, $I_{o\circ}$ is the intensity of solar radiation at wavelengths less than 1550 A, (normal incidence is assumed), and σ is the absorption cross section. For CO, $\sigma \simeq 1.6 \times 10^{-20}$ cm^2; $I_o(\lambda < 1550\ \text{A}) \simeq 2.8 \times 10^{12}$ photons/cm^2 -sec. During hover, about 2×10^{-4} g/cm^2 of CO are deposited a approximately uniformly over an area of 2×10^8 cm^2; thus $n_{CO} \simeq 4.3 \times 10^{18}$ molecules/cm^2. Thus, from Eq. (12) we have $R_{CO*} \simeq 1.8 \times 10^{11}$ molecules/cm^2 -sec. The number of H_2 molecules deposited during hover (assuming no escape) is about 6×10^{18} molecules/cm^2. If we then assume that one formaldehyde molecule is produced for every CO molecule excited, (very unlikely, since the reaction mechanism also involves collision between CO* and H_2), we find that the rate of formation of formaldehyde must be less than 9×10^{-12} g/cm^2 -sec. Thus, the time required to build up a microgram/cm^2 of formaldehyde on the lunar surface by the above process would be more than 28 hours. To produce carbohydrates in significant concentration by polymerization of formaldehyde would take even longer.

Ammonia can be synthesized photochemically by the action of the Lyman-α line (1216 A) on a mixture of hydrogen atoms and nitrogen. The Lyman-α line, which is particularly strong in the solar spectrum (photon flux of 3.9×10^{11} photons/cm^2 -sec), can effect the transition:

$$H(^2P) \leftarrow H(^2S) \quad . \tag{13}$$

The number of hydrogen atoms released during hover is of the order of 9.0×10^{17}/cm^2. If we assume that the rate of formation of $H(^2P)$ atoms via Eq. (13) during the hover period is equal to the Lyman-α flux, and if the quantum yield of ammonia is unity, we find that photochemical reaction would have to proceed for more than 25 hours to provide a microgram/cm^2 of ammonia on the lunar surface.

The photolysis of water vapor can lead to the production of hydrogen peroxide via the primary absorption reactions [Eqs. (2) and (3)] cited above, followed by

$$2OH \rightarrow H_2O_2 \tag{14}$$

or

$$O(^1D) + H_2O \rightarrow H_2O_2 \ , \qquad (15)$$

We can use the analogue of Eq. (12) with $n_{H_2O} \simeq 1.7 \times 10^{19}$ molecules/cm^2, $I_o \simeq 9 \times 10^{12}$ photons/cm^2 -sec, $\sigma \simeq 1.3\ 10^{-18}$ cm^2 to calculate the rate of photochemical decomposition of water on the lunar surface. If we assume a quantum yield of one-half, then it would be possible to form microgram/cm^2 quantities of hydrogen peroxide in times of the order of 5 minutes.

We discussed above the photolytic decomposition of CO_2 and NO. On the lunar surface, approximately 3-6 hours might be required to decompose a microgram/cm^2 of CO_2 to CO and O or NO to N and O. The atoms might in turn react further.

In several experiments in recent years, amino acids have been synthesized by the action of an electric discharge on mixtures of simple inorganic molecules such as CO_2-N_2-H_2-H_2O; CO-N_2-H_2-H_2O; CO_2-NH_3-H_2-H_2O. There has been speculation that similar reactions could be initiated by the action of ultraviolet light. Groth (Ref. 7) did produce amino acids by irradiation of a gaseous mixture of CH_4, NH_3, and H_2O with xenon resonance light at 1470 and 1295 A, total intensity 10^{16} photons/sec. However, the gas pressures he used were CH_4, 400 torr; NH_3, 150 torr; and H_2O, 100 torr; and irradiation had to be continued for 24 hours before unequivocal results were obtained. It is interesting to note that at a lower water vapor pressure, 15 torr, amino acids were not formed, although there were small yields of methyl and ethyl amines. Thus, if photochemical reactions are the only ones that can occur among the LEM exhaust products, significant quantities of amino acids cannot be expected within the time of the mission.

We have yet to explore the chemical reactions produced by the more energetic particles of the solar wind, and the effects of the radiation damaged lunar surface on chemical contamination.

3. Catalytic Reactions on the Lunar Surface

Catalysis is by its very nature highly specific and can be discussed only in terms of particular reactions on particular catalytic surfaces. It is difficult to apply the data available in the vast catalysis literature to the specific problems of the lunar surface. Even if we knew more about the nature of the lunar

surface, we still could not predict reaction rates among LEM exhaust products from any information currently available on the catalytic nature of oxide surfaces.

On the basis of the environment to which it has been exposed, the lunar surface should be catalytic in nature. However, it is not possible to predict what reactions might be catalyzed and to what extent. In general, oxide catalysts are activated by prolonged degassing at elevated temperature. Furthermore, in most of the studies that have been made of the enhancement of catalytic activity by irradiation, the effects have been no larger than those produced by more efficient vacuum degassing (Ref. 8). It seems clear that the parts of the lunar surface that have been subject both to solar wind and to temperatures of 400°K in a vacuum environment for the order a billion years, should have maximum catalytic activity for the particular materials involved.

Because the main contaminant introduced from the LEM exhaust is expected to be water, it should be pointed out that water commonly poisons oxide catalysts (Ref. 9). Thus, if the rate of chemisorption of water vapor exceeds the rate of any potential catalytic reaction, the lunar surface may be effectively poisoned.

In addition to possible strained, high-energy surface sites formed by long term degassing and proton bombardment from the solar wind, there will be positively charged sites on the moon that might react rapidly with incoming neutral combustion products. The positive charge on the lunar surface is due to a competition between the photoelectric effect and the accretion of electrons from outer space. The work function of most silicate minerals is about 10 ev. The He II 304 line whose output from the sun is about 15 ergs/cm^2 -sec or 2.3×10^{11} photons/cm^2 -sec, each of energy 40 ev, should be particularly effective in inducing emission of photoelectrons from the lunar surface. The net result of the competition is a maximum surface density of photoelectrons of $3.6 \times 10^5/cm^2$, a maximum surface charge of 5.75×10^{-10} coulombs/m^2, and a maximum number of 0.28 positive charges on 5μ particles (Refs. 10 and 11).

We have been concerned to this point about the possible effect of radiation and solar wind on the catalytic properties of the lunar surface prior to the introduction of the LEM contaminants. It is also conceivable that the radiation environment

may interact with adsorbed species to produce reactions that might not occur to the same extent in a homogeneous system exposed to the same degree of radiation. A recent review of the subject (Ref. 12) unfortunately does not include examples that are pertinent to the LEM contamination problem.

4. Summary

Photochemical reactions are possible in the exhaust gas during hover but they will not alter the exhaust composition to a measurable extent. The calculated rate of photochemical decomposition of H_2O, N_2, CO_2, and NO during hover are summarized in Table 7.

Table 7

PHOTOCHEMICAL REACTIONS IN THE EXHAUST GAS DURING HOVER

Reactant	Products	Maximum Rate of Reaction, Molecules/cm^2 -sec
H_2O	H + OH or H_2 + O	5×10^{18}
N_2	$N_2^+ + e^-$	2×10^{8}
CO_2	CO + O	5×10^{11}
NO (E > 7 ev)	N + O	2.2×10^{12}
NO (E > 10 ev)	$NO^+ + e^-$	8.5×10^{9}

Photochemical reactions between adsorbed gases on the lunar surface will be of greater importance. Maximum rates of formation and the times required to form microgram/cm^2 quantities of formaldehyde, ammonia, hydrogen peroxide, and a number of atomic species were calculated. The data are summarized in Table 8. Further reactions among the radicals produced are possible but cannot be predicted quantitatively. The results in Tables 7 and 8 are judged to have an uncertainty of about a factor of 2.

Table 8

PHOTOCHEMICAL REACTIONS ON THE LUNAR SURFACE

Reactants	Products	Rate of Formation of Product, g/cm^2 -sec	Time to Form 1μ g/cm^2 of Product, hrs
$CO + H_2$	HCHO	9.6×10^{-2}	29
$H + N_2$	NH_3	10^{-11}	28
H_2O	H_2O_2	5.5×10^{-9}	0.05
CO_2	CO + O	1.7×10^{-10}	2
NO	N + O	1.1×10^{-10}	2.5

A number of experiments in which amino acids were synthesized from mixtures of simple inorganic gases were evaluated with respect to the LEM contamination problem. Unless the lunar surface is highly catalytic, amino acids are not anticipated in detectable concentration.

Due to the high vacuum and radiation environment of the moon, the lunar surface should have maximum catalytic activity for the particular materials involved. However, it is impossible to predict the reactions that might be catalyzed or to calculate even the order of magnitude of the reaction rates.

C. Bibliography

The following listing is intended primarily to aid an experimental investigation of the expected LEM cabin bacterial population and the ecology of the suited astronaut on the Lunar surface. The experimental program may be conducted independently of, or in conjunction with, a physiological investigation. Generally, the integration of microbiological and physiological programs necessitates sacrificing some of one of these, usually the former. Most microbiological studies therefore, have been limited to monitoring some pathogens, rather than the total ambient ecology. To predict the composition and density of contaminants derived from human ecological debris, a comprehensive experimental determination of the total human ecology, at the expected environmental conditions, will be necessary.

1. NASA 1965 Summer Conference on Lunar Exploration and Science, NASA SP-88, Falmouth, Mass., July 19-31, 1965.

2. Life Sciences and Space Research, ed. by M. Florkin, A Session of the Fifth International Space Science Symposium, Florence, 12-16 May, 1964, John Wiley and Sons, Inc., N.Y., 1965.

3. Conference on Nutrition in Space and Related Waste Problems, NASA SP-70, Univ. of Tampa, Fla., April 27-30, 1964.

4. Problems of Space Biology, Vols. 1, 3 ed. by N. M. Sisakyan and V. I. Yazdovsky, trans. by Joint Publ. Research Service, JPRS-25287, 29 June 1964.

5. Pilgrim, A. J., Fosberg, J. M., and Anderson, J. H., "Manned Environmental System Assessment" Proc. XV Internat. Astronautical Congress, Warsaw, 1964, Vol. IV.

6. Helvey, W. M., et al., Effects of Prolonged Exposure to Pure Oxygen Human Performance, Republic Aviation Corp. RAC 393-1, Final Report on Contract NAS r-92, 30 Nov., 1962.

7. Riely, P. E., Geib, D. and Shorenstein, D., Determination of the Indigenous Microflora of Men in Controlled Environments, Republic Aviation Div., Fairchild Hiller Corp./Aerospace Medical Research Labs., Wright-Patterson AFB, Ohio AMRL-TR-65, Final Report AF Contract AF 33(615)-1814.

8. Gall, L. S. and Riely, P. E., Determination of Aerobic and Anaerobic Microflora of Human Feces, Republic Aviation Corp., Report AMRL-TR-64-107, Oct., 1964. Final Report on AF Contract AF 33(615)-1748.

9. Moyer, J. E., and Lewis, Y. Z., Microbiological Studies of the Two Man Space Cabin Simulator: Interchange of Oral and Intestinal Bacteria, School Aerospace Medicine, Brooks AFB, Texas, SAM-TDR-64-3, March 1964.

10. Aviation and Space Medicine, V. V. Parin, ed., NASA TT-F-228, Dec. 1964.

11. Aerospace Medicine & Biology - A Continuing Bibliography, NASA-SP-7011 (05) Dec. 1964, NASA-SP-7011 (11) May 1965, NASA-SP-7011 (12) June 1965.

12. Studies in Radiotelemetry in Physiology and Medicine, Joint Publ. Research Service JPRS-27600, 30 Nov. 1964.

13. Markelova, L. et al., A Human in a Spaceship, Joint Publ. Research Service JPRS-27880, 16 Dec. 1964.

14. Iyerusalimskiy, N. D. and Spirin, A. S., Microbiological Synthesis In Industry and Protein Biosynthesis, Joint Publ. Research Service JPRS-30486, 8 June 1965.

15. Apollonov, A. and Mirolyubov, V., Effect of Altitude on the Organism of Fliers in Flight, transl. by A.F. Syst. Com., Wright-Patterson AFB, Ohio, 7 April 1965.

16. The Effects of Weightlessness and Other Stresses Associated With Flight in Space on Pathogenicity and Immunity - Final Report - Michigan State Univ., East Lansing - Grant Ns G-514, 1964.

17. "Space-Oriented Ecophysiology in the USSR," A.T.D. Press Special Express Issue, Vol. 3 No. 243, 14 June 1965.

18. Soviet Literature on Life Support Systems. Part A: Biosciences - Surveys of Soviet-Bloc Scientific and Technical Literature, Library of Congress, Aerospace Tech. Div. AD-609827, 30 December 1964.

19. Vedenov, M. F. and Kremyanskiy, V. I., On the Specific Character of Biological Structures, Joint Publication Research Service JPRS-30737, 22 June 1965.

20. "Second International Symposium on Basic Environmental Problems of Man in Space," Paris, 14-18 June 1965.

21. Interdisciplinary Studies of the Effects of the Space Environment on Biological Systems, Semi-annual Status Report, Okla. City Univ., NASA-CR-63790, 30 April 1965.

22. Michel, E. L., Smith, Jr., G. B. and Johnston, R. S., Gaseous Environment Considerations and Evaluation Programs Leading to Spacecraft Atmosphere Selection, NASA TN D-2506, January 1965.

23. Moyer, J. E., "Microbiologic Problems of Sealed Cabin Environments," Developments in Industrial Microbiology, 1964, pp. 216-223, Vol. 5.

24. McNall, E., "Microbiologic Examination of Spacecraft," published by the Dynamic Science Corporation, Pasadena, California, 1966.

25. Bioastronautics Data Book, Paul Webb, M.D. ed., NASA SP-3006, Prepared for NASA by Webb Assoc., Yellow Springs, Ohio, 1964.

26. Davis, N. S., et al., Effects of Simulated Space Environments on the Viability of Microorganisms, Nat. Res. Corp., Cambridge, Mass., 12 March 1963, Quarterly Status Report, Oct. 16, 1962 through Jan. 15, 1963.

27. "A Symposium on Toxicity in the Closed Ecological System," M. Homma and H. J. Crosby, eds., 29-31 July 1963, Palo Alto, Calif.

28. Nette, I. T., et al., Growth of Some Mycobacteria on Petroleum and Petroleum Products, Vol. 1 Joint Publications Research Service JPRS-31360, 2 August 1965.

29. Investigations in Space-Related Biology, Miami University, Coral Gables Institute of Molecular Evolution, First Annual Report, 1 June 1965.

30. McNall, E. G. and Duffy, W. T., Microorganisms in Solid Materials, Phases I, II, III, IV, Dynamic Science Corp., South Pasadena, Calif., Final Summary Report 23 April 1965.

31. Biological Studies, National Academy of Sciences, Part of U. S. Space Science Program, Report to COSPAR, 1963, Warsaw, 3 June 1963.

32. Haldane, J. B. S., "Life at High Pressure." Science News, IV, 1947, Penguin Books, New York.

33. Behnke, A. R., Johnson, F. S., Poppen, J. R. and Motley, E. P., "The Effect of Oxygen on Man at Pressures From 1 to 4 Atmospheres," Amer. J. Physiol., 1934-35, 110, 565.

34. Bean, J. W., "Effect of Oxygen At Increased Pressures." Physiol. Rev., 1945, 25, 1.

35. Welch, B. E., Morgan, T. E., Ulvedal, F., and Henderson, W. W., "Observations in the SAM Two-man Space Cabin Simulator." Aerospace Med., 1961, 32:7, 583, 591, 603, 610.

36. Ernsting, J., "Some Effects of Oxygen Breathing," Proc. Roy. Soc. Med., 1960, 53:96.

37. Clark, C. D., and Augerson, N. W., "Human Acceleration Tolerance While Breathing 100% Oxygen at 5 Psia Pressure," presented at Aerospace Medical Association Meeting, April 26, 1961.

38. Malmo, R. B. and Finan, J. L., "A Comparative Study of Eight Tests in a Decompression Chamber," Amer. J. Psychol., 1944, 57, 389-405.

39. Beerens, H. et al., "Classification des Bacteroidaceae," VIII International Congress for Microbiology, August 19-24, 1962, Montreal, Canada.

40. Brandia, S. A., et al., "Functional Changes in the Organism at Rest and at Work During Prolonged Inhalation of Gas Mixtures Containing Large Amounts of Oxygen," Fiziol. Zh. SSSR Sechenov, July 1960, 46:801.

41. Campbell, J. A., "Further Observations on Oxygen Acclimatisation," J. Physiol., 1947, 63, 325.

42. Dehnert, J., "Zur normalen Intestinalbesiedlung. Grenzen Der Kulturellen Analyse Der Stuhlflora," Wien. Klin. Wschr. 1961, 73:43-44, 729-733, in Excerpta Med. IV Microb., 1962, 15, 373.

43. Dubos, R. J., and Schaedler, R. W., "The Effect of the Intestinal Flora on the Growth Rate of Mice, and on Their Susceptibility to Experimental Infections," J. Exp. Med., 1960, 111, 407.

44. Gall. L. S., Tenzer, D. B., and Helvey, W. M., "Bio-Ecology of Digestion," USAF-Air Force Systems Command, Symposium-Workshop, Biologistics for Space Systems, May 1-3, 1962.

45. Haenel, H., "Some Rules in the Ecology of the Intestinal Microflora of Man," J. Appl. Bact., 1961, 24:3, 242.

46. Hall, A. L. and Martin, R. J., "Prolonged Exposure in the Navy Full Pressure Suit at Space Equivalent Altitudes," Aerospace Med., 1960, 31, 116.

47. Huhtanen, C. N., Rogers, M. R., and Gall, L. S., "Improved Techniques for Isolating and Purifying Rumen Organisms," J. Bact., 1952, 64, 17.

48. Juhlin, I., and Ericson, C., "A New Medium for the Bacteriologic Examination of Stools (LSU Agar)." Acta. Path. Microbiol. Scand., 1961, 52, 2, 185.

49. Lambertson, C. J., "A Philosophy of Extremes for the Gaseous Environment of Manned Closed Ecological Systems," I.A.S. Proceedings, April 1960.

50. Langdon, D. E., et al., "Post Flight Respiratory Symptoms Associated with 100% Oxygen and g Forces," Aerospace Med., 1961, 32, 713.

51. Lowman, J. T., "Diagnostic Confusion Associated with Spherocytes in Coombs'- Positive Acquired Hemolytic Anemia," J. Lancet., 1962, 82, 431.

52. Manual of Microbiological Methods, Society of Amer. Bacteriologists, McGraw-Hill, 1957.

53. Pearman, E., "Some Life Sustaining Problems of Space and Lunar Exploration," Environmental Quarterly, June 1962.

54. Pearman, E. and Helvey, W. M., "Space Environment and Life Sciences Facilities at Republic Aviation," Inst. Environ. Sci., Annual Proceedings, 1961, Washington, D. C.

55. Rogosa, M., Mitchell, J. A. and Wiseman, R. F., "A Selective Medium for the Isolation and Enumeration of Oral Lactobacilli," J. Dent. Res., 1951, 30, 682.

56. Zubrzycki, L. and Spaulding, E. H., "Studies on the Stability of Normal Fecal Flora," J. Bact., 1962, 83:968.

57. Bergeim, O., Hanszen, A. H., Pincussen, L. and Weiss, E., "Relation of Volatile Fatty Acids and Hydrogen Sulphide to Intestinal Flora," J. Infect. Dis., 69, 155-166, 1941.

58. Dubos, R., Schaedler, R. W., Costello, R. and Hoet, P., M.D., "Indigenous, Normal and Autochthonous Flora of the Gastro-intestinal Tract," J. of Exp. Med., 122, 67-76, 1965.

59. Watson, E. D., Hoffman, N. J., Simmers, R. W. and Rosebury, T., "Aerobic and Anaerobic Bacterial Counts of Nasal Washings: Presence of Organisms resembling Corynebacterium acnes," J. Bact., 83, 144, 1962.

60. Rosebury, Theodor, Microorganisms Indigenous to Man, published by the Blakiston Division, McGraw-Hill Book Company, Inc., New York, 435 pp., 1962.

61. Marples, Mary J., The Ecology of the Human Skin, published by Charles C. Thomas, Springfield, Illinois, 970 pp., 1965.

62. Huhtanen, C. N., Rogers, M. R. and Gall, L. S., "Improved Techniques for Isolating and Purifying Rumen Organisms," J. Bact., 64, 17-23, 1952.

63. Breed, Robert S., Murray, E. G.D. and Smith, Nathan R. (Editors), Bergey's Manual of Determinative Bacteriology, 7th Edition, Baltimore, The Williams & Wilkins Company, 1957.

64. Shehadeh, N. H. and Kligman, A. M., "The Effect of Topical Anti-Bacterial Agents on the Bacterial Flora of the Axilla," J. Invest. Derm., 40, 61-71, 1963.

65. Pillsbury, D. M. and Kligman, A. M., "Some Current Problems in Cutaneous Bacteriology," (Chapter 11) in Modern Trends in Dermatology, 2nd series, Butterworth, pp. 187-213, 1954.

66. Marples, M. J. and Bailey, M. J., "A Search for the Presence of Pathogenic Bacteria and Fungi in the Interdigital Spaces of the Foot," Brit. J. Derm., 69, 379-388, 1957.

67. Krassilnikov, N. A., "Guide to the Identification of Bacteria and Actinomycetes," Academy of Science, USSR, 1949.

68. NASw-738, "Study of Normal Fecal Bacterial Flora of Man," Office of Space Sciences, National Aeronautics and Space Administration, Washington, D. C., July 26, 1965.

69. Gall, L. S., NAS9-4172, "Effect of Diet and Atmosphere on Intestinal and Skin Flora," 1963.

70. AF33(615)-3255, "Research on Microbiological Flora of Human Subjects Undergoing Conditions of Simulated Enviroment."

71. Silen, W., Harper, H. A., Mauasley, D. L. and Weirich, W. L., "Effect of Antibacterial Agents on Ammonia Production Within the Intestine," Proc. Soc. Exp. Bio. and Med., 88, 138, 1955.

IV. CONTAMINANT DISTRIBUTION

A. Far Field Distribution [F. Koch]

1. General

The gas plume issuing from the LEM descent rocket engine nozzle into the vacuum around the moon interacts with the lunar surface causing contamination of the surface. The rocket plume has two major flow regimes. Adjacent to the nozzle exit there is a compressible continuum fluid flow regime, but as the gas continues to expand out from the nozzle the density decreases, and a free molecular flow, far field regime develops.

When the LEM vehicle, in its landing trajectory, is at an appreciable altitude, only the fully developed far field of the exhaust plume intersects the moon. This interaction produces the far field contamination that has been analyzed and determined by assuming free-molecular point-source flow of the exhaust gas in the lunar gravitational force field.

These reasonable simplifications make it possible to determine the primary-impact mass flux distribution on the lunar surface for a given position of LEM. If all the gas sticks to the surface (accommodation coefficient equal to unity) this distribution is the contamination flux distribution. Some of the gas can rebound from the surface (accommodation coefficient less than unity) necessitating additional analysis that is very involved and further, requires some speculation as to the nature of the lunar surface. Thus, as a first approximation, only the primary contamination flux distributions are considered herein that should give conservative contamination levels. The total contamination at a fixed lunar point is then obtained by integrating the contamination flux at that point over the time interval of the LEM landing trajectory for which the far field contamination flux calculation is valid.

The point source characteristics (velocity and density factor distributions) necessary for this analysis are obtained by a subsidiary analysis using the flow properties of the rocket exhaust plume calculated by the method of characteristics.

2. Formulation

a. Assumptions and Flow Model: Several assumptions are made in defining the flow model to describe the transfer of the descent

rocket exhaust gas to the lunar surface and to determine the resultant surface contamination distribution. The moon is assumed to be a sphere with no atmosphere to interfere with the exhaust gas moving toward the lunar surface. The lunar gravitational force field becomes a governing factor in analyzing this flow.

Method of characteristics calculations show that the far field flow of the rocket exhaust plume resembles a free molecular point source flow. The streamlines become straight and appear to radiate from a point near the nozzle exit and the magnitude of the velocity approaches the limiting velocity of the gas. The density varies approximately inversely with the square of the distance from the virtual source center and is also a function of the conical angle between the flow direction and the nozzle centerline.

For the present problem (determination of the far field contamination), the continuum flow region around the nozzle exit is very small in comparison to the free molecular flow region that extends to the lunar surface and its effect on the contamination is assumed to be negligible. In other words, the outer boundary of the continuum flow regime is assumed to shrink to a point (the LEM center of gravity) when considering the pertinent distances in the problem (e.g., LEM altitude). This point then becomes the center of a free molecular point source flow with characteristics equal to those of the far field of the exhaust plume. The source characteristics are given by two distributions that are independent of the distance from the source center; a velocity distribution that has a constant magnitude and a density factor distribution (i.e., product of density and the square of the radial distance from the source center) that is axisymmetric about the nozzle centerline.

Because the exhaust velocity of the gas is very close to its limiting value, the random thermal component of the molecular velocity for each of the species in the exhaust gas is small and assumed to be negligible. Thus, all of the molecules emanating from the source have the same velocity. This assumption, coupled with the fact that the trajectories are independent of molecular weight, lead to the conclusion that the flux of far field contamination to the lunar surface is homogeneous (no differences between fluxes of the individual exhaust species to the surface due to differences in molecular weight).

The flow model thus consists of a moving, free molecular-flow point source in the lunar gravitational force field. The velocity of the gas molecules flowing from the source is the vector sum of the velocity at which the source (LEM) is moving and the source exhaust velocity. At ignition of the descent engine the LEM velocity is approximately half the exhaust velocity and so must be included in the analysis. The random thermal velocity is considerably

smaller. The molecules follow orbital trajectory flight paths that may intersect the spherical lunar surface where, as a first approximation, they can be assumed to be fully adsorbed.

b. Analysis and Equations for Contamination Calculation: The total far field contamination distribution on the lunar surface is obtained by integrating at each of a series of fixed lunar points, the time history of contamination flux for the time period of the far field portion of the LEM landing trajectory. The input data (LEM position and velocity and the point source exhaust velocity and density factor distribution) are such that the integration must be done numerically by determining the flux at discrete times over the powered descent phase of the LEM trajectory.

The principal equation in the flux calculation is the standard gravitational-force-field particle-trajectory equation (e.g., Ref. 13) that defines the flight path of a particle as a conic section. This equation is most easily solved in a spherical coordinate system with origin at the center of the moon and with polar axis going through a known point on the trajectory. A particle moves in a plane and its coordinates (r and θ, see Fig. 3) at any time are related by the trajectory equation

$$r(\theta) = \frac{p}{1 + e \cos(\theta - \theta_*)} , \tag{16}$$

where

$$p = 2r_o \left(\frac{q_p}{Q}\right)^2$$

$$e^2 = 1 + 4 \left(\frac{q_p}{Q}\right)^2 \frac{(q_o^2 - Q^2)}{Q^2}$$

$$\cos \theta_* = \frac{2q_p^2 - Q^2}{\sqrt{Q^4 + 4q_p^2(q_o^2 - Q^2)}}$$

$$q_p = q_o \sin \Theta_o$$

$$Q = Q_m \sqrt{\frac{R}{r_o}}$$

Q_m = escape velocity on the surface of the moon ($r = R$).

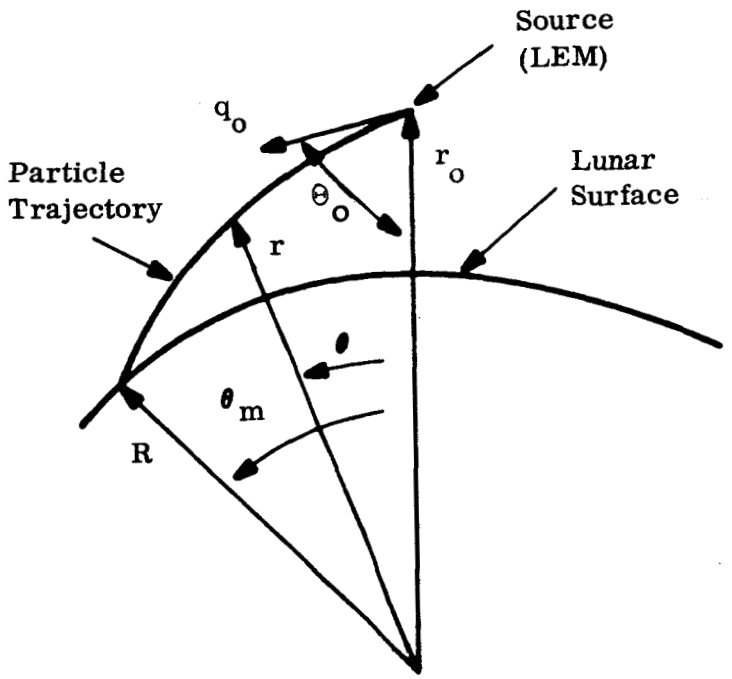

Fig. 3 Nomenclature for a Particle Trajectory Plane

For a given particle velocity (magnitude, q_o, and direction, Θ_o) at the source point, r_o, the relative position of the impact point on the lunar surface, θ_m, can be determined by setting $r = R$.

To calculate the total contamination at a fixed point on the lunar surface, the particle trajectory equation must be applied repeatedly to the source as it moves along the LEM trajectory. The movement of the source means that the local coordinate system for the particle trajectories rotates relative to the fixed point. Furthermore, the particle trajectory equation does not explicitly determine which particle will land at the fixed point. To circumvent these difficulties, a different, indirect approach must be taken. Therefore, at a given time or equivalently for a given position of the source, we calculate the velocity that a particle must have at the source to intersect the fixed point and this velocity uniquely determines the particle that lands there.

The fixed point where the total contamination is to be calculated is referenced to the same spherical coordinate system used for the LEM trajectory. This fixed coordinate system is shown in Fig. 4, with origin at the center of the moon, polar axis passing through the LEM touchdown point, and meridional reference plane coincident with the LEM trajectory plane at touchdown. In this system, the coordinates of the fixed point and the source are $(R, \bar{\theta}_m, \bar{\delta})$ and (r_o, θ_L, Δ), respectively. The coordinates of the fixed point in local particle trajectory coordinates (R, θ_m, δ) are found from the following transformation equations:

$$\cos \theta_m = \cos \theta_L \cos \bar{\theta}_m + \sin \theta_L \sin \bar{\theta}_m \cos(\Delta - \bar{\delta}) , \tag{17a}$$

$$\sin(\Sigma - \delta) = \frac{\sin \bar{\theta}_m \sin(\Delta - \bar{\delta})}{\sin \theta_m} \tag{17b}$$

where Σ is the angle between the local LEM trajectory plane and the LEM position plane defined by the touchdown point and the position vector of LEM, r_o.

Substituting the value of θ_m from the transformation equation [Eq. (17a)] into the trajectory equation [Eq. (16)] is not sufficient to determine the initial velocity components (radial, q_r, and perpendicular, q_p) of the required trajectory. These components have to be found, when they exist, by solving simultaneously the trajectory equation and the vector sum equation for the total velocity of the particle at the source. The trajectory equation, in terms of the velocity components with $r(\theta) = R$ and $\theta = \theta_m$, becomes

$$2q_r q_p \sin \theta_m + (1 - \cos \theta_m)Q^2 = (\bar{r} - \cos \theta_m)q_p^2 , \tag{18}$$

where $\bar{r}$ is the ratio of the initial position radius, r_o, to the radius of the moon, R. The source exhaust velocity, q_J, and the velocity of LEM, q_{LEM}, are added vectorially to determine the total initial velocity of the particle. In terms of the velocity components, this equation is

$$(q_p - q_{LEM} \sin \Theta \cos \delta)^2 + (q_r - q_{LEM} \cos \Theta)^2 = q_J^2 - q_{LEM}^2 \sin^2\Theta \sin^2\delta . \tag{19}$$

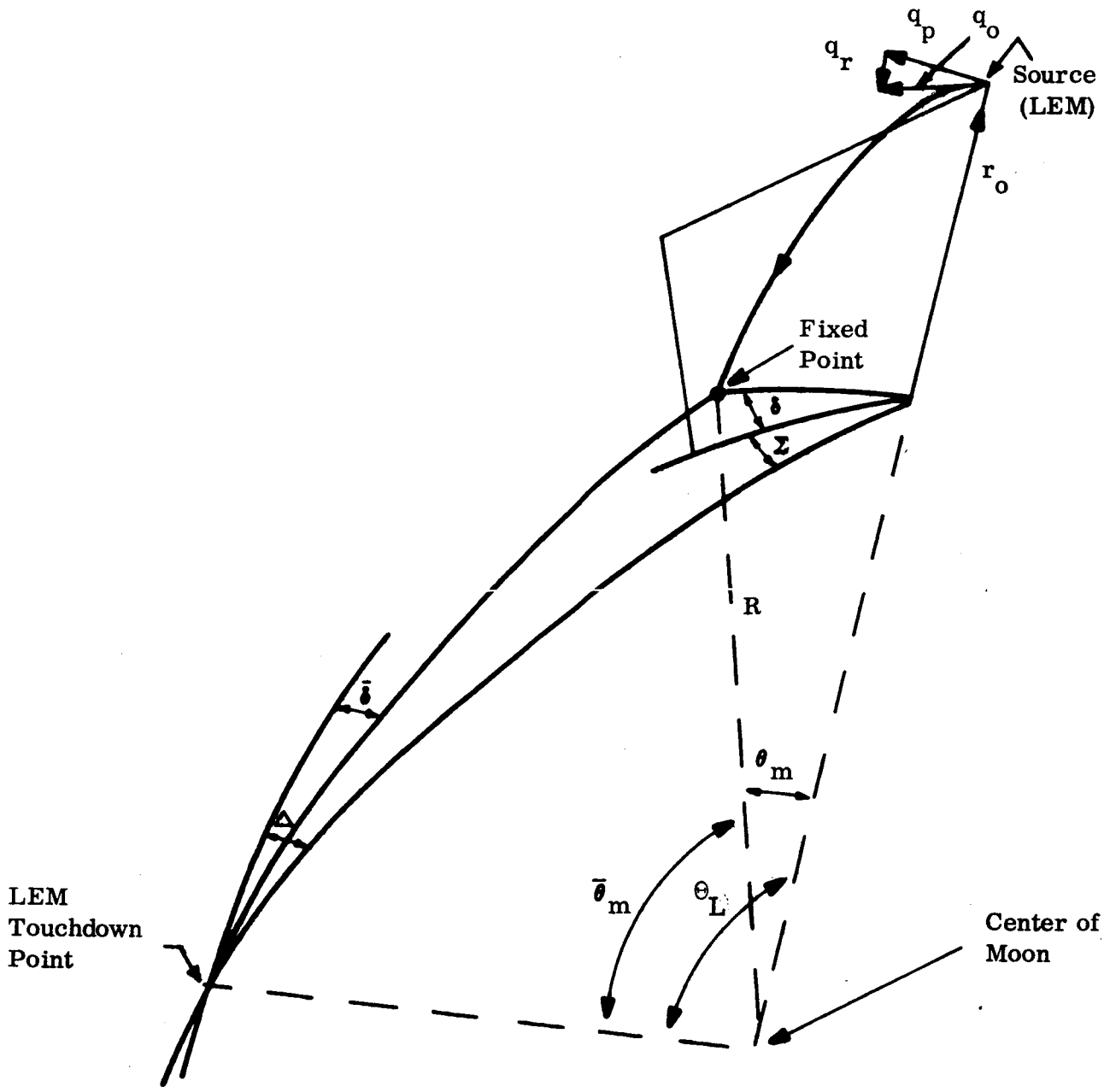

Fig. 4 Coordinate Systems

Having determined the initial velocity components by numerical solution of Eqs. (18) and (19), the angle between the local source velocity and the nozzle centerline, φ, is calculated by the following equation:

$$\cos\varphi = \Big[q_r \cos\beta \cos(\Theta - \alpha) + q_p [\cos\beta \cos\delta \sin(\Theta - \alpha) - \sin\beta \sin\alpha] - q_{LEM} \cos\beta \cos\alpha \Big] \Big/ q_J \ ,$$

where α is the angle between the nozzle centerline and the LEM velocity vector in the local LEM trajectory plane, and β is the angle the centerline makes with this plane (see Fig. 5). The angle φ is needed to find the value of the density factor distribution, $D(\varphi)$, of the point source that corresponds to the particle trajectory where

$$D(\varphi) \equiv \rho(\varphi, r_J) r_J^2 \ .$$

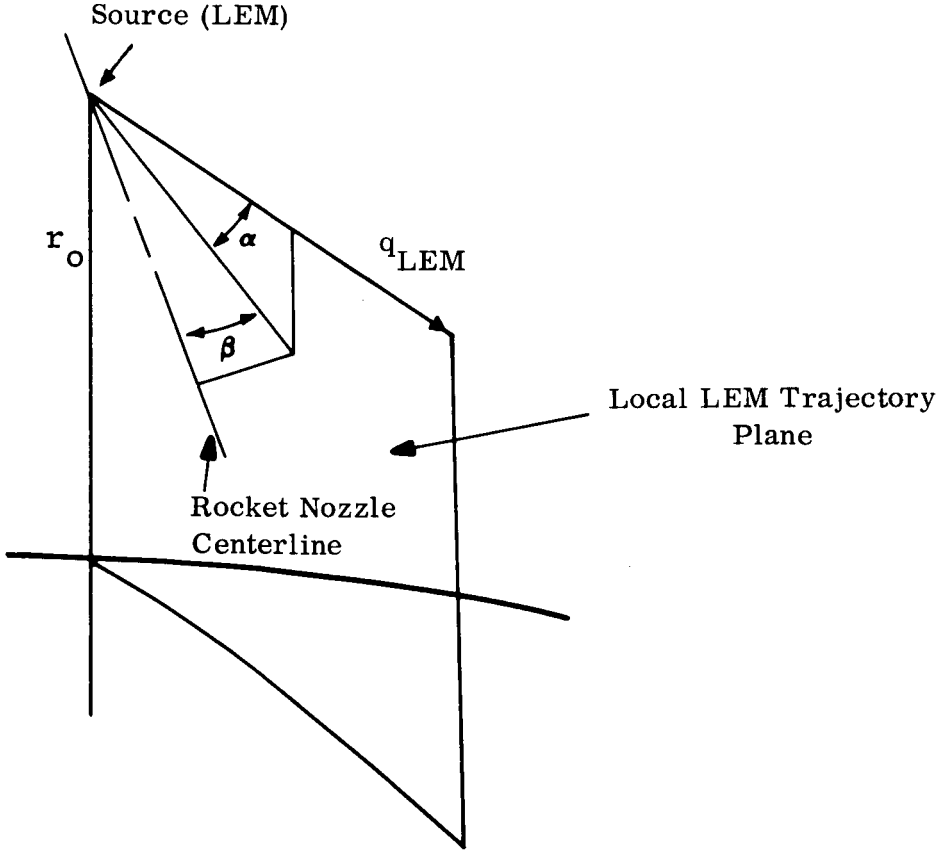

Fig. 5 Nozzle Centerline Orientation

Now that the particle trajectory that intersects the fixed point has been determined, the contamination flux transported along this trajectory must be calculated. This is done by equating the flow rate at the source to that impacting the lunar surface along a differential "streamtube" of the trajectory:

$$\rho_m q_m dA_m dt_m = \rho_J q_J dA_J dt_J \ .$$

In this equation, subscripts m and J refer to conditions at the moon's surface and at the source, respectively. It is necessary to include both time differentials to account for variable particle transport times between the source and the lunar surface. The preceding equation is rearranged to define the contamination flux, I, as

$$I(t_J) = \rho_m q_m \left(\frac{dt_m}{dt_J}\right) = \frac{dA_J}{dA_m} \rho_J q_J \ ,$$

to facilitate the anticipated integration by using the t_J time scale. It should be noted that $I(t_J)$ is not the true build-up rate at the fixed point. However, the integrated result is independent of the time scale. The differential area ratio is derived from the trajectory equation by assuming a differential area at the source and computing the resultant differential area at the moon's surface. This area ratio is incorporated in a flow expansion factor, F, defined as

$$F \equiv \frac{1}{q_J}\left(\frac{dA_m}{dA_J}\right)\left(\frac{r_J}{R}\right)^2$$

$$= \frac{\left[Q^2(1 - \cos\theta_m)\left(\frac{q_r - q_{LEM}\cos\theta}{q_p}\right) + \left(\frac{q_o^2 + q_J^2 - q_{LEM}^2}{2}\right)\sin\theta_m\right]\sin\theta_m}{q_p^2\sqrt{q_r^2 + Q^2(\bar{r} - 1) - q_p^2(\bar{r}^2 - 1)}}$$

The contamination flux then becomes

$$I(t_J) = \frac{\left[\rho_J r_J^2\right]}{\left[\frac{1}{q_J}\left(\frac{dA_m}{dA_J}\right)\left(\frac{r_J}{R}\right)^2\right]R^2} = \frac{D(\varphi)}{FR^2} \quad .$$

The total contamination at the fixed point, $C(\bar{\theta}_m, \bar{\delta})$, is then calculated by integrating the flux from the time the descent rocket engine is ignited, t_i, until the time, t_f, that it is turned off or that the assumptions of the mathematical model described herein are no longer valid

$$C(\bar{\theta}_m, \bar{\delta}) = \int_{t_i}^{t_f} I(t_J)\, dt_J \quad .$$

Because the contamination flux is not given as an analytical function of time, but can only be calculated at discrete instants of time over the course of the LEM descent, this integration must be done numerically.

This entire procedure is repeated at as many fixed points as desired or needed. It might be mentioned here that the selection of the fixed points is completely arbitrary. However, one convenient set of points are those located on concentric rings around the LEM touchdown point. The over-all calculation procedure is summarized in Table 9.

c. Subsidiary Analysis for Point Source Characteristics: The point source characteristics (velocity and density factor distributions at the source center) are input data for the far field contamination calculation described above. These characteristics are chosen so that the source flow field approximates the flow in the far field of the rocket plume and thus depend on the rocket engine throttle setting. The plume flow field for each throttle setting is calculated by the method of characteristics and even though this method assumes continuum flow, the properties needed for this calculation (velocity, flow direction and density) are fairly accurate when the flow becomes

Table 9

OUTLINE OF FAR FIELD CONTAMINATION CALCULATION

A. Select a Fixed Point on Lunar Surface Relative to LEM Touchdown Point $(\bar{\theta}_m, \bar{\delta})$

B. Determine the Time History of Contamination Flux at the Point $[I = I(t_J)]$

1. Transform Point to Local LEM Coordinates (θ_m, δ)
2. Compute Initial Velocity Components of the Trajectory that Intersects the Point
3. Calculate Flow Expansion Factor Between Source and the Point (F)
4. Find Angle Between Local Source Velocity and Nozzle Centerline (φ) to Evaluate $D(\varphi)$
5. Solve for Resultant Parameters at the Fixed Point
   a. Contamination Flux (I)
   b. Impact Angle* (φ_m)
   c. Impact Velocity* (q_m)

C. Integrate Contamination Flux to Get Total Contamination at the Fixed Point $[C(\bar{\theta}_m, \bar{\delta})]$

*These parameters are important in determining accommodation coefficients.

very rarefied. For practical purposes, the boundary between the two flow regions of the plume is assumed to be where the velocity obtains a value within 1 or 2 percent of the limiting velocity of the gas.

For a true source flow, the density, $\rho(\varphi, r_J)$, varies inversely with the square of the radial distance, r_J, from the source center so that a density factor distribution, $D(\varphi)$, at the source center is:

$$D(\varphi) = \rho(\varphi, r_J) r_J^2 .$$

In our approximate case, the above expression is calculated at several axial stations in the rocket plume. The definition of radial distance used for these calculations is the length of the extension of the local velocity vector to its intersection with the nozzle centerline. Because the far field is not truly a point source flow, the radial distances do not intersect the centerline at a common point and the calculated distributions are not exactly alike. The differences between these distributions decrease for the downstream stations so that an approximate limit distribution can be determined and assumed to be the density factor distribution of the point source. Based on this result, the constant magnitude of the source velocity is determined by equating the mass flow rate of the source with that of the rocket. Its value is generally just under the limiting velocity of the gas.

3. Results and Conclusions

The calculations are carried out using an IBM 7094-II digital computer. The time dependent input data for this calculation are given in Table 10. The data shown in this table are required for each instantaneous position of LEM considered over the entire time span of the far field calculation. In addition to these data, a number of constants are required (e.g., Q_m, R, t_f, and the locations of the fixed points).

Table 10

TIME DEPENDENT INPUT DATA FOR IBM CALCULATION

A. LEM Landing Trajectory
   1. LEM Trajectory Coordinates (h, θ_L, Δ)
      h is LEM Altitude ($r_o \equiv h + R$)
   2. Orientation of Local LEM Trajectory Plane (Σ)
   3. LEM Velocity in Trajectory Plane
      [Magnitude (q_{LEM}), Direction (Θ)]

B. Source Characteristics of Descent Engine
   1. Exhaust Speed (q_J)
   2. Nozzle Centerline Orientation Relative to LEM Velocity Vector (α, β)
   3. Density Factor Distribution [$D(\varphi)$]
      (φ - Conical Angle Between Local Source Velocity and Nozzle Centerline)

Results for a simplified LEM trajectory based on Ref. 2 ($\beta = \Sigma = \Delta = 0$, constant throttle setting) are listed in Table 11. The arrangement of the data in this table is such that the columns indicate the contamination variation along great circle arcs emanating from the touchdown point; and that the rows indicate the variation on circles concentric with the touchdown point. Contamination concentration is given in units of slugs/ft^2. From this table, it can be seen that the most rapid fall-off in contamination occurs at $\bar{\delta} = 90°$ and thus may be a preferred direction of travel from LEM. It should be noted that for any value of $\bar{\delta}$, the contamination falls off very rapidly from the indicated maximum value at the touchdown point. Notice should also be given to the fact that 1° in θ_m corresponds to 18.85 miles along the lunar surface.

A more detailed presentation of the contaminant concentration in the vicinity of the touchdown point is shown in Fig. 6 in which contamination in units of kg/m^2 is plotted as a function of distance from the touchdown point in meters. As a final point, the total mass deposited on the area covered by Table 11 (as determined by a surface integration) is only about 10 percent of the total mass emitted by the source. Results for an actual LEM trajectory are presented elsewhere (Ref. 3).

B. Near Field Distribution (T. Luzzi)

1. Saltation

a. General: Considered here is the so-called near field erosion problem. We define this problem as the study of lunar contamination by the LEM rocket exhaust gases when the vehicle is close enough to the moon such that a region of continuum fluid mechanics exists from the exhaust nozzle down to the lunar surface.

The nature of the interaction of exhaust gases with the lunar surface depends strongly on the nature of the lunar surface. As the nature of the lunar surface is largely unknown, the best one can do in analyzing the contamination problem is to pick various surface models, analyze the contamination produced in each, and thus establish certain broad limits on the near field contamination.

Herein, we will consider an erosive model for the lunar surface. It can be seen that the lunar surface material directly under the LEM will be the most seriously contaminated. It is quite possible that eroded material could be picked up and blown into an area where the astronaut will be taking samples of lunar soil. These particular samples then could be highly contaminated. One can see then that a dust model in a sense represents a maximum amount of contamination in that the most seriously contaminated particles are deposited in an area where lunar soil samples could be taken.

Table 11

TOTAL FAR FIELD CONTAMINATION VARIATION ABOUT THE LEM TOUCHDOWN POINT

$C(\bar{\theta}_m, \bar{\delta}) \times 10^6 \frac{\text{slugs}}{\text{ft}^2}$ $\quad t_f = 500$ sec $\quad \Delta t_J = 5$ sec

$\bar{\theta}_m$ \ $\bar{\delta}$	0°	15°	30°	45°	60°	75°	90°	105°	120°	135°	150°	165°	180°
0°	.517637	.517637	.517637	.517637	.517637	.517637	.517637	.517637	.517637	.517637	.517637	.517637	.517637
.1°	.0668305	.0344611	.0154097	.0086938	.0059712	.0047924	.0043730	.0044529	.0049679	.0059191	.0072383	.0084399	.0088219
.2°	.0186321	.0087009	.0036105	.0020224	.0014118	.0011681	.0011126	.0011956	.0014294	.0018542	.0024496	.0029961	.0031635
.3°	.0073469	.0036973	.0015656	.0008736	.0006061	.0004983	.0004733	.0005161	.0006394	.0008708	.0012142	.0015416	.0016450
.4°	.0044776	.0021553	.0008813	.0004856	.0003339	.0002718	.0002569	.0002804	.0003527	.0004950	.0007163	.0009340	.0010045
.5°	.0032103	.0014367	.0005689	.0003023	.0002087	.0001682	.0001583	.0001727	.0002194	.0003149	.0004682	.0006227	.0006729
.6°	.0024559	.0010341	.0003973	.0002112	.0001406	.0001121	.0001050	.0001148	.0001471	.0002151	.0003220	.0004419	.0004792
.7°	.0019543	.0007866	.0002937	.0001519	.0000991	.0000781	.0000730	.0000802	.0001038	.0001544	.0002393	.0003283	.0003566
.8°	.0016246	.0006235	.0002243	.0001124	.0000719	.0000561	.0000523	.0000579	.0000758	.0001148	.0001813	.0002518	.0002741
.9°	.0013906	.0005101	.0001755	.0000851	.0000534	.0000412	.0000384	.0000428	.0000569	.0000877	.0001409	.0001981	.0002158
1.0°	.0012253	.0004251	.0001389	.0000654	.0000402	.0000308	.0000287	.0000322	.0000435	.0000684	.0001117	.0001589	.0001733
1.5°	.0007471	.0001848	.0000493	.0000205	.0000115	.0000083	.0000078	.0000092	.0000136	.0000237	.0000423	.0000634	.0000691
2.0°	.0004725	.0000940	.0000217	.0000079	.0000039	.0000026	.0000024	.0000030	.0000049	.0000096	.0000187	.0000295	.0000320
2.5°	.0003443	.0000547	.0000110	.0000034	.0000015	.0000009	.0000008	.0000010	.0000019	.0000041	.0000087	.0000143	.0000155
3.0°	.0002702	.0000356	.0000060	.0000015	.0000006	.0000003	.0000002	.0000003	.0000007	.0000018	.0000040	.0000067	.0000072
3.5°	.0002357	.0000243	.0000033	.0000007	.0000002	.0000001	.0000001	.0000001	.0000003	.0000007	.0000017	.0000028	.0000029
4.0°	.0002127	.0000169	.0000018	.0000003	.0000001	.0000000	.0000000	.0000000	.0000001	.0000002	.0000005	.0000007	.0000006
4.5°	.0001983	.0000116	.0000009	.0000001	.0000000	.0000000	.0000000	.0000000	.0000000	.0000000	.0000000	0	0
5.0°	.0001842	.0000080	.0000005	.0000000	.0000000	.0000000	.0000000	.0000000	.0000000	0	0		
5.5°	.0001710	.0000055	.0000003	.0000000	.0000000	.0000000	.0000000	.0000000	0				
6.0°	.0001568	.0000039	.0000001	.0000000	.0000000	.0000000	0	0					
6.5°	.0001428	.0000027	.0000001	.0000000	.0000000	0							
7.0°	.0001324	.0000019	.0000000	.0000000	0								
7.5°	.0001234	.0000013	.0000000	.0000000									
8.0°	.0001148	.0000008	.0000000	0									
8.5°	.0001068	.0000005	.0000000										
9.0°	.0001015	.0000002	.0000000										
9.5°	.0000993	.0000001	.0000000										
10.0°	.0000967	.0000000	0										

Note: 1° of $\bar{\theta}_m$ equals 18.85 miles on the lunar surface

1 slug/ft^2 = 157 kg/m^2

Mass = 63.5 slugs

As will be discussed, the rigorous analysis of the problem of rocket plume interaction with an erosive surface in a vacuum environment is very difficult. Roberts (Refs. 14, 15, and 16) has studied this problem analytically. His erosion model assumes that the particles, once picked off the surface, are suspended in the continuum fluid flow beneath the rocket.

However, our contract studies indicate that another erosion process may occur. Particles can be picked up by the fluid and fall back to the surface many times before moving out of the influence of the continuum flow. This process, called saltation, is very common in desert dust storms and is discussed thoroughly in Ref. 17.

An analytical model of the saltation process is developed. This model, together with the plume-surface interaction gas dynamics developed in Refs. 14, 15, and 16 are applied to the study of lunar erosion by the LEM upon landing. Contamination of the region in the neighborhood of the LEM landing site is determined to within an order of magnitude accuracy.

b. Flow Field Model: A rigorous analysis of a rocket exhausting into a vacuum onto a dusty surface is a very complicated one. To make progress, one must devise a simple analytical model of the flow field for use in an erosion analysis. The model that we have chosen (Fig. 7) was proposed by Roberts (Refs. 14, 15, and 16) and is discussed briefly in Ref. 1. The flow field model will enable us to determine the aerodynamic shear stress on the surface. It will also enable us to establish a criterion for determining approximately the extent of the influence of the continuum flow on the eroded particles. With such a model we describe the eroded particle contamination of the lunar surface in the near neighborhood of the LEM to within an order of magnitude. Roberts' model has also been used in calculating the thermal histories of the eroded material (Sec. IV.C).

The aerodynamic shear stress on a hemispherical protuberance on the surface beneath the LEM, τ (see Refs. 14, 15, and 16), can be expressed in terms of the rocket thrust, T_{hr}, coefficient of friction, C_F, height off the surface, h, and radial distance from the axis of LEM descent, r_i, as

$$\tau = \frac{T_{hr}\, C_F}{\pi} \left(\frac{k+4}{2h}\right)^2 \left(\frac{r_i}{h}\right)^2 e^{-\left[\frac{k+4}{2}\left(\frac{r_i}{h}\right)^2\right]} \tag{20}$$

$$k = \gamma(\gamma - 1)M_n^2 \tag{21}$$

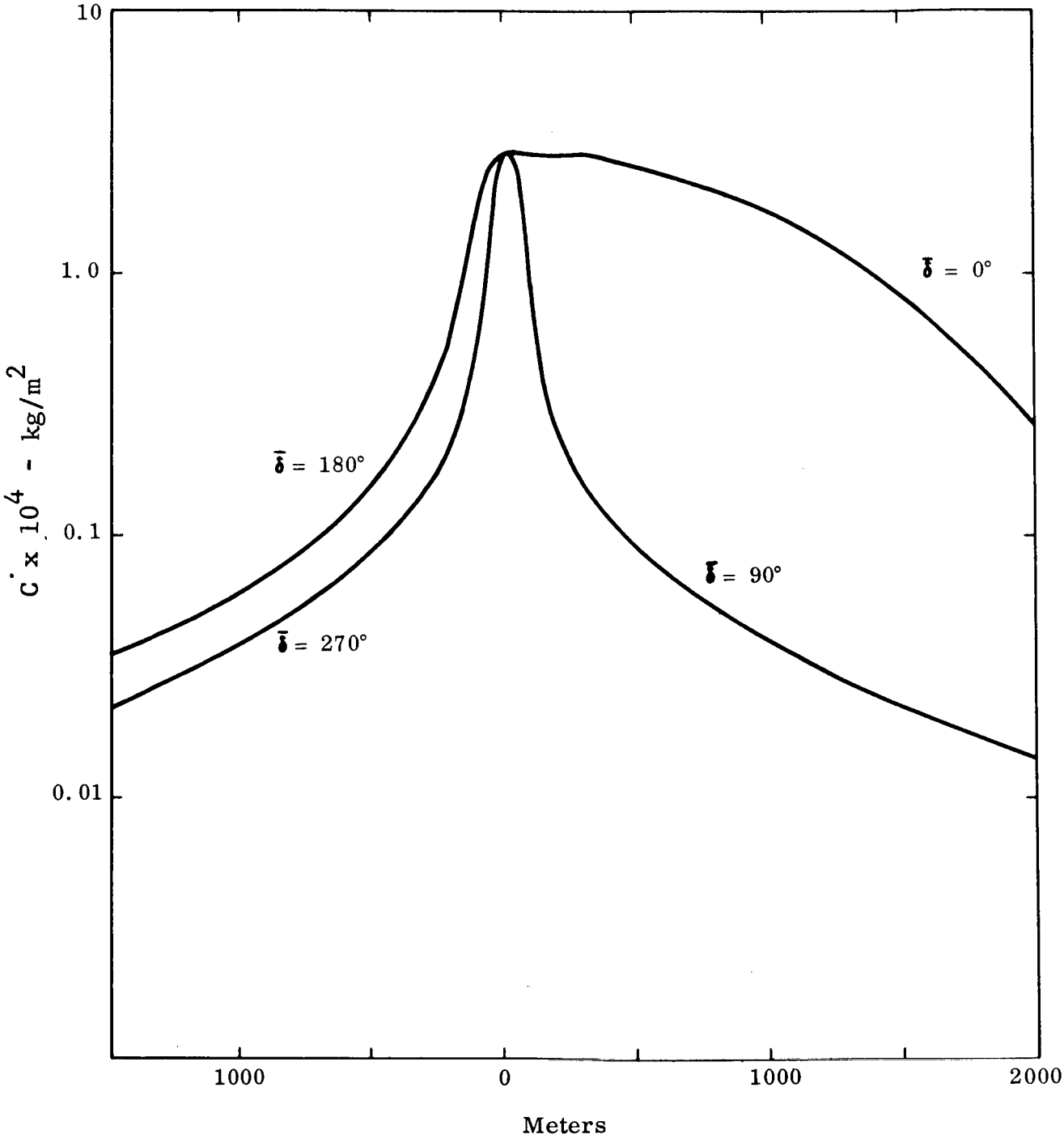

Fig. 6 Contaminant Density Versus Distance from Touchdown Point

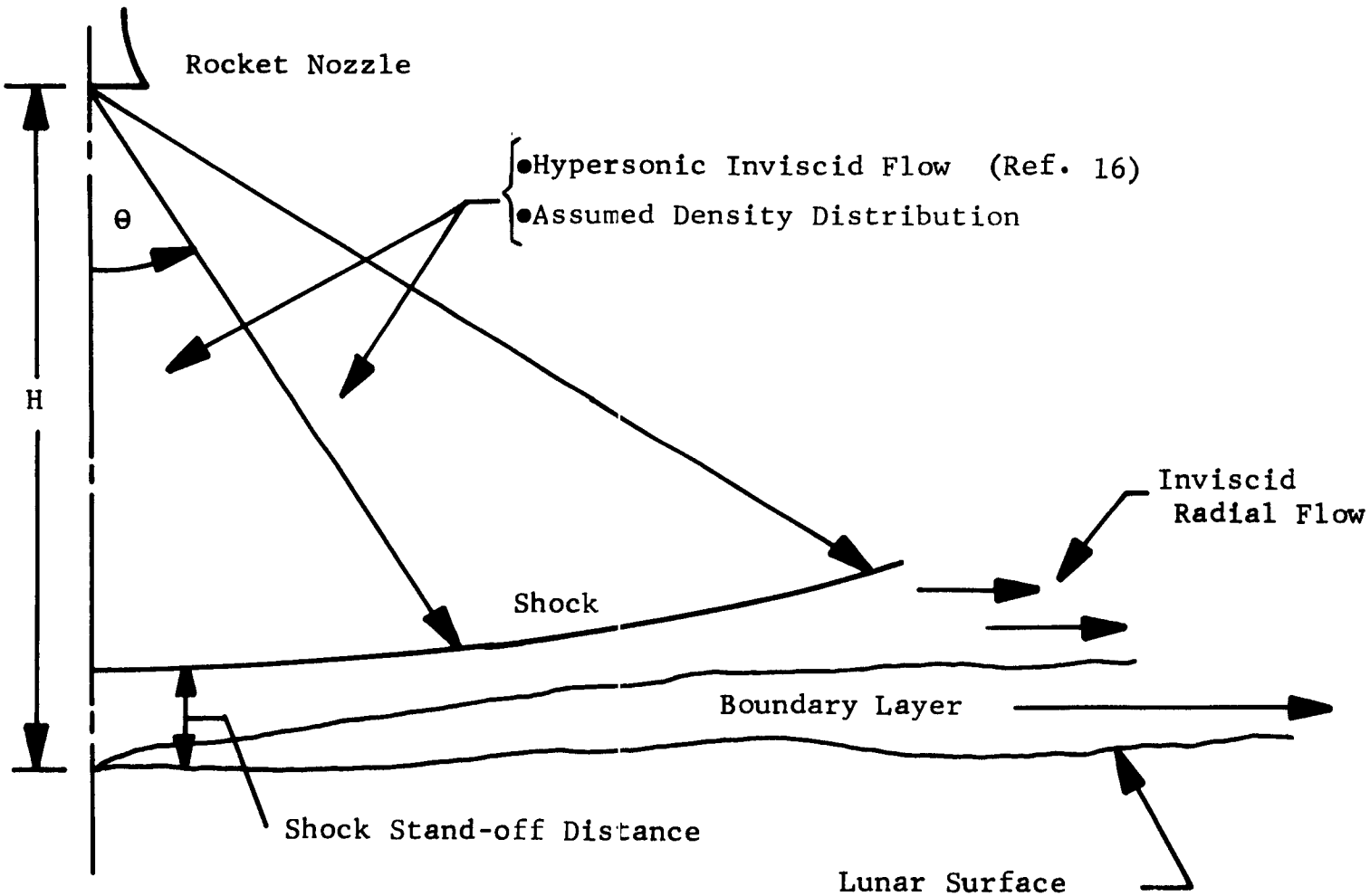

Fig. 7 Near-Field Flow Analytical Model

where γ is the ratio of specific heat and M_n is the Mach number of the flow at the exit plane of the rocket nozzle.

Investigation of Eq. (20) show that the shear stress is a maximum when the exponent

$$\frac{k+4}{2}\left(\frac{r_i}{h}\right)^2 = 1 ,$$

and decreases to zero as the exponent approaches infinity. We arbitrarily assume that the influence of the continuum flow under the shock wave ceases when the aerodynamic shear stress is 1 percent of the maximum value. We call this position the "edge of the plume", R. The expression for R obtained from Eq. (20) is

$$R = \frac{4}{(k+4)^{\frac{1}{2}}} h . \qquad (22)$$

It is expected that this approximate representation of the flow field will give realistic values of the effect of the flow on the eroded particles above heights of about 3 meters.

c. Model of Motion of Eroded Particles: A qualitative description of possible erosion processes is given in Refs. 1 and 17. The nature of the erosion process and, hence, the erosion model that is chosen depends on the grain size and the characteristics of the fluid flow field. Bagnold (Ref. 17) found that desert sand of .025 cm mean diameter was moved by two processes, saltation and surface creep. He found that 3/4 of the sand was moved by saltation and 1/4 by surface creep. Roberts' analysis (Ref. 16) indicates that for particle sizes between roughly 10 and 1000 microns, the erosion process "cuts-off" or ceases above a certain altitude and that altitude is a function of the particle size. The smaller the particle, the higher is the altitude of erosion cut-off. Finally, discussions with many people indicate that a reasonable dust particle size could vary between 10 and 1000 microns. From the above, it appears that the saltation process is the most probable erosion process and, hence, it will be the basis for the erosion model used in establishing the eroded particle distribution. Thermal transfer equations that are used in establishing the temperature history of eroded particles (Sec. IV.C) are decoupled from the trajectory equations. In establishing the temperature, the less complicated suspension erosion process is used to avoid unnecessary expenditure of computer time.

In the saltation process, a particle is moved along the surface under the action of the fluid shear forces, bounded up into the fluid flow by an elastic collision with a stationary particle, and accelerated in the streamwise direction by the fluid drag forces. The particle then falls to the surface and is bounced up into the fluid again. An exact description of the process would be very complex. We have constructed an analytical model of this saltation process which is shown in Fig. 8. The particle receives its initial impulse normal to the fluid flow direction from an elastic collision process as shown in Fig. 8. The expected acceleration from the first hop is determined and lumped into a velocity increment. This increment is added to the streamwise velocity at the apex of the first trajectory. The particle then falls on a new trajectory toward the surface where it again hops up into the gaseous stream. This process is continued until the particle reaches the edge of the plume at which point the angle of inclination and velocity are recorded, to be used as initial conditions for the ballistic trajectory out into the far region.

The continuum region will be divided into a number of positions, i, from which particles are eroded. A particle "picked up" from a position, i, can experience one or more hops before leaving the continuum flow region. For example, V_{ij}, refers to the initial velocity magnitude of a particle picked up initially at position i that has experienced its j^{th} hop. The positions i correspond to an area i in the continuum region. Thus, the erosion rate from area i is the erosion rate per unit area at position i multiplied by the area, i.

Consider a row of particles on the surface, and sitting on this row is a particle that juts or sticks out into the flow stream. Further downstream, say some 5 or 6 particle diameters away, consider a particle slightly embedded in this row of particles. This surface is under the influence of the fluid shear stresses, hence, the first particle could move along the surface and bounce off the embedded particle up into the gas stream. One could simplify the model even further by replacing the embedded particle by a plane at some angle with respect to the surface. Our collision model could then be characterized by two parameters, the distance between the plane and the particle and, secondly, the angle of the plane. The above model leads to an initial trajectory angle and velocity for the ballistic trajectory of the particle while under the influence of the continuum flow. The two parameters could be adjusted as a result of some experiment. The two parameters used in this analysis are the number of particle diameters between the plane and the accelerating particle, α, and the initial trajectory angle, taken as 45° in this analysis. Thus, the initial velocity of a particle at position i is

$$V_{ij} = \left(\frac{2\pi D\alpha}{m}\right)^{\frac{1}{2}}$$

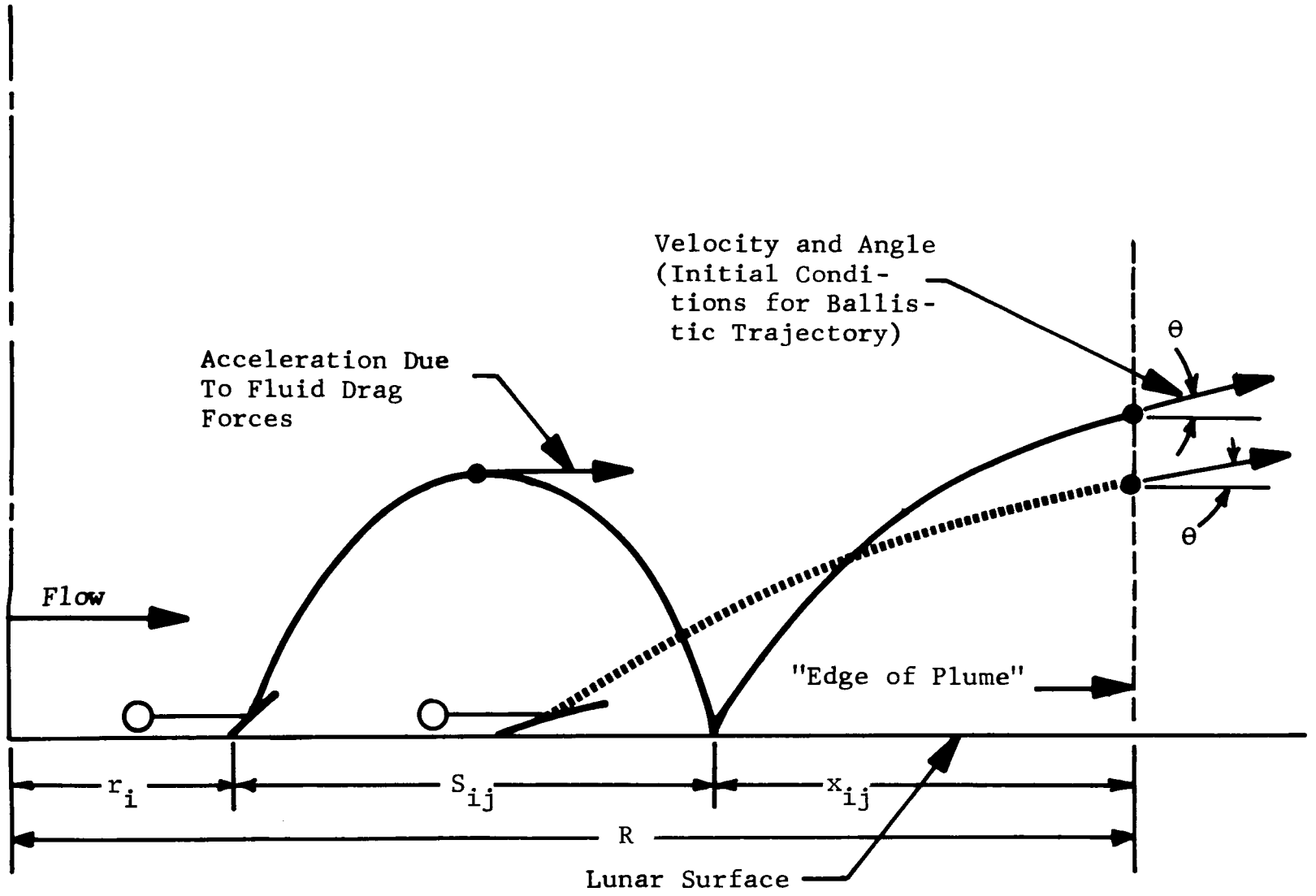

Fig. 8 Saltation Model: Near-Field Trajectories

The initial horizontal (V_{Hij}) and vertical (V_{Vij}) velocity of the particle will be

$$V_{Hij} = V_{Vij} = \frac{\sqrt{2}}{2} V_{ij} \quad . \tag{24}$$

The initial trajectory angle, θ_{ij}, is

$$\theta_{ij} = \arctan \frac{V_{Vij}}{V_{Hij}} = \frac{\pi}{4} \quad . \tag{25}$$

In Eqs. (23), (24), and (25), $j = 1$ because they refer to the initial hop of a particle. The horizontal distance moved by a particle in ballistic flight with no external forces in the horizontal direction is given by the following expression

$$S_{Pij} = \frac{V_{ij}^2 \sin 2\theta_{ij}}{g} \quad , \tag{26}$$

where g is the acceleration due to gravity. If an increment in velocity is imparted to the particle at the apex of the trajectory ΔV_{ij}, the horizontal distance covered is given by the following expressions:

$$S_{ij} = \frac{V_{ij}^2 \sin 2\theta_{ij}}{g} + \frac{V_{ij}^2 \sin \theta_{ij}}{g} \frac{\Delta V_{ij}}{V_{ij}} \quad . \tag{27}$$

The horizontal V_{HFij} and vertical V_{VFij} velocities at the end of a trajectory for a particle experiencing a velocity increment at the apex are

$$V_{HFij} = V_{ij} \left(\cos \theta_{ij} + \frac{\Delta V_{ij}}{V_{ij}} \right) \tag{28}$$

$$V_{VFij} = V_{ij} \sin \theta_{ij} - \left[\frac{gS_{ij}}{V_{ij}\left(\cos \theta_{ij} + \frac{\Delta V_{ij}}{V_{ij}}\right)} + \frac{\frac{\Delta V_{ij}}{V_{ij}} \frac{S_{Pij}}{2}}{V_{ij} \cos \theta_{ij}\left(\cos \theta_{ij} + \frac{\Delta V_{ij}}{V_{ij}}\right)} \right] . (2$$

The initial velocity magnitude of the $j + 1$ trajectory can be obtained from the final velocity of the j trajectory, thus,

$$V_{i(j+1)} = \sqrt{V_{HFij}^2 + V_{VFij}^2} \quad . \tag{30}$$

The initial trajectory angle used for all trajectories in this analysis will be $45°$. Therefore, the initial horizontal and vertical velocities for all trajectories can be obtained from Eq. (25).

Roberts (Ref. 16) gives an approximate expression for the gas velocity beneath the shock wave as a function of the radial distance from the center of the plume. Grossman (Ref. 18) has calculated the velocity of dust particles suspended in a gas stream. The characteristics of the gas stream are those of Roberts' (Ref. 16), namely, the flow beneath the shock wave of a plume impinging on a solid surface. Grossman showed, to a good approximation, that the particles increase their velocity almost linearly with distance from the axis from zero to some maximum value, a fraction of the maximum gas velocity beneath the shock wave. The maximum particle velocity is a function of the particle size and occurs approximately at the "edge of the plume" as defined in this report. Values of the ratio of the maximum particle velocity to gas velocity at the edge of the plume, Ω, for different particle sizes are given in Table 12.

Using Roberts' approximate expression for the gas velocity and solving for the velocity at the edge of the plume, we have

$$u_{gas} = \sqrt{(R_{gas}\ T_c)(k + 4)}\ \frac{R}{h} \quad , \tag{31}$$

Table 12

PARTICLE-GAS VELOCITY RATIO, Ω, VERSUS PARTICLE DIAMETER, D(cm)

Ω	D
.01	2.5
.02	0.25
.06	.025
.14	2.5×10^{-3}
.32	2.5×10^{-4}
.55	2.5×10^{-5}
.72	2.5×10^{-6}
.78	1.3×10^{-6}

where R_{gas} is the gas constant and T_c is the combustion chamber temperature. Assuming that the velocity increment per trajectory is proportional to the length of the ballistic trajectory and the particle size, through Ω, we have

$$\Delta V_{ij} = \Omega \, u_{gas} \frac{S_{Pij}}{R} \, . \tag{32}$$

From Eqs. (31) and (32) we have an approximate expression for the velocity increment per trajectory in terms of the trajectory length:

$$\Delta V_{ij} = \Omega \sqrt{RT_c(k+4)} \frac{S_{Pij}}{h} \, . \tag{33}$$

The objective of the velocity analysis is to determine the horizontal and vertical velocities at the edge of the plume, R, as a function of the radial position, r_i. Thus, we must determine these velocities at the position x_{ij} for the last trajectory in

the continuum region (see Fig. 8). If the length x_{ij} is less than half the total trajectory length of the final hop, the velocity increment, ΔV_{ij}, is not considered when calculating the edge of the plume horizontal, $V_{\alpha i}$, and vertical, $V_{\beta i}$, velocities. Thus,

$$V_{\alpha i} = V_{ij} \cos \theta_{ij} , \tag{34}$$

$$V_{\beta i} = V_{ij} \sin \theta_{ij} - \frac{g x_{ij}}{V_{ij} \cos \theta_{ij}} . \tag{35}$$

If x_{ij} is greater than half the total trajectory length of the final hop, the velocity increment, ΔV_{ij}, must be considered when calculating $V_{\alpha i}$ and $V_{\beta i}$. Thus,

$$V_{\alpha i} = V_{ij} \left(\cos \theta_{ij} + \frac{\Delta V_{ij}}{V_{ij}} \right) \tag{36}$$

and

$$V_{\beta i} = V_{ij} \sin \theta_{ij} - \left[\frac{g x_{ij}}{V_{ij} \left(\cos \theta_{ij} + \frac{\Delta V_{ij}}{V_{ij}} \right)} + \frac{\frac{\Delta V_{ij}}{V_{ij}} \frac{S_{Pij}}{2}}{V_{ij} \cos \theta_{ij} \left(\cos \theta_{ij} + \frac{\Delta V_{ij}}{V_{ij}} \right)} \right] . \tag{37}$$

The value x_{ij} can be obtained from the following:

$$x_{i(j+1)} = R - \left(r_i + \sum_j S_{ij} \right) . \tag{38}$$

To determine the number of hops for each r_i, the expression

$$L_{ij} = r_i + \sum_j S_{ij} \tag{39}$$

is used in the computer program. The positions r_i are determined by dividing R into increments of equal length. For example, taking 10 increments,

$$\Delta r = \frac{R}{10} \tag{40}$$

$$r_1 = \Delta r \ , \qquad r_2 = 2\Delta r \text{ etc.} \tag{41}$$

d. Erosion Rate: Roberts (Ref. 16) gives approximate relations for the erosion rate of material in the continuum region. The expression for the erosion rate at r_i, $(dy/dt)_i$ in meters per second is

$$\left(\frac{dy}{dt}\right)_i = \frac{2\sqrt{2}\, C_F}{C_{PA}\, e} \frac{T_{hr}\left(\xi_i\, e^{(1-\xi_i^2)} - \frac{\Gamma_T}{\xi_i}\right)}{\pi \left(h\sqrt{\frac{2}{k+4}}\right)^2 \rho_T \sqrt{R_{gas}\, T_c}} \ , \tag{42}$$

where C_{PA} is the spherical particle packing coefficient and is approximately 0.5 and ρ_T is the dust particle density.

$$\xi_i = \sqrt{\frac{k+4}{2}}\, \frac{r_i}{h} \tag{43}$$

$$\Gamma_T = \Gamma_g + \Gamma_{coh} \tag{44}$$

$$\Gamma_g = \frac{\rho_T g D C_{PA} \tan \epsilon}{\frac{C_F}{e} \frac{T_{hr}}{\pi \left(h\sqrt{\frac{2}{k+4}}\right)^2}} \tag{45}$$

$$\Gamma_{coh} = \frac{A_{coh} D^{-3}}{\frac{C_F}{e} \frac{T_{hr}}{\left(h\sqrt{\frac{2}{k+4}}\right)^2}} \tag{46}$$

Γ_g is indicative of the adhesiveness of the particles. Roberts indicates that $C_{PA} \tan \epsilon$ is about 0.4. Γ_{coh} is indicative of the cohesiveness of the particles. From angle of repose measurements of small particle dust piles in a vacuum, the value of A is approximately 6.9×10^{-18} kilogram meters (Ref. 16).

The erosion area A_{ri} under the continuum regions is

$$\left.\begin{aligned} A_{ri} &= \pi r_i^2 && i = 1 \\ A_{ri} &= 2\pi(\Delta r)(r_i) && i = 2, \ldots \end{aligned}\right\}. \tag{47}$$

The erosion rate from these areas, E_{ri}, is

$$E_{ri} = \frac{A_{ri}}{D^3}\left(\frac{dy}{dt}\right)_i . \tag{48}$$

The ballistic trajectory length, S_{FRi}, for each r_i measured from the edge of the plume is

$$S_{FRi} = \frac{\left(V_{\alpha i}^2 + V_{\beta i}^2\right)\sin 2\theta_{FRi}}{2g} , \tag{49}$$

where

$$\theta_{FRi} = \arctan \frac{V_{\beta i}}{V_{\alpha i}} . \tag{50}$$

The particle build-up rate per unit area E_{rAi} at a distance $R + S_{FRi}$ from the LEM axis is

$$E_{rAi} = \frac{E_{ri}}{\pi\left[\left(R + S_{FRi}\right)^2 - \left(R + S_{FR(i+1)}\right)^2\right]} \qquad i = 1 \qquad (51)$$

$$E_{rAi} = \frac{E_{ri}}{\pi\left[\left(R + S_{FR(i-1)}\right)^2 - \left(R + S_{FRi}\right)^2\right]} \qquad i = 2, \ldots . \qquad (52)$$

A flow chart of the computer program is shown in Fig. 9.

e. Results and Conclusions: The analysis of the report has established a technique for studying the erosion of a solid surface by a rocket exhausting into a vacuum atmosphere. The analysis is a steady state analysis in that it assumes that the mass flow rate from the rocket and the height off the surface are constant in time. This will give the particle build-up per unit time in the neighborhood of the LEM landing site for each eroded particle size. Analysis of the erosion problem due to any LEM landing trajectory can be obtained by summing results of the appropriate steady state analyses. The following conclusions are obtained:

- Using the foregoing computer program, the erosive particle build-up has been calculated for three particle diameters (1, 0.1, 0.01 mm) and four altitudes (3, 6, 10, 25 meters), the results are reported elsewhere (Ref. 3).
- The above computation indicates that the saltation model is a good one in that most particles make many hops before leaving the continuum flow region.
- For particles between 100 and 1000 microns, most of the erosion falls within 100 meters of the LEM touchdown point. However, deposition beyond 100 meters is not negligible.
- Most of the erosion takes place when the vehicle is very close to the surface. In fact, for any LEM trajectory one can estimate the erosion contamination fairly accurately by considering the deposition that takes place during the last 3 meters of rocket altitude.
- Calculations indicate that there is practically no erosion for heights above 25 meters from the surface.

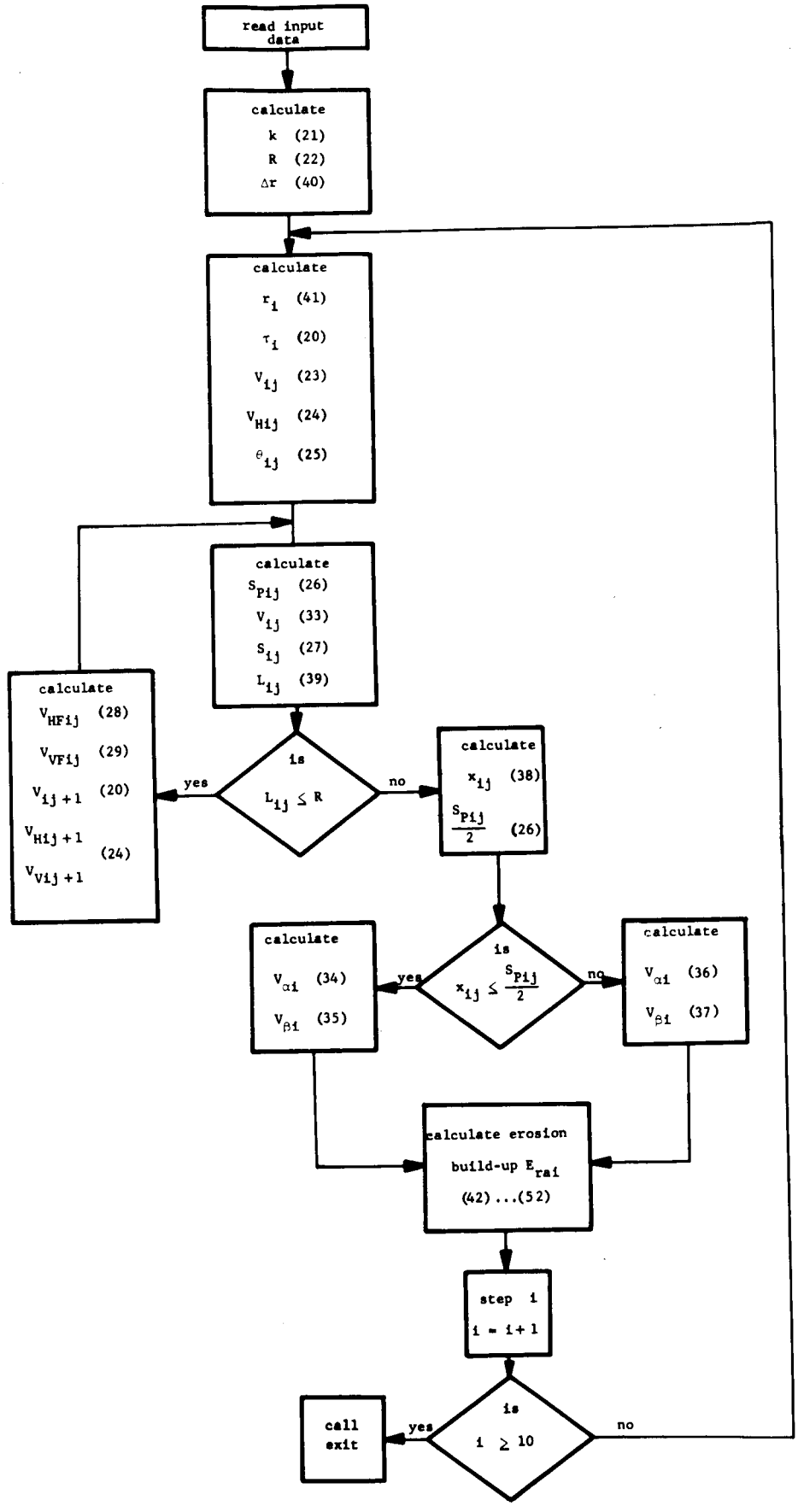

Fig. 9 Computer Program Flow Chart
( ) Refer to Equations

- Both adhesive and cohesive forces have been considered when calculating the erosion at any place in the flow. Cohesion and, hence, the erosion rate, has been expressed in terms of a parameter that can be easily changed for any computer run. For the computations above, the constant was obtained from the results of experimental data reported in Ref. 16.
- It has been assumed that a particle does not change its velocity magnitude on striking the surface. It is further assumed that after striking the surface, a particle leaves at a 45° angle. The computer program can be easily changed to consider inelastic effects and different leaving angles.

As indicated above, the preceding work analyzes the erosion build-up per unit time by a rocket exhausting into a vacuum. Adjustable parameters have been included in the program such that the assumptions of the analytical model may be checked. Use of the program with appropriate checking should enable one to calculate the contamination due to eroded material to within the required accuracy of an order of magnitude.

C. Heat Transfer to Particles (Suspension) [D. Weiss]

1. General

Rocket exhaust gases impinging on a bed of particles will impart both momentum and heat to the particles. Depending on size and density, the particles will be eroded, heated, and blown away, and will fall at some distance away from their points of erosion.

Presented herein are the results of a study of the motion and temperature history of spherical particles in a vacuum environment that are affected in this way. The study was motivated by the need to estimate chemical and thermal contamination of the lunar surface as a consequence of a manned lunar landing. A dust model (or particulate model) was assumed for the lunar surface.

The study relies quite heavily on the previous work of Roberts (cf. Sec. IV.B) providing a readily available model of the exhaust gas, and of the gas-surface interaction phenomena. Previous work performed at Grumman By Grossman (Ref. 18) set up the groundwork for the calculations of the motion of individual spherical particles blown away by the jet impingement.

The transient heat transfer to the particle as it is borne by the gas was assumed to take place by forced convection only. Gas radiation to the particle was taken to be insignificant in comparison. However, radiation cooling of the particle to zero-temperature space was included. Lunar particles were assumed to be somewhat similar in composition to silica rock and the thermal properties and density selected accordingly.

2. List of Symbols

A	Surface area of spherical particle
$\bar{a}$	Local speed of sound
C_D	Drag coefficient
C_{SP}	Specific heat of lunar material
C_p	Specific heat of gas at constant pressure
$\tilde{c}$	Particle packing coefficient

F_G Gas radiation flux

F_S Surface radiation flux

g_c Acceleration due to gravity at earth's surface

g_L Acceleration due to gravity at moon's surface

h_B Height of emergence

H_c Heat-convection surface coefficient

H_R Heat-radiation surface coefficient

h H_c/K

h_n Height of nozzle exit plane above lunar surface

K Thermal conductivity of lunar material

$\bar{K}$ $\gamma(\gamma - 1)\ M_n^2$

k Thermal conductivity of gas

k_n Roots of the characteristic equation

M_n Mach number at nozzle exit

m Mass of spherical particle

Nu Nusselt number

Pr Prandtl number

p Static pressure

p_c Chamber pressure

p_r Shock recovery pressure

p_s Stagnation pressure

R_e	Reynolds number
$\bar{R}$	Gas constant
R	Radius of spherical particle
r_n	Radius of nozzle exit (Ft.)
r_o	Initial location of particle
T_L	Temperature of spherical particle
$\bar{T}$	T_G-T
T_G	Recovery temperature of gas
T_1	Initial temperature of spherical particle
T_s	Stagnation temperature of gas
T_∞	Static temperature of gas
u	Velocity of spherical particle ralative to lunar surface and in a direction parallel to lunar surface
u_B	Velocity of particle as it exits from exhaust plume
u_o	Initial velocity of lunar particle
V	Velocity of gas parallel to lunar surface
γ	Ratio of specific heats
ϵ_G	Emissivity of gas
e_s	Emissivity of surface
θ	Angle measured from centerline of nozzle exit

κ diffusivity of lunar material

λ Mean free path for gas molecules

μ Absolute viscosity of gas

μ_c Absolute viscosity of gas at rocket chamber temperature

ρ Static density of gas

ρ_L Density of lunar material

ρ_s Stagnation density of gas

σ Stefan-Boltzmann constant

τ_m Maximum boundary layer shearing stress

ζ Temperature recovery factor

3. Exhaust Gas Model

An analysis of the momentum and energy interaction between the rocket exhaust gas and lunar particles requires a knowledge of the exhaust-gas, flow-field properties. A brief description of this flow field taken from the work of Roberts (Ref. 14) follows.

The rocket is assumed to be hovering in a vertical position close to the lunar surface. Its plume is divided into two portions, the inner high density region and the rarified outer region (see Fig. 10).

The gas is assumed to issue isentropically from the exhaust nozzle and to expand symmetrically outwards from the nozzle centerline extension. Expansion also takes place (but less rapidly) away from the nozzle exit plane along the centerline. As the gas approaches the surface, a standing shock wave is formed a short distance off the surface, and parallel to it. Below the shock wave the gas is assumed to turn away from the centerline and flow in a radial direction parallel to the surface, forming a laminar boundayy layer on the surface. It is the surface shearing stress set up by this boundary layer that is responsible for erosion of the surface (which is assumed to be particulate in this analysis).

All the interaction between the gas and the lunar particles will presumably take place in the inner region, which is governed by continuum flow theory. The rarified outer region is governed by free-molecular-flow equations. From some reasonably selected edge of the continuum flow, the particle is assumed to travel in a ballistic trajectory within the free-molecular-flow regime, until it lands.

The equations from Ref. 14 for evaluating the gas plume flow field are as follows: Surface pressure distribution is expressed as

$$\frac{p}{p_s} = (\cos\theta)^{\bar{K}+4} \tag{53}$$

$$\frac{p_s}{p_c} = \frac{\bar{K}+2}{2}\left(\frac{p_r}{p_c}\right)\left(\frac{h_n}{r_n}\right)^{-2} \tag{54}$$

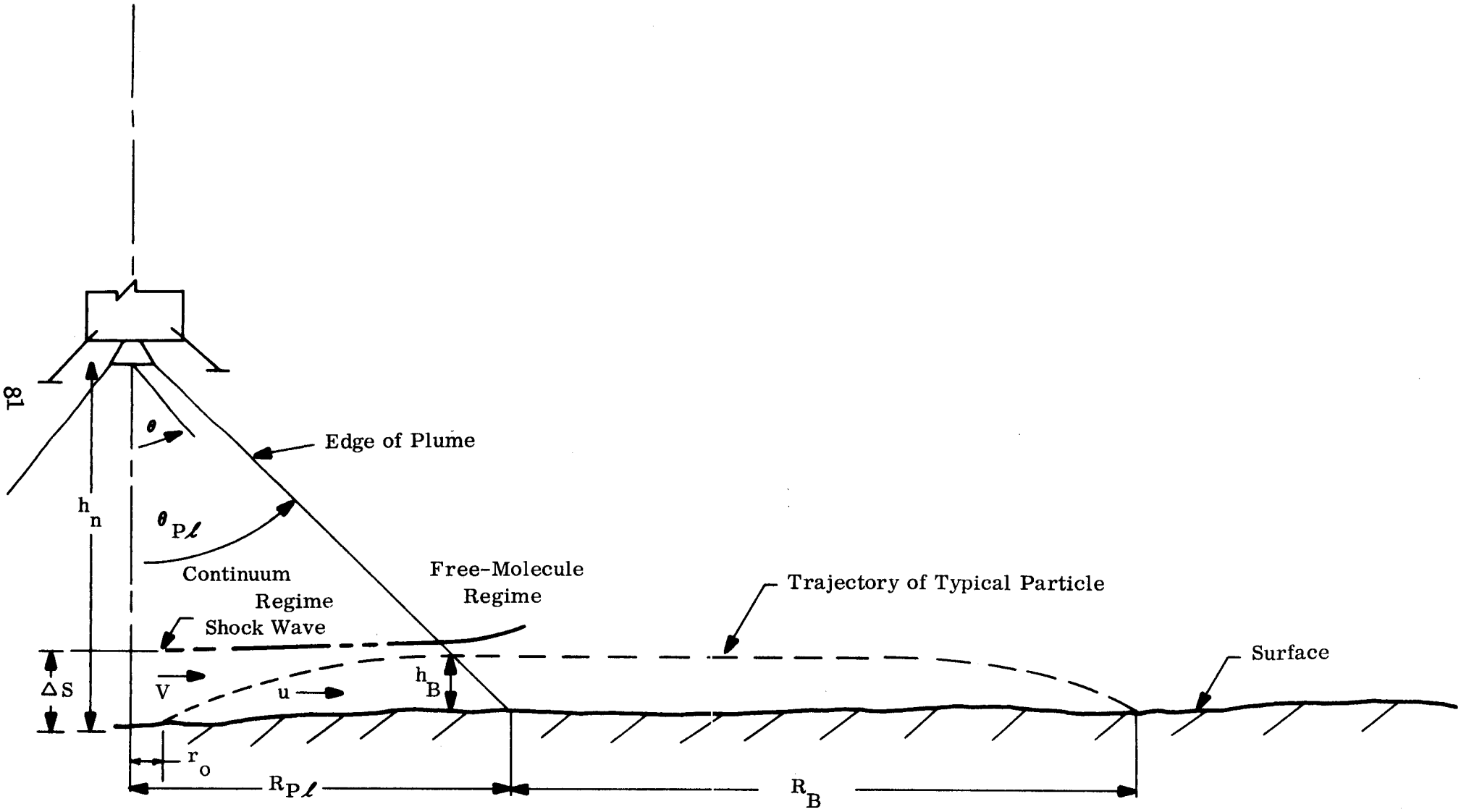

Fig. 10 Sketch of Gas Plume and Particle Trajectory

$$\bar{K} = \gamma(\gamma - 1)\, M_n^2 \tag{55}$$

$$\frac{p_r}{p_c} = (1+\gamma M_n^2)\ (1+\frac{\gamma - 1}{2}\, M_n^2)^{-\frac{\gamma}{\gamma-1}}\ , \tag{56}$$

where p_s is the stagnation pressure at the plume centerline on the lunar surface; θ is the azimuth angle measured from the plume centerline (see Fig. 10); p_r is the normal-shock recovery pressure; h_n is the height of the nozzle exit plane above the lunar surface; r_n is the radius of the exit plane of the nozzle; M_n is the exit Mach number; p_c is rocket chamber pressure; and γ is the ratio of specific heat.

Assuming that isentropic relations for a perfect gas apply, the gas temperature, T, and density, ρ, can be expressed as

$$T_\infty = T_s(\cos\theta)\ \frac{(\gamma - 1)\ (\bar{K}+4)}{\gamma} \tag{57}$$

$$\rho = \rho_s(\cos\theta)\ \frac{\bar{K} + 4}{\gamma}\ , \tag{58}$$

where T_s is the stagnation temperature that was set equal to the rocket chamber pressure T_c; and ρ_s is the stagnation density obtained from the equation of state for a perfect gas

$$\rho_s = \frac{p_s}{\bar{R}T_s} \tag{59}$$

$\bar{R}$ being the gas constant.

4. Motion of a Particle in the Gas

To calculate the convective heating rates from the gas to the particles, it is necessary to determine the relative velocities of the gas over the particles as the particles travel through the continuum portion of the gas plume. In addition, to determine the landing site of the particle, we must know its exiting velocity from the continuum portion of gas plume. To accomplish these, we refined somewhat an existing analysis made at Grumman in 1962 (Ref. 18), programmed at that time for the IBM 7090 computer.

In this analysis, the particle velocities were determined by a simple force balance between the drag forces and inertial forces on the particle, i.e.,

$$C_D A \frac{\rho}{2} (V - u)^2 = m \frac{du}{dt} \quad , \tag{60}$$

where V and u are the radial velocities of the gas and particle, respectively, in a direction parallel to the surface; ρ is the gas density; C_D, m, and A are the drag coefficient, the mass, and the surface area of the particle, and t is time.

The radial gas velocity, V, can be derived from the gas flow field equations, assuming isentropic flow, and can be expressed in the following form,

$$V = \left\{ \frac{2\gamma g_c \bar{R} T_s}{(\gamma - 1)} \left[1 - (\cos \theta)^{\frac{(\gamma-1)(\bar{K}+4)}{\gamma}} \right] \right\}^{\frac{1}{2}} \tag{61}$$

where g_c is the acceleration due to gravity.

No specific mechanism was assumed by which the particles would be lifted from the surface. The magnitude of the initial velocity of the particle was assumed. It turns out that the trajectories of the particles within the continuum regime of the gas plume and the ballistic trajectory of the particle are not very sensitive to the assumed value of the initial velocity.

Equation (60) was solved numerically (Ref. 18) using a Taylor expansion technique. The current refinement to Ref. 18 was for the purpose of evaluating the local drag coefficient as the particle's Reynolds number varied in the gas stream. In Ref. 18, C_D was assumed constant.

The drag coefficient was taken from an empirical equation presented in Hoerner (Ref. 19):

$$C_D = 0.95 + \frac{5}{\sqrt{R_e}} \quad . \tag{62}$$

Because C_D depends on R_e, and R_e cannot be calculated until the particle velocity is known, an iteration scheme was utilized as follows: An initial value of C_D was assumed, from which particle velocity and R_e were obtained. From this R_e, a new C_D was calculated and the iteration continued until no significant change in R_e was noticed.

In this manner, C_D, u, and R_e were calculated at various radii from the plume centerline.

5. Particle Heat Transfer

The heat balance on a particle as it is carried along by the hot gas can be represented as convected heat + gas radiation = radiation cooling + heat conducted and absorbed.

The following sections discuss each of these separately:

a. Heat Convection: The convective heat transfer coefficient was calculated from a Nusselt-type equation for average values around a sphere. Average values were considered more appropriate than local values because of the uniform surface heating resulting from the probable spinning of the particle. In addition, the assumption of a uniform heating rate around the sphere surface enables us to use a spherical conduction model in which the isotherms are concentric spheres, simplifying the mathematics of the transient internal heat conduction considerably.

The equation used is

$$Nu = .37\ Re^{.6}\ Pr^{.33} \quad , \tag{63}$$

where

$$Nu = \text{Nusselt No.} = \frac{H_c R}{k} \quad ,$$

$$Re = \text{Reynolds No.} = \frac{\rho(V - u)R}{\mu} \quad ,$$

$$Pr = \text{Prandtl No.} = \frac{C_p \mu}{k} \quad ,$$

which is valid for a range of Reynolds numbers from 20 to 150,000 (Ref. 20). The required transport and thermodynamic properties were evaluated at free-stream conditions.

The high relative velocity of the gas over the sphere results in a boundary layer around the sphere causing the gas temperature in this layer to rise due to compression and friction.

In calculating heat convection, the value of the gas temperature used as the driving potential is usually called the recovery temperature, and is expressed as

$$T_G = T_\infty + \zeta(T_s - T_\infty)$$

where ζ is the recovery factor. For laminar flow the recovery factor has been shown to be approximately equal to $\sqrt{Pr}$.

b. Gas Radiation: The radiation flux intensity (F_G) to a non-reradiating black body surrounded by a hot radiating gas at temperature T_∞ is

$$F_G = \sigma\ \epsilon_G\ T_\infty^{\ 4} \quad , \tag{64}$$

where σ is the Stefan Boltzmann constant, and ϵ_G is the emissivity of the gas.

A constant value of F_G obtained by Luzzi (Ref. 21) was used in our calculations and, as seen in the results, this value proves to be insignificant compared to convection heat transfer.

c. Radiation Cooling: Radiation from the surface of a particle to zero temperature space (F_S) is

$$F_S = \sigma \epsilon_s A T_L^4 \quad , \tag{65}$$

where ϵ_s is the surface emissivity, A the surface area of a particle, and T_L the surface temperature of the particle.

Because of the nonlinear dependence on the surface temperature, it would be very complex to attempt to include this expression for the radiation flux as a boundary condition to the transient heat conduction equation (which will be discussed subsequently).

An alternate and much simpler method was used; this was to calculate the surface temperature decrement resulting from the radiation cooling at intervals along the particle path.

If it is assumed, for the purpose of calculating the radiation cooling only, that the conductivity of the particle is infinitely large, then the temperature decrement ΔT_{LR}, due to radiation cooling, can be expressed as

$$\Delta T_{LR} = \frac{\sigma \epsilon_s A T_L^4}{m C_L} \quad . \tag{66}$$

This method of handling the radiation cooling is probably accurate enough for most purposes.

d. Heat Conduction and Absorption: As mentioned previously, the assumption of a uniform heating rate around the surface of a spherical particle enables us to use a conduction model in which the isotherms are concentric spheres; that is, the temperature, T, will depend only on the radii, r, and the time, t.

The appropriate conduction equation is

$$\frac{\partial T}{\partial t} = \kappa\left(\frac{\partial^2 T}{\partial r^2} + \frac{2}{r}\frac{\partial T}{\partial r}\right) \quad , \tag{67}$$

with the following boundary conditions:

$$\text{at} \quad r = o, \quad T = T \quad ,$$

$$r = R, \quad \frac{\partial T}{\partial r} = -h(T_G - T_L) \quad ,$$

and at $t = o, \quad T = T_1$;

where $\kappa = K/\rho_L C_{sp}$ is the thermal diffusivity; ρ is the density; K is the thermal conductivity; C_{sp} is the specific heat of the spherical particle; h is the ratio of the convective surface coefficient to the thermal conductivity, H_c/K; T_G is the temperature of the gas, and R is the surface radius of the sphere.

To facilitate the derivation with the use of a non-zero temperature for the surrounding gas, we set

$$\bar{T} = T_G - T \quad .$$

Equation (67) then becomes

$$\frac{\partial \bar{T}}{\partial t} = \kappa\left(\frac{\partial^2 \bar{T}}{\partial r^2} + \frac{2}{r}\frac{\partial \bar{T}}{\partial r}\right) \quad , \tag{68}$$

with the following boundary conditions:

$$\text{at} \quad r = o, \quad \bar{T} = \bar{T} \quad ,$$

$$r = R, \quad \frac{\partial \bar{T}}{\partial r} = -h\bar{T}_L \quad ,$$

and at $t = o, \quad \bar{T}_1 = T_G - T_1$.

Following the procedure in Carslaw and Jaeger (Ref. 22), we let

$$\bar{u} = \bar{T}r \quad .$$

Then Eq. (68) becomes

$$\frac{\partial \bar{u}}{\partial t} = \kappa \frac{\partial^2 \bar{u}}{\partial r^2} \quad , \tag{69}$$

with the boundary conditions

at $r = o$, $\bar{u} = o$;

at $r = R$, $\frac{\partial \bar{u}}{\partial r} = -(h - \frac{1}{R})\ \bar{u}_L$;

at $t = o$, $\bar{u} = \bar{T}_1 r = (T_G - T_1)\ r$.

Using the standard method of solving Eq. (69) as in Ref. 22, we get

$$\bar{T} = \frac{2(T_G - T_1)h}{r} \sum_{n=1}^{\infty} e^{-\kappa k_n^2 t} \frac{R^2 k_n^2 + (Rh - 1)^2}{k_n [R^2 k_n^2 + h(Rh - 1)]} \sin k_n R \sin k_n r \quad , \tag{70}$$

$n = 1, 2, \ldots \infty$

where k_n are roots of the characteristic equation

$$Rh - 1 + Rk_n \cot k_n R = 0 \quad . \tag{71}$$

Equations (70) and (71) were included in the computing program (see flow chart, Fig. 11).

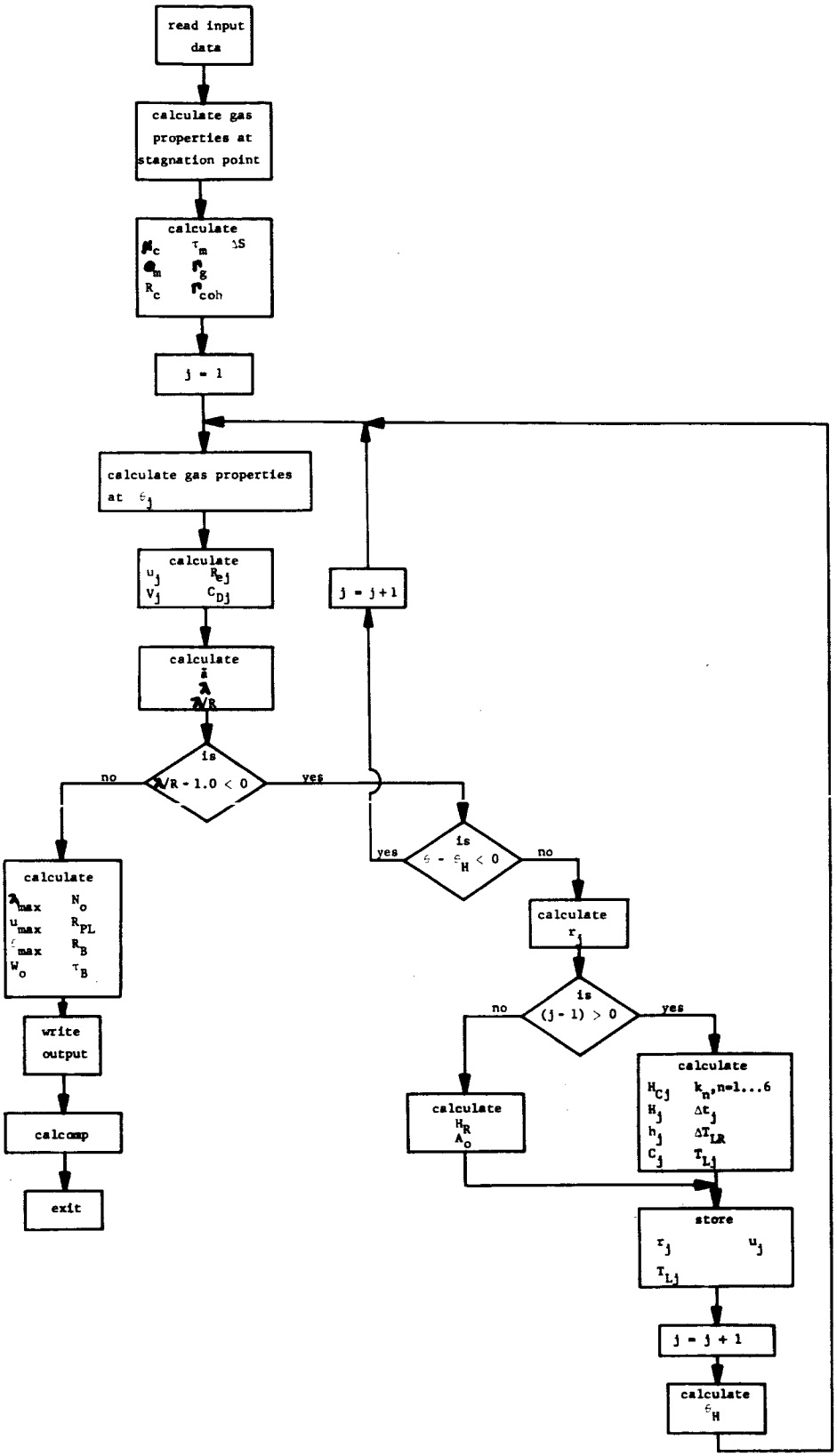

Fig. 11 Computer Flow Chart

6. Discussion of Results

Equation (70) was derived for a constant gas temperature and a constant convection coefficient, H_c . In our problem, however, the recovery gas temperature varies across the plume and the convection coefficient will vary due to the changes in the relative velocity between the particle and the gas as the particles travel through the plume.

One way of dealing with these variations is to divide the plume into small intervals and assume constant values of the gas temperature and constant H_c across each interval, using the calculated temperature at the end of one interval as the initial temperature for the next interval. This method is called the stepwise method in contrast to the spanwise method.

In the spanwise method, the plume is also divided into intervals, but Eq. (70) is used from the initial station to the end of the first interval, then from the initial station to the end of the second interval, and so on for all the intervals, and finally, from the initial station, all the way to the edge of the plume.

For each of these spanwise calculations, the gas temperature used was the value at the end of the interval. The convection coefficient used was the average value between the initial station and the end of the interval.

Theoretically, the stepwise method should give more accurate results, mainly because local conditions in the gas are taken into account more accurately. One of the disadvantages of the stepwise method is that it has a tendency to build up numerical errors and become numerically unstable. There is good evidence from the calculations to indicate that the lower the density of the plume and the smaller the radius of the particle, the more the tendency of the stepwise method to become unstable. Because of the very low density of the plume, especially at the outer regions, and the small particle diameters used, we used the spanwise method for our calculations.

As can be seen in Fig. 12, the calculations predict that the temperature of particles originating near the rocket nozzle centerline may rise very rapidly. The smaller the particle diameter the more rapid the rise. The curves show the maximum temperature that the surface of the particles will reach for various particle radii and nozzle heights. As the nozzle approaches the lunar surface, the particles can reach even higher temperatures.

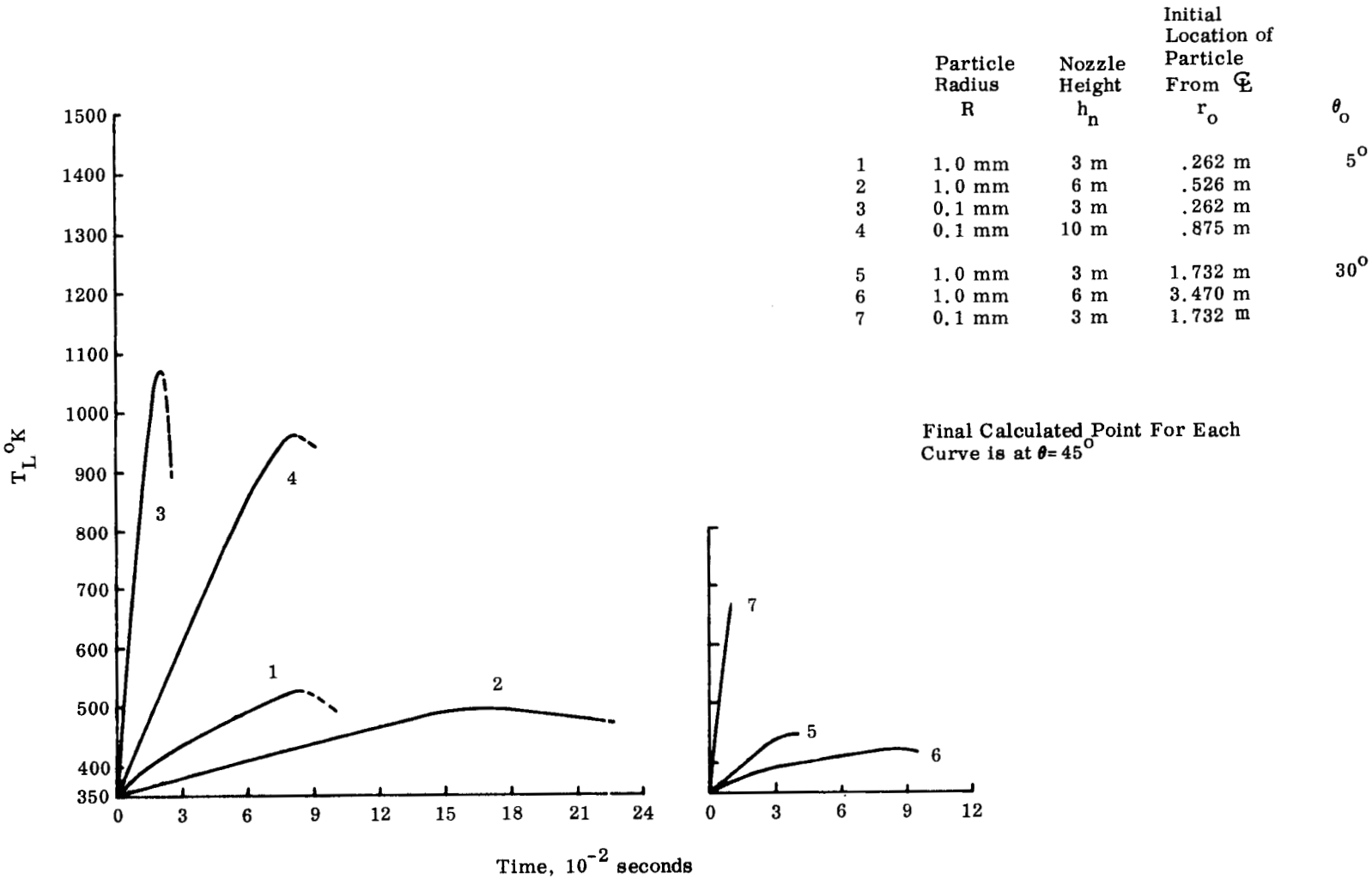

Fig. 12. Temperature History of Lunar Particle Surface

The dotted portion of the curves are not considered accurate because of the very low densities at the outer edge of the plume. Cooling of the particles by radiation to space during the free flight outside the plume is not shown in Fig. 12. Convection calculations were made, up to a θ of 45°. The particle temperatures for other nozzle heights and particle sizes can be obtained with the existing computer program.

Provisions are included in the program for calculating the landing sites of the particles, and also the rates at which particles are eroded from the surface. Therefore, the program can be used, if desired, to calculate the redeposited particle distribution on the surface and the associated temperature history for a suspension model.

7. Conclusions

Calculations show that:

1) Particles originating near the rocket nozzle centerline, smaller than 0.1 millimeter radii, blown away by the hot LEM exhaust gas, may reach temperatures in excess of 1100°K very quickly. This is much greater than the maximum subsolar temperature shown in Fig. 1 (also cf. Ref. 23).

2) Particles of 0.1 mm radii may fall as far as 130 meters from the rocket nozzle centerline.

D. Adsorption of Rocket Exhaust Gas on the Lunar Surface Using a Solid Lunar Surface Model [L. Aronowitz and J. Scanlon]

1. General

Adsorption of the LEM descent rocket exhaust gas on lunar surface material can introduce significant amounts of contaminants into the samples of the lunar surface that the Apollo astronauts will bring back to earth for scientific analysis. Discussed herein is a model used for quantitative calculations of the amount of rocket gas adsorbed on the lunar surface, and the subsequent desorption of these surface contaminants.

The model chosen for the lunar surface is a rough plane. This choice agrees well with the recent Soviet photographs of the lunar surface. The composition of the lunar surface material, shown in Table 13, was chosen to be similar to that of certain meteorites.

Table 13

LUNAR SURFACE MATERIAL COMPOSITION

SiO_2	46%
MgO	40%
FeO	9%
Al_2O_3	5%

2. Formulation

As the LEM descends toward the touchdown site, gas molecules from the rocket exhaust will strike the lunar surface. While the LEM altitude is above 100 or 200 feet, the molecules striking the surface are in the free molecular flow regime. At lower altitudes, the gas contacting the lunar surface in the vicinity of the LEM is in the continuum flow regime. The formulation uses gas-dynamic equations appropriate to the continuum regime.

At each point of the lunar surface in contact with the gas, there will be a flux density of f molecules per unit area per unit time from the gas to the surface. Of these impinging molecules,

a fraction S will be physically or chemically adsorbed, while the remaining fraction, $(1 - S)$, of impinging molecules will rebound. Quantity S is termed the "sticking coefficient." The adsorbed gas molecules may gradually desorb from the surface. If N is the number of molecules stuck to a unit area of lunar surface, then a fraction, D, of these molecules will be desorbed per unit time where D is called the desorption coefficient. Note that D is here defined as a fraction and therefore differs from the D defined in Sec. IV.E.

In general, the value of S depends on the average velocity of the impinging molecules and on the species of molecule and the chemical composition of the surface. The value of D depends on the specie of molecule, the chemical composition of the surface, and the surface temperature, T. The rate of change of N is given by

$$\frac{dN}{dt} = fS - DN \ . \tag{72}$$

For a given species, the value of S can be considered relatively constant, but f and D will vary as the pressure and temperature at the lunar surface change due to impingement of the rocket exhaust plume.

Flux, f, is related to gas pressure, p, at the lunar surface. Each of the molecules that strike the surface and stick to it transfer momentum, $M\bar{u}$, to the surface where M and $\bar{u}$ are, respectively, the average molecular mass and the average component of molecular velocity normal to the surface. If the molecule rebounds elastically instead of sticking, it transfers momentum $2M\bar{u}$ to the surface. The pressure, p, which is the momentum transferred to a unit area per unit time by the f impacting molecules, is given by

$$p = fM\bar{u}S + f2M\bar{u}(1 - S) = M\bar{u}f(2 - S) \ . \tag{73}$$

Thus

$$f = \frac{p}{M\bar{u}(2 - S)} \ . \tag{74}$$

In Eq. (74), the effects of inelastic collisions are neglected. The root mean square value of u can be substituted for $\bar{u}$ in Eq. (72) without introducing significant error. Thus,

$$\bar{u} = \sqrt{\frac{kT_g}{M}} , \tag{75}$$

where k is Boltzmann's constant and T_g is the gas temperature. The value of T_g for the rocket gas near the lunar surface in the vicinity of the LEM is of the order of T_c, the temperature of the gas in the combustion chamber of the rocket. The average value of $T_g = 0.64T_c$ was used in Eq. (75). The values of S for the principal species of gas in the exhaust, shown in Table 20, were found with the aid of a computer program (cf. Sec. IV.G) developed at Grumman under Contract NASw-1027 (Ref. 4). Values of D were found using the expression $D = 1/\tau$, where τ, the adsorption lifetime (Refs. 25 and 26) is given by (see discussion of thermal lifetimes in Sec. IV.F)

$$\tau = \tau_o \, e^{Q/(RT)} . \tag{76}$$

In Eq. (76), τ_o is a parameter characteristic of lunar surface material, R is the gas constant, Q is the heat of adsorption of the species on the lunar surface material, and T is the lunar surface temperature. Uncertainties in the calculated values of S and D are briefly considered later in this section.

The value of T in Eq. (76) varies as the lunar surface is heated by the impinging rocket plume and subsequently cools after the engine shuts down. As discussed, the constant value $T = T_o$ was used to calculate D, where T_o is the ambient lunar surface temperature. Therefore, changes in D with T [see Eq. (76)] have been ignored and the computed distributions of adsorbed gas are valid only at distances greater than 30 ft from the touchdown point where heating of the surface by the rocket plume can be ignored (cf. Table 23). No attempt was made to compute distributions at distances of less than 30 ft taking into account variations in T because existing data on variation of D with T under lunar environmental conditions are inadequate. The sensitivity of D to changes in T and other parameters is illustrated in Fig. 66. The value of T during rocket plume impingement and subsequent cooling have been calculated (Sec. IV.H), and can be used to compute adsorbed gas distributions when the necessary data are available (see Sec. V.B). The computation can be simplified by fitting an analytic expression for T during cooling, taken from Chap. 2 of Ref. 22, to the T distribution discussed in Sec. IV.H. Lunar surface thermal parameters for use in the analytic expression are given in Sec. IV.H.

The descent trajectory chosen for the calculation has zero horizontal velocity and constant negative vertical velocity. This corresponds well with pretouchdown to touchdown conditions in current trajectory planning (Ref. 3).

The following solution has been found for Eq. (72):

$$N_i(t) = \left(1/e^{\int_o^t D_i dt'}\right)\left(N_{io} + S\int_0^t f_i\, e^{\int_o^{t'} D_i dt''}\, dt'\right) \qquad (77)$$

where N_i is the number of adsorbed molecules per unit area of the i^{th} species, and N_{io} is the value of N_i at $t = 0$. A computer program was written to evaluate Eq. (77).

3. Results

Values of the desorption coefficient, D, were calculated for the 10 species of exhaust gas contaminants shown in Table 14. The values for $\tau = 1/D$ [Eq. (76)] in Table 14 were calculated using the values $T = 365°K$ and $\tau_o = 10^{-13}$ sec. Note that the values of Q in Table 14 that were used to calculate τ are the same as the values of E in Table 20 expressed in different units. The assumption of constant T ignores the heating of the lunar surface by the impinging descent rocket plume. This neglect would lead to erroneous results in the immediate vicinity of the touchdown point. At distances of about 30 ft or more from the touchdown point, the lunar surface heating effects of the rocket on D become unimportant (cf. Table 27) and the assumption of constant T is valid.

From Eq. (77) it is seen that τ plays the role of a time constant in the decay of the amount of adsorbed contamination. The Apollo astronauts will not begin collecting samples for a time period greater than 1×10^3 sec after touchdown, and will not collect any further samples after, at most, 1.4×10^5 sec. If τ is small compared with 1×10^3 sec, then none of the adsorbed contaminant will remain by the time the samples are collected. Table 14 shows that H, H_2, CO, and CO_2 will desorb so rapidly that they will not be present in the samples. The other species will only appear in regions of the lunar surface where they are chemically adsorbed.

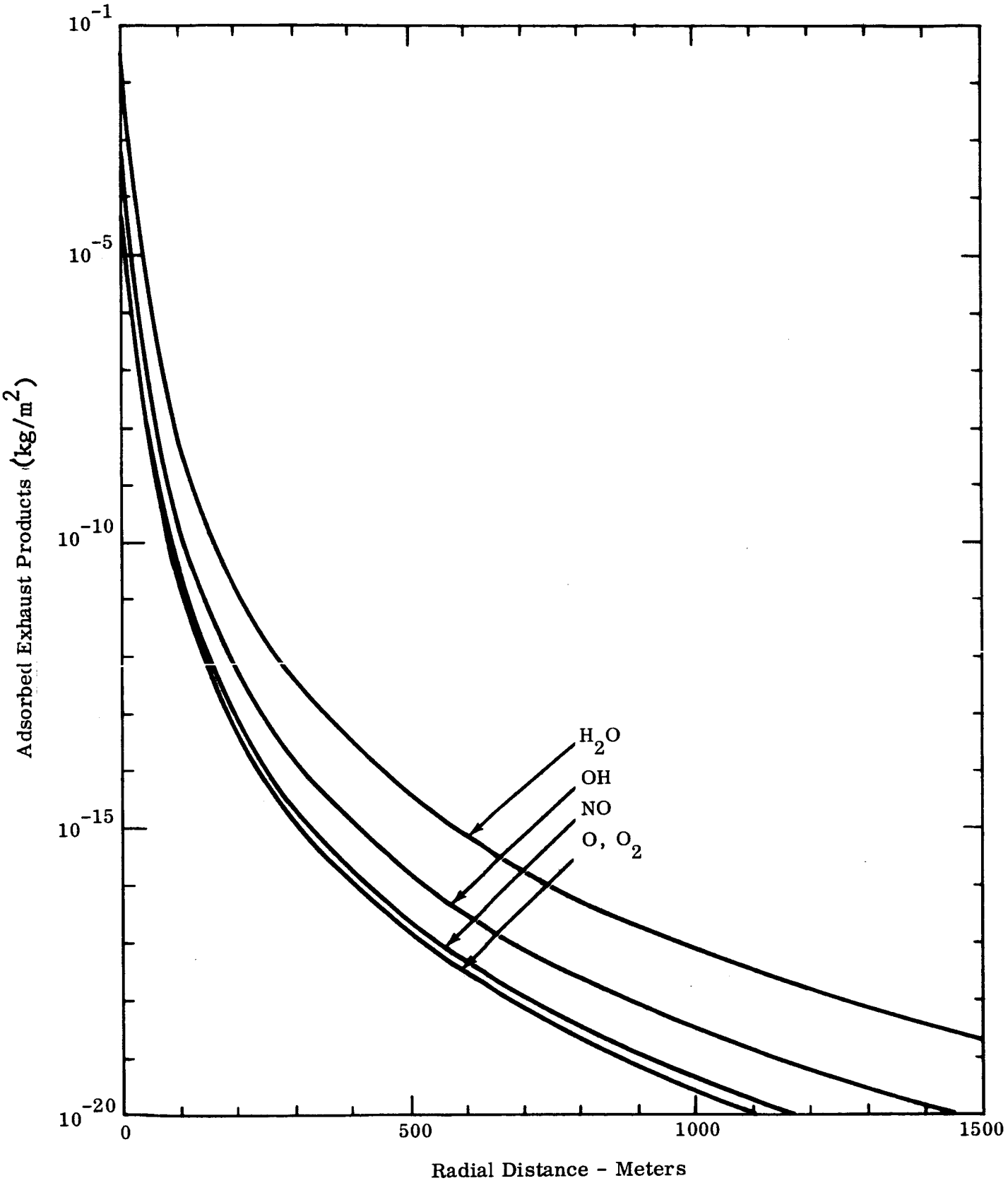

Fig. 13 Density of Rocket Exhaust Species Adsorbed on the Lunar Surface Versus Radial Distance from LEM

If τ is large compared with 1.4×10^5 sec, there will be negligible desorption during the lunar stay period and the density of the adsorbed contaminant will remain the same as its value when the descent rocket is shut down. The density of adsorbed contaminant species on areas where they are chemically adsorbed is shown in Fig. 13. The values in Fig. 13 were computed using the values of D in Table 14. Figure 13 plots density in kg/m^2 versus distance from touchdown point in meters. The reader must again be cautioned that Table 14 and Fig. 13 are, at best, rough order of magnitude estimates. Insufficient data exist at present to make reliable estimates of values for S and D in Eq. (77) (cf. Sec. V.B).

Table 14

VALUES OF $\tau = 1/D$ FOR $T = 365°K$ AND $\tau_o = 10^{-13}$ sec

Species	Q cal/mole		τ sec	
	Phys.	Chem.	Phys.	Chem.
H	$.090(\times 10^4)$	$2.1(\times 10^4)$	$< 10^{-12}$	.37
H_2	.23	2.3	$< 10^{-10}$	6.0
H_2O	1.4	6.0	$< 10^{-4}$	$> 10^{22}$
CO	.69	2.3	$< 10^{-8}$	6.0
CO_2	.92	2.3	$< 10^{-7}$	6.0
N_2	.46	4.6	$< 10^{-10}$	$> 10^{14}$
NO	.72	15	$< 10^{-8}$	$> 10^{76}$
O	.58	8.1	$< 10^{-9}$	$> 10^{35}$
O_2	.46	4.6	$< 10^{-10}$	$> 10^{14}$
OH	.92	10	$< 10^{-7}$	$> 10^{46}$

4. Conclusions

The approximations made in the computer program, which were discussed earlier in this note, do not introduce significant error into the results. Far more serious is the present lack of data on the values of parameters S and D under lunar environmental conditions, and of the variation of D with temperature. It should be noted that D appears exponentially in Eq. (77) and the computed results are sensitive to errors in D. Therefore the results presented herein can be treated only as qualitative guidelines. The results should be recalculated when better data are available.

E. Atmosphere [F. Pomilla and N. Milford]

1. General

To interpret the measurements that will be made of the gases in the lunar atmosphere during and after the LEM stay on the moon, estimates are made of the contamination of the ambient lunar atmosphere by the exhaust gases. Adopting as source function for the atmospheric contaminants the appropriate fraction of the space and time distribution of the LEM gases striking the lunar surface, calculations have been made of two models of lunar atmosphere contamination. The first model, valid for later times, gives the average over the moon of the contaminant gas density as a function of solar wind velocity and time. In the second model, an appropriate diffusion equation is solved to give the contaminant density as a function of position on the lunar surface, solar wind velocity, and time.

The contamination calculations are based on models of lunar atmospheres with time dependent gas sources developed at Grumman and described in detail in the Grumman Research Department report "Variations in the Lunar Atmosphere" (Ref. 26). To make the present description of the lunar atmosphere contamination calculations reasonably self-contained, an outline of the models covered in that Grumman report is included here. In the following paragraphs, the space-independent and space-dependent models (I and II, respectively) of atmosphere contamination are formulated and the basic contamination equations solved. The numerical results are then presented in the form of graphs of the atmospheric contaminant distribution with position on the moon and time after initial ignition of LEM descent rockets, and finally the implications are discussed. During the LEM stay-time, the contamination of the atmosphere is shown to be both appreciable and nonuniform in distribution, with the subsequent trend towards a uniform distribution proceeding at different rates for different exhaust gas species.

2. Model I Formulation

a. Assumptions: In this simplified model of the lunar atmosphere, the exhaust gases from the LEM are assumed to spread uniformly over the lunar surface, attain the temperature of the surface and then be reemitted into the ambient lunar atmosphere at a uniform time rate. In turn, these exhaust gases are assumed

lost from the atmosphere through the mechanisms* of (a) collisions (elastic and charge exchange) with the solar wind, (b) interactions with solar photons producing photoionization and photodissociation, and (c) thermal evaporation from the top of the atmosphere, as well as by (d) sticking to the lunar surface.

Because the ambient lunar atmosphere is extremely rarefied ($< 10^{-9}$ of the earth's atmosphere), the mean free path of the exhaust gases is very large so that the assumption of a uniform distribution over the lunar surface is reasonable for long times after rocket shutoff. This model then should give the asymptotic values of the gas densities approached by space dependent distribution models.

b. Equations: If the total number of particles, N, of a given species of gas is contained in the volume, V, between the surface of the moon (of radius r_o) and a spherical surface at height h, then

$$N = nV \quad ,$$

where n is the number density of the gas species in question and the "scale volume" is

$$V = \frac{4}{3}\pi \left[(r_o + h)^3 - r_o^3 \right] \quad ,$$

while the "scale height" for a gas of particles of mass m is

$$h = \frac{kT}{mg} \quad .$$

The number density, n, is taken as constant throughout the volume, V, and therefore it also represents the average surface

*We follow Hinton and Taeusch (Ref. 27), hereafter referred to as H and T, in evaluating the losses from the atmosphere due to mechanisms (a) - (c).

number density. Then, in this simple model, n is time dependent only and its time rate of change is given by

$$\frac{dn}{dt} + An = \frac{1}{V}\left[B + C(t)\right] \quad , \tag{78}$$

where

AN = the number of particles of a given species of gas lost per second from the atmosphere via the H and T mechanisms,

B = the number of particles of a given species of gas emitted from the H and T surface sources per second, exclusive of the contribution from the LEM exhaust, and

C(t) = the number of particles of a given species of exhaust gas reemitted per second from the lunar surface.

Following our assumption that the exhaust gases are reemitted from the lunar surface at a constant time rate, we let

$$C(t) = D \cdot u(t) \quad ,$$

where $u(t)$ is the step-function of time

$$u(t) = \begin{cases} 1, & 0 \leq t \leq \tau \\ 0, & t > \tau \end{cases} \quad ,$$

τ is the total time interval during which this exhaust gas is being reemitted, and

D = number of particles of a given species of exhaust gas reemitted per second from the lunar surface.

c. Solutions: The solutions of Eq. (78) are easily found (Ref. 26) to be:

for $0 \leq t \leq \tau$

$$n(t) = \frac{B+D}{AV} + \frac{e^{-At}}{V}\left(N_o - \frac{B+D}{A}\right)$$

and

for $t > \tau$

$$n(t) = \frac{B}{AV} + \frac{e^{-At}}{V}\left[N_o - \frac{B - D(e^{A\tau}-1)}{A}\right] \quad ,$$

in which we have used the initial condition

$$n = \frac{N_o}{V} \quad \text{at} \quad t = 0 \quad .$$

For those exhaust gas species that are initially present in the H and T model atmosphere, viz., H_2O and H,

$$N_o = \frac{B}{A} \quad ,$$

which is the equilibrium value for those species, while for all the other gas species in the exhaust,

$$N_o = 0 \quad ,$$

as these are not initially present in the H and T model atmosphere.

The expressions used for evaluating the quantities A and B are identical with the H and T expressions for their loss and source terms, respectively. Thus, using H and T notation,

$$A = \beta \left\{ J\left(\bar{\gamma}\sigma'_{e\ell} + \sum X\sigma_1\right) + \sum \sigma\Phi_o + \frac{\pi r_o^2}{\beta V}\,\bar{c}\; e^{-r_o/h}\left(1 + \frac{r_o}{h}\right)\right\} \quad ,$$

and

$$B = XJ\pi r_o^2 + J_s 4\pi r_o^2 \quad ,$$

where

J = total positive ion flux in the solar wind per cm^2 per sec

and

J_s = the flux of particles of the given species into the lunar atmosphere due to (a) neutralization and diffuse reflection of solar wind ions, and (b) to actual sources in the lunar surface crust.

Following H and T, we have taken $J_s = 1.5 \times 10^5$ moles per cm^2 per sec for H_2O, and $J_s = 0$ for all the other exhaust species. The four terms on the right hand side of the expression for A are the rates of escape of particles of a given species per second from the lunar atmosphere due to the following processes:

(a) Loss of a particle as a result of its gaining enough energy from an elastic collision with a solar wind proton. The effective cross section for such collisions is $\sigma'_{e\ell}$ and $\bar{\gamma}$ is the average geometric probability that a particle receiving enough energy in such a collision will be ejected from the atmosphere and not hit the moon's surface.

(b) Loss of a particle as a result of having undergone a charge exchange collision with a solar wind positive ion and thereby receiving enough energy to reach the slightly positively charged lunar surface and recombine there. The effective charge exchange cross section is σ_1 and X is the fraction of positive ions of a particular kind in the solar wind. Following Aller (Ref. 28), we have taken $X = .86$ for H and $X = 0$ for all the other exhaust species.

(c) Loss of a particle as a result of interacting with the solar photon flux Φ_o (Ref. 29) and thereby being ionized or dissociated with the cross sections for each of these processes being designated by σ.

(d) Loss of particles due to thermal escape of particles (with r.m.s. speed $\bar{c}$) at the height h (Jean's escape mechanism).

We have written the rate of reemitted exhaust gas, D, in the form

$$D = \frac{N_A f Y M}{w \tau} ,$$

where

Y = mole fraction of a given species of gas in the exhaust,

M = total mass of exhaust gas in grams, arbitrarily chosen as 10^7 grams,

N_A = Avogadro's number,

w = molecular weight of the given species of gas,

f = fraction of exhaust gas of the given species that hits the surface and is reemitted in a time τ.

Table 15 contains the various values we have taken for the parameters entering into the quantities A, B, and D. β is the fraction of the particles of a given species in the atmosphere that is exposed to the sun.

3. Model II Formulation

a. Assumptions: In this model, the initial space distribution of the LEM exhaust gas as it impinges on the lunar surface is taken as known input from the far field and near field gas dynamics calculations (cf., Sections IID2,3; VA,B of this report). The gas particles in this initial distribution subsequently undergo a three dimensional diffusion into the thin lunar atmosphere. It is assumed that this can be adequately represented by a diffusion of the particles in two dimensions across the lunar surface

Table 15

VALUES OF THE INPUT PARAMETERS FOR MODELS I AND II

Exhaust Species (S)	$\bar{\nu}$	$\beta^{\dagger}$	$\bar{\gamma}$	$\sigma_{e\ell}(H^+,S) \times 10^{16}(cm^2)$	$\sigma'_{e\ell}(H^+,S) \times 10^{16}(cm^2)$	$\sigma_{ex}(H^+,S) \times 10^{15}(cm^2)$	$\sigma_{ex}(He^+,S) \times 10^{15}(cm^2)$	$\Sigma\sigma\ \Phi_o \times 10^6(sec^{-1})$	$A \times 10^5(sec^{-1})$ $J = 10^9$	$J = 10^{12}$
H_2O	.36	.5	.5	5.8	5.8	2.0	2.0	19.0	1.01	65.5
N_2	.32	.5	.5	11.3	0.65	1.0	0.4	5.0	0.296	46.4
H_2	.13	1.0	1.0	5.8	5.8	0.5	0.1	1.0	14.3	116.6
CO	.096	.5	.5	11.2	0.65	2.7	2.7	5.0	0.383	132.9
CO_2	.037	.5	.5	16.8	0.45	1.0	1.0	10.0	0.55	50.9
H	.019	1.0	1.0	4.5	4.5	2.0	0.03	0.45	14.6	231.8
OH	.016	.5	.5	3.1	3.1	1.0	1.0	5.0	0.283	33.1
NO	.0024	.5	.5	11.1	0.55	1.0	1.0	5.0	0.30	50.4
O_2	.0015	.5	.5	10.3	0.45	1.0	0.7	5.0	0.298	48.2
O	.0014	.5	.5	6.9	6.9	0.5	0.4	1.0	0.0794	29.4

†These values of β are for Model I only.

with concurrent loss mechanisms occurring in the vertical column of gas of scale height, h, for each species. As in Model I, the atmospheric number density, n, for each species is assumed uniform over the scale height, h, and the particles are assumed to be thermalized upon striking the lunar surface. In addition to the loss mechanisms of H and T used in Model I, we consider in Model II (in some detail) the adsorption and desorption occurring at the lunar surface for each gas species.

b. Equations: Choosing the diffusion coefficient D' as a constant for each species of exhaust gas, the diffusion equation for the particle density n (particles/cm^3) is

$$\frac{\partial n}{\partial t} = D'\nabla^2 n + q(r,\theta,\varphi,t) + Kn \quad , \tag{79}$$

where q is a source function ($cm^{-3}sec^{-1}$) that is not explicitly dependent on the number density n at each point (r,θ,φ), and K is the time rate coefficient (sec^{-1}) of the loss term which is explicitly n dependent. The constant diffusion coefficient D' is given by

$$D' = \frac{1}{3}\lambda v \quad ,$$

where

λ = mean free path of a gas particle

v = velocity of reemission of a gas particle from the lunar surface.

c. Solution: The three dimensional diffusion problem [Eq. (79)] is reduced to two problems: (a) a one dimensional uniform vertical distribution of height h above the lunar surface with appropriate loss mechanisms in the vertical column as in Model I plus adsorption at the base of the column, and (b) a two dimensional diffusion along the spherical lunar surface. Choosing the usual spherical polar coordinates (r,θ,φ) with origin at the center of the moon and the LEM touchdown point as the pole, the three dimensional diffusion equation [Eq. (79)]

reduces to the two dimensional equation

$$\frac{\partial n(\mu,t)}{\partial t} = \frac{D'}{r_o^2} \frac{\partial}{\partial \mu} \left[(1 - \mu^2) \frac{\partial n}{\partial \mu} \right] + q(\mu,t) + Kn \quad , \qquad (80)$$

when

$r = r_o$ = radius of moon

$\mu = \cos \theta$

and

n is taken as φ independent.

Taking the source function q as consisting of point sources of the form

$$q = q_o \, \delta(\mu - \nu) \, \delta(t) \quad ,$$

at times t after the exhaust impinges on the lunar surface, the initial condition

$$n(\mu,o) = 0 \quad ,$$

and using Laplace transform techniques to solve Eq. (80), we obtain (Ref. 26)

$$n(\mu,t) = q_o \sum_{\ell=o}^{\infty} \Theta_\ell(\mu) \, \Theta_\ell(\nu) \, e^{-\left[|K| + \frac{D'}{r_o^2} \ell(\ell+1) \right] t} \quad , \qquad (81)$$

where the Θ_ℓ are normalized Legendre functions of the first kind†.

---

†If n is taken as φ dependent and

$$q = q_o \, \delta(\mu - \nu) \, \delta(\varphi - \varphi') \, \delta(t) \quad ,$$

the only effect produced in Eq. (81) is the replacement of the Θ_ℓ functions by the spherical harmonics $Y_{\ell,m}(\mu,\varphi)$.

If we divide the moon's surface into small areas, $\sin\theta_i \Delta\theta_i \Delta\varphi_j$, and represent the exhaust gas reemitted at a time t_k from each area element as a point source located at $(\theta_i \varphi_j)$, then the total particle density of a given gas specie at an observation point (θ,φ) at the time t can be shown (Ref. 26) to be

$$n(\theta,\varphi,t) = \sum_{i,j,k} q_o(\theta_i,\varphi_j,t_k) \sum_{\ell=o}^{\infty} \sqrt{\frac{2\ell+1}{2}}\, \Theta_\ell (\cos\alpha) \cdot h_{\ell k}(t) \quad , \quad (82)$$

where

$$\cos\alpha = \cos\theta \cos\theta_i + \sin\theta \sin\theta_i \cos(\varphi - \varphi_j) \quad ,$$

$$h_{\ell k}(t) = e^{-\left[|K| + \frac{D'}{r_o^2} \ell(\ell+1) \right] (t - t_k)} U(t - t_k) \quad ,$$

$$U(t - t_k) = 0 \quad \text{for} \quad t \leq t_k$$

$$= 1 \quad \text{for} \quad t > t_k$$

and

$$q_o(\theta_i,\varphi_j,t_k) = \frac{32.17 \times 10^{-2}}{2.205(30.48)^2} \frac{N_A Ym(\theta_i,\varphi_j)}{wh} (1 - f_1) \Delta\theta_i \Delta\varphi_j \sin\theta_i \quad (\text{in cm}^{-3})$$

for h in km. The far-field gas dynamics calculation yields the total mass per unit area, $m(\theta_i\varphi_j)$ (in slugs/ft^2), of LEM exhaust gas that impinges on the lunar surface at point (θ_i,φ_j), and we have assumed that a fraction, f_1, of these fast particles of a given specie stick to the lunar surface for periods that are long compared to the observation time t. The contributions from the near-field calculations can be expressed in a similar way. The total source coefficient, $q_o(\theta_i,\varphi_j,t_k)$, is in general a sum of the near plus far-field contributions. The other parameters in

the q_o expression have already been defined above in Model I. The coefficient K of the loss term is given by

$$K = - A - \frac{1}{4} \frac{\bar{c} f_2}{h} ,$$

where we have assumed, in addition to the loss mechanisms in Model I, represented again by the coefficient A as defined above, that a fraction, f_2, of the $\frac{1}{4} n_o \bar{c}$ thermalized particles of a given gas species that hit the lunar surface (per cm^2 per sec.) stick to the surface.

Table 16 contains the values of the chemical sticking coefficients f_1 and f_2 and the desorption times τ_o, which were obtained from Sections II.D5, and V.D of this report, for the various species of exhaust gas. The diffusion coefficients $D'(= \frac{1}{3} \lambda v)$, together with the values of $\bar{c}$ and λ are also listed in Table 16 for an assumed constant temperature (T) lunar surface of 300°K. The values in this table are obtained from the relations

$$\bar{c} = .158 \sqrt{\frac{T}{w}} \quad (km/sec)$$

$$\lambda = \frac{\bar{c}^2}{g_m} \sin 2\alpha \quad , \quad g_m = 162 \times 10^{-5} \frac{km}{sec^2}$$

$$v = \bar{c} \cos\alpha \quad ,$$

and therefore,

$$D' = \frac{1}{3} \frac{\bar{c}^3}{g_m} \sin 2\alpha \cos\alpha \quad ,$$

where we have chosen $\alpha = 45°$ as the average angle of reemission from the lunar surface for the thermalized gas particles.

Table 16

VALUES OF SOME OF THE INPUT PARAMETERS FOR MODEL II

Exhaust Species	f_1	f_2	τ_o(sec)	$\bar{c}$(km/sec)	$\lambda(10^2 km)$	$D'(km^2/sec)$
H_2O	0.9750	0.99912	∞	0.645	2.57	39.0
N_2	0.947	0.99885	∞	0.517	1.65	20.1
H_2	0.9926	0.99760	3.2×10^3	1.93	23.0	10.5×10^2
CO	0.874	0.99768	8.7×10^3	0.517	1.65	20.1
CO_2	0.779	0.99767	8.7×10^3	0.412	1.05	10.2
H	0.997	0.99732	1.5×10^2	2.73	46.0	29.6×10^2
OH	0.987	0.99947	∞	0.664	2.72	42.6
NO	0.985	0.99965	∞	0.499	1.54	18.1
O_2	0.933	0.99885	∞	0.483	1.44	16.4
O	0.985	0.99934	∞	0.684	2.89	46.6

4. Model I Results

For each species of the exhaust gas we have calculated in Model I $n(t)$ for $0 \leq t \leq 10^7$ seconds with $\tau = 1000$ seconds, $J = 10^9$ cm^{-2} sec^{-1} and $\bar{J} = 10^{12}$ cm^{-2} sec^{-1}. In all cases $T = 300°K$ and $F = 1(= f)$. These results are shown in Figs. 14-33 assembled together at the end of this section.† It should be noted that the number density $n(t)$ (particles/cm^3) in each figure is the total of the H and T ambient atmosphere plus the LEM exhaust for that particular gas species. Results for additional values of the parameters were calculated at Grumman and they appear in Ref. 26.

†In the figures, the symbols NO(TT) and TT represent $n(t)$ in particles/cm^3 and t in seconds, respectively. Since the log-log plots necessarily distort the values NO(TT) = 0, it should be understood that NO(TT) = 0 at TT = 0 for all gases except H_2O and H.

5. Model II Results

For each species of the exhaust gas, we have calculated in Model II $n(\theta,\varphi,t)$ for $10^3 \leq t \leq 10^7$ seconds at several values of θ when $J = 10^9$ cm^{-2} sec^{-1} and $T = 300°K$ for the case of no sticking, $F_1 = F_2 = 0 (= f_1 = f_2)$ and the case in which the sticking coefficients have the values listed in Table 16. The results are shown in the log graphs of Figs. 34-65, (assembled together at the end of this section) where N(PHE) is the value of $n(\theta,\varphi,t)$ in particles/cm^3 and T is the time t in seconds. Zero time corresponds to the start of the powered descent of LEM, which is some 500 seconds before touchdown. It should be noted that the number density, N(PHE), in each figure is that for the LEM exhaust only, excluding the H and T ambient atmosphere. The values 0.01° and 90° chosen for θ (indicated by THETA on the figures) correspond to the distances of approximately 300 meters and 2500 km, respectively, from the LEM touchdown point, which is the pole of our spherical coordinate system. The results presented in Figs. 34-65 hold for all values of φ .

Results for additional values of the parameters were calculated at Grumman and they appear in Ref. 26. Of course, if the number density for each exhaust species is desired at still other values of the parameters, the Grumman computer program is available for such additional computations.

6. Conclusions

a. Model I: The results presented in Figs. 14-33 for this simple model represent an "averaged" contamination of the lunar atmosphere by the LEM exhaust gases. This model should yield the asymptotic values of the contaminant gas densities approached by space dependent distribution models, such as our Model II, at times long after rocket shutoff.

In Model I we have asusmed that the total mass of LEM exhaust (nominally chosen as 10 metric tons) hits the lunar surface, spreads uniformly over the surface, accommodates to the temperature of the surface (chosen to have a value of 300°K) and is reemitted in its entirety (F = 1 = f) into the lunar atmosphere at a constant rate in the time interval τ (chosen as 1000 seconds). In the actual powered descent phase of the LEM, the trajectory of the LEM and the exit velocities of the exhaust gases are such that approximately 90 percent of the total exhaust will be lost into space,

and of the remaining approximately 10 percent which does strike the surface, some will stick for long periods of time. However, Model II does take cognizance of the actual LEM descent characteristics and surface sticking of exhaust particles and, therefore, the results (cf. Figs. 34-65) are more realistic estimates of the intensities and distributions of the LEM contaminants in the lunar atmosphere.

In making comparisons between the Model I and Model II results, it should be recalled that our Model I results (Figs. 14-33) give the total of the H and T ambient atmosphere plus the LEM exhaust number density for each gas species in the exhaust, while Model II results (Figs. 34-65) give the number density for the LEM exhaust gas species only. Of the species present in the LEM exhaust, H_2O and H are also present in the H and T ambient atmosphere. Furthermore, a total mass of 10 metric tons of exhaust strikes the lunar surface in Model I, while approximately 1 metric ton of exhaust strikes it in Model II. Then, making the appropriate comparisons of the results for Model I (Figs. 14-33) with the results for Model II (Figs. 34-65), at times after a uniform distribution has been reached, it is seen that Model II number densities do approach the Model I densities. (H_2 is an exception, which is probably due to crude $\beta(=1)$ value chosen for it in Model II).

It is seen from Figs. 14-33 that H_2O, N_2, and CO make the largest contributions in this simple model over periods greater than 1 day. Water vapor, the contaminant of greatest selenophysical interest, reaches a maximum particle density of approximately 20 times that predicted (Ref. 27) for its abundance in the ambient atmosphere. It is clear from the comparison of Figs. 13-23 with Figs. 24-33 that, except for hydrogen (H), the effect of an increase in the solar wind flux (J) is to decrease the density and decay times of the contaminants. The solar wind tends to sweep the atmosphere clean of all contaminants except H. In the case of H, the solar wind protons (H^+) are neutralized and diffusely reflected by the lunar surface and thus add to the H content of the atmosphere. This effect, of course, increases with an increase in solar wind flux.

b. Model II: For this more realistic model, the space and time distributions of the particle number densities for the LEM contaminant gases in the lunar atmosphere are shown in Figs. 34-65. Results are obtained for the region of prime interest for the first Apollo mission, that is, within 300 meters of LEM touchdown, for

a simulated LEM descent trajectory that lies wholly in the plane of a lunar great circle. This was chosen as the lunar meridianal plane, i.e., the $\varphi = 0$ plane. Results are also shown for the particle density at a large distance ($\sim$ 2500 km) from the LEM touchdown point. The total mass of the LEM exhaust gases was arbitrarily chosen as 10 metric tons, of which 1 metric ton reaches the surface of the moon from the far-field gas flow. This is confined almost exclusively to the region enclosed by the 10° latitude circle about the LEM touchdown point (pole). The number density calculations were performed 1) using the sticking coefficients in Table 16 and also 2) under the assumptions of no sticking to the lunar surface. The sticking coefficients used (Table 16) were obtained from Sec. IV.F and G. We have included only chemical sticking since the physical sticking coefficients have desorption times that are very short ($\sim$ several seconds) compared to the relatively long times ($\lambda/\bar{c} \sim 10^3$ seconds) needed for the diffusion equation [Eq. (79)] to be applicable.

It is clear from the figures that the single most important loss mechanism is that of adsorption to the lunar surface. Unfortunately, this effect is probably also the least well known of the loss mechanisms due to the general lack of knowledge of the physical and chemical properties of the lunar surface. This, combined with the fact that the solar wind itself is not well known, makes the theoretical determination of the structure of the lunar atmosphere and its contamination somewhat uncertain, and at best only order of magnitude estimates can be expected.

In Model II, only the far-field input has been considered since estimates of the near-field contribution to the atmosphere indicate that it is small compared to the far-field contribution.

Our results presented in Figs. 34-65 are for an average solar wind flux of 10^9 positive ions per cm^2 per second of which about 86 percent are protons. These are estimates obtained from Mariner II and satellite measurements and reasonably approximate average solar wind parameters. However, since the first Apollo mission will be near the time of solar maximum, it is anticipated that the solar wind will be more intense than average. Larger solar wind fluxes will lead to smaller decay times for the exhaust contaminants and thereby effect a faster removal of the contaminants from the lunar atmosphere.

For both models, the values of the parameter $\bar{\gamma}$ chosen for each gas species are given in Table 15. We recall that this parameter

is an attempt to represent the geometric probability that a particle receiving enough energy in a collision to enable it to escape will actually escape and therefore be lost to the atmosphere. Following the reasoning of H and T in Ref. 27, we have chosen $\bar{\gamma} = 1$ for the light gases H and H_2 and $\bar{\gamma} = 1/2$ for the remaining heavy gases in the LEM exhaust.

In Model II we have chosen $\beta = 1$ for all the exhaust gas species. This parameter represents the fraction of the particles in the atmosphere that are exposed to the sun. As distinguished from Model I, where the exhaust gases were assumed uniformly distributed over the lunar surface so that $\beta = 1/2$ was chosen as a reasonable value (except for the light gases H and H_2 where $\beta = 1$ was chosen), the values of $\beta = 1$ in Model II account for the fact that the gases except H and H_2, diffuse slowly from the sunlit side (where LEM in the first Apollo mission will land) to the dark side. For H and H_2, which diffuse quickly, the value $\beta = 1$ is probably crude. In fact, in the case of H, which has in addition to the LEM exhaust source an additional source due to neutralization of the solar wind protons, there should probably be two parameters β instead of one.

The values of the cross sections listed in Table 15 are reasonable estimates gleaned from the limited literature on these collision processes. The literature is particularly scant on photodissociation cross sections, so that these were estimated from the more abundant literature on total photoabsorption cross sections.

Finally, it should be pointed out that the results for very early times ($\lesssim 10^3$ sec) are not valid, since for the diffusion theory to apply the gas molecule must have undergone at least several hops along the surface.

The present computer calculations have shown that:

a) For a given latitude (θ) on the lunar surface, the particle density for any atmospheric contaminant species is not a function of the longitude φ. Thus the results presented in Figs. 34 through 65 are all at $\varphi = 0$.

b) In the region of LEM touchdown, the particle density of the contaminants in the atmosphere does not change with distance for distances of 30 meters to 300 meters from touchdown.

It is seen from Figs. 34 through 65 by comparing the no sticking ($F = F = 0$) results at $\theta = 0.01°$ with those at $\theta = 90°$, that the light molecules H and H_2 are uniformly distributed in the atmosphere over half the moon's surface in a couple of hours, while the heavier contaminants CO_2 and O_2 require approximately six days to attain such a uniform distribution. The other contaminants have distribution times between these extremes with that of H_2O being approximately two days. From additional calculations performed at Grumman it is found that in these stated times the uniform distribution is over the full surface of the moon. It is also clear that for the case of no sticking, the particle number densities of the contaminants are sufficiently large for significantly long times both in the vicinity of LEM touchdown and also at great distances that they should be readily detectable by standard instruments. Indeed, if the present experimental and theoretical estimates of 10^6 particles/cm^3 for the ambient lunar atmosphere are correct and there is no sticking of the exhaust contaminants to the surface, then the total particle number density of the contaminants in the vicinity of the LEM is of the order of the ambient atmosphere for the first day after touchdown. However, in the event that sticking to the surface occurs to the extent that we have estimated, those contaminants will be detectable in the atmosphere only by more sensitive instruments in the vicinity of LEM touchdown and then only during the first few hours after touchdown. After this time period, only trace amounts ($< 10^{-4}$ particles/cm^3) of such contaminants will be present in the lunar atmosphere. At great distances from the LEM touchdown, such contaminants will never be present in more than trace amounts. The contaminants H, H_2, CO, and CO_2 with zero sticking coefficients will predominate in the lunar atmosphere, with CO and CO_2 being most prevalent and most persistent.

For completeness, it should be pointed out that by making certain approximations, it is possible to obtain an analytical formula that yields rough estimates of the atmospheric density of the various contaminant species in the neighborhood of the LEM touchdown site ($\theta = 0°$):

$$n \approx \frac{q_o R^2}{2D'(t - t_k)} e^{-|K|(t-t_k)}$$

for $10^3 \lesssim t - t_k \lesssim 10^5$, except H and H_2, and $10^3 \lesssim t - t_k \lesssim 10^4$ for H and H_2, where the symbols have the designations given to them above.

Finally, the amount of atmospheric contamination for other values of the sticking coefficients can be estimated roughly from the figures (except for H, H_2, CO, CO_2). In addition to the two cases of zero sticking and large sticking, there is the additional (trivial) case of complete sticking, $F_1 = F_2 = 1.0$, which corresponds to zero atmospheric contamination (except for a small orbital component that decays with the time constant A^{-1}) at all times after the first contact of the LEM exhaust gases with the surface. Thus, it is possible to interpolate roughly between these three values of the sticking coefficients to find the contamination for intermediate sticking values.

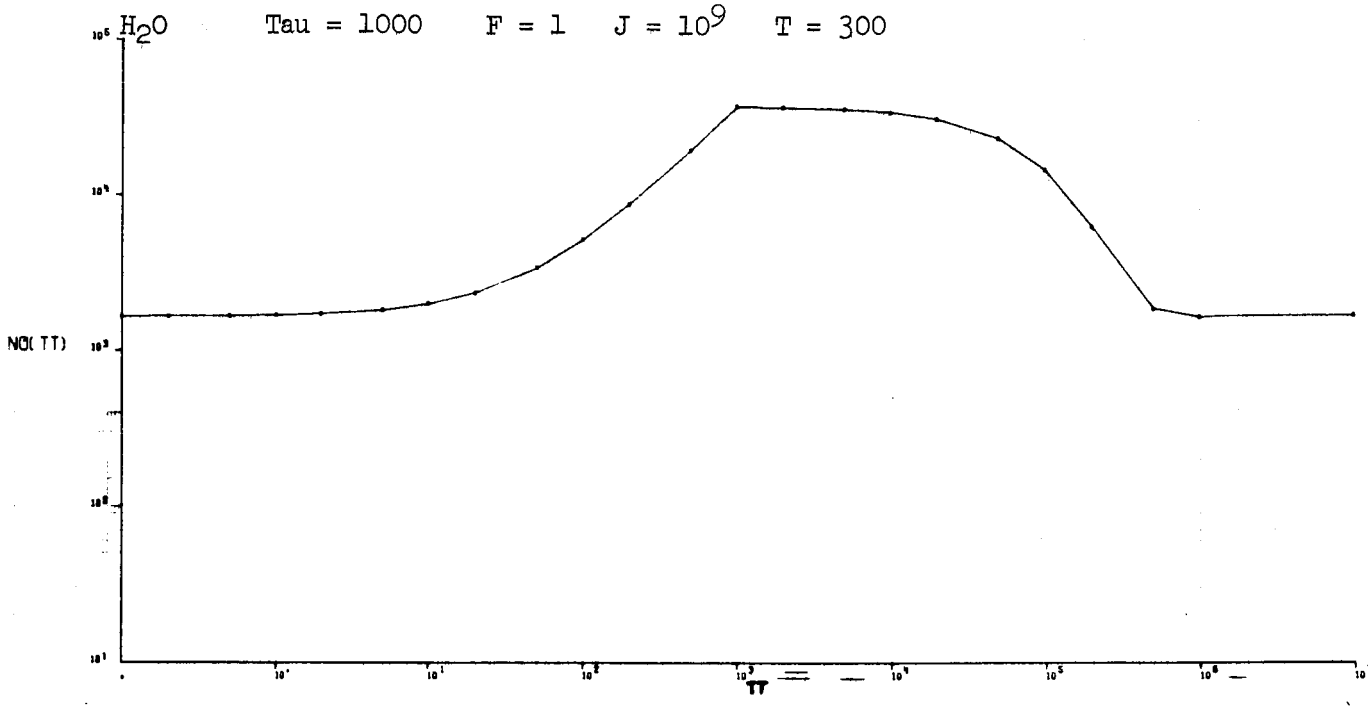

Fig. 14 Model I - H_2O Variation of LEM Exhaust Contamination With Time (Number of Particles/cm^3 versus Time in Seconds)

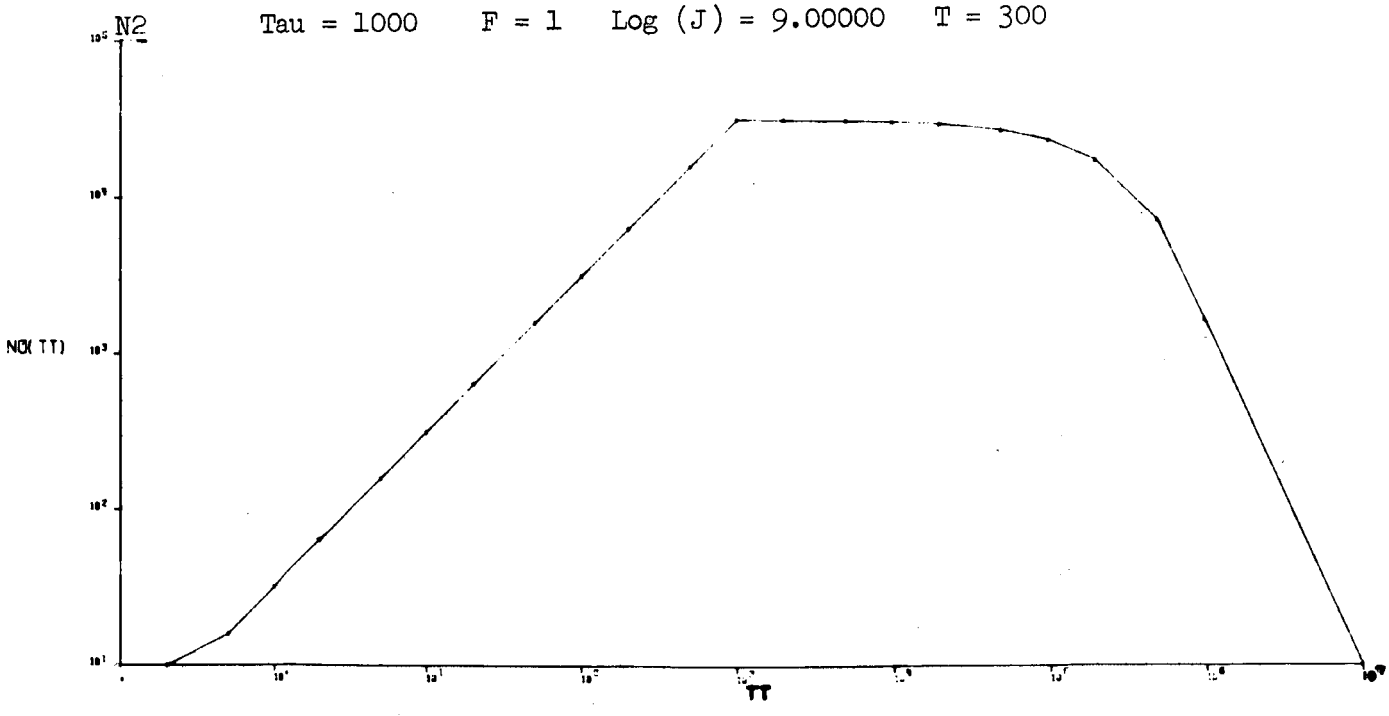

Fig. 15 Model I - N_2 Variation of LEM Exhaust Contamination With Time (Number of Particles/cm^3 versus Time in Seconds)

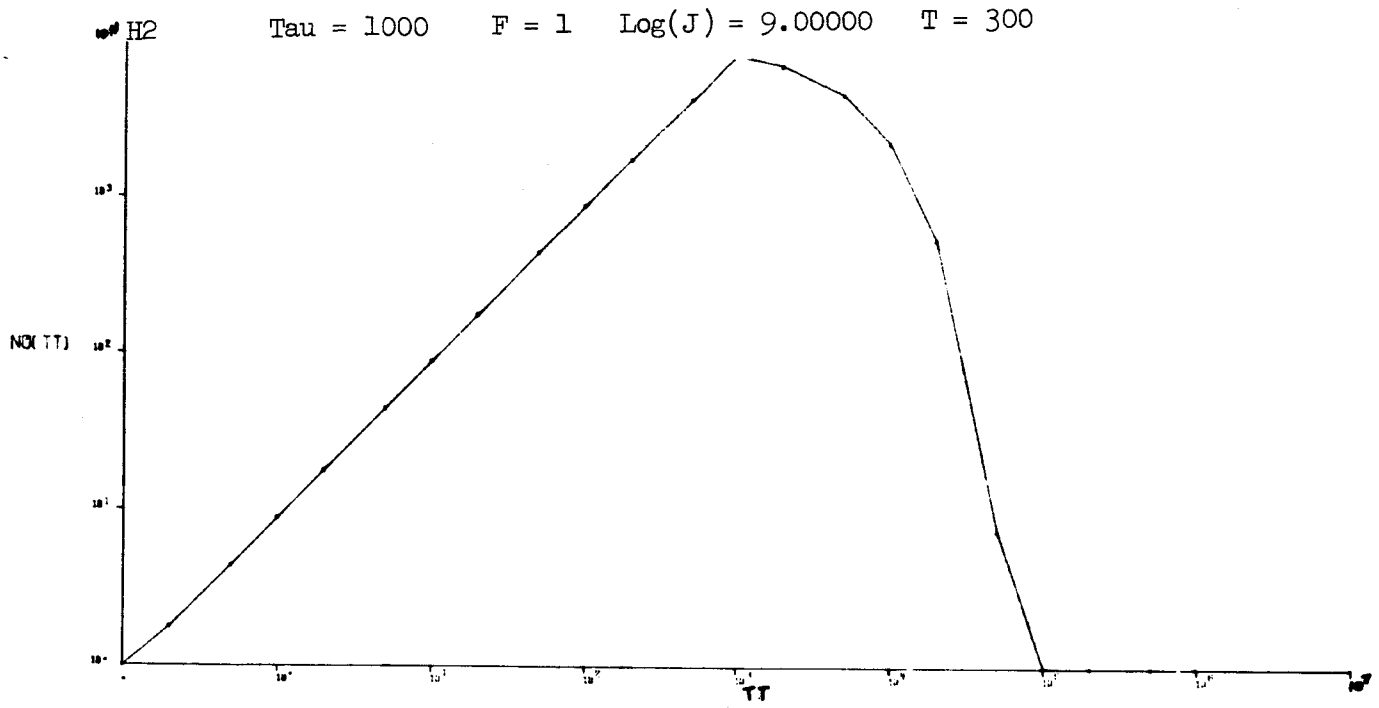

Fig. 16 Model I - H_2 Variation of LEM Exhaust Contamination With Time (Number of Particles/cm^3 versus Time in Seconds)

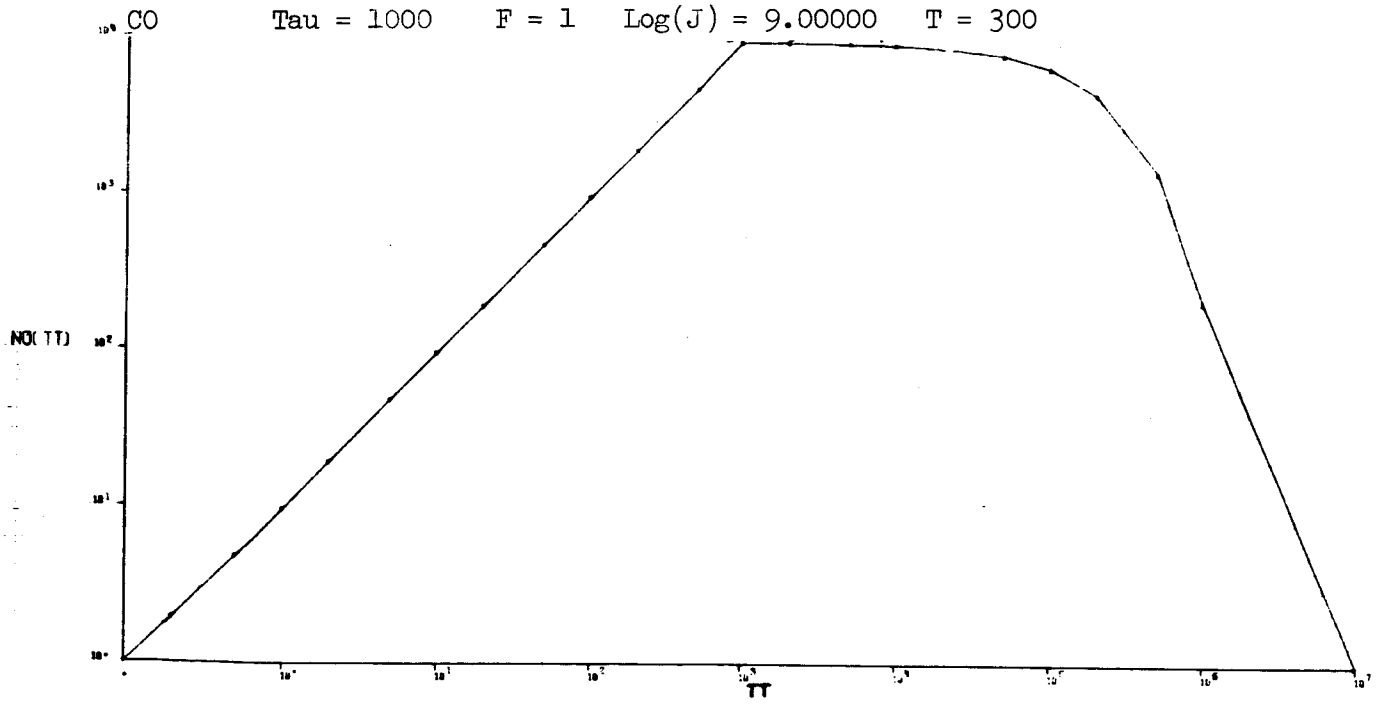

Fig. 17 Model I - CO Variation of LEM Exhaust Contamination With Time (Number of Particles/cm^3 versus Time in Seconds)

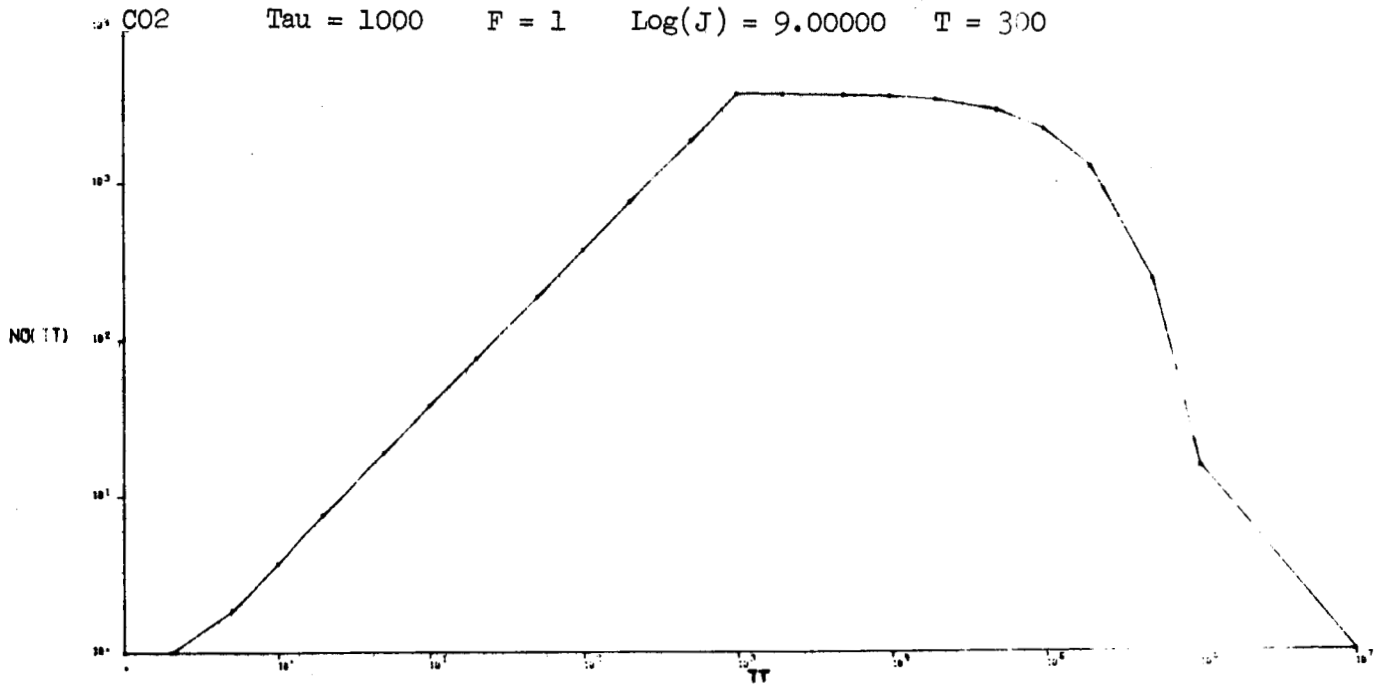

Fig. 18 Model I - CO_2 Variation of LEM Exhaust Contamination With Time (Number of Particles/cm^3 versus Time in Seconds)

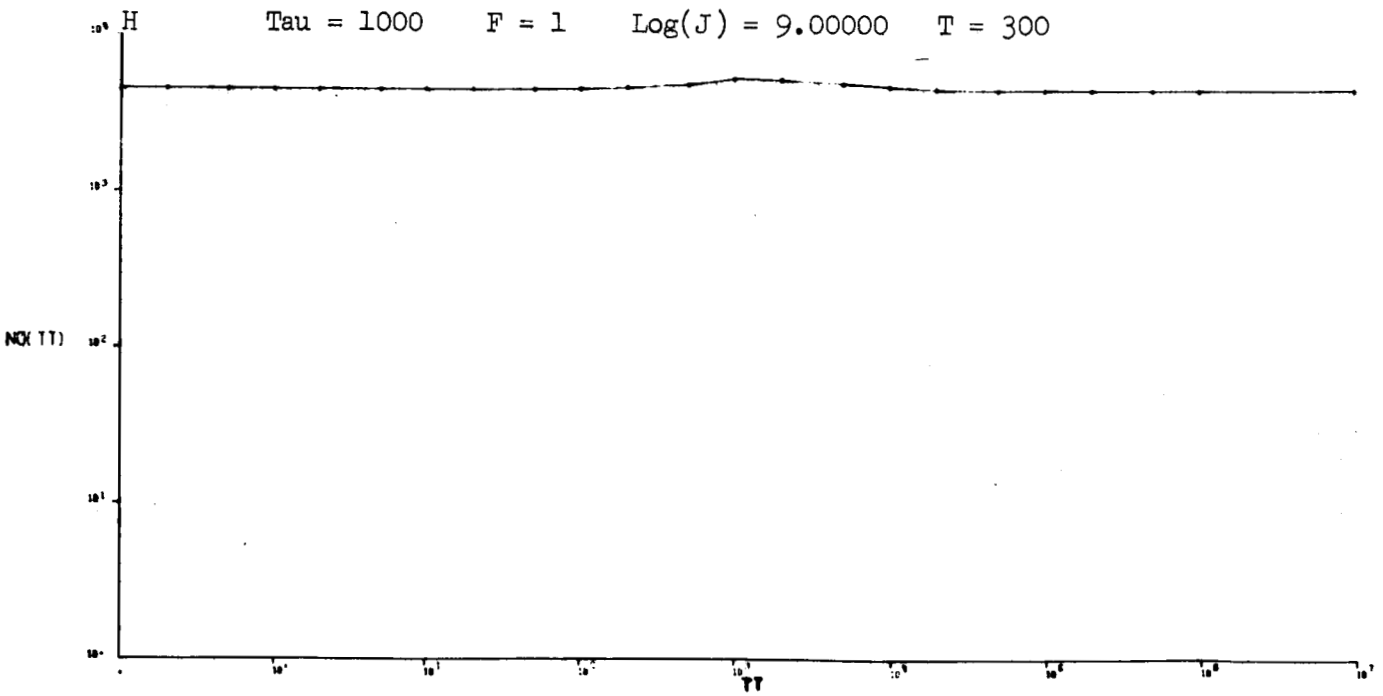

Fig. 19 Model I - H Variation of LEM Exhaust Contamination With Time (Number of Particles/cm^3 versus Time in Seconds)

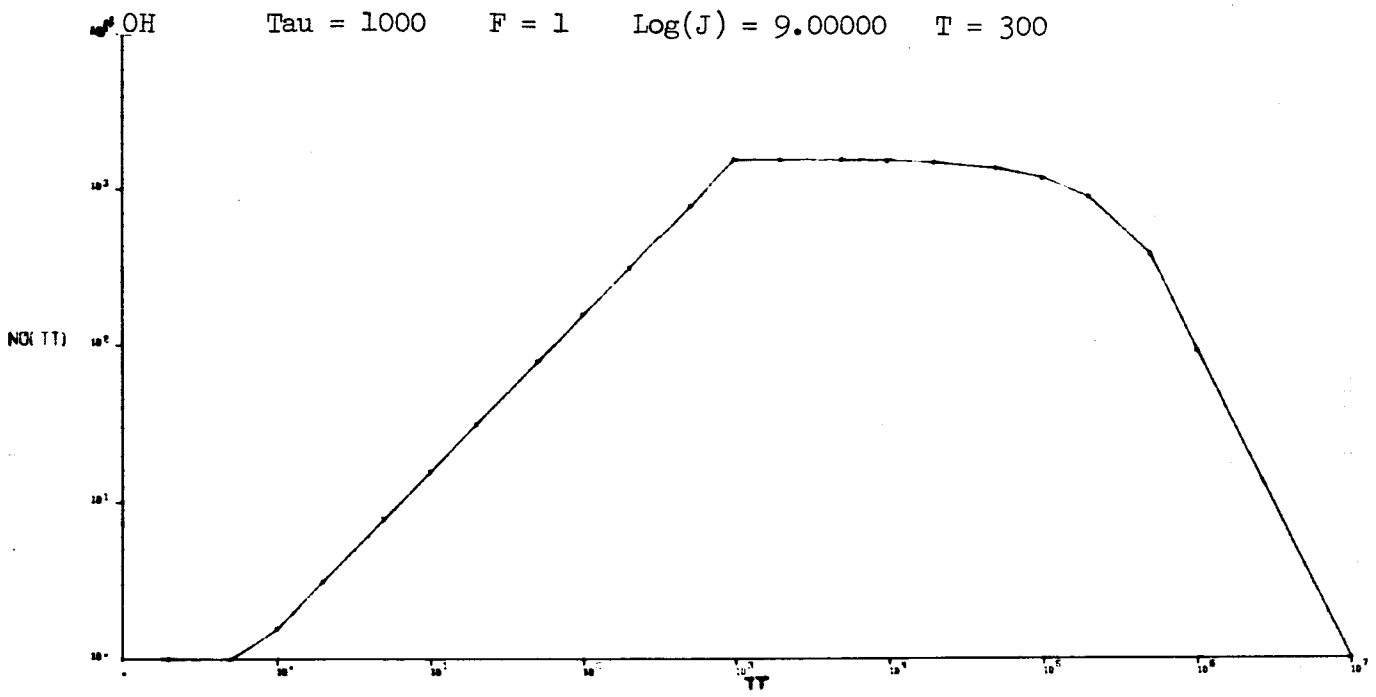

Fig. 20 Model I - OH Variation of LEM Exhaust Contamination With Time (Number of Particles/cm^3 versus Time in Seconds)

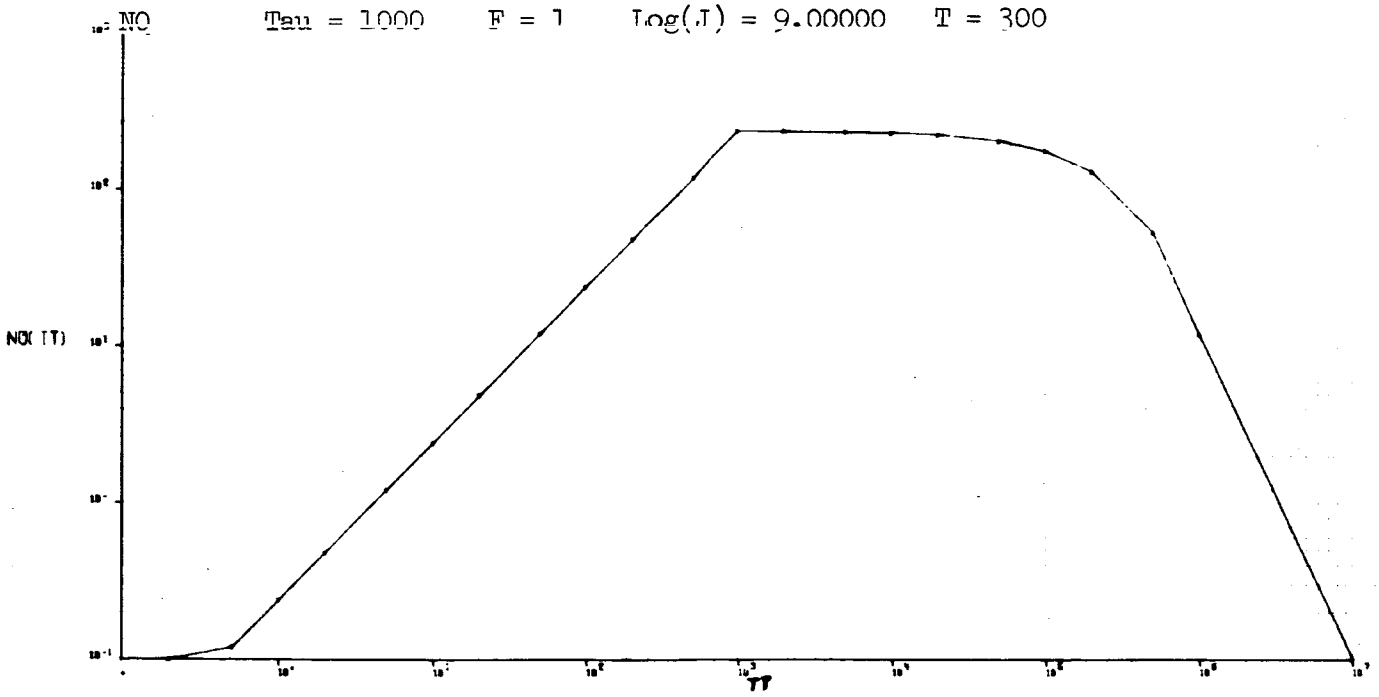

Fig. 21 Model I - NO Variation of LEM Exhaust Contamination With Time (Number of Particles/cm^3 versus Time in Seconds)

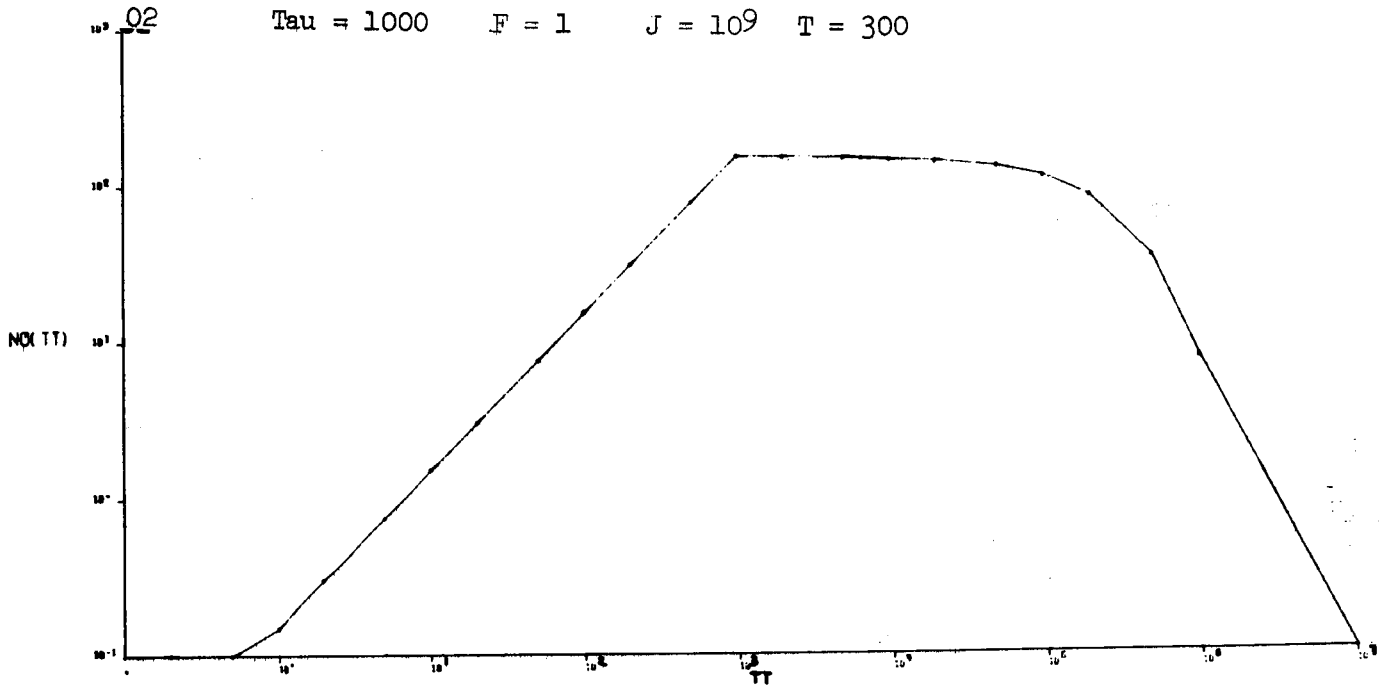

Fig. 22 Model I - O_2 Variation of LEM Exhaust Contamination With Time (Number of Particles/cm^3 versus Time in Seconds)

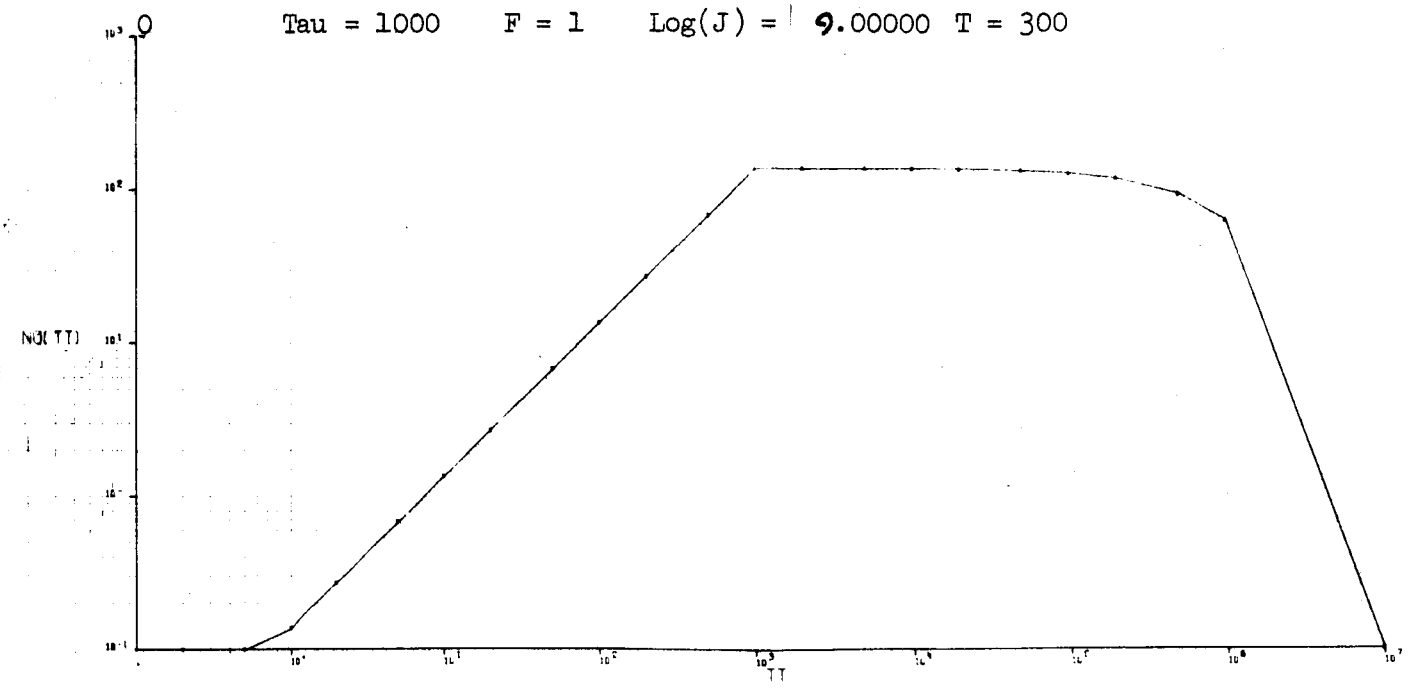

Fig. 23 Model I - O Variation of LEM Exhaust Contamination With Time (Number of Particles/cm^3 versus Time in Seconds)

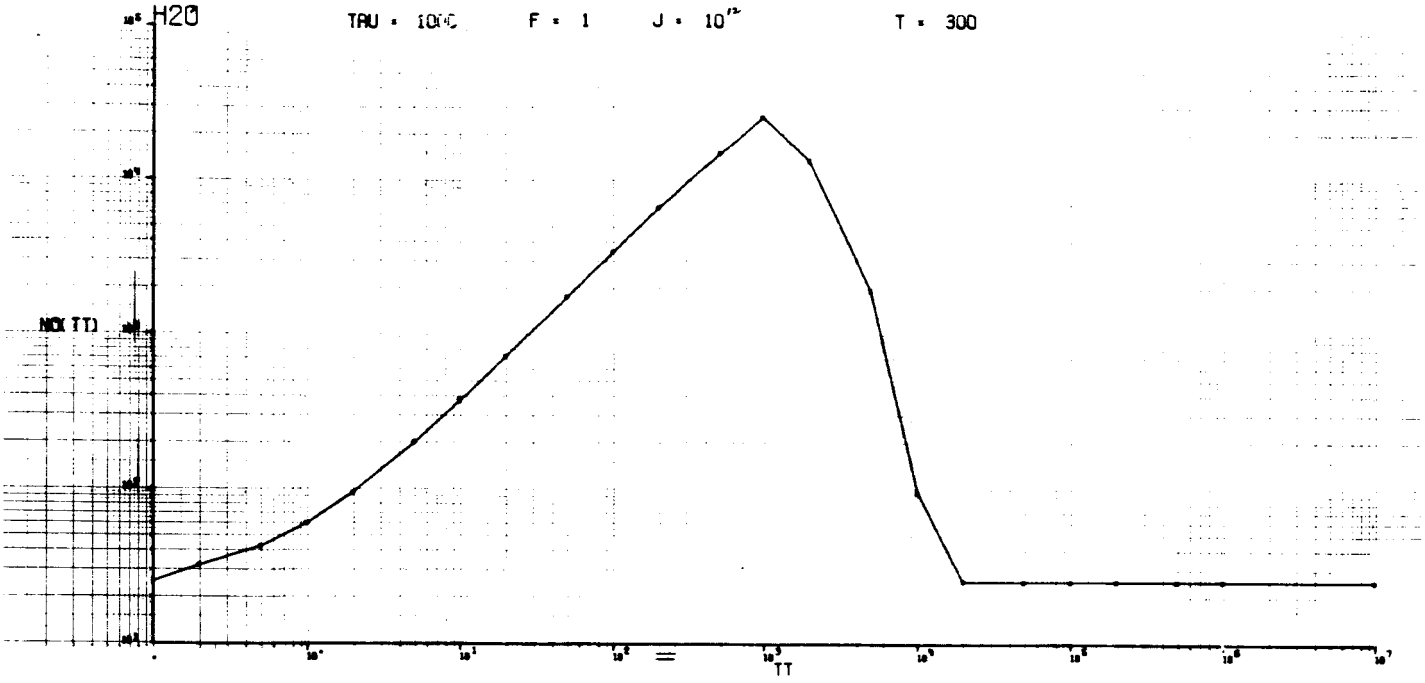

Fig. 24 Model I - H_2O Variation of LEM Exhaust Contamination With Time (Number of Particles/cm^3 versus Time in Seconds)

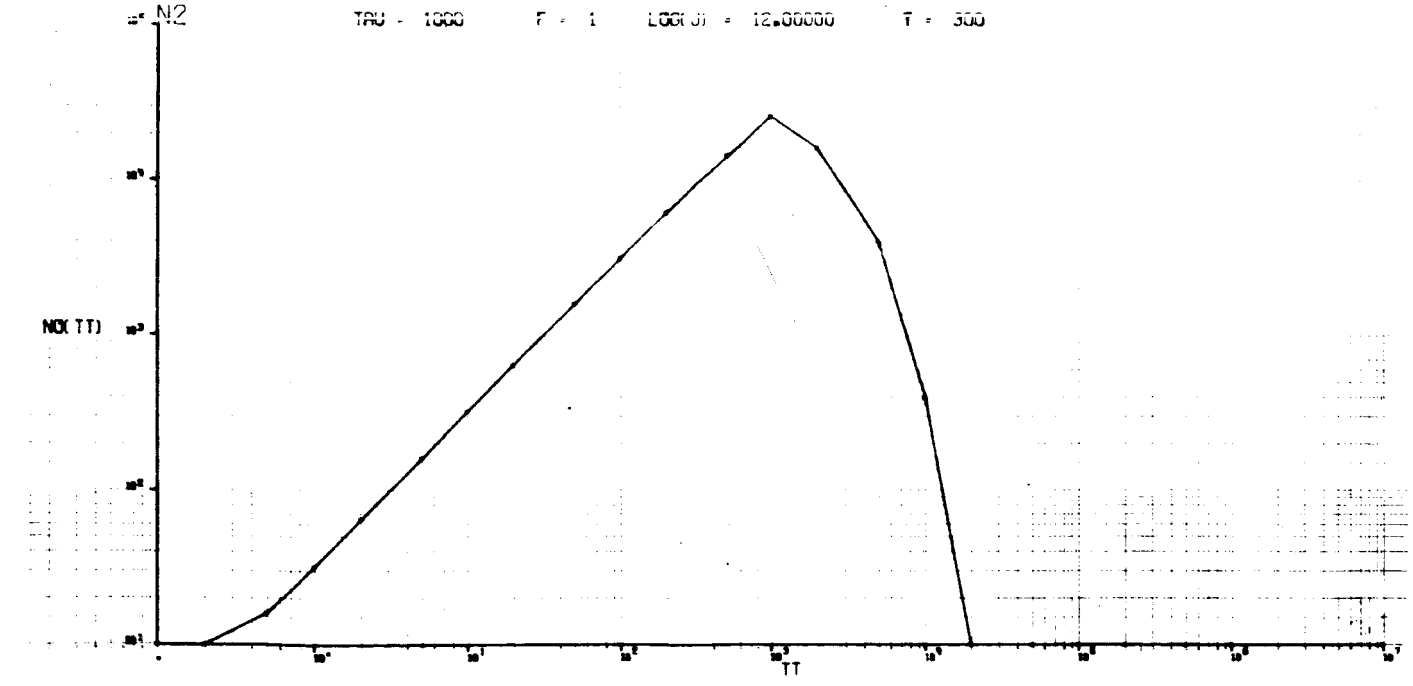

Fig. 25 Model I - N_2 Variation of LEM Exhaust Contamination With Time (Number of Particles/cm^3 versus Time in Seconds)

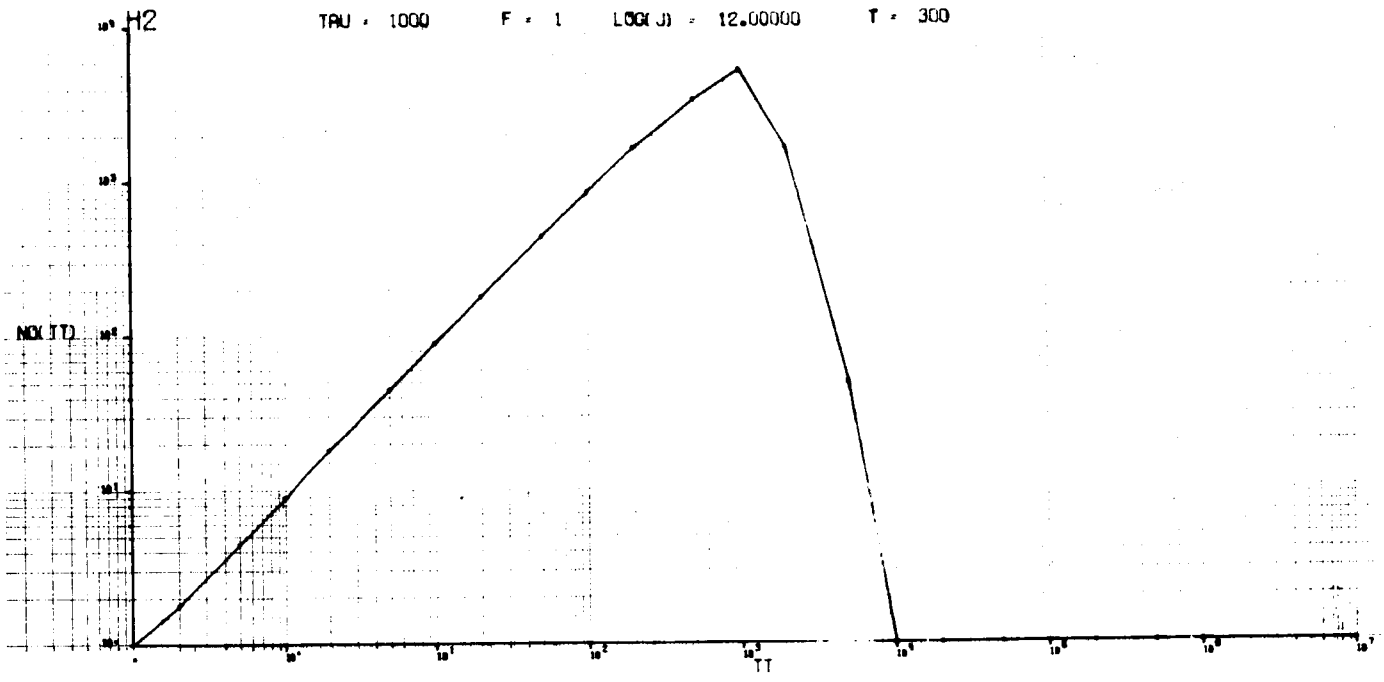

Fig. 26 Model I - H_2 Variation of LEM Exhaust Contamination With Time (Number of Particles/cm^3 versus Time in Seconds)

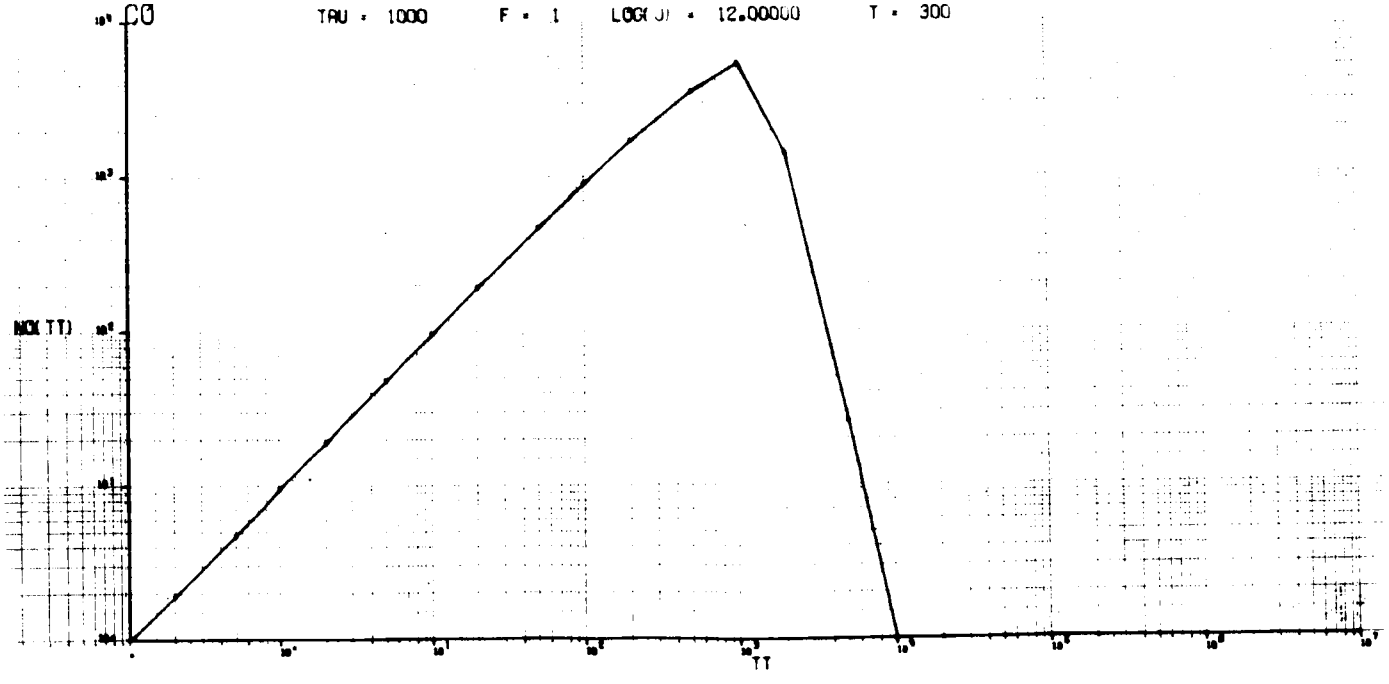

Fig. 27 Model I - CO Variation of LEM Exhaust Contamination With Time (Number of Particles/cm^3 versus Time in Seconds)

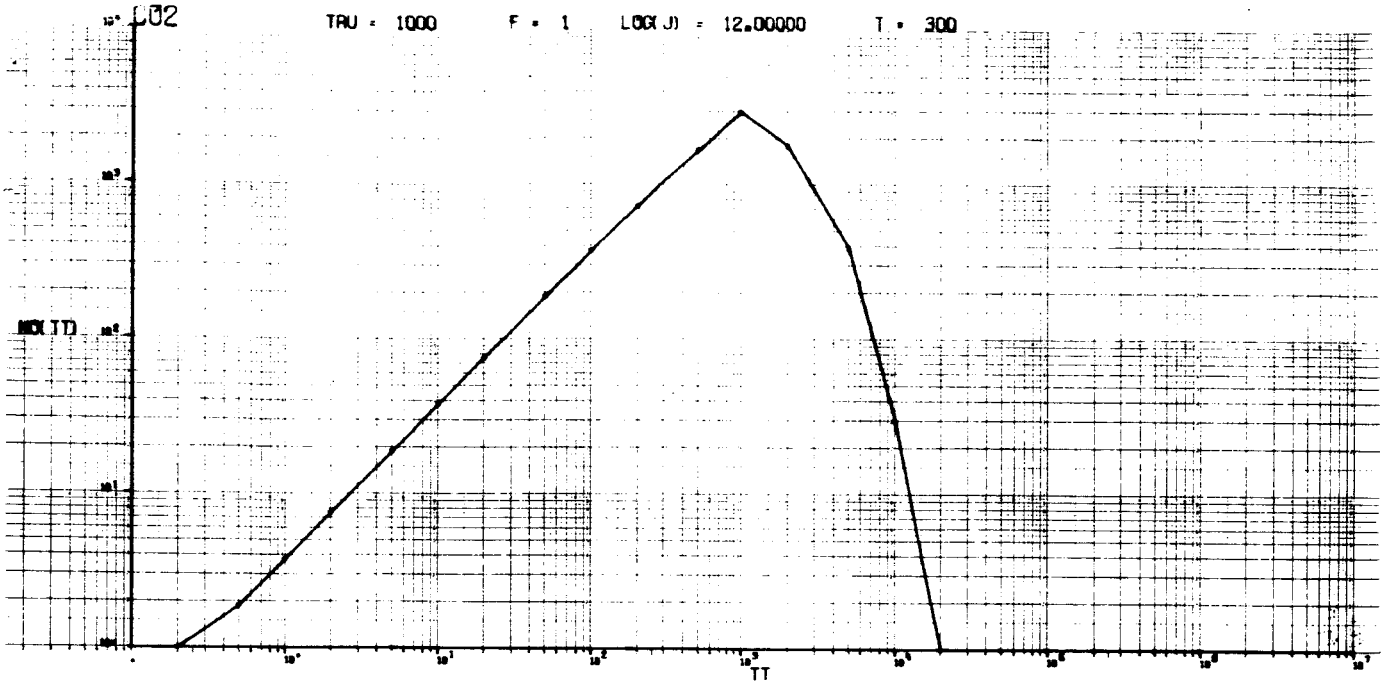

Fig. 28 Model I - CO_2 Variation of LEM Exhaust Contamination With Time (Number of Particles/cm^3 versus Time in Seconds)

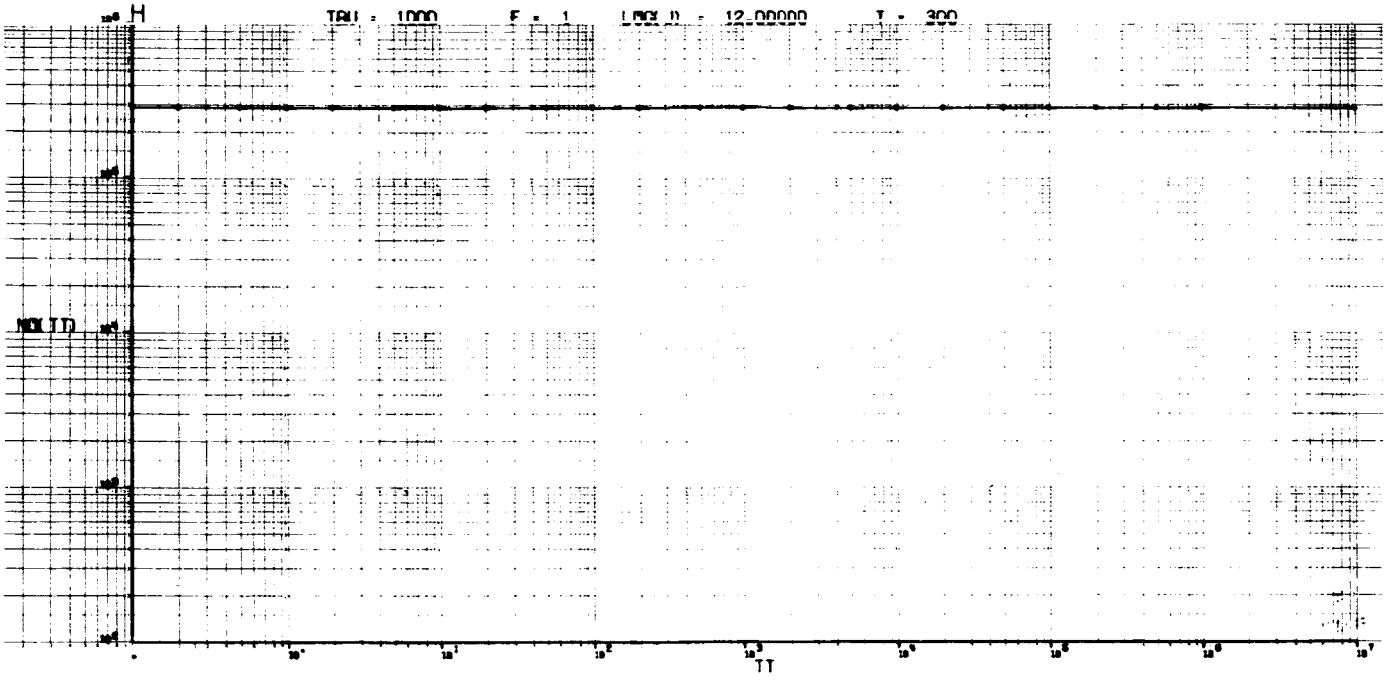

Fig. 29 Model I - H Variation of LEM Exhaust Contamination With Time (Number of Particles/cm^3 versus Time in Seconds)

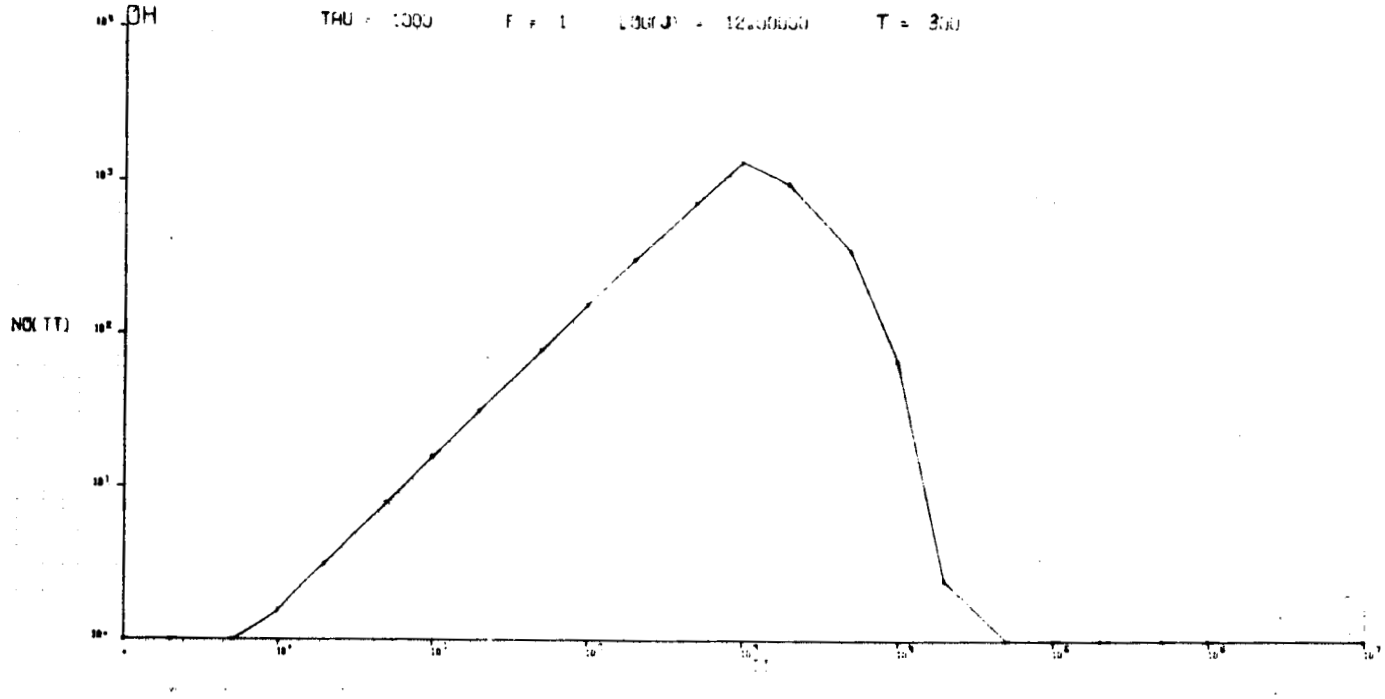

Fig. 30 Model I - OH Variation of LEM Exhaust Contamination With Time (Number of Particles/cm^3 versus Time in Seconds)

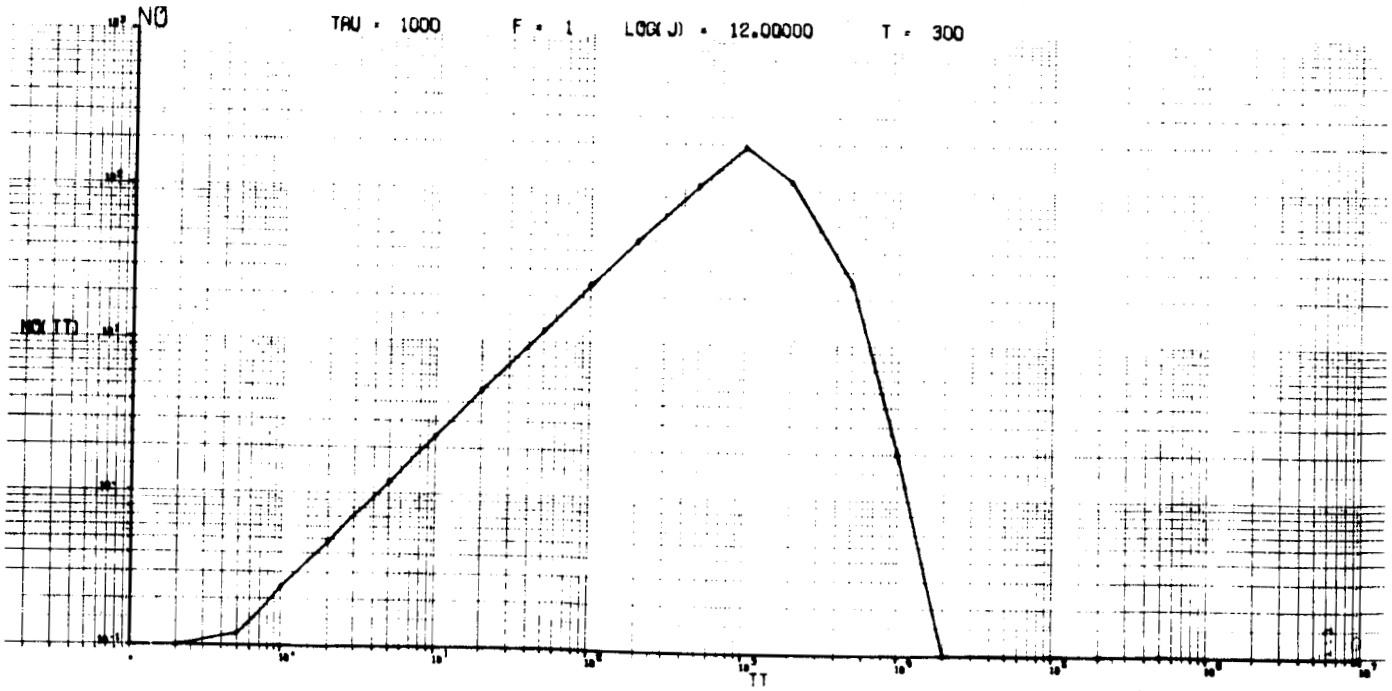

Fig. 31 Model I - NO Variation of LEM Exhaust Contamination With Time (Number of Particles/cm^3 versus Time in Seconds)

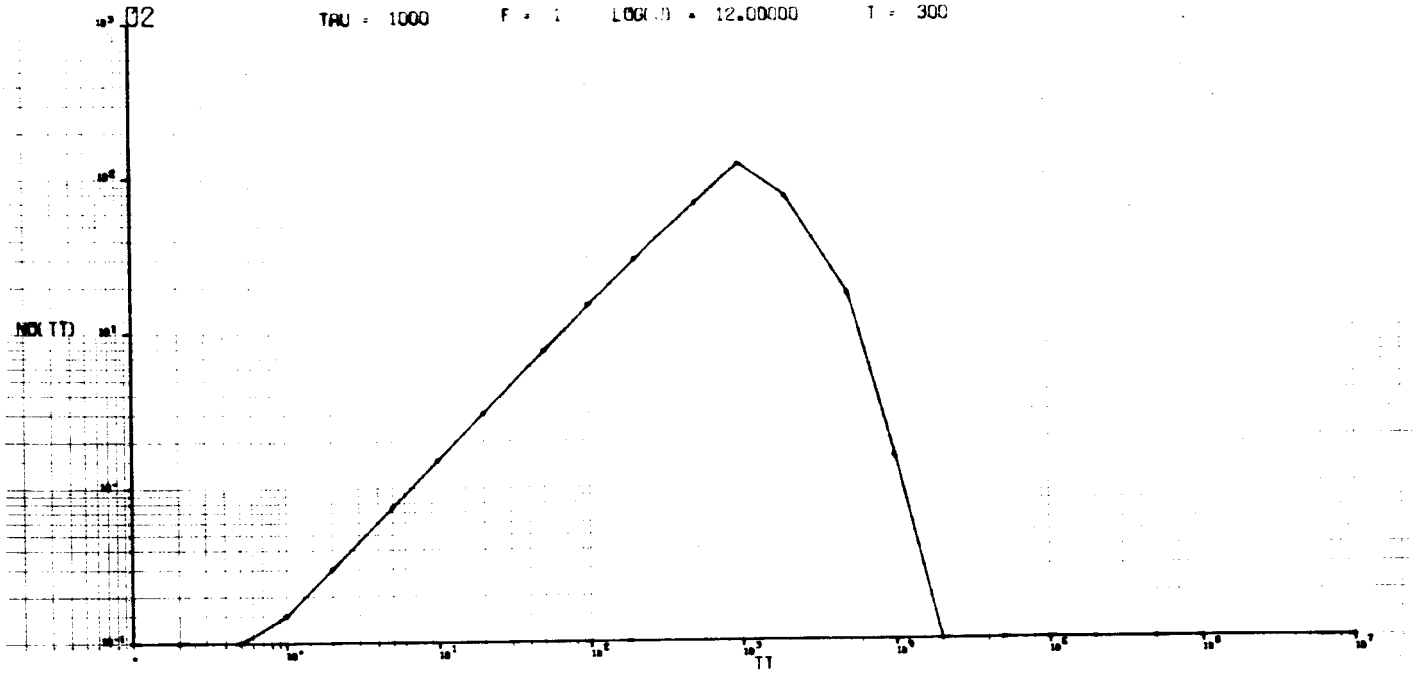

Fig. 32 Model I - O_2 Variation of LEM Exhaust Contamination With Time (Number of Particles/cm^3 versus Time in Seconds)

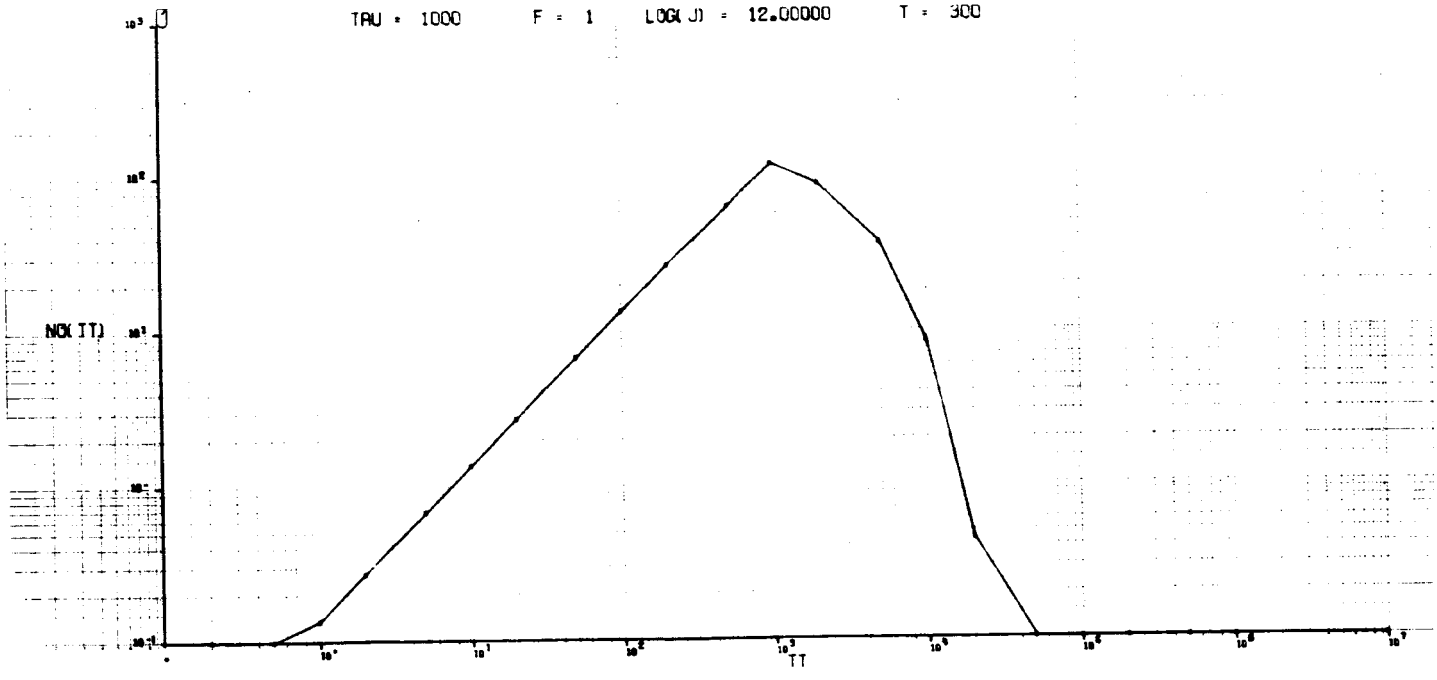

Fig. 33 Model I - O Variation of LEM Exhaust Contamination With Time (Number of Particles/cm^3 versus Time in Seconds)

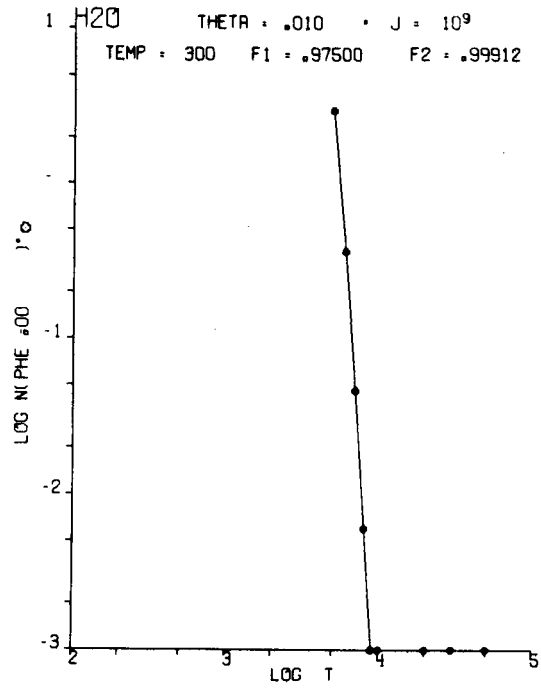

Fig. 34 Model II - H_2O Variation of LEM Exhaust Contamination with Time at 300 Meters from LEM Touchdown
$F_1 = 0.975$, $F_2 = 0.99912$

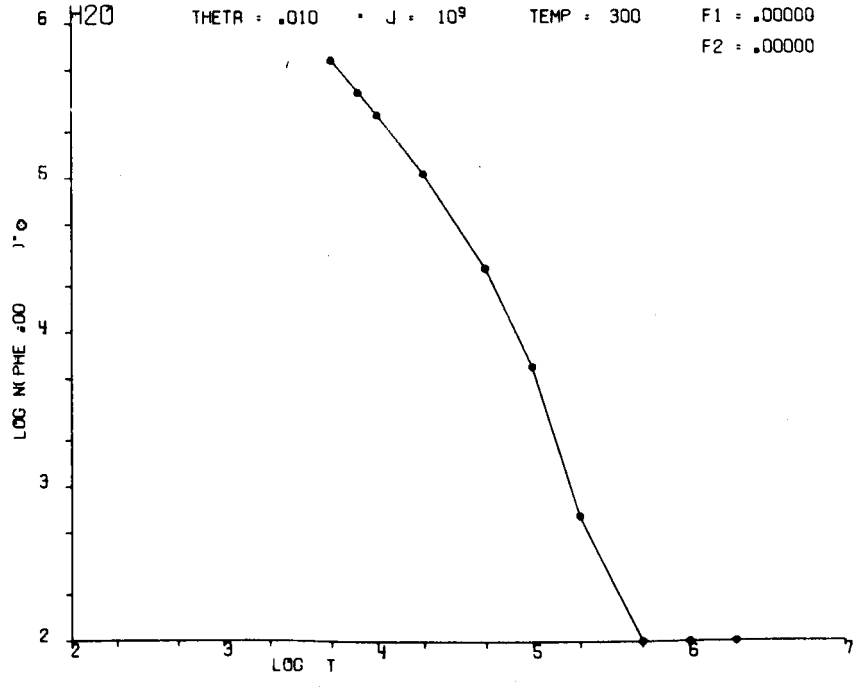

Fig. 35 Model II - H_2O Variation of LEM Exhaust Contamination with Time at 300 Meters from LEM Touchdown
$F_1 = 0$, $F_2 = 0$

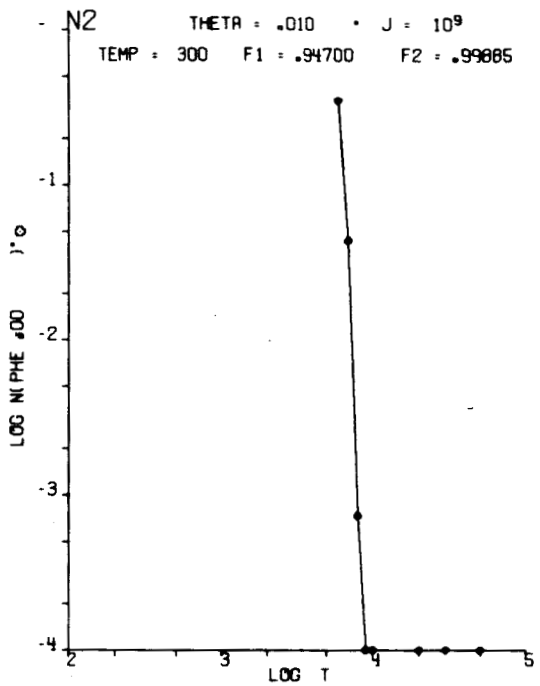

Fig. 36 Model II - N_2 Variation of LEM Exhaust Contamination with Time at 300 Meters from LEM Touchdown
$F_1 = 0.947$, $F_2 = 0.99885$

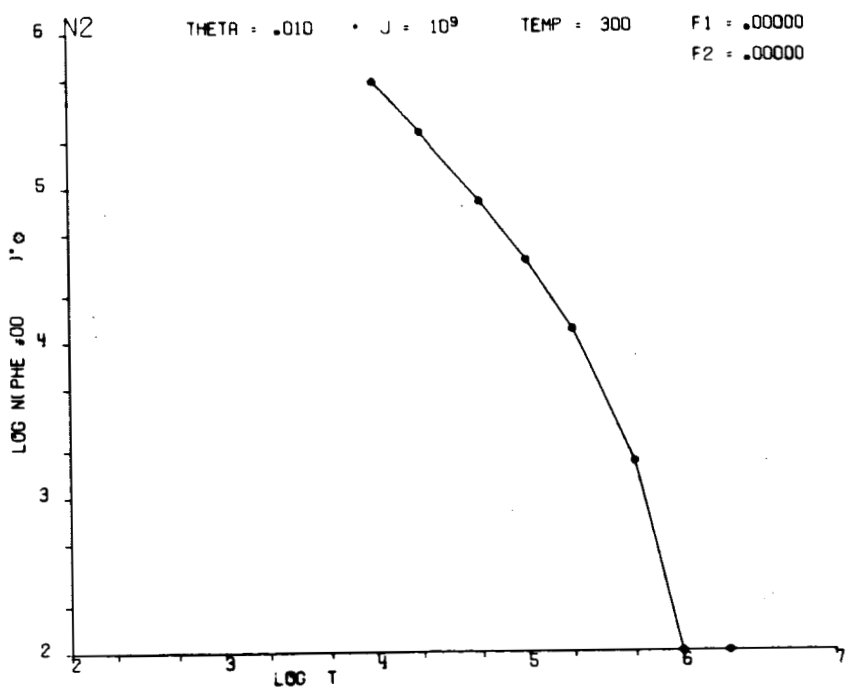

Fig. 37 Model II - N_2 Variation of LEM Exhaust Contamination with Time at 300 Meters from LEM Touchdown
$F_1 = 0$, $F_2 = 0$

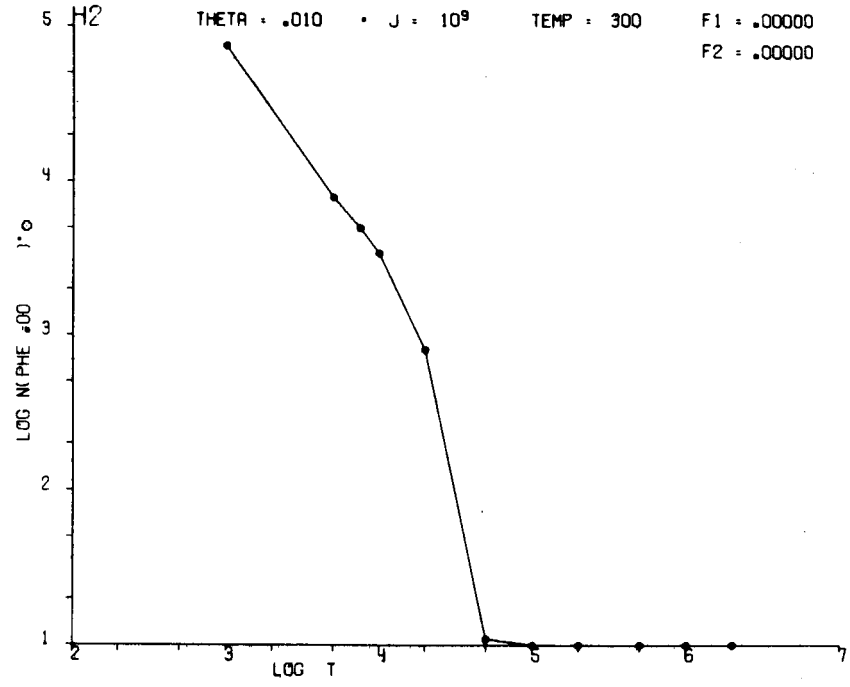

Fig. 38 Model II - H_2 Variation of LEM Exhaust Contamination with Time at 300 Meters from LEM Touchdown
$F_1 = 0, F_2 = 0$

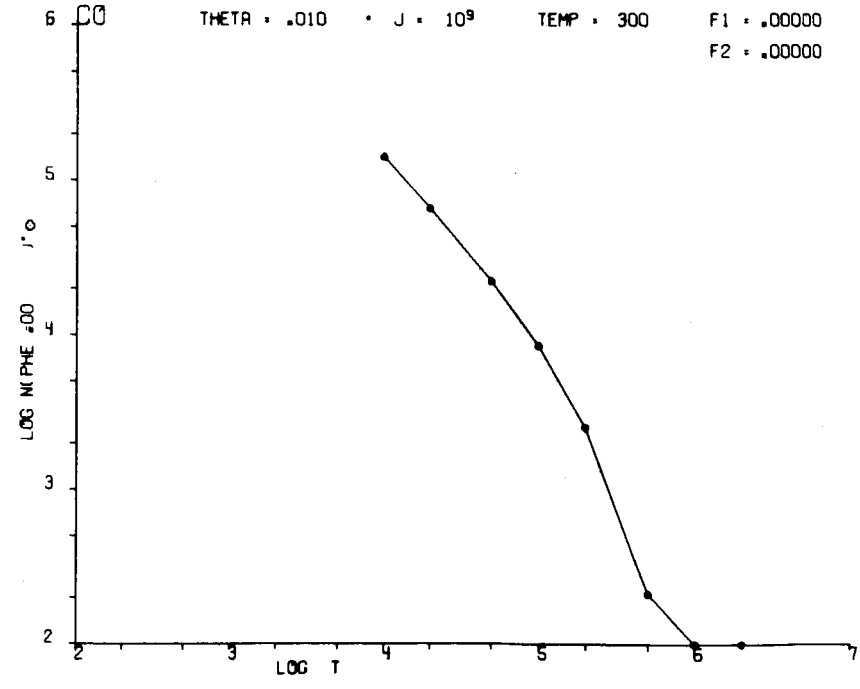

Fig. 39 Model II - CO Variation of LEM Exhaust Contamination with Time at 300 Meters from LEM Touchdown
$F_1 = 0, F_2 = 0$

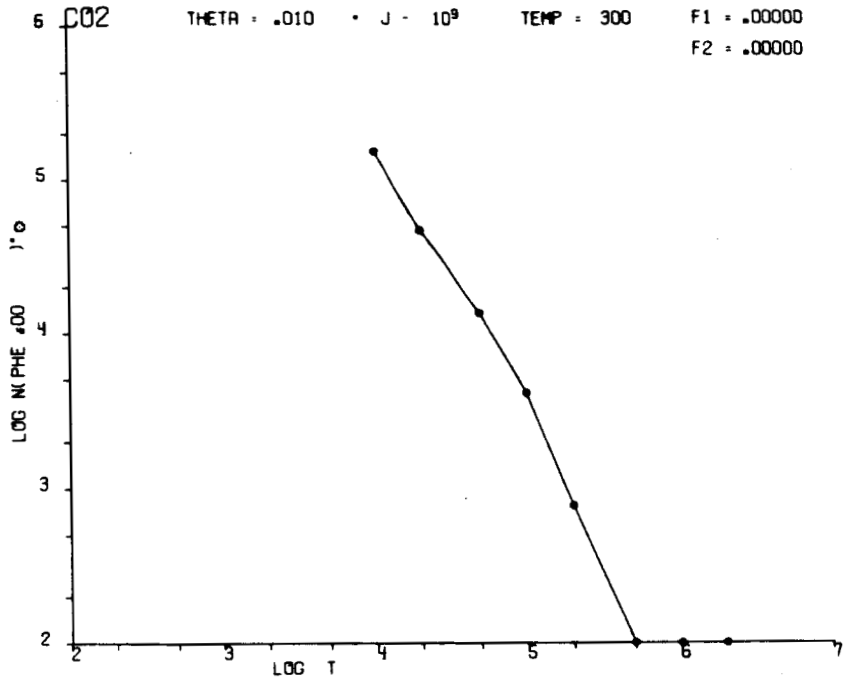

Fig. 40 Model II - CO_2 Variation of LEM Exhaust Contamination with Time at 300 Meters from LEM Touchdown
$F_1 = 0$, $F_2 = 0$

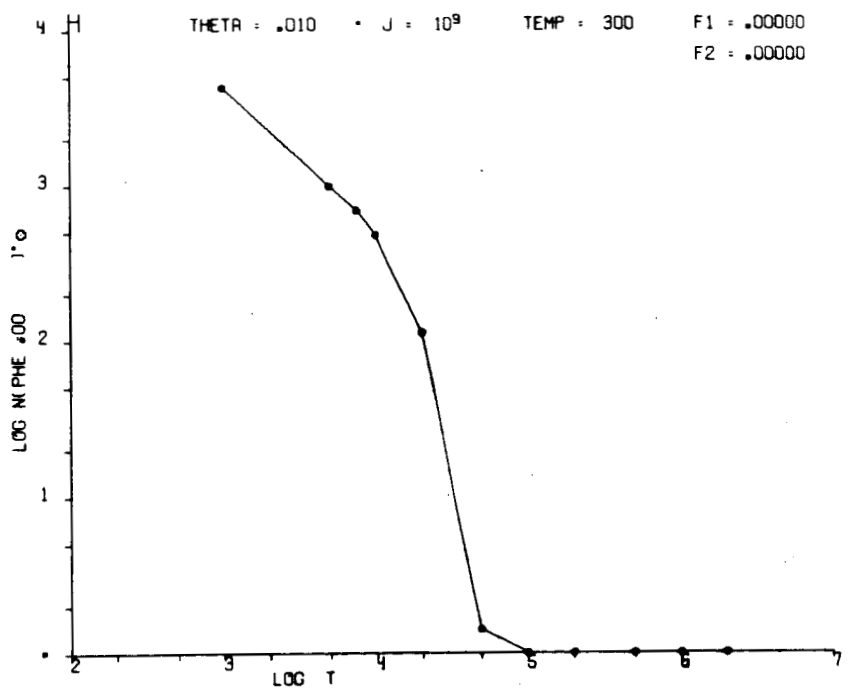

Fig. 41 Model II - H Variation of LEM Exhaust Contamination with Time at 300 Meters from LEM Touchdown
$F_1 = 0$, $F_2 = 0$

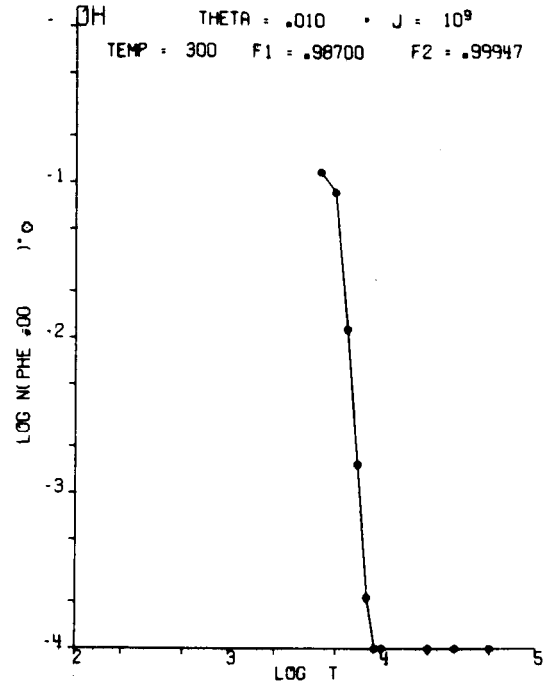

Fig. 42 Model II - OH Variation of LEM Exhaust Contamination with Time at 300 Meters from LEM Touchdown $F_1 = 0.987$, $F_2 = 0.99947$

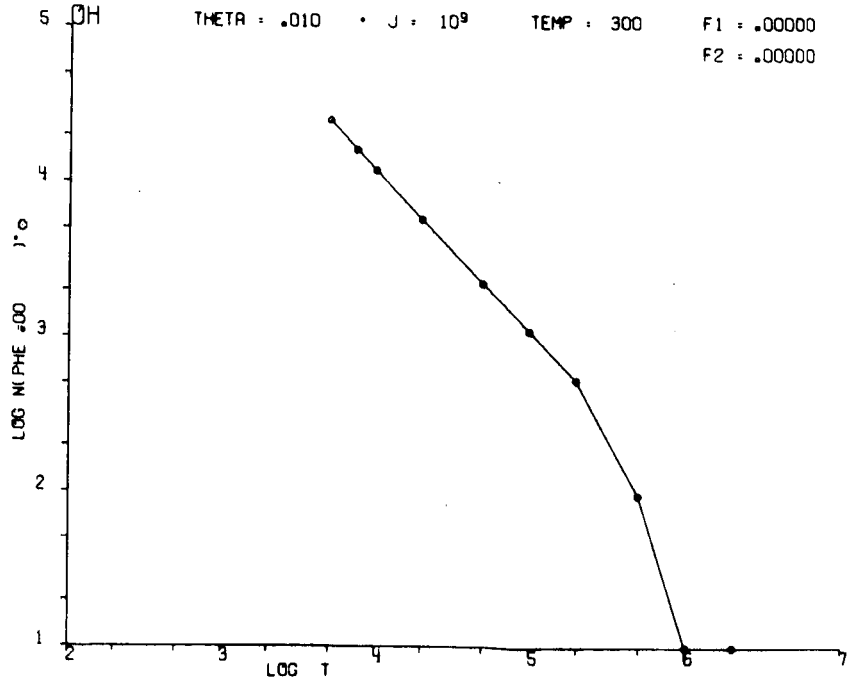

Fig. 43 Model II - OH Variation of LEM Exhaust Contamination with Time at 300 Meters from LEM Touchdown $F_1 = 0$, $F_2 = 0$

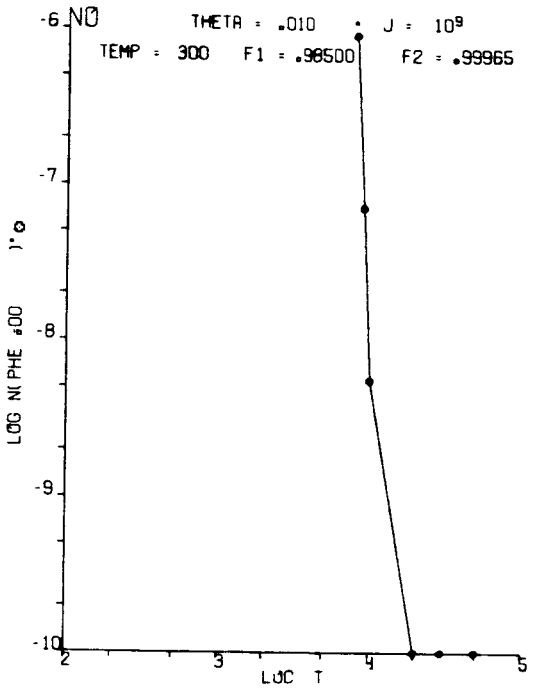

Fig. 44 Model II - NO Variation of LEM Exhaust Contamination with Time at 300 Meters from LEM Touchdown $F_1 = 0.985$, $F_2 = 0.99965$

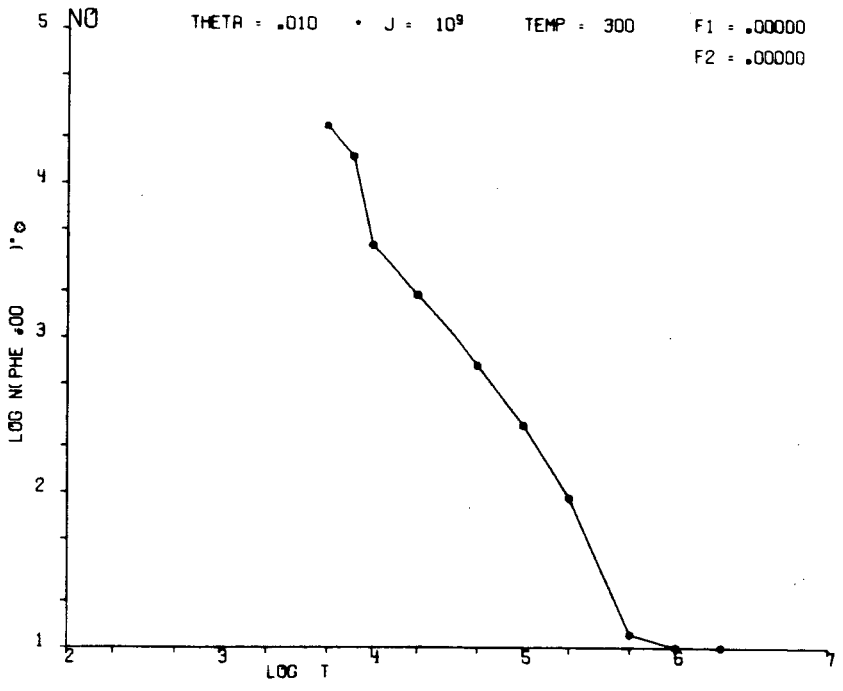

Fig. 45 - Model II - NO Variation of LEM Exhaust Contamination with Time at 300 Meters from LEM Touchdown $F_1 = 0$, $F_2 = 0$

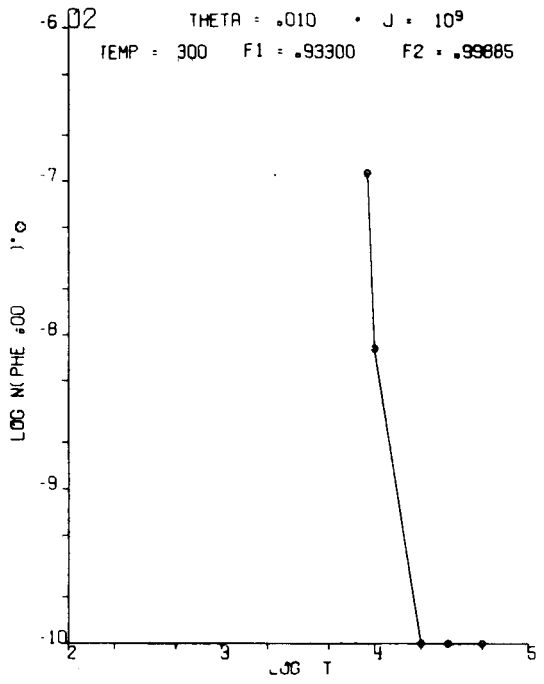

Fig. 46 Model II - O_2 Variation of LEM Exhaust Contamination with Time at 300 Meters from LEM Touchdown
$F_1 = 0.933$, $F_2 = 0.99885$

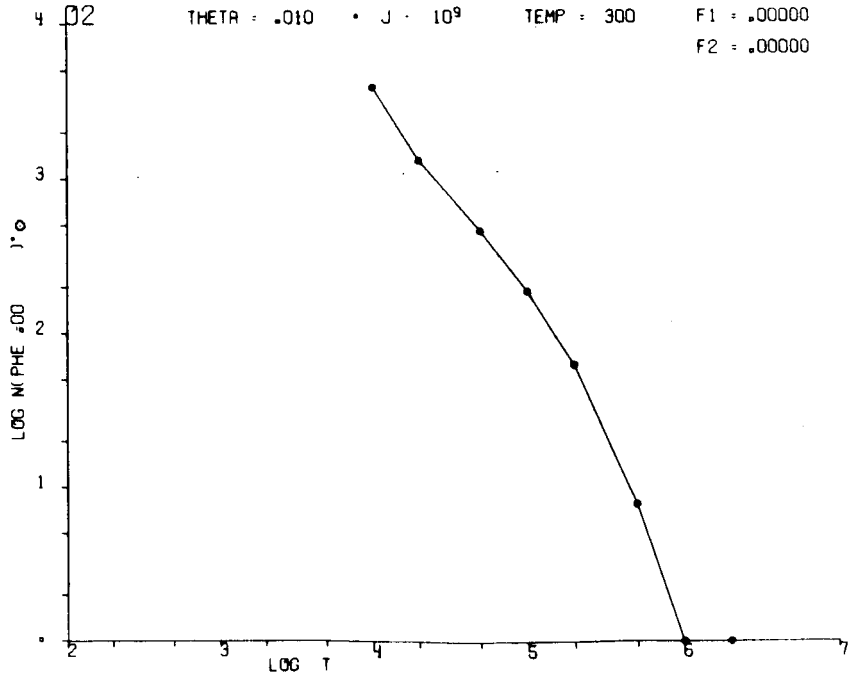

Fig. 47 Model II - O_2 Variation of LEM Exhaust Contamination with Time at 300 Meters from LEM Touchdown
$F_1 = 0$, $F_2 = 0$

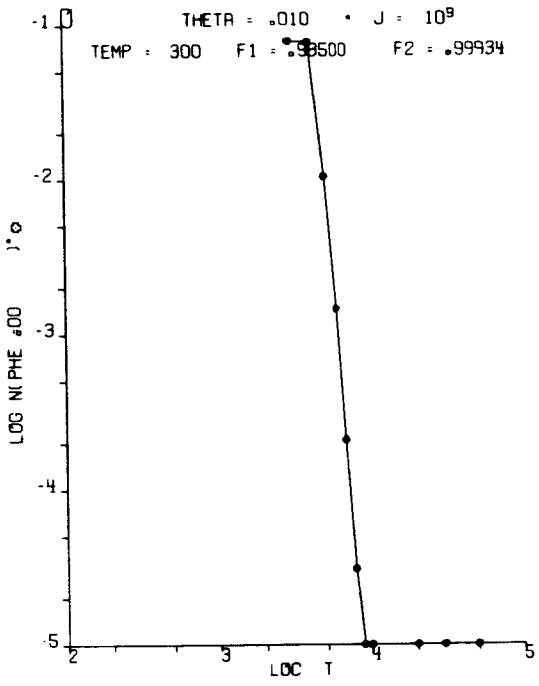

Fig. 48 Model II - O Variation of LEM Exhaust Contamination with Time at 300 Meters from LEM Touchdown $F_1 = 0.985$, $F_2 = 0.99934$

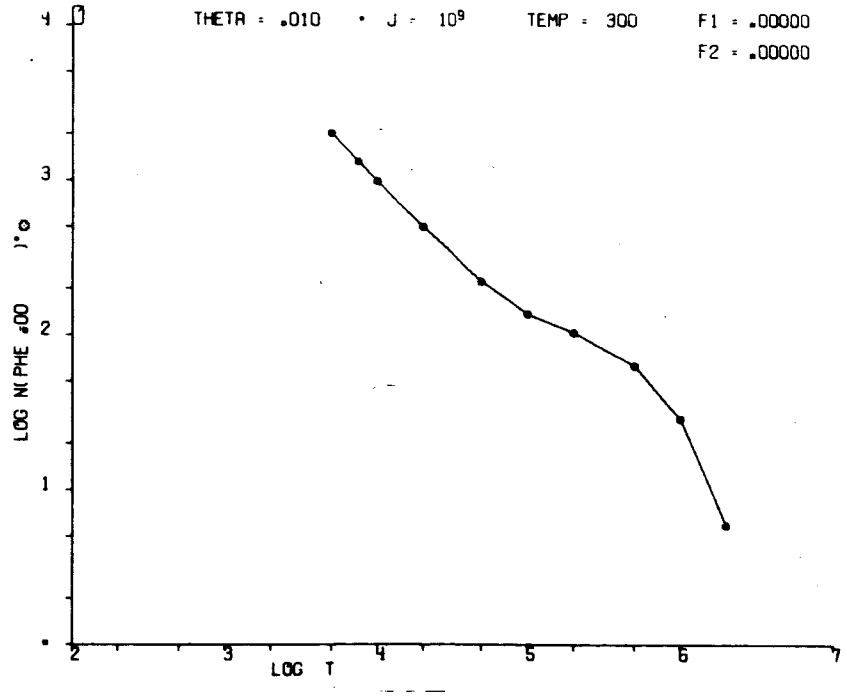

Fig. 49 Model II - O Variation of LEM Exhaust Contamination with Time at 300 Meters from LEM Touchdown $F_1 = 0$, $F_2 = 0$

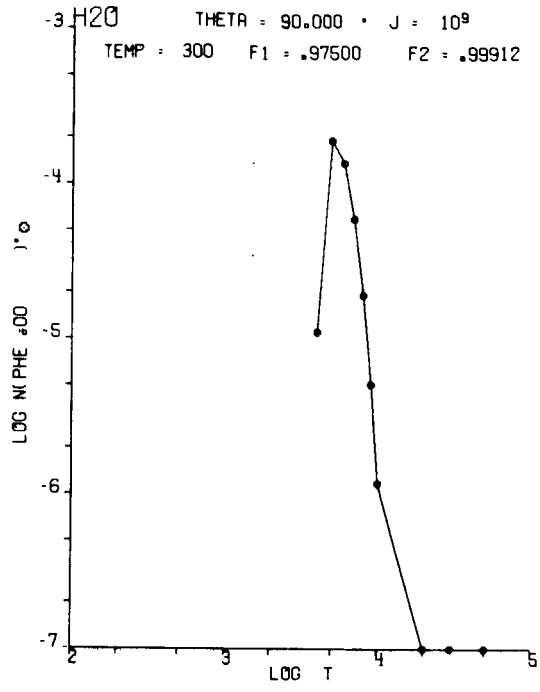

Fig. 50 Model II - H_2O Variation of LEM Exhaust Contamination with Time at 2700 km from LEM Touchdown
$F_1 = 0.975$, $F_2 = 0.9912$

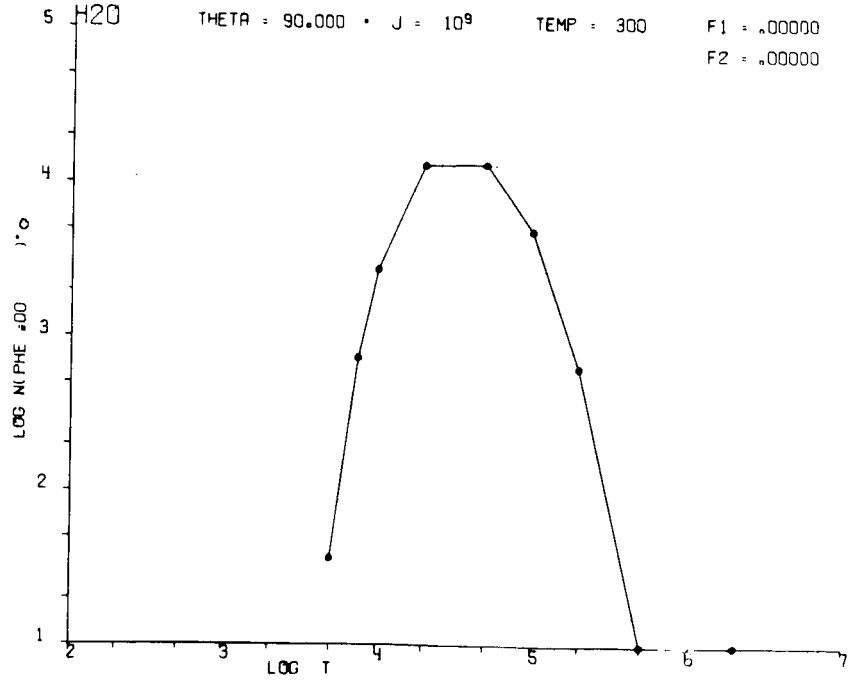

Fig. 51 Model II - H_2O Variation of LEM Exhaust Contamination with Time at 2700 km from LEM Touchdown
$F_1 = 0$, $F_2 = 0$

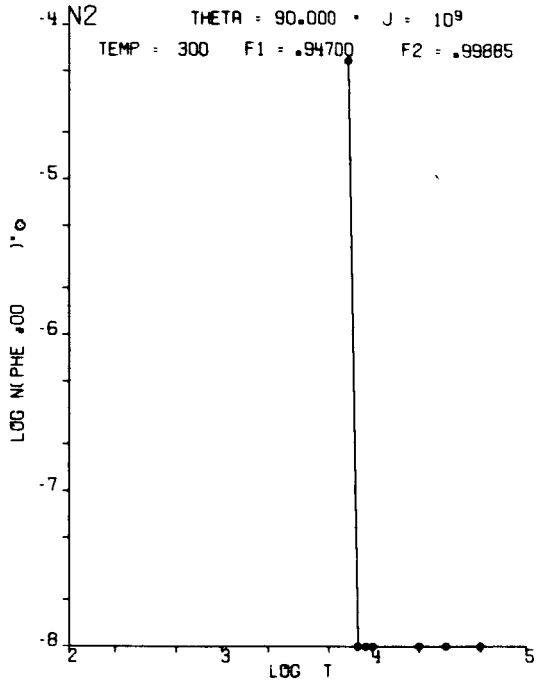

Fig. 52 Model II - N_2 Variation of LEM Exhaust Contamination with Time at 2700 km from LEM Touchdown $F_1 = 0.947$, $F_2 = 0.99885$

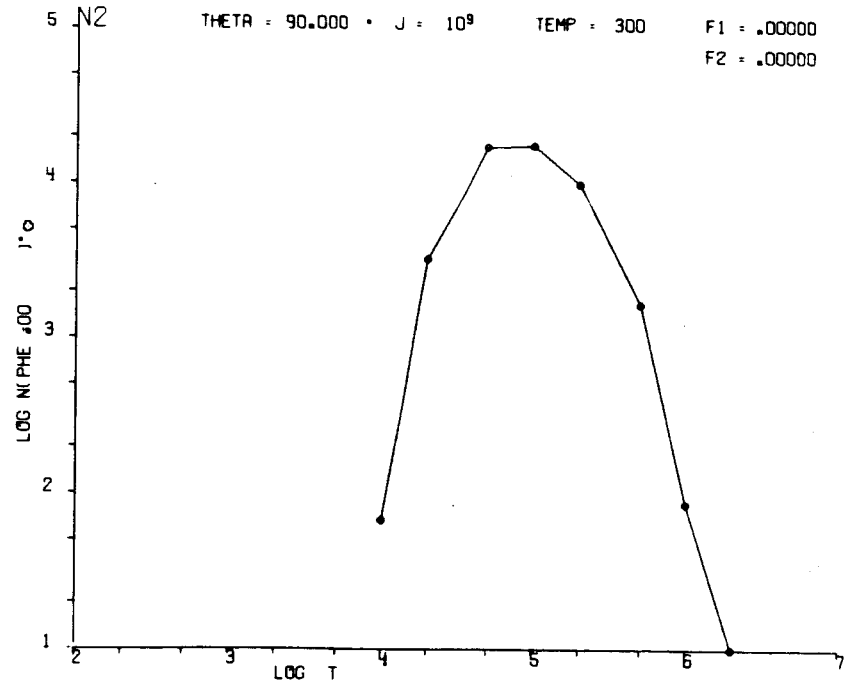

Fig. 53 Model II - N_2 Variation of LEM Exhaust Contamination with Time at 2700 km from LEM Touchdown $F_1 = 0$, $F_2 = 0$

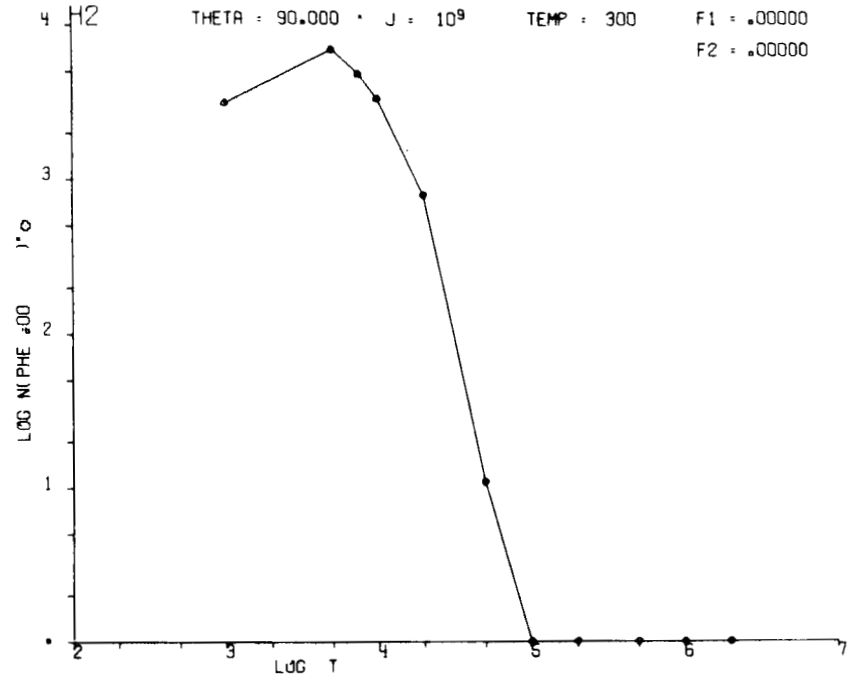

Fig. 54 Model II - H_2 Variation of LEM Exhaust Contamination with Time at 2700 km from LEM Touchdown
$F_1 = 0$, $F_2 = 0$

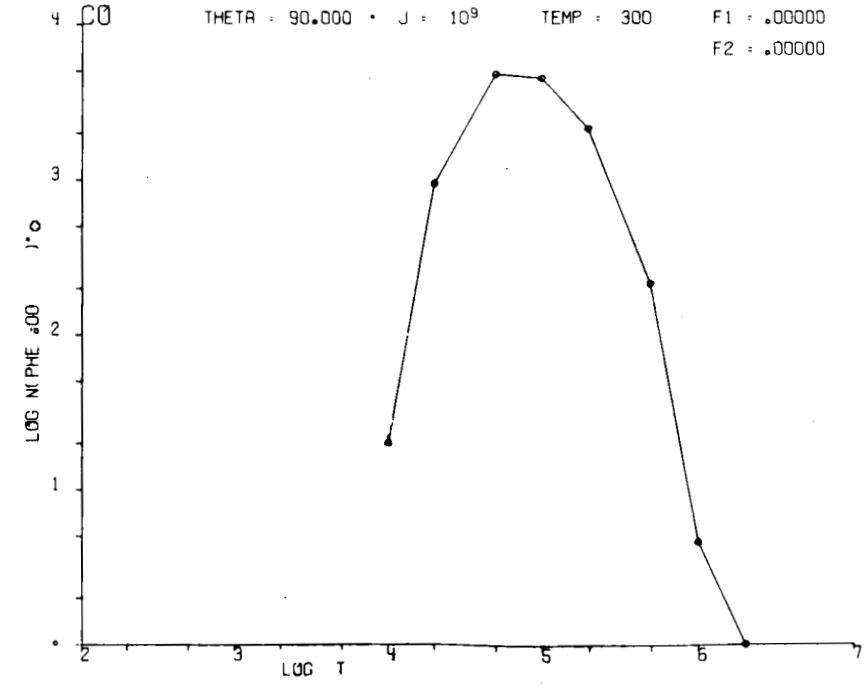

Fig. 55 Model II - CO Variation of LEM Exhaust Contamination with Time at 2700 km from LEM Touchdown
$F_1 = 0$, $F_2 = 0$

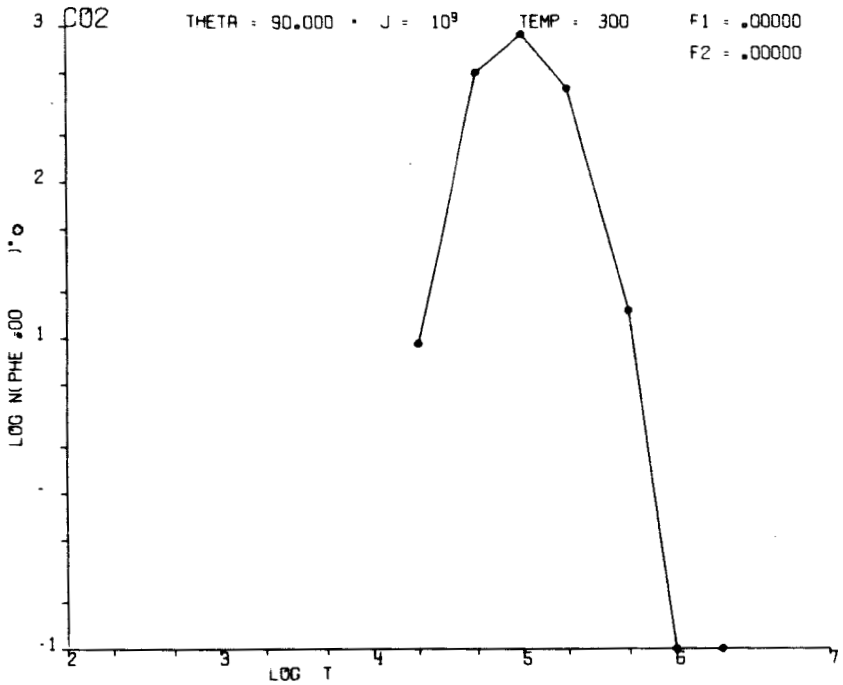

Fig. 56 Model II - CO_2 Variation of LEM Exhaust Contamination with Time at 2700 km from LEM Touchdown
$F_1 = 0$, $F_2 = 0$

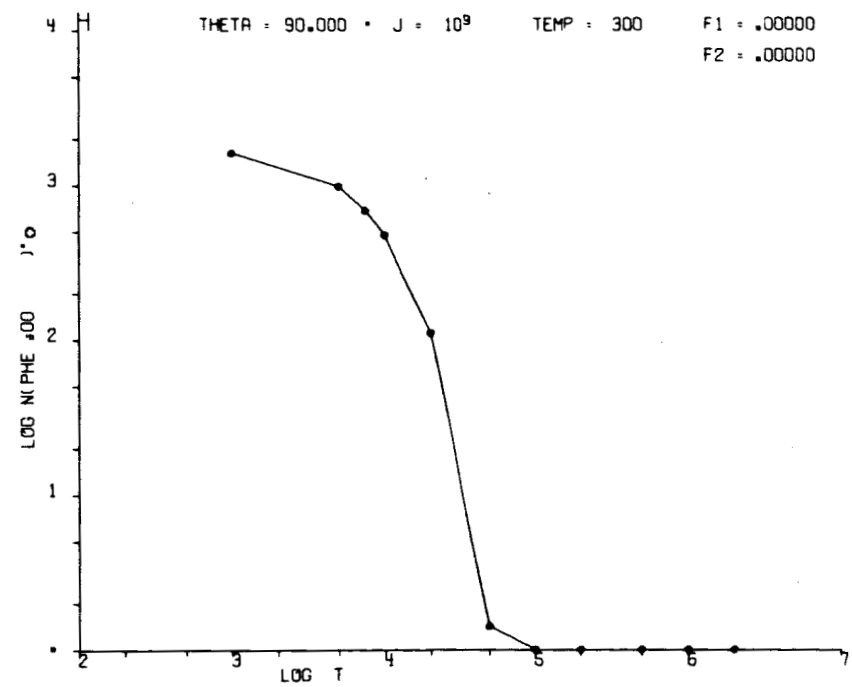

Fig. 57 Model II - H Variation of LEM Exhaust Contamination with Time at 2700 km from LEM Touchdown
$F_1 = 0$, $F_2 = 0$

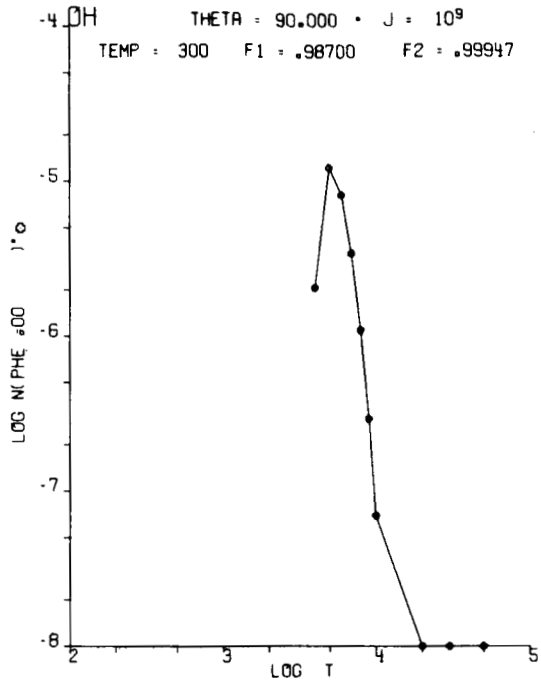

Fig. 58 Model II - OH Variation of LEM Exhaust Contamination with Time at 2700 km from LEM Touchdown
$F_1 = 0.987$, $F_2 = 0.99947$

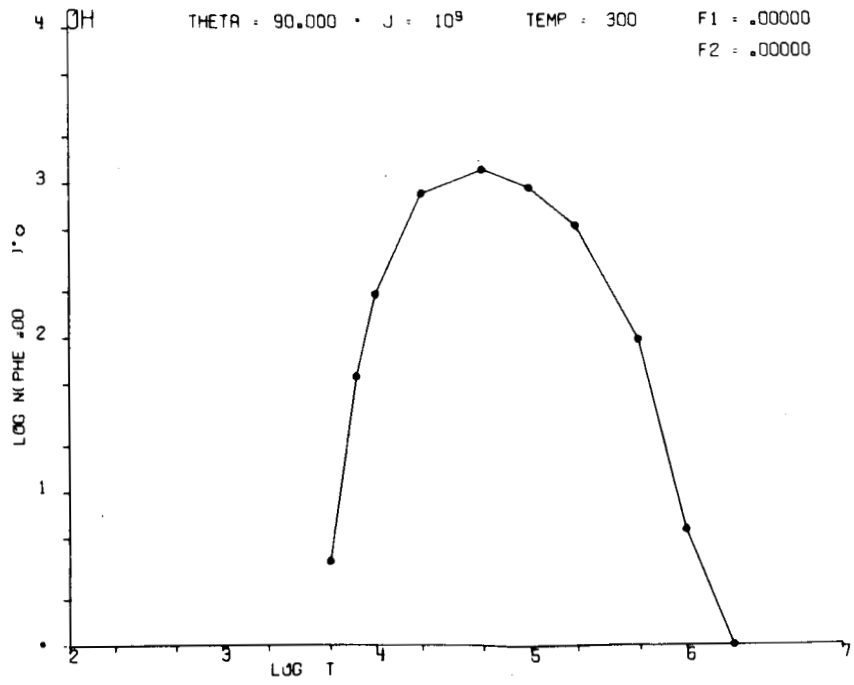

Fig. 59 Model II - OH Variation of LEM Exhaust Contamination with Time at 2700 km from LEM Touchdown
$F_1 = 0$, $F_2 = 0$

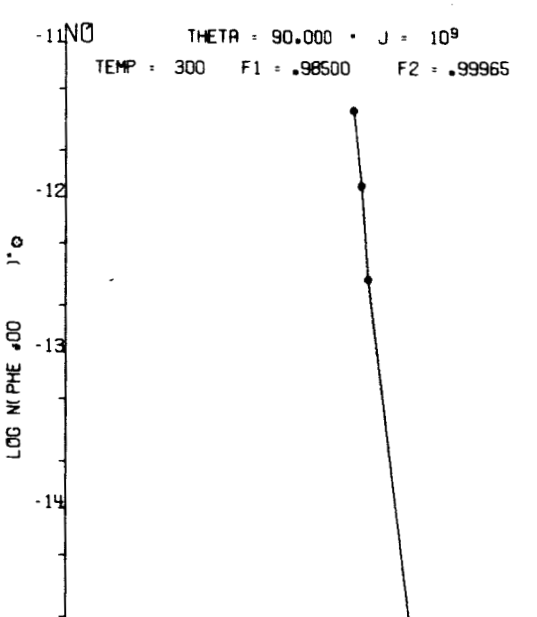

Fig. 60 Model II - NO Variation of LEM Exhaust Contamination with Time at 2700 km from LEM Touchdown
$F_1 = 0.985$, $F_2 = 0.99965$

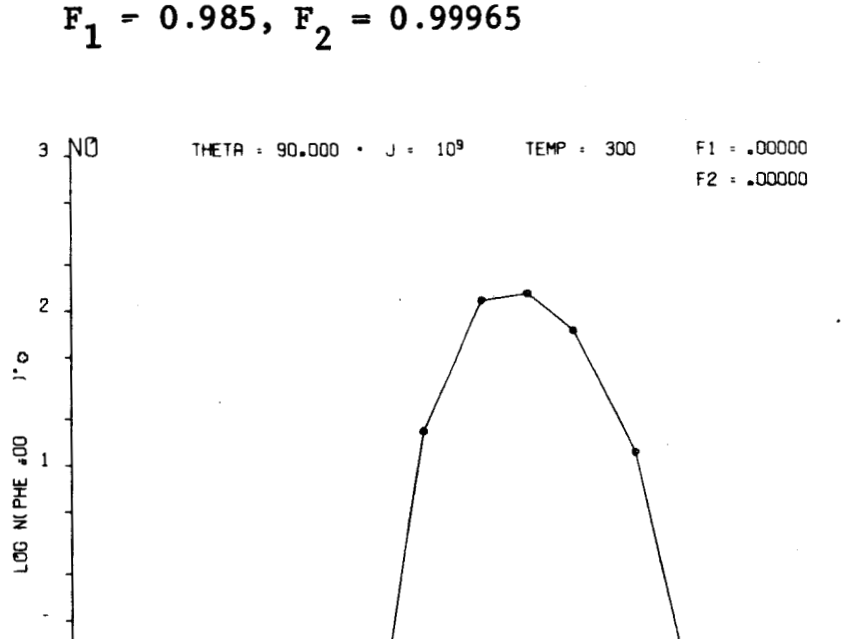

Fig. 61 Model II - NO Variation of LEM Exhaust Contamination with Time at 2700 km from LEM Touchdown
$F_1 = 0$, $F_2 = 0$

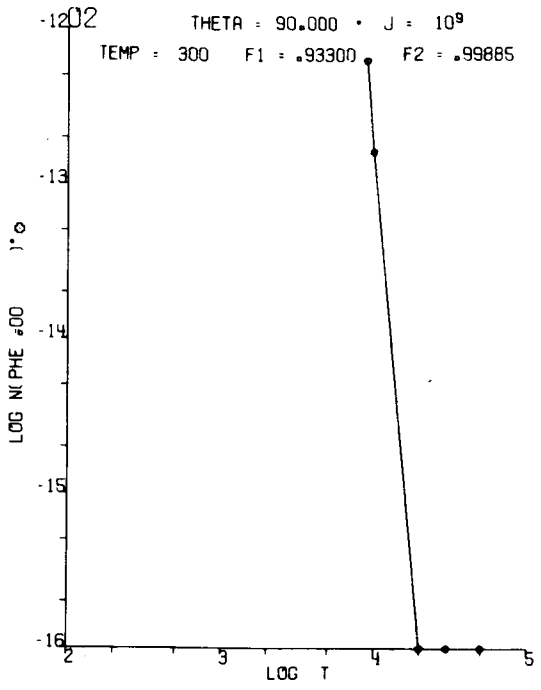

Fig. 62 Model II - O_2 Variation of LEM Exhaust Contamination with Time at 2700 km from LEM Touchdown
$F_1 = 0.933$, $F_2 = 0.99885$

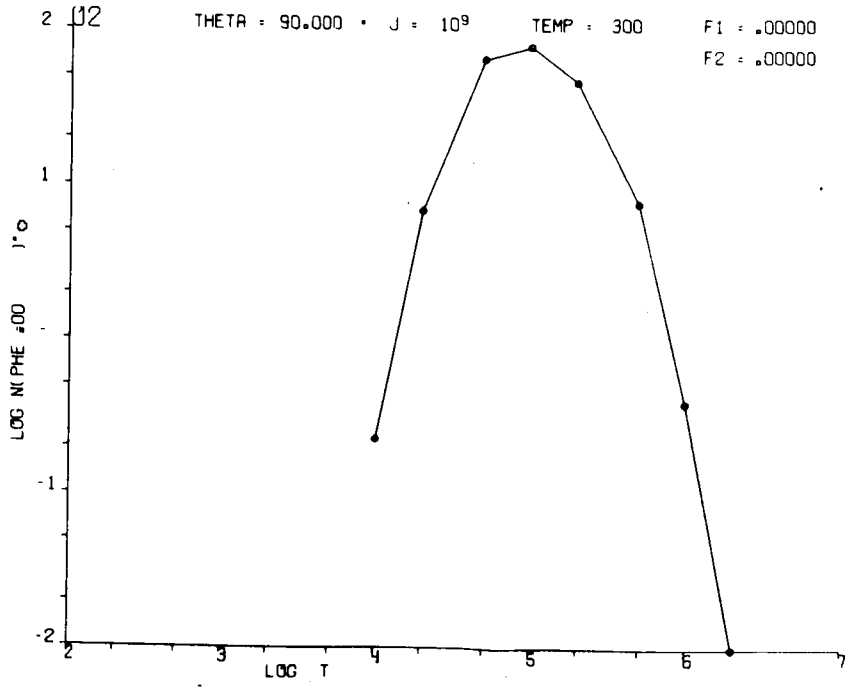

Fig. 63 Model II - O_2 Variation of LEM Exhaust Contamination with Time at 2700 km from LEM Touchdown
$F_1 = 0$, $F_2 = 0$

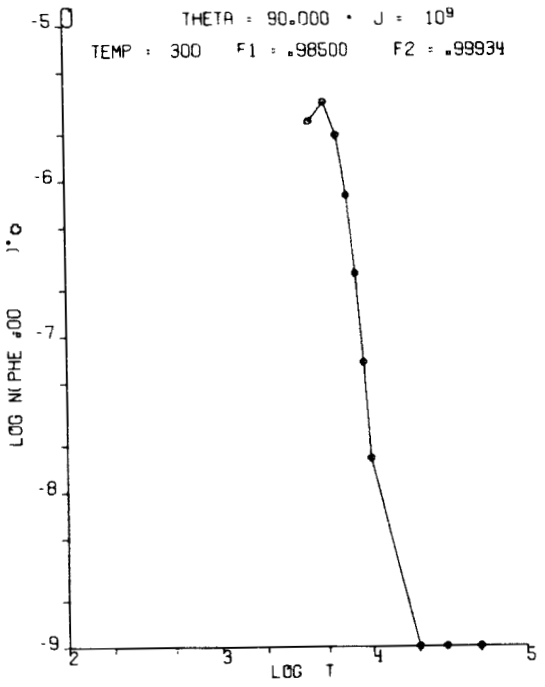

Fig. 64 Model II - O Variation of LEM Exhaust Contamination with Time at 2700 km from LEM Touchdown
$F_1 = 0.985$, $F_2 = 0.9934$

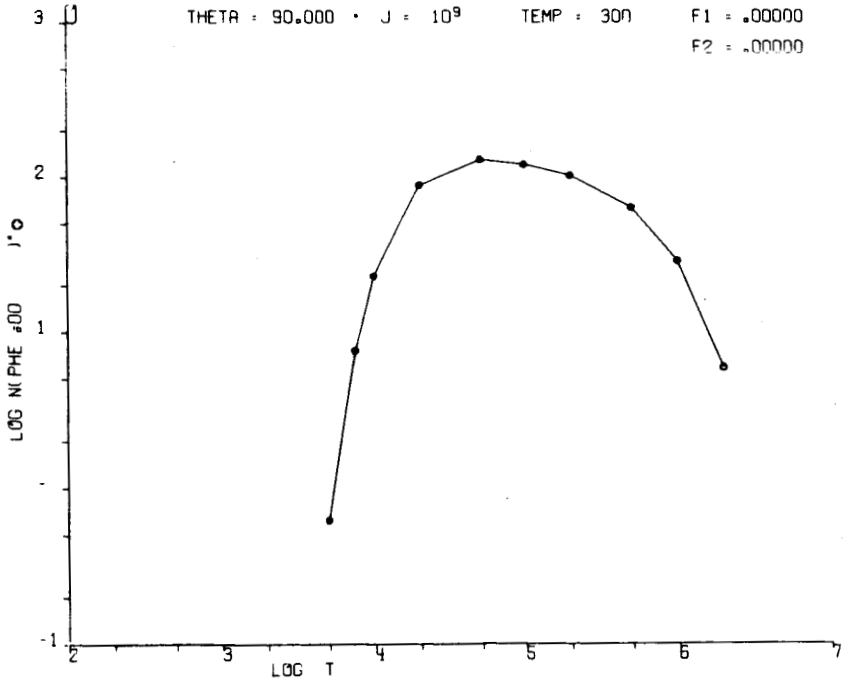

Fig. 65 Model II - O Variation of LEM Exhaust Contamination with Time at 2700 km from LEM Touchdown
$F_1 = 0$, $F_2 = 0$

F. Desorption of LEM Exhaust Gases From the Lunar Surface [M. Sidran]

1. General

To estimate the contamination that will result from the interaction of the LEM exhaust with the lunar surface, the physical and chemical properties of the surface and the state of the impinging gases must be evaluated. Gas molecules colliding with the surface may rebound elastically, react chemically to form new species, or become adsorbed at an active surface site. This section discusses the fate of the adsorbed molecules. The thermal lifetimes of adsorbed gases are calculated. Desorption mechanisms such as solar wind sputtering and out-gassing by micrometeorite collisions are briefly discussed. The lifetimes of desorbed molecules in the lunar atmosphere are considered. Finally, the effects of high energy solar radiation on adsorption and desorption processes are described.

2. Discussion

The properties of the lunar surface depend on both its composition and its interaction with the lunar environment. Depending on their thermal history, portions of the surface have probably cooled in the absence of an atmosphere to form a rock foam of very low density. The constant rain of micrometeorites pulverizes and fractures the surface; the impacts shock the crystalline structure, producing a disordered lattice. Ejected dust particles may be transported to other portions of the surface where they form a layer, possibly welded into a fairy castle structure in the hard vacuum (Ref. 30). Some of the original projectile energy is dissipated as heat that can outgas the surface, and can melt part of the rock, possibly giving a glassy material on cooling (Ref. 31).

Low energy solar wind particles sputter away the surface atoms, especially the lighter elements, many of which leave the surface with velocities in excess of the escape velocity. Others are driven deep into crevices and pores. Laboratory measurements on sputtering indicate that the surface can be welded into a porous, brittle crust rich in metallic atoms, and poor in oxygen (Ref. 32).

High energy solar wind particles penetrate the bulk material, producing lattice defects that migrate to the surface at lunar temperatures. These sinter the dust grains together and form surface defect sites for adsorption and catalysis.

The high energy electromagnetic radiation from the sun ionizes the surface by ejecting photoelectrons.

Due to the effects of all the above processes, the lunar surface is a highly active site for promoting chemical reactions and adsorption of LEM gases.

The effects of ionization by solar radiation, and of collisions with solar particles, on the exhaust gas molecules in the atmosphere are neglected in first approximation because of the low probability of their occurrence. We therefore assume that most of the gas released into the atmosphere exists in the form in which it left the vehicle. However, the effect of these agents on the process of adsorption itself must be considered. Although little data are available, the preliminary experiments indicate that high energy radiation increases the probability and binding energy of chemisorption, leading to practically infinite adsorption lifetimes.

3. Results

a. Thermal Desorption of LEM Gases: The approximate lifetimes (Ref. 25) of molecules physically adsorbed on silicate rocks are shown in Table 17 for 14 LEM exhaust gases at $404^{\circ}K$, about the temperature of the sub-solar point, and at $126^{\circ}K$, the temperature of dark, cold shadowed crevices where sunlight never reaches. (τ_o in Tables 17 and 18, and Fig. 66 is a parameter of the lunar surface material, cf. Ref. 25) There is actually a range of lifetimes for each molecule, since the lifetime is a sensitive function of the heat of adsorption, Q, which varies with position on the surface according to the activity of local trapping sites. If we define significant lifetimes as those greater than 10 seconds, then only H_2O and OH (at $T = 126^{\circ}K$) have significant lifetimes for physical adsorption.

Table 18 shows the chemisorbed lifetimes (Ref. 25) of 10 exhaust gases. Only H_2, H, and CO, and CO_2 have short chemisorbed lifetimes at $404^{\circ}K$. All other lifetimes are effectively infinite.

The effect of lunar temperature cycling on adsorption lifetimes can be calculated exactly (Ref. 25). For H_2O in Table 17, and for H_2, H, and CO in Table 18, the exact calculation yields a multiplication factor of about an order of magnitude for the

Table 17

LIFETIMES OF LEM GASES ADSORBED PHYSICALLY ON SILICATE ROCK ($\tau_o = 10^{-13}$) 404°K AND AT 126°K (TEMPERATURE OF CREVICES)

Gas	Q cal/mole	T = 126°K	T = 404°K
N_2	4300-2300	10^{-6} to 10^{-9} sec	10^{-11} to 10^{-12} sec
H_2	3000-1500	10^{-8} to 10^{-11} sec	10^{-12} sec
CO	4800-7000	$10^{-5} - 10^{-1}$ sec	$10^{-11} - 10^{-9}$ sec
CO_2	7000-10,000	$10^{-1} - 10^{4}$ sec	$10^{-9} - 10^{-8}$ sec
H	900	10^{-12} sec	10^{-13} sec
NO	7400	0.5 sec	10^{-9} sec
O_2	4400	10^{-5} sec	10^{-11} sec
N	2300	10^{-9} sec	10^{-12} sec
NH_3	7200	0.3 sec	10^{-9} sec
CH_4	5200	10^{-4} sec	10^{-11} sec
C_2H_2	6600	10^{-2} sec	10^{-10} sec
H_2O	15,000-30,000	$10^{13} - 10^{39}$ sec	10^{-5} to 10^{3} sec
O	5800	10^{-3} sec	10^{-10} sec
OH	9200	10^{3} sec	10^{-8} sec

Table 18

LIFETIMES OF CHEMISORBED LEM GASES ON SILICATE ROCKS ($\tau_o = 10^{-13}$)

Gas	Q cal/mole	T = 126°K	T = 404°K
OH	60,000-90,000	10^{20} sec	10^{20}-10^{36} sec
H_2O	60,000	10^{20} sec	10^{20} sec
CO_2	23,000	10^{20} sec	0.4 sec
H_2	23,000	10^{20} sec	0.4 sec
O_2	46,000-72,000	10^{20} sec	10^{12}-10^{26}
CO	23,000	10^{20} sec	0.4
O	80,000	10^{20} sec	10^{20}
N_2	45,000	10^{20} sec	10^{11}
NO	150,000	10^{20} sec	10^{20}
H	20,000	10^{20} sec	10^{-2}

tabulated lifetimes. In all other cases, however, the use of a constant temperature (404°K) gives a reasonable approximation to the exact lifetime.

The lifetimes of LEM gases not shown in the tables may be found from Fig. 66, after data on their heats of adsorption Q become available. Figure 66 shows the variation of lifetime with Q for (constant) lunar temperatures, the sub-solar 404°K, the mean 303°K, the dark 126°K, and two other temperatures that might be found in dark crevices, 202°K and 256°K.

Gases thermally desorbed from the surface at 400°K will have a distribution of mean velocities shown in Table 19. Many

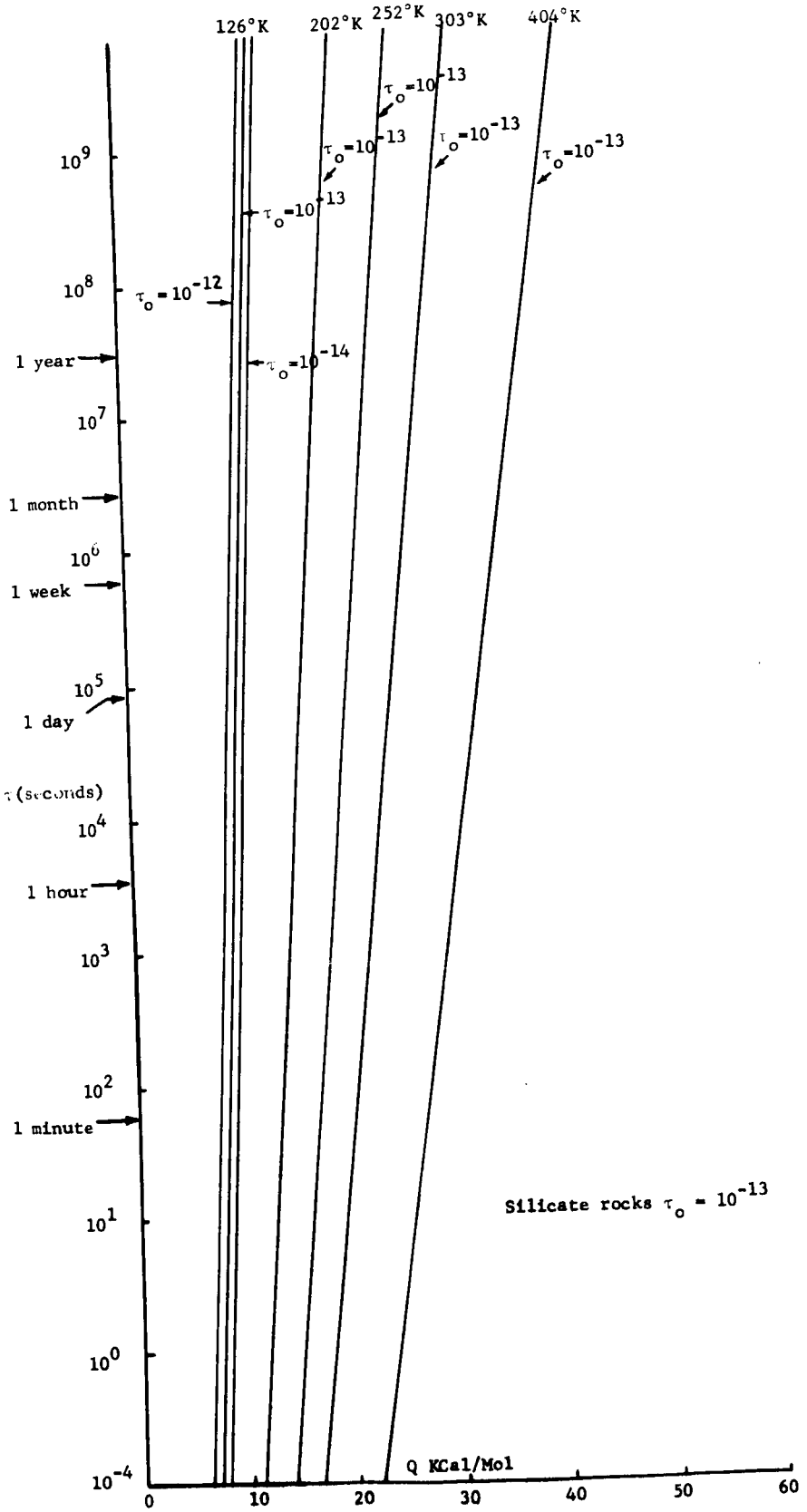

Fig. 66 Thermal Lifetimes versus Heats of Adsorption

Table 19

MEAN THERMAL VELOCITIES AND THERMAL LIFETIMES IN LUNAR ATMOSPHERE OF DESORBED LEM GASES AT $400^{\circ}K$

Gas	Molecular Weight	Mean Thermal Velocity (cm/sec)	Thermal Lifetime in Atmosphere (sec)
N_2	28	6×10^4	5×10^{11}
H_2	2	2×10^5	4×10^3
CO	28	6×10^4	5×10^{11}
CO_2	44	5×10^4	2×10^{17}
H	1	3×10^5	4×10^3
NO	30	6×10^4	2×10^{12}
O_2	32	6×10^4	1×10^{13}
N	14	8×10^4	8×10^6
NH_3	17	8×10^4	8×10^7
CH_4	16	8×10^4	4×10^7
C_2H_2	26	6×10^4	8×10^{10}
H_2O	18	8×10^4	2×10^8
O	16	8×10^4	4×10^7
OH	17	8×10^4	8×10^7

of these will follow trajectories that intersect the surface in the far field. Each collision with the surface will give a thermalized distribution of velocities; the more energetic particles will escape from the moon. The lifetime of each gas in the lunar atmosphere for a Maxwellian velocity distribution at 400°K is given in Table 19. A more general discussion of loss mechanisms is found in Sec. IV.E of this report.

b. Desorption by Solar Wind Sputtering and Micrometeoroid Impact: Sputtering of the lunar surface by protons and alpha particles in the solar wind can modify the picture considerably. Light atoms adsorbed on the surface will be driven off with velocities in excess of the escape velocity. Some sputtered atoms will escape from the moon, but many will be driven in the direction of motion of the incoming particle, into holes and crevices to be readsorbed, and perhaps later resputtered.

The sputtering yield in atoms per proton depends on the atomic weight of the sputtered atom. It is estimated (Refs. 32 and 33) that the yield for oxygen is 0.05 or 0.1 per proton. This yield would also hold for C and N atoms, and probably for H. Thus, atoms and molecules adsorbed on the surface might have a higher escape rate from the moon than those not adsorbed. A surface area of 1 cm^2 would be cleared in several years. However, this does not consider the microscopic roughness or the area of the pore.

Outgassing by micrometeoroid impact is estimated to be, very roughly, as effective as outgassing by sputtering (Ref. 33). This outgassing depends on desorption by heating of the surface. The released material will have thermal velocities corresponding to the temperatures of the heated surface, which may or may not exceed the escape velocity.

4. Conclusions

The chief contaminants of the lunar surface would be OH, H_2O, and N_2, which have relatively high concentrations in the LEM exhaust, and practically infinite thermal lifetimes for chemisorption, even at the lunar day temperature. At the temperature of dark unheated crevices, H, CO_2, OH, H_2O, H_2, CO, and N_2 have both long thermal lifetimes and high concentrations.

Desorbed molecules would impact the surface outside the near field, and spread around the moon in a relatively short time.

All species have solar wind sputtering, photon absorption, and micrometeorite outgassing as significant desorption mechanisms that would clear the exposed surfaces in a time estimated at several years. This does not include pores inside the fairy castle structure that might have adsorbed surface gases, but would not receive the direct solar wind.

G. Calculation of Sticking Probabilities [L. Aronowitz]

1. General

The probability, S, of an impacting molecule sticking to the lunar surface was calculated using methods developed in the Research Department of Grumman under a contract with the Fluid Physics Branch, Research Division, Office of Advanced Research and Technology, NASA HQ. In that study, a machine program was developed which allows the calculation of the three dimensional classical trajectories of gas molecules directed at a crystal lattice that is represented by a set of harmonic oscillators which are point centers of potential (a Lennard-Jones 6-12 potential). A detailed discussion of the study can be found in Ref. 4. The study allows examination of chemisorption in which the binding energies are of the order of 1-10 ev and also physical adsorption with energies in the neighborhood of 0.1 ev (cf. Sec. VIII of Ref. 1).

2. Formulation and Results

The value of S for a molecule making a single impact with the surface is $S = 1 - R$ where R is the probability for the molecule rebounding from the surface. The value of R is given by (Ref. 4)

$$R = \frac{\overline{p_z^2}}{2m_g A} ,$$

where m_g is the mass of the impinging gas molecule. The quantity A is determined from

$$A = \frac{E}{E_i \cos^2\theta_i} , \tag{83}$$

where E is the energy with which the molecule is bound to the surface, θ_i is the angle between the incident velocity and the normal to the surface, and E_i is the incident kinetic energy of the molecule. The value of $\overline{p_z^2}/(2m_g)$ is found from the expressions

$$\frac{\overline{p_z^2}}{2m_g} = 0.5 \cos^2\theta_i (1 + A)(1 - \alpha_p)(1 - e^{-1/A}) \qquad (84)$$

and

$$\alpha_p = - \frac{4\mu \cos \theta_i \exp[-a'(\omega_n \sigma / V_i)]}{(1 + \mu)^2} , \qquad (85)$$

where

$\mu = m_\ell / m_g$, and

m_ℓ is the mass of a lattice atom.

The value of $\exp[-a(\omega_n \sigma / V_i)]$ was taken to be 0.85 on the basis of information on Debye frequencies for silicates supplied by Arthur D. Little, Inc. To calculate the values of μ, a lunar surface composition, similar to that of certain meteorites was selected. The composition is shown in Table 13. The values of R for each incident species of exhaust gas molecule were calculated for each species of surface atom and then the results were averaged over the distribution of atoms given in Table 13.

Values of R were calculated for far field molecules that were assumed to have an E_i corresponding to a velocity of the order of 3000m/sec and an average value of $\theta_i = 45°$. Little reliable data exist on the value of E to be used for these species under lunar environmental conditions. Values of E were taken from a variety of scattered sources. In general, it was attempted to find a representative value of E for both physical adsorption and chemical adsorption on a silicate surface. The values of E used and the corresponding R values are shown in Table 20. No great reliability can be claimed for these values. Better experimental adsorption and desorption data for simulated lunar conditions are urgently needed.

If the lunar surface is smooth, then S would simply be equal to 1 - R. However, as shown by the Luna 9 photographs and other evidence, it is more likely that the surface is extremely rough on a scale of a few centimeters or less. The value of S is higher for a rough surface than for a smooth surface. On a rough surface a molecule that rebounds from the wall of a cavity in the

Table 20

PARAMETERS FOR EXHAUST MOLECULES

Molecule	E (ev)		R		S	
	Phys.	Chem.	Phys.	Chem.	Phys.	Chem.
H	.039	.900	.215	.007	.880	.997
H_2	.100	1.00	.163	.0146	.912	.993
H_2O	.600	2.60	.254	.0489	.855	.975
CO	.300	1.00	.762	.225	.384	.874
CO_2	.400	1.00	.917	.362	.917	.362
N_2	.200	2.00	1.00	.101	0	.947
NO	.311	6.48	.139	.030	.139	.030
O	.250	3.50	.528	.030	.641	.985
O_2	.200	2.00	.129	.127	.932	.933
OH	.390	4.40	.061	.026	.969	.987

surface will have a substantial probability of striking another wall of the cavity before escaping from the surface. Therefore, each impacting molecule will have to rebound several times on the average before escaping from the surface, greatly increasing its probability of capture.

To illustrate this increase in S with roughness, consider a two dimensional example. Consider the surface to be made of rectangular corrugations each of width y and depth h as shown in Fig. 67. Assume that a parallel beam of molecules all moving with the same velocity is incident on the surface. The molecular flux is uniform and constant. The value of the flux is I_o molecules per unit area per unit time measured in a plane at right angles to the molecular velocity. The velocity makes an angle θ_i with

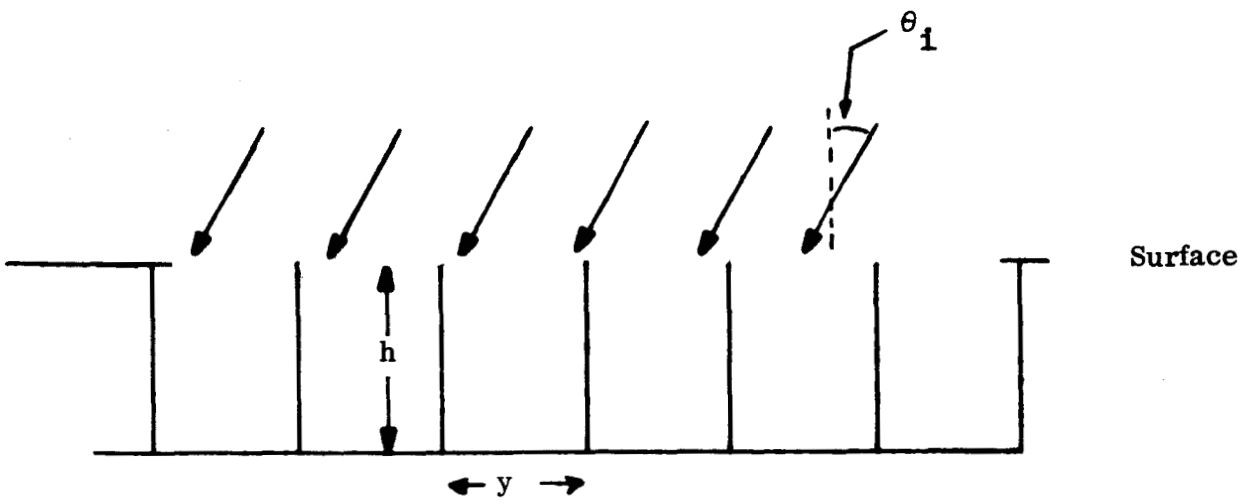

Fig. 67 Two Dimensional Corrugated Surface

the normal. In Fig. 67 the flux of particles incident on the left side of a corrugation (side 1) is given by $I_o \sin \theta_i$. Assume that fraction R of these molecules is reflected. Assume that all the reflected molecules have the same speed, but that their directions are uniformly distributed over an angle π. Let $dI_r(1) = RI_o \sin \theta_i \, dz$ be the number of molecules per unit time that are reflected from an element of side 1 of the corrugation. The element is at depth z below the surface and has width dz (see Fig. 68). Let dI(1) be the number of molecules per unit time reflected from dz that escape from the corrugation without making any further collisions with the walls. Then

$$dI(1) = (\alpha/\pi)dI_r(1) = (\alpha/\pi)RI_o \sin \theta_i \, dz$$

where $\alpha = \arctan(y/z)$.

If θ_i is in the range $\theta_o < \theta_i < \pi/2$, where $\theta_o = \arctan(y/h)$ (i.e., all the incident particles strike side 1), then integration yields

$$I(1) = \frac{I_o y R \sin \theta_i \left[\theta_i \cot \theta_i - \ell n(\sin \theta_i)\right]}{\pi} . \qquad (86)$$

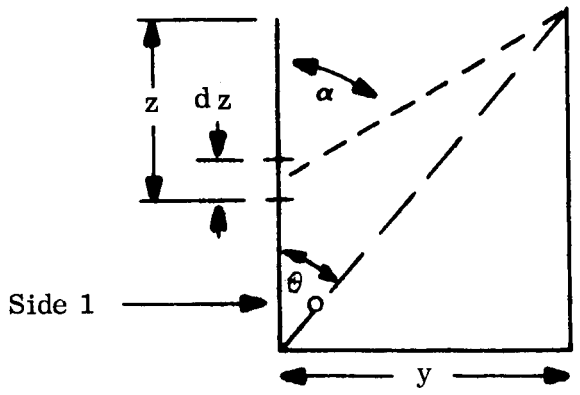

Fig. 68 Corrugation $\theta_o < 0_i < \pi/2$

If $0 < \theta_i < \theta_o$, then some of the incident molecules strike the bottom of the corrugation. The number of molecules reflected from an element dx of the bottom (see Fig. 69) is

$$dI_{rB} = I_o R \cos \theta_i \, dx = I_{rB} \, dx$$

where $I_{rB} = I_o R \cos \theta_i$. For the bottom, the number of molecules reflected from dx that strike side 1 is

$$dI_{B1} = \frac{dI_{rB}\gamma_1}{\pi}$$

and the number of molecules from dx striking side 2 is

$$dI_{B2} = \frac{dI_{rB}\gamma_2}{\pi}$$

where $\gamma_1 = \text{arcot } (x/h)$ and

$$\gamma_2 = \text{arcot } \left(\frac{y - x}{h}\right) .$$

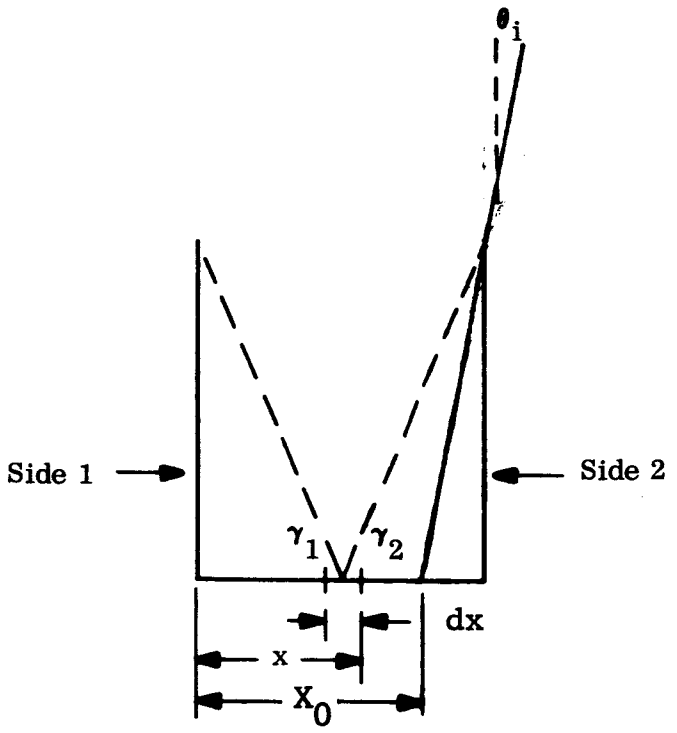

Fig. 69 Corrugation: $0 < \theta_i < \theta_o$

The number of molecules dI(B) reflected from dx per unit time that escape from the corrugation without further collisions is given by

$$dI(B) = dI_{rB} - dI_{B1} - dI_{B2} = dI_{rB}\left(1 - \frac{\gamma_1 + \gamma_2}{\pi}\right) .$$

Integration yields

$$I(B) = I_{rB}\int_0^{X_0}\left(1 - \frac{\gamma_1 + \gamma_2}{\pi}\right) dx , \qquad (87)$$

where $X_0 = y - h \tan \theta_i$ (see Fig.69). Using the standard expression

$$\int \operatorname{arcot}(x/a)\, dx = x \operatorname{arcot}(x/a) + (a/2)\, \ell n\, (a^2 + x^2) , \qquad (88)$$

the expression for I(B) may be integrated.

When $0 < \theta_i < \theta_o$, the number of molecules escaping from the corrugation after having made only a single collision is given by the sum of those which escape from side 1 and from the bottom after only a single collision. The number making only a single collision with side 1 is obtained by setting $\theta_i = \theta_o$ in Eq. (86) The number of those escaping after only a single collision with the bottom is found from Eq. (87).

The rate at which molecules enter the corrugation is

$$I_o y \cos \theta_i \tag{89}$$

The fraction, F, of molecules entering the corrugation that escape after only a single collision can be found for the case where $\theta_o < \theta_i < \pi/2$ from the ratio of Eq. (86) to Eq. (89). The value of F for $0 < \theta_i < \theta_o$ is found from the ratio of the sum of Eq. (86) with $\theta_i = \theta_o$ and Eq. (87) to Eq. (89). Using Eq. (88) to evaluate the integral in Eq. (87) yields the following value for F:

for $\theta_o < \theta_i < \pi/2$

$$F = \frac{R}{\pi}\left[\theta_i - \tan \theta_i \ \ell n(\sin \theta_i)\right] \tag{90}$$

and for $0 < \theta_i < \theta_o$

$$\begin{aligned} F = \frac{R}{\pi}\Big\{ & \tan \theta_i(\theta_o \cot \theta_o - \ell n \sin \theta_o) \\ & + \cot \theta_o\left[\frac{\pi}{2}(\tan \theta_o - \tan \theta_i) - (\tan \theta_o - \tan \theta_i) \cot^{-1} (\tan \theta_o - \tan \theta_i\right. \\ & + \frac{1}{2} \ell n \frac{1 + \tan^2\theta_i}{\left[1 + \tan^2\theta_o\right]\left[1 + (\tan \theta_o - \tan \theta_i)^2\right]} \\ & \left. - \theta_i \tan \theta_i + \theta_o \tan \theta_o\right]\Big\} \end{aligned} \tag{91}$$

Table 21 shows values of F/R from Eq. (90) and Eq. (91) for various values of θ_o and θ_i

Table 21

VALUES OF F/R

θ_o	θ_i	F/R
0°	30°	.29
	45°	.36
	60°	.41
	90°	.50
30°	30°	.29
	45°	.36
	60°	.41
	90°	.50
60°	30°	.15
	60°	.41
	90°	.50
90° (smooth surface)	$0 < \theta_i < \pi/2$	1.00

Table 21 makes it evident that a considerable fraction of molecules make multiple collisions with a rough surface before escaping.

As a rough approximation assume that, on the average, half the molecules at a rebound will escape from the lunar surface while the remaining half make at least one further collision. Using this assumption the number escaping from the surface is

$$\frac{R}{2} + \frac{R}{2}\left(\frac{R}{2}\right) + \frac{R}{2}\left(\frac{R}{2}\right)^2 + \frac{R}{2}\left(\frac{R}{2}\right)^3 + \ldots = \sum_{n=1}^{\infty} \left(\frac{R}{2}\right)^n$$

and

$$S = 1 - \sum_{n=0}^{\infty} \left(\frac{R}{2}\right)^n .$$

The series for S can be evaluated, since $R/2 < 1$, yielding

$$S = \frac{1 - R}{1 - (R/2)} \qquad (92)$$

The values of S in Table 20 were calculated using Eq. (92).

In deriving Eq. (92) it was assumed that R remains constant. This is probably not the case. At each collision with the wall a molecule will exchange energy with the wall and "accommodate" its kinetic energy to that representative of the temperature of the surface. This results in a decrease of R with each collision and a somewhat larger value of S than predicted by Eq. (92). While the equation could be modified to take account of accommodation such a refinement is scarcely justifiable. The value of S is a sensitive function of E (cf. Table 20). Since so little is known about values of E for molecular interactions with lunar surface materials, the values of S in Table 20 are only rough order of magnitude estimates. As previously noted, reliable experimental data on adsorption and desorption under simulated lunar environmental conditions is urgently needed.

Since existing data on adsorption under lunar environmental conditions do not permit accurate calculations of R, the use of Eq. (92) to determine S has little practical advantage over the simpler expression $S = 1 - R$. However the derivation of Eq. (92) is of interest in another connection. The methods used in deriving Eq. (92) can be used to find the distribution of the flux of molecules to sides 1 and 2. By extending the method, the distribution of molecules adsorbed on the walls of the corrugation as a function of distance below the surface can be determined. This distribution gives an estimate of the depth below the surface to which far field contamination will penetrate into a porous lunar surface.

Values of S for the ten molecular species in Table 20 were also calculated for incident molecular kinetic energies corresponding to a temperature $T = 300°K$. Results are shown in Table 22. These values were used in the calculation of atmospheric contamination in Sec. IV.E of this report. It should be remarked that

the use of Eqs. (83), (84) and (85) in calculating S for molecules in this range of kinetic energy will give less accurate results than their use for the energies in Table 20 (see Ref. 4).

Table 22

VALUES OF S FOR T = 300°K

Molecule	S	
	Phys.	Chem.
H_2	.974	.978
H_2O	.996	.999
N_2	.988	.989
CO	.992	.998
CO_2	.994	.998
O_2	.988	.999
NO	.992	1.00
OH	.994	.999
H	.943	.997
O	.990	.999

H. Thermal Effects of the LEM Descent Engine [A. Wechsler]

1. General

The objectives of the thermal analysis carried out at Arthur D. Little, Inc., are to determine the temperature distribution on the lunar surface and within the shallow subsurface in the vicinity of the LEM during and after its descent. The thermal effects of the LEM descent engine are of significance to the study of contamination of the lunar surface for several reasons:

- The reactivity of the surface materials may change if they are heated to sufficiently high temperatures.
- The absorption and desorption of exhaust gases on the surface and subsurface layers will be affected by the temperatures reached and the time at which elevated temperatures are attained.
- The safety of the astronaut may depend upon how rapidly the surface temperatures in the immediate vicinity of the LEM return to their predescent values.
- The thermal history of any lunar surface or subsurface samples gathered by the astronaut from the vicinity of the LEM should be known.

We have assessed the perturbances in the normal thermal behavior of several types of lunar surface materials caused by the heating of the LEM descent engine.

2. Methods of Analysis

Two approaches were used in ascertaining the thermal effects of the LEM descent - (1) computer calculations using several lunar models to determine in detail the variation of surface and subsurface temperatures with time, depth, and distance from the LEM and (2) simplified analyses to determine maximum temperatures of the surface and the anticipated depth of penetration of the transient heat wave.

a. Computer Calculations: We have used a computer program, originally developed for NASA by Mr. Ingrao's group at Harvard University. The basic approach used, and the details of the numerical technique are given in Refs. 34 and 35.

In the basic approach given by Ref. 35, the heat conduction equation takes the form:

$$\rho c(x,T)\ \frac{\partial T}{\partial \theta} = \frac{\partial}{\partial x}\left[k(x,T)\ \frac{\partial T}{\partial x}\right] + Q(x,\theta) \qquad (93)$$

where

- x = depth beneath the surface
- T = absolute temperature
- ρ = density of material
- $c(x,t)$ = heat capacity (function of depth and temperature)
- $k(x,T)$ = thermal conductivity (function of depth and temperature)
- $Q(x,\theta)$ = source term (usually taken as zero)
- θ = time

The surface medium is divided into six layers, each consisting of an arbitrary number of sublayers or depth integration steps. Three models of the surface were considered in the original program; temperature-independent properties, linear temperature-dependent properties, and conductivity with a radiation contribution. The heat conductivity equation is written for each layer in finite difference form using forward and central differences. Equations are written for the boundary between two layers and for the surface. The sets of difference equations are solved to provide the surface temperature distribution during lunations and eclipses.

The original program was modified and rewritten (Ref. 36) for several reasons:

- The logical design of the existing program was such that the important computations were not logically isolated from the input, output, and control steps.
- The fundamental difference equation was coded explicitly wherever needed instead of being isolated in a subroutine.
- The thermal models of the lunar material were substituted analytically in the heat flow equation before the difference equation was derived, making it impossible to change models without recoding the difference equations.

- The integration step size control was not as useful as was required.

The modified approach was taken from an analog computing technique. Each layer l_i was made up of n_i slices of thickness Δx_i, and the thermal properties of each slice given by the following model:

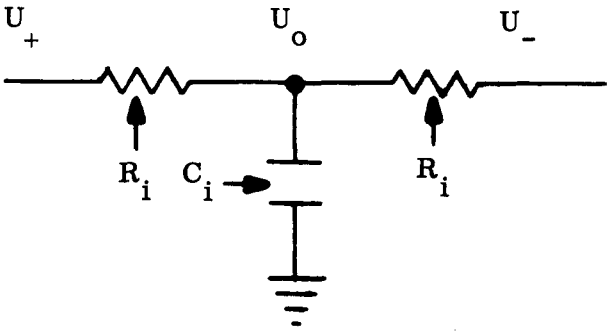

where $R_i = \frac{1}{2}\frac{\Delta x_i}{k_i}$ and $C_i = \rho_i c_i \Delta x_i$; U represents the temperature and k_i, ρ_i, c_i are the thermal conductivity, density, and specific heat in the i^{th} layer. Assuming that k_i, ρ_i, and c_i are constant over an integration step, the above network is described by:

$$C_i \dot{U}_o = \frac{U_+ - U_o}{R_i} + \frac{U_- - U_o}{R_i} \quad . \tag{94}$$

These equations form a set of simultaneous first order differential equations that may be solved. The integration step size φ is forced to satisfy the inequality $\varphi \leq aR_iC_i$, where a is an input parameter less than 1. The lower boundary condition is specified by a constant temperature constraint. The surface boundary condition is maintained by an iterative solution to the surface boundary constraint, namely

$$q_{in}(U_s) = q_f(U_s) \quad , \tag{95}$$

where $q_{in}(U_s)$ is the total flux into the surface from the LEM exhaust plus the absorbed solar radiation minus the reradiation to space, and $q_f(U_s)$ is the heat flux conducted into the surface. The equation is solved for U_s by an iterative technique similar to Newton's method that uses first differences to approximate derivatives.

Because of the nature of this approach, there is no need for special considerations at the interlayer boundaries. A first estimate of the initial temperature is made, and the system is relaxed over at least one lunation prior to solving the problem with the LEM heat flux parameters. The temperature distribution of the surface and subsurface layers is then found. Input parameters required are discussed in Sec. C. The thermal properties may be specified in the form:

$$\rho = \rho_o$$

$$c = c_o + c_1 T$$

$$k = k_o + k_1 T + k_2 T^2 + k_3 T^3$$

for each of up to 20 layers.

b. Simplified Analyses: To estimate the maximum temperatures of the lunar surface and subsurface, a simplified analysis may be used and the results compared to more rigorous calculations. The maximum surface temperature that can be attained may be calculated assuming no conduction into the lunar surface. The boundary equation for the surface then becomes:

$$Q_{LEM} + I(1 - A_s) = \epsilon_s \sigma T_s^4 ,$$

where Q_{LEM} represents the heat flow from the LEM exhaust, I is the solar incidence, A_s is the albedo of the moon, ϵ_s is the emittance of the lunar surface and T_s is the surface temperature.

The maximum temperature excursion produced by the LEM exhaust at various depths in the subsurface may be found by several approximate methods. Certainly it will be lower than the maximum at the surface. If all of the heat from the LEM that reaches the surface during the descent flows into the surface and is contained in a

skin of depth S_1, and after the end of the descent this heat is allowed to flow into the surface, but not to space, the temperature may be found (as a function of depth) in analytical form. This method is used, for example, when a flat sheet of molten rock is intruded into another rock at a constant temperature. A more appropriate solution may be obtained as follows: Assume that the subsurface material prior to the LEM descent is at constant temperature. Heat is supplied at the surface at a constant rate Q_{LEM} per unit area for time τ. At time τ, the heat supply ceases and the surface $x = 0$ is thermally insulated. The temperature at time θ, for $\theta > \tau$ is (Ref. 22):

$$T = \frac{2Q_{LEM}\alpha^{\frac{1}{2}}}{k}\left\{\theta^{\frac{1}{2}}\text{ierfc}\ \frac{x}{2\sqrt{\alpha\theta}} - (\theta - \tau)^{\frac{1}{2}}\text{ierfc}\ \frac{x}{2\sqrt{\alpha(\theta - \tau)}}\right\} . \qquad (96)$$

where α is the thermal diffusivity ($k/\rho c$) of the surface layer. This expression would overestimate the temperature because the surface is assumed to be insulated. Furthermore, all of the flux from the LEM does not go into the surface. This may be partially considered by using an average value heat flux in the calculations, rather than the maximum value of the flux.

3. Input Data

a. Lunar Models: A recent review of the aspects of the lunar environment and the probable nature of the lunar surface has been given by Glaser (Ref. 37). Recent investigations point to a surface material similar to a consolidated powder or vesicular rock. The very recent findings of Luna 9 seem to support these conclusions. Rather than select a particular lunar surface modek, we have chosen several possible models as representative of those which may be found in various lunar locations. They are:

1) Homogeneous dust model
2) Homogeneous vesicular rock
3) Homogeneous solid rock
4) Particulate surface layer - vesicular rock substrate
5) Particulate surface layer - solid rock substrate
6) Vesicular rock surface layer - solid rock substrate
7) Particulate surface layer - rubble substrate
8) Homogeneous rubble.

The thickness of layers 4, 5, and 6 was chosen on the basis of early calculational results indicating the depth of penetration of the thermal perturbation into the homogeneous layer.

b. Thermal Parameters of Lunar Materials: The thermal properties of possible lunar materials in vacuum have been summarized by Wechsler and Glaser (Ref. 38). Based upon these data, and more recent unpublished data on powdered materials at low temperatures (Ref. 39), we have chosen the following values for the important lunar surface properties:

Table 23

VALUES OF LUNAR THERMAL PARAMETERS

Material	Density (gm/cm^3)	Specific Heat (joules/gm °K	Thermal Conductivity (watt/cm °K)
Particulate	1.1	$0.502 + 7.4 \times 10^{-4} T$	$4.6 \times 10^{-6} + 3.05 \times 10^{-13} T^3$
Vesicular Rock	0.9	$0.502 + 7.4 \times 10^{-4} T$	$1.5 \times 10^{-3} + 20 \times 10^{-6} T$
Solid Rock	2.6	$0.502 + 7.4 \times 10^{-4} T$	$0.020 + 1.0 \times 10^{-5} T$
Rubble	1.9	$0.502 + 7.4 \times 10^{-4} T$	$2.0 \times 10^{-3} + 20 \times 10^{-6} T$

c. Landing Site and Time: It has been usually accepted that the LEM will land within $\pm 5°$ of the equator. For purposes of estimating the incident solar flux, we have assumed that it will land on the equator. The exact position (longitude) is not yet specified. The value may be taken as an arbitrary position; however, the time relative to the terminator must be specified. We have used the information provided by Grumman Aircraft Engineering Corporation and assumed that the LEM landing will be at a longitude of $45°$ with respect to the terminator.

d. LEM Trajectory: When the LEM is in the hover position, the heat transfer from the exhaust gas to the surface has a maximum value significantly less than 0.3 watt/cm^2. The heating of the surface, even under assumed steady state conditions, would be nominal. We have therefore restricted our attention to the localized heating produced during descent. The LEM altitude trajectory that was the most serious for surface heating (vertical descent) was supplied by Grumman.

e. Heat Flux from LEM to Surface: The heat flux from the LEM exhaust to the surface is the sum of a convective flux and a radiative flux. Data on the convective flux as a function of time from the start of the descent and distance from the LEM landing site (assuming vertical descent) were provided by Grumman. The convective heat flux to the surface was given in the form:

$$Q_{conv} = h(T_g - T_s) \ , \tag{109}$$

where h is a tabulated function of time and distance, T_g is the effective (or total) exhaust gas temperature, and T_s is the lunar surface temperature. The input data for the convective coefficient h were obtained from internal Grumman calculations. Because h itself is a function of the surface temperature, the values used are not exact for each lunar surface model we have chosen. Nevertheless, these were the most accurate data available.

The radiation from the LEM exhaust nozzle (and exhaust cavity) to the surface may be expressed by the equation:

$$Q_{rad} = \sigma F_{NS} \epsilon_N T_N^4 \ ,$$

where F_{NS} is the "view factor" by which the element of lunar surface "sees" the nozzle, and is given by:

$$F_{NS} = \frac{1}{2}\left[1 - \frac{(d - R_N)(d + R_N) + H^2}{\sqrt{[(d + R_N)^2 + H^2][(d - R_N)^2 + H^2]}}\right] .$$

H is the LEM elevation, d is the radial distance of the surface element from the landing site, R_N is the nozzle exit radius, ϵ_N is the nozzle emittance (0.9) and T_N is the constant nozzle temperature.

The total flux from the LEM is given as

$$Q_{LEM} = Q_{conv} + Q_{rad} = h(T_g - T_s) + \sigma F_{NS} \epsilon_N T_N^4 \ .$$

f. Radiation from the Lunar Surface to Space: It has previously been mentioned that the lunar surface radiates to space. The surface material under the LEM is covered in part by a shield behind the LEM exhaust nozzle. Thus, the surface elements near the landing site "see" both space and the exhaust shield. In an attempt to consider the portion covered by the shield, and also the fact that significant heat may be reflected by the shield to the surface, we have chosen the following equation for the flux emitted by the lunar surface during and after the LEM descent:

$$Q_{surf\ rad} = \sigma \epsilon_s (1 - F_{ss}) T_s^4 ,$$

where ϵ_s = the surface emittance, and F_{ss} is the viewfactor of the rocket nozzle shield given by:

$$F_{ss} = \frac{1}{2}\left[1 - \frac{(d - R_s)(d + R_s) + (H + 2.450)^2}{\sqrt{[(d + R_s)^2 + (H + 2.450)^2][(d - R_s)^2 + (H + 2.450)^2]}}\right]$$

4. Results of Analyses

a. Results of Simplified Analyses: Table 24 shows maximum possible surface temperatures for several distances from the LEM landing site. In these calculations, the surface temperature, in the absence of the LEM, would be 362 °K. It can be seen that for distances greater than 10 feet, the temperature perturbation produced by the landing is small. Also shown in Table 24 are values of the maximum surface temperature as calculated by a Grumman computer program in which heat flow into a dust surface was assumed. In these calculations, the surface temperature in the absence of the LEM was 387 °K (the subsolar point was used in the calculations).

Table 24

MAXIMUM LUNAR SURFACE TEMPERATURES (°K) DURING LEM DESCENT

	Distance from LEM Site (ft)					
	0	5	10	20	50	100
Maximum Surface Temperatures	1839	898	649	513	407	368
Maximum Surface Temperatures (Calculated by Grumman)	1572	875	574	442	394	387

Except for large distances from the LEM landing site, where heating by the exhaust is negligible, the surface temperature estimated from our simplified analysis is higher than that obtained from more rigorous analyses which include conduction heat transfer into the surface material.

We have estimated the subsurface temperatures after the descent of the LEM using the analytical model described above. Equation (96) shows several important factors which will also be observed in the computer results:

1) The rise in temperature above the initial value at any depth will be directly proportional to the assumed average LEM heat flux.

2) For constant values of thermal diffusivity and time, the temperature rise at any depth will be inversely proportional to the thermal conductivity of the material.

3) At the surface ($x = 0$) the temperature rise will decrease continuously after the LEM heat flux is terminated.

The average value of the LEM heat flux at various distances from the landing site were obtained from the following equation:

$$Q_{LEM,\ average} = \frac{1}{\tau} \int_0^{\tau} \left[h(t)\,(T_g - T_s) + \sigma \epsilon_N T_N^4 F_{NS}(t) \right] dt \qquad (97)$$

where $h(t)$ and $F_{NS}(t)$ are the convective heat transfer coefficient and nozzle view factors, and vary with time (t) and distance from the landing site in the manner given by Table 25. T_s was assumed to be zero, and ϵ_N to be 0.9, and τ is the time of descent. Values of the average LEM heat flux for various distances from the landing site are given below:

Table 25

HEAT FLUX TO THE LUNAR SURFACE

Distance (d) from Landing Site	$Q_{LEM\ average}$ (watt/cm^2)	Ratio of $\frac{(Q_{LEM,\ average})_{d = d}}{(Q_{LEM,\ average})_{d = 0}}$
ft.		
0	3.85	1
5	1.38	0.36
10	0.63	0.16
20	0.24	0.062
50	0.15	0.039
100	0.0022	0.00057

We have calculated the subsurface temperature distribution given by Eq. (108) for three models — homogeneous solid rock, homogeneous vesicular rock, and homogeneous particulate material at the landing site. As explained earlier, subsurface temperatures for other distances from the landing site may be obtained directly from the appropriate ratios Q_{LEM}, $d = d/Q_{LEM}$, $d = 0$ given in the above table. In the calculations we have assumed the thermal property values given by Table 23, corresponding to a mean temperature of about 300°K.

The results of the calculations are shown in Fig. 70. The temperature rise above the initial temperature is plotted as a function of time (from the initiation of the descent) for various depths within the surface. Three sets of curves are shown corresponding to solid rock, vesicular rock and particulate material.

Examination of the figure shows several significant results:

1) The maximum subsurface temperature rise of the solid rock is much less than that of the vesicular rock or particulate material. The maximum temperature rise in the subsurface material at depths of 1 to 2 centimeters is reached at times of 30 to 150 seconds after the initiation of the LEM descent.

2) The maximum subsurface temperature rise of the vesicular rock is greater than that of the solid rock, but less than that of a particulate surface material. The maximum temperature rise in the subsurface material at depths of 1 to 3 centimeters is attained at times of 100-1500 seconds after the initiation of the LEM touchdown.

3) The maximum subsurface temperature rise of the particulate material is the largest of the three models considered. The maximum temperature rise in the subsurface material at depths of 0.25 to 1 centimeter occurs at times of 1000 to 20,000 seconds ($\sim$ 20 min. - 6 hours) after the initiation of the LEM touchdown.

4) As the thermal conductivity (and diffusivity) of the surface material is decreased, the maximum temperature rise at shallow fixed subsurface depths generally increases and the time at which this maximum rise occurs increases. For example,

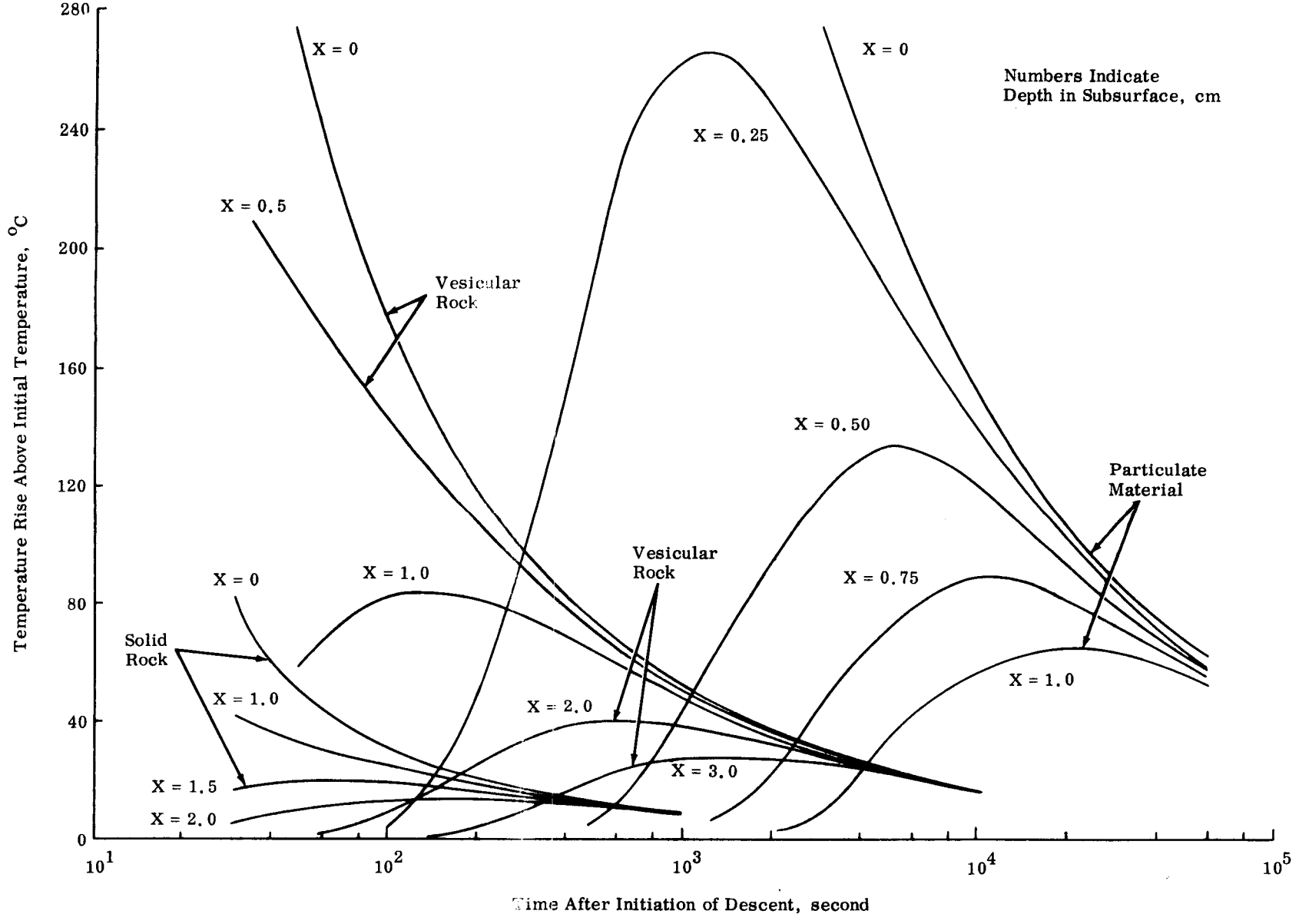

Fig. 70 Subsurface Temperatures Calculated From Simplified Analysis

at a depth of 1.0 cm the maximum temperature rise and corresponding time of the maximum are shown in Table 26.

Table 26

MAXIMUM TEMPERATURE RISE AT DEPTH = 1 cm

	Max. Temp. Rise (°C)	Time of Max. Rise (sec)
Solid Rock	44	< 30
Vesicular Rock	84	130
Particulate Material	64	2×10^4

In this case the maximum subsurface temperature for the particulate material was not greater than that for the vesicular rock because of the long time required to achieve the maximum.

5) At depths greater than 1 cm below the surface, regardless of its nature, the maximum temperature rise at the landing site caused by the LEM heat flux is less than 100°C. At distances greater than 10 feet from the landing site, this subsurface temperature rise would probably not be more than 15°C.

These calculations demonstrate that the temperature excursions in the subsurface are quite small, and the contamination effects of these excursions should also be small.

Comparison of the results of the computer program, shown in Table 27 and Fig. 71, with the analytical results using the simplifying assumptions given in 4.a shows good agreement. Temperature transients (during heating and cooling) as obtained from the computer analyses are more pronounced because of surface radiation cooling, and the use of the actual LEM heat flux rather than an assumed average heat flux. Maximum temperatures occur in the subsurface at nearly the same times in both calculations and are of the same order of magnitude. For example, at the landing site computer results for the vesicular rock model indicate that a maximum temperature rise of approximately 100°K occurs at 1 cm depth 160 seconds after the initiation of the descent. The simpli-

Table 27

MAXIMUM TEMPERATURES (°K) AT SURFACE AND SUBSURFACE LOCATIONS

MODEL 1 HOMOGENEOUS DUST

Radial Distance (ft)	0	5	10	20	50	100	Pre-Descent Temperature
Depth (cm)							
0	1640 (28)	811 (22)	600 (21)	476 (13)	383 (5)	363 (5)	361
0.1	807 (46)	425 (90)	380 (90)	365 (100)	358 (110)	356**	356
0.2	539 (170)	375 (350)	358 (350)	354 (350)	352 (400)	352**	352
0.5	383 (1800)	342*	338*	337*	337*	336**	336
1.0	313*	311**	311**	311**	311**	311**	310
2.0	262**	262**	262**	262**	262**	262**	261

MODEL 2 HOMOGENEOUS VESICULAR ROCK

0	1490 (28)	573 (26)	441 (22)	383 (15)	356 (8)	353** (8)	352
0.2	718 (34)	446 (30)	394 (27)	367 (23)	353 (20)	352** (18)	351
0.5	527 (60)	394 (60)	369 (50)	357 (44)	351** (44)	351**	350
1.0	437 (160)	369 (150)	357 (130)	351 (130)	348** (130)	348**	348
2.0	386 (550)	353 (500)	347 (450)	345 (450)	344**	344**	344
5.0	346*	334*	332**	332**	332**	332**	331

Table 27 (Cont.)

MODEL 3 HOMOGENEOUS SOLID ROCK

0	705 (28)	365 (26)	334 (22)	321 (15)	315** (8)	315** (7)	315
0.4	405 (36)	334 (32)	323 (27)	317 (23)	314** (21)	314** (19)	314
1.0	354 (70)	322 (60)	317 (60)	314 (48)	313** (48)	314**	313
2.0	332 (180)	316 (160)	313 (170)	312**	312**	312**	311
6.0	311 (1100)	306** (800)	306**	306**	306**	306**	305
10.0	302*	300** (1800)	300**	300**	300**	300**	299

MODEL 4 PARTICULATE SURFACE LAYER - VESICULAR ROCK SUBSTRATE

Particulate Layer 0.1 cm thick

0	1640 (28)	775 (28)	600 (21)	472 (13)	377 (5)	357 (3)	355
0.1	607 (38)	348 (60)	323 (70)	316 (70)	312** (80)	312**	311
0.2	433 (60)	320 (120)	312 (120)	310 (130)	309**	309**	308
0.5	381 (110)	316 (180)	310 (180)	308** (200)	308**	308**	307
1.0	348 (250)	311 (300)	307** (300)	306**	306**	306**	306
6.0	295*	291**	291**	291**	290**	290**	290

MODEL 5 PARTICULATE SURFACE LAYER - SOLID ROCK SUBSTRATE

Particulate Layer 0.1 cm thick

0	1639 (28)	773 (28)	597 (21)	468 (13)	370 (5)	350**	349
0.1	531 (38)	294 (60)	269 (70)	262 (80)	259*	259*	257
0.3	275 (60)	253 (130)	251** (150)	251** (170)	251**	251**	250
0.5	270 (80)	252 (150)	251** (160)	251** (180)	251**	251**	250
1.1	263 (130)	251** (200)	250** (250)	250**	250**	250**	250
2.1	257 (300)	250** (350)	250** (450)	250**	250**	250**	250

Table 27 (Cont.)

MODEL 6 VESICULAR ROCK SURFACE LAYER - ROCK SUBSTRATE

Vesicular Layer 1.25 cm thick

0	1435 (28)	549 (26)	414 (22)	354 (15)	326 (7)	323** (7)	322
0.1	874 (32)	465 (27)	384 (25)	343 (20)	323 (13)	321** (13)	321
0.5	500 (60)	361 (60)	335 (50)	322 (45)	315** (45)	315**	314
1.25	333 (170)	310 (150)	306 (150)	304** (150)	304**	304**	303
4.0	308 (700)	300** (550)	300** (800)	299**	299**	299**	299
8.0	297 (1700)	294** (1300)	294**	294**	294**	294**	293

MODEL 7 HOMOGENEOUS RUBBLE

0	1370 (28)	506 (26)	407 (22)	367 (14)	349 (7)	347** (6)	346
0.2	556 (38)	397 (32)	368 (27)	354 (25)	346 (21)	345** (20)	345
0.5	438 (90)	366 (80)	353 (70)	347 (70)	344** (60)	344**	344
1.0	388 (250)	352 (250)	345 (200)	343 (250)	341**	341**	341
2.0	358 (900)	340 (750)	338 (850)	337*	336**	336**	336
5.0	326*	322*	321**	321**	321**	321**	320

MODEL 8 PARTICULATE SURFACE LAYER - RUBBLE SUBSTRATE

Particulate Layer 0.1 cm thick

0	1640 (28)	809 (25)	599 (21)	471 (13)	375 (5)	354** (3)	353
0.1	578 (38)	330 (60)	306 (70)	299 (70)	296** (100)	296**	295
0.2	367 (60)	298 (130)	293 (130)	292** (150)	291**	291**	291
0.5	331 (140)	295 (200)	291** (200)	290** (250)	290**	290**	290
1.0	310 (350)	291 (400)	289** (450)	289**	289**	289**	288
6.0	274**	273**	273**	273**	273**	273**	273

Notes:

At depths greater than those indicated, the temperature approaches 230°K

Values in parentheses are times (in seconds after initiation of descent) at which maximum temperature occurs

*Temperature rising at end of calculations (2000 sec)

**Temperature within one degree of predescent temperature at 2000 sec or at maximum temperature

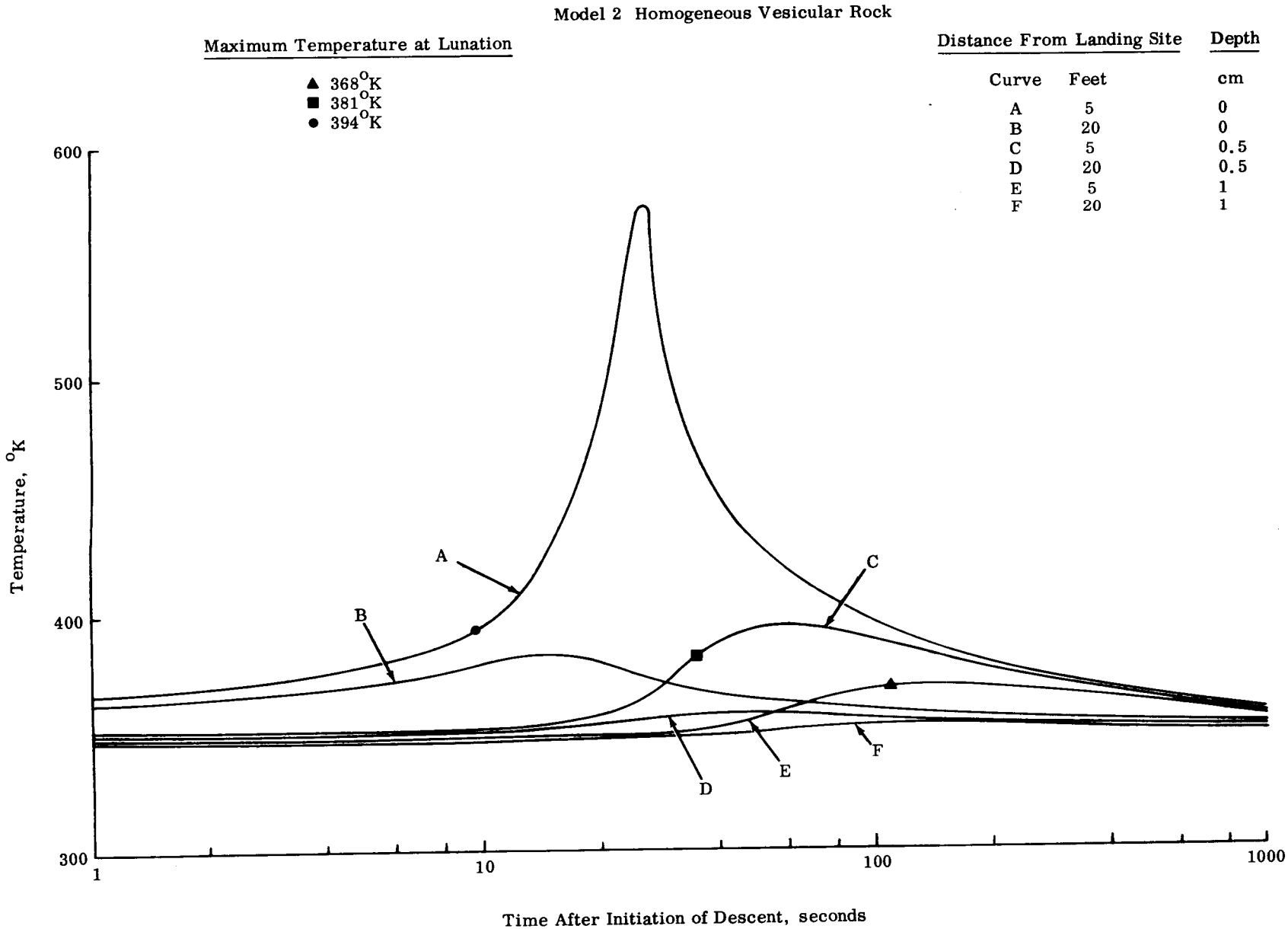

Fig. 71 Variation of Surface and Subsurface Temperature With Time-Results of Computer Calculations

fied analyses indicate a maximum temperature rise of 84°C at 1 cm depth 130 seconds after the initiation of the descent. Computer calculations for the solid rock show a maximum temperature rise of 11°C at 2 cm depth 180 seconds after the initiation of the descent. In the simplified analyses, a rise of 14°C after 160 seconds was obtained. Larger differences exist between the computer calculations and the results of the simplified analyses for the homogeneous dust layer because of the large variation in thermal conductivity with temperature of this material. At increasing distances from the landing site, there are significant differences in the maximum temperatures obtained from the computer and simplified analyses. This is caused by the assumption of average flux occurring over the entire 27.6 second descent time in the simplified analyses rather than the true heat flux pattern included in the computer analyses. However, the simplified analyses can be used to estimate the temperature rise for conditions other than those used in the computer calculations.

b. Results of Computer Calculations: Maximum temperatures at and below the surface for the postulated lunar models are shown in Table 27. Temperatures prior to the LEM descent are also given. Values in parentheses indicate the time from the initiation of the descent at which the maximum temperatures occur. Where no times are given, the temperatures were still increasing at the end of the time period used for the computations (2000 seconds). The double asterisk indicates: 1) the maximum temperature reached was within one degree of the pre-descent temperature or 2) the temperature after 2000 seconds was within one degree of the pre-descent value. The maximum temperature reached at the points with no indicated times will be less than those reached at the preceding depth indicated in the table. For example, for a homogeneous dust model at zero radial distance from the LEM landing site and at a depth of 0.5 cm, a maximum temperature of 383°K is reached 1800 seconds after the initiation of the descent. At 1 cm depth in the same location, the temperature rises to 313°K after 2000 seconds and continues to rise. The maximum temperature that will be reached at 1 cm will be significantly less than 383°K.

The results of the computer calculations show that for radial distances greater than 20 feet from the LEM landing site, the maximum temperature attained (for any model) is 600°K. At the surface, the highest temperatures are attained for the particulate (or dust) models. At depths below 1 centimeter, the maximum temperature reached is approximately 440°K. At 1 centimeter depth

the highest temperatures are reached for the vesicular model rather than for the dust model because of the large attenuation of the heat flux by the low thermal conductivity of the dust. At depths below 1 centimeter, temperatures during the LEM landing are comparable to the normal temperature variations attained during lunations. At distances greater than 50 feet from the LEM landing site, the maximum temperature at the surface is only about 20°C higher than the pre-descent temperatures.

The time dependence of the temperature for the various models can be inferred from the tables and is shown for the homogeneous vesicular model in Fig. 71. The six curves represent the temperature-time history in a homogeneous vesicular model for the surface and two subsurface locations, at 5 and 20 feet from the LEM landing site. The filled symbols on Curves A, C, and E represent the maximum lunation temperature attained at the surface and at depths of 0.5 cm and 1 cm for the model. The surface temperature 5 feet from the LEM landing site peaks sharply as the LEM descends and decreases rapidly due to radiation cooling of the surface. The temperature rises to its maximum value at 20 feet from the landing site in a horter time than at 5 feet because the maximum heat flux is reached at an earlier time. (See Sec. 3 for discussion of the variation of heat flux with time.)

To make the computer calculations more representative of an actual physical system, we assumed that the convective heat flux ceased immediately when the LEM engine is turned off, but that the radiative flux from the nozzle decreases exponentially with a 5 second time constant. This affects primarily the surface temperatures near the LEM, i.e., at 0 and 5 feet radial distances.

The surface temperatures calculated for the layered models are similar to those calculated for the homogeneous models using the same surface material layer. Subsurface temperature rises are smaller than those for the homogeneous models because of the high attenuation factor of the low thermal conductivity surface layer.

I. Sampling for an Indigenous Lunar Ecology [S. Penn]

1. General

Sampling for an extraterrestrial ecology, although one of the more exciting objectives of lunar exploration, will require the most demanding sampling methods. The presence of simple organic compounds in lunar material would probably be accepted (as were those found in meteorites) by some as sufficient proof of life in space. Unless confidence could be established in the sampling methods, this would remain a minority view. One positive proof of an indigenous lunar ecology would be the fossilized remains of former life.

The presence of men on the moon and their capacity for contaminating lunar samples by exuding human ecological debris could vitiate the quality of all investigations of the indigenous lunar ecology. Evidence of a viable lunar ecology may never be completely accepted but with a large number of experiments, a level of confidence may be established for the data.

2. Principles of Lunar Ecological Sampling

All lunar exobiological investigations have one thing in common, namely obtaining samples of the surface and near surface ecology for subsequent investigations. The detection of organic matter in situ is not presently planned (Ref. 40). The technique for obtaining and preparing the specimens and bringing them to the test area is somewhat vague at present. Similarly the experiments to be performed and the way in which the data will be recorded is largely undetermined. For simplicity, we are concerned herein only with specimens that will be returned to earth for study, hence the astronaut may or may not take the samples, but will be called upon to recover and stow them aboard the Apollo spacecraft. We shall also limit our subsequent objective to seeking data on terrestrial-like life, relegating the investigation of unusual forms (such as silicon rather than carbon based life) to future missions.

The level of contamination of any specimen, organic or not, could be greatly reduced if taken at some depth beneath the lunar surface. This in fact may be the most propitious location for an indigenous ecology even prior to the introduction of the contaminants. Unlike the terrestrial ecology where the density of

organic material is greatest near the surface, and decreases sharply with depth, the lunar environment may preclude this arrangement. A cover of surface material may be essential for most organisms to survive. Hence, sampling at depth may be the only way to obtain an exobiological specimen. It is entirely possible that a number of ecological horizons, corresponding to temperature and moisture variations could exist at depth. The presence of ecological horizons at depth might escape detection unless deliberately sampled for.

With each successive vehicle landing on the moon, the opportunity for obtaining an uncontaminated sample of the lunar ecology decreases. Sampling is invariably time dependent. Variations can be expected in samples to be obtained between the first mission and all later ones. In fact, within the time span of the first manned landing, significant variations can be expected between samples obtained at a single site. These may be due to:

- Settlement of eroded material
- Infall of micro-meteoritic material
- Activity of astronauts (mechanical)
- Activity of products of rocket exhaust, LEM cabin, and astronaut leakage (chemical)
- Solar wind bombardment of surface exposed by the rocket exhaust.
- Mutation or reduction of organic contaminants so that they cannot be distinguished as terrestrial in origin.
- Normal thermal changes during the lunar day.

3. Sterilization Technology

It is apparent that the degree of confidence that can be placed on a sample is directly proportional to the extent to which the sampling tools and return containers are free of terrestrial life forms. Despite great strides that have been made by the food and medical industries, sterilization technology in use today is still very inadequate for the purposes of exobiological sampling. For very practical reasons, no attempt is ever made to remove all

of the viable organisms (Ref. 41). Instead, most, though by no means all, of the the pathogens in our food and drugs may be killed with one or more shotgun methods that have been learned principally by trial and error.

For the investigation of an extra-terrestrial ecology it may not be sufficient to kill organisms by merely reducing them to a mass of less complex peptides. Absolute sterilization mandates the irreversible reduction of all organic molecules to their inorganic components (e.g., C, O_2, H_2O, CO_2). Some reduction techniques are currently in use and have been known for some time. Among these are heat, chemical reagents, and photons. As most commercial sterilization techniques are less concerned with absolute sterility then economy, some factor, such as time or temperature is sacrificed. The level of sterility required for exoecological sampling equipment must obviously exceed commercial standards if any confidence is to be expected in the results obtained with them.

The antithesis of sterilization, i.e., the combination of inorganic material to form organic like or proto life molecular structures, must also be noted. There is abundant evidence to confirm the "spontaneous generation" of possible proto life, including some that are capable of replication (Refs. 42 through 47). The discrimination of indigenous proto life from that which might inadvertently be generated from contaminants may not be possible without the use of tracers. For the first missions at least, the element of time required for the generation of proto life may be important.

4. Contamination With Human Ecological Debris

In addition to the data that have been derived from manned earth orbiters, a number of investigators have confined human subjects within various controlled environments to obtain physiological data (Refs. 48 through 53). In instances, the pathogens of feces have been monitored as well as some nonpathogenic flora (Ref. 48). Deep sea and high altitude simulations establishing man's compatibility with his environment, have generally been intended to qualify the equipment used to maintain the environment, with little or no effort expended to measure the ambient ecology. One such investigation, soon to be conducted at Grumman, will seek to qualify the LEM Environmental Control System by having a suited subject perform various tasks in a simulated LEM cabin environment. There are at present no plans to monitor the ambient

ecology. It seems evident that an evaluation of the contamination of the indigenious lunar ecology with human ecological debris will be greatly dependent upon knowledge of the nature of the human ecology in the space suit and LEM cabin environments.

On the lunar surface, gasses are expected to leak from a number of areas of the suit at an estimated rate of 200 cc per minute. Because of the minute size of the leaks, they may be regarded as molecular filters, selectively passing gasses and some smaller organisms, while screening and thereby concentrating the larger ones. The consequence of this concentration may in itself be a problem area worthy of further consideration.

Leakage from the LEM cabin may similarly contaminate the moon with human ecological debris. For several reasons, this source of contamination may be of less significance than that exuded by the roving astronaut. In order for the astronaut to leave the cabin, it must be depressurized, thereby venting all of its atmosphere over much of the area that he will traverse. The initial density of organic contaminants will predictably diminish with their radial distance from the LEM.

Following prolonged exposure to the lunar environment, little of the original organic materials are likely to retain their molecular structure, and their subsequent recognition as the inorganic contaminants derived from human ecological debris is problematical. The low density of organic contaminants (in areas remote from the LEM), their exposure to the lunar reduction environment, and the considerable time lapse between the LEM depressurization and the final sampling operation, could combine to exceed the level of sterilization expected from commercial sterilization techniques. By contrast, leakage from the astronaut's suit need travel only negligible distances to contaminate grab samples with viable organisms which would then experience little direct exposure to the lunar environment before being sealed in a sample return container.

The reduction or sterilization of most viable organic material when exposed to the lunar environment is a reasonable assumption. Despite the lack of quantitative data, there are indications that some organisms can survive the lunar environment in a suspended state (Ref. 54). The survival and adaptation of some terrestrial organisms to the lunar environment is, in a sense, an assumption upon which much of our concern is based.

5. Characteristics of an Effective Exobiological Sampling System

It is evident that in the search for an indigenous lunar ecology, a sophisticated, fully integrated system is mandatory. The object of this report is not as much to select a sampling system, as to define some of the parameters for exobiological sampling and to suggest some possible tools and techniques that may be applicable for the Apollo program.

Within the framework of the Apollo program the factors necessary for exobiological sampling are as follows:

- All surfaces that may be exposed to the sample should be totally free of organic material, not merely sterile in its ordinary commercial sense. This is equally applicable for vacuum rated lubricants which may contain trace amounts of organic contaminants. As an alternative, it may be possible to separate interaction surfaces with a film of soft metal, such as with aluminum or gold. The presence of minute amounts of such metals in the specimen would be readily discernible and effectively inert. Teflon has been recommended as a suitable material for sealing lunar biological sample return containers (Ref. 40). As teflon has an organic molecular structure, its use presupposes that it will not degrade in the lunar environment. Such a supposition must be carefully verified.

- Samples should be taken at depth as well as at the surface because of the possibility of an ecology developing beneath the protective crust.

- Percent recovery must be noted. Voids or lost material may be significant.

The above parameters are as applicable for a fully automated system (i.e., one that would land an instrumented package on the moon to obtain, process and store a sample for later recovery) as they are for a roving astronaut collecting grab samples.

Each phase of each lunar landing is expected to be progressively more deleterious, giving rise to greater quantities of organic contaminants and their accumulation. (The exhaust of

the descent rocket will contain the least amount of organic material, followed by the depressurization of the LEM and leakage of the astronaut's suit, each of which is progressively more likely to contain organic contaminants.) In short, the optimum sample should be that which is taken at the earliest stage in the sequence of operations consistent with engineering and payload restrictions. Carried to extremes, this could suggest a sampling device that would be dropped from a lunar orbiter.

All lunar probes, sampling devices, or systems may generally be classified in one of four possible concepts (see Fig. 72).

- Concept 1 - Introduced from a Lunar Orbit (Fig. 73)

  Use of a lunar impacter for sampling would, as noted, probably be least affected by the contamination associated with soft landers, the depressurization of the LEM cabin, and leakage from the astronaut's suit.

  With an impact velocity of the order of 2.5 km/sec, a vehicle that could survive the impact, sample, and then emit some sort of signal for its subsequent recovery would necessitate an imposing shock absorbing system. Even then the impact area might be so greatly altered that the sample could be meaningless. It may be possible to eject a secondary module or modules from the vehicle that could obtain samples in a less disturbed area near the initial impact. With much of the original impact energy absorbed by the "mother" vehicle, the sample probes would experience only the relatively milder secondary impact. The "mother" vehicle could furnish the means for the location and subsequent recovery of the smaller probes. The Russian Luna 9 is reported to have been ejected from a larger (mother) vehicle, which relied upon retro rockets to reduce its impact velocity. A lunar hard lander that could telemeter data back following its impact, precluding the need for its recovery, may be a mission objective worthy of consideration, even if independent of the Apollo.

  The use of a soft lander or one which will use retro rockets to halt its descent (to some moderate height) and then fall to the moon is currently being considered

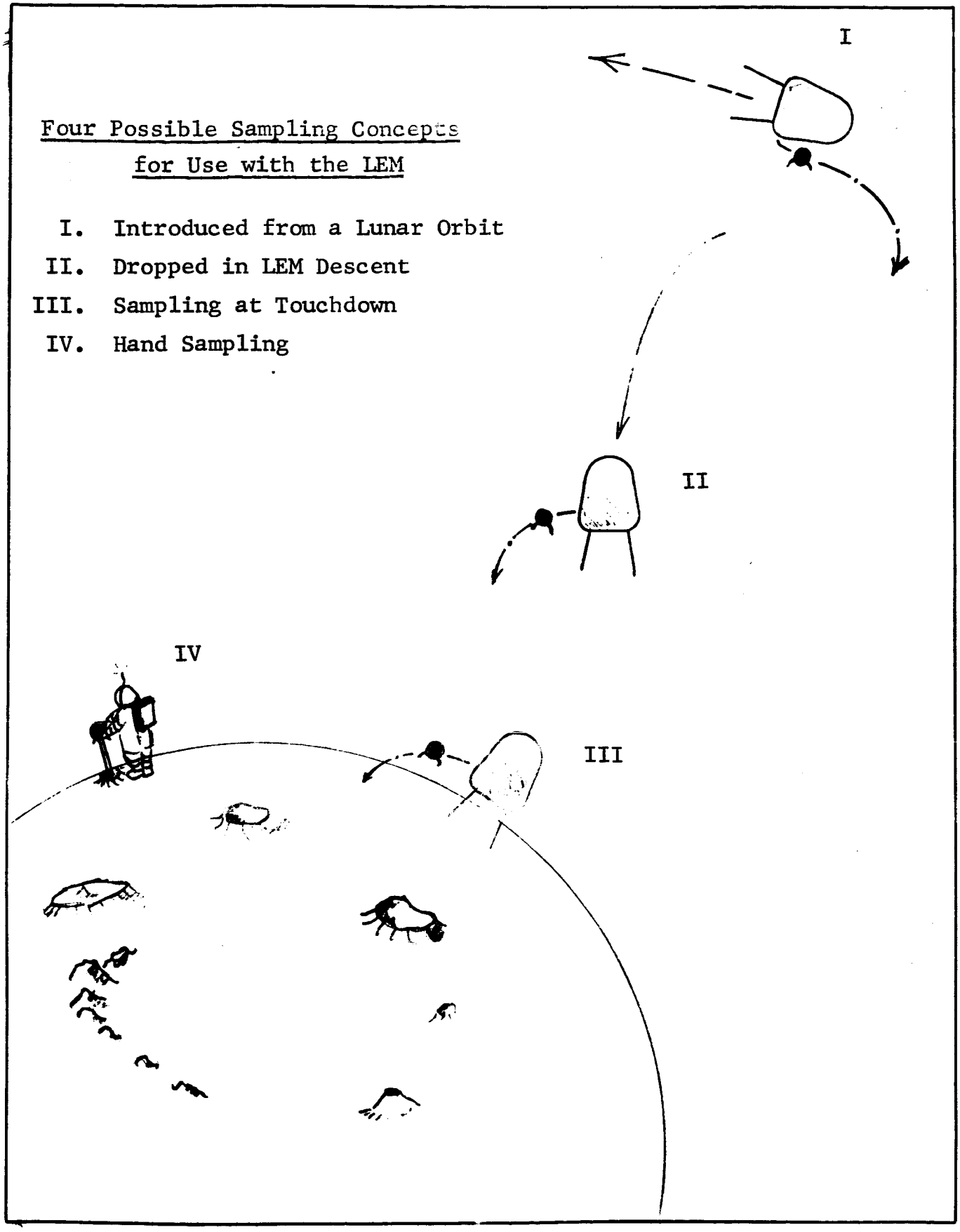

Fig. 72 Sampling the Moon for a Viable Ecology

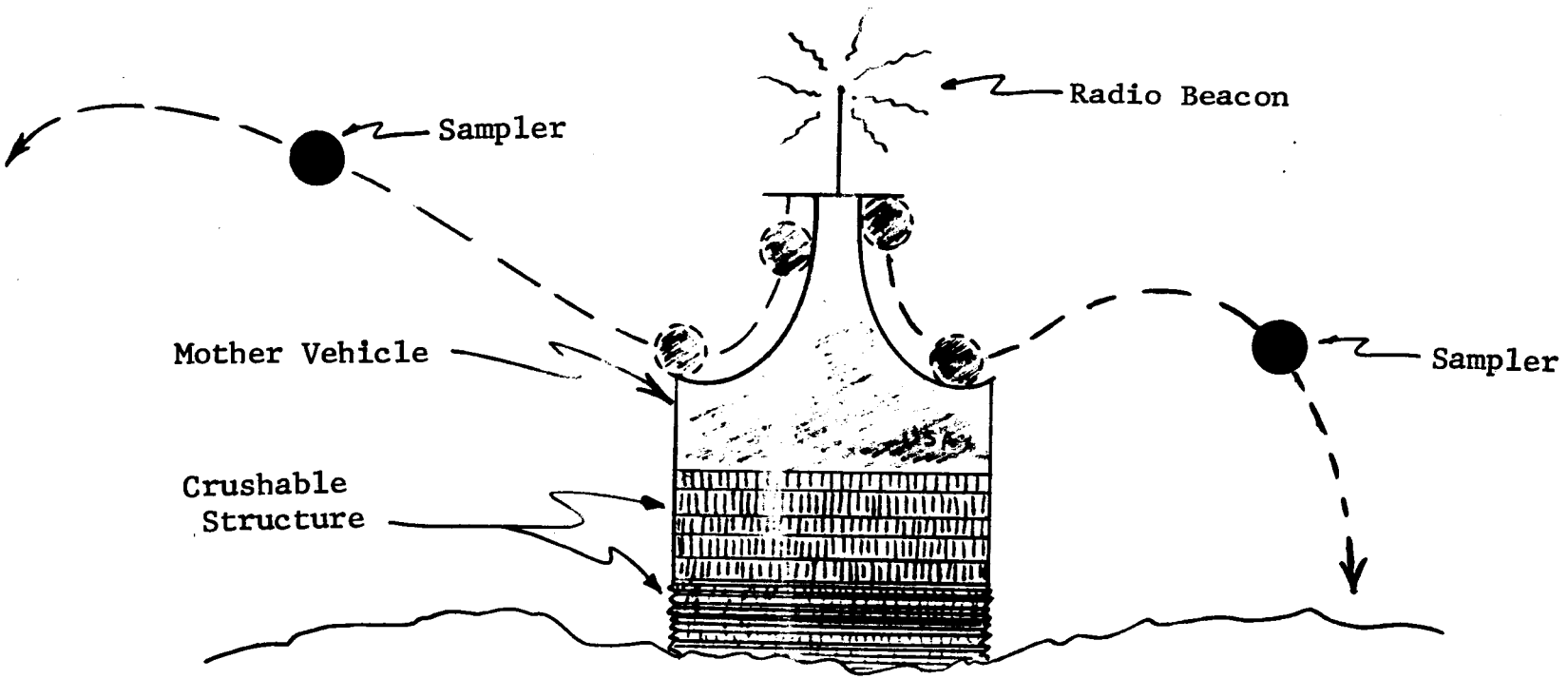

Fig. 73 Sampling for a Viable Lunar Ecology: Concept I – Introduced from a Lunar Orbit, A Possible Hard Lander

for post Apollo missions. In one scheme, a "mother" vehicle would eject a number of penetrometers and hover while relaying back data. Although the use of retro rockets for a soft or semi-soft lander would introduce an additional source of contamination, the quantity of contaminant would be less that that introduced by the LEM. By using retrorockets to reduce the descent when several hundred or thousand feet above the moon, rather than stopping it when a few feet from the surface (required for the LEM), considerably less, if any, of the contaminant would ultimately appear in the sample.

That the level of contamination to be expected would be smaller with devices introduced from a lunar orbiter is partially offset by its inherent degree of complexity, particularly if an elaborate communication system is required for their subsequent recovery.

- Concept 2 - Dropped in LEM Descent

When the LEM is descending to the lunar surface, but prior to touchdown, it may be possible to eject a sampling device at a height of 200 to 2000 feet. The level of contamination of the sample due to the rocket exhaust should be considerably less than that which would subsequently be obtainable.

The device could be similar to one which could be inserted from a lunar orbit (Concept 1) but need not contain the elaborate array of retrorockets and communication equipment. The location and recovery of the device should be relatively simple.

The principal disadvantage of this concept stems from the additional burden that it imposes upon the astronauts during the critical landing maneuver. Lacking attitude controls, it may be difficult to assure a precise orientation of the module at impact.

- Concept 3 - Sampling at Touchdown

Following the landing of the LEM it is unlikely that an uncontaminated specimen of the indigenous ecology could be obtained at the surface. Even if the surface

were not eroded by the rocket exhaust, the integrity of exobiological samples taken in the vicinity of the vehicle would be questionable, if only for the changes thermally and chemically induced by the rocket.

Within this concept there are two possible variances; a device attached to the landing gear of the LEM, or one ejected from it prior to the egress of the astronaut. The principle objection to the first is that the touchdown area will experience the greatest thermal changes, and chemical contamination due to the rocket exhaust; hence sampling there may not be too meaningful. Ejection of a sampling device to some distance from the vehicle is preferable.

The advantage gained by this method over having the astronaut place a device on the moon is that the contamination introduced by the depressurization of the LEM cabin and leakage from the astronaut's suit and the repressurized LEM is avoided. When compared with the quality possible with devices injected from orbit or dropped from some intermediate height above the moon, this concept is less promising.

- Concept 4 - Hand Sampling

Barring an unprecedented degree of sophistication, the biochemical level of contamination should be greatest in grab samples and shallow cores obtained from the lunar surface. If a sub-surface ecology is indeed the nature of the lunar biosphere, grab samples might at best yield negative results. Although the method may be the least complicated it could also be the least fruitful. An exception is the sampling of natural structural features such as deep craters, fissures, caves, etc., which might experience little direct exposure to the sun's radiation and the rocket exhaust and may support an indigenous ecology. It is improbable that such features, if they exist at all, could be remotely sampled. As considerable judgement will probably be required to effectively sample them, it is evident that some form of hand sampling will be required, despite its inherently high contamination potential.

6. Possible Techniques for Minimizing Sample Contamination

To minimize the erosional and highly contaminating effects of the retrorocket, it may be possible to shield one or more areas near the landing site to subsequently obtain relatively uncontaminated samples from them.

During the descent to the lunar surface, a package could be ejected from the LEM, which at or slightly before impact would expand to form a thin protective shield or blanket for the material beneath it. The shield could be a mass of silicon grease, possibly a rapidly forming foam, or a foam contained within a flexible skin, a sort of flat balloon. The impact of the package could disturb the structure of the moon's surface but the direct exposure of the surface to the rocket exhaust might otherwise erode it, with the consequence that no sample of the surface would be obtainable.

An exposed foam, though evolving gases while forming, would probably off gas to space in preference to the material below. The nature of the gas could be well established in advance so that its detection in the samples would not be unexpected. The gas pressure above the foam would tend to protect the shield from the impingement of rocket gases, though this would be strongly influenced by its distance from the point of touchdown. A "spin-off" of the prelaunched shield would be to establish ground control for the landing maneuver. With sufficient development, the shield diameter, thickness, etc., could be predictable. It could also contain bright colors and perhaps luminesce. Knowing the diameter of the shield, the astronaut, when sighting upon it, could estimate his altitude. If the package could be assured of a vertical fall with no horizontal motion, the shape of the shield may help to guide him in the selection of a landing site.

Anticipating a disc, he would be justified in avoiding the site if instead it appears as an ellipse with a minor axis of half its major axis, thereby indicating a 50% slope. Irregularities of its perimeter, when correlated with the thickness of the shield, its viscosity, etc., may reveal a degree of roughness at the landing site that may be too hazardous. It is evident that for the astronaut, the secondary advantages of the shield may far outweigh its significance for exobiological sampling.

The success of the sampling mission will to a great measure be dependent upon the discretion of the astronaut. Natural

structural features that experience little direct exposure to solar radiation, may also suffer less from the rocket exhaust. Hence, grab samples, though generally frowned upon, would be preferred from these areas and could contain fewer contaminants. Statistical sampling such as with an orderly grid system or radiating from the LEM may be more feasible for later missions, or for an unvarying, homogeneous plain.

Leakage from the astronaut's suit, particularly at the joints, is expected to contain a high percentage of contaminants that could influence exobiological sampling. Determination of the sources of leakage may not necessarily lead to their elimination. We may still be able to assure a level of confidence in ecological sampling with a fresh approach to the use of hand tools.

A list of hand tools that are normally used for terrestrial sampling and which may be applicable on the moon appears in Table 28. The hand or powered coring tools that have been proposed for lunar geological sampling may not assure an uncontaminated ecological specimen. The lubricants normally used to cool drill bits and remove the cuttings from the hole (water or air) will probably not be used on the moon. Instead, other lubricants and impregnated drill bits may be used (Ref. 55). These may be unacceptable for ecological sampling while being perfectly acceptable for stratigraphic or petrological investigations. The use of impregnated drill bits, bearings, hand tools, etc., while solving some technical problems could create additional sources of contamination.

That we are experiencing some difficulty selecting a lunar ecological sampling tool stems from the paucity of similar tools for terrestrial use. Biologists tend to rely upon conventional hand and power driven tools. To date, no tools have been suggested that could assure a pristine lunar ecological sample.

We may tentatively assume that all of the contaminants due to the retrorockets, the LEM, and the astronauts will remain on or near the lunar surface. Hence a tool that could penetrate the surface, take a specimen, and then be withdrawn without exposing the specimen to the surface layer or other contaminants, could obtain relatively pristine samples. One possible configuration would be a tool consisting of three concentric telescoping tubes with the inner and outer one tapering to a tip of claw-like radial springs, not unlike a drafting pencil within a protective shroud (see Fig. 74).

Table 28

HAND TOOLS USED FOR GEOLOGICAL SAMPLING

Tool	Type of Sample	Nature of Material to be Sampled
1. File	Powder	Very hard and dense. Fine grain. Smooth rock face.
2. Striking Hammer and Star Drill or Chisel	Chips, Hand Specimens	
3. Pick		Coarse grain, low porosity.
4. Stone Hammer		Thin edges or projections.
5. Wedge		Fissures.
6. Crowbar		
7. Handsaw		Very porous or loosely cemented.
8. Auger Drill	Soil	Dense, packed, fine grained soil.
9. Spoon Sampler		Less dense, fine grain.
10. Scoop Shovel		Loose particles, gravel to dust.

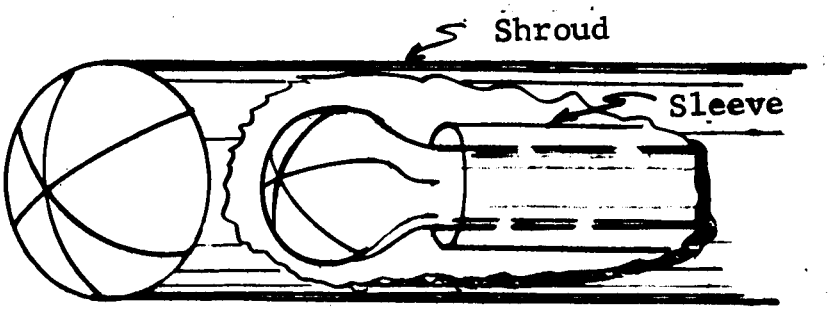

a.

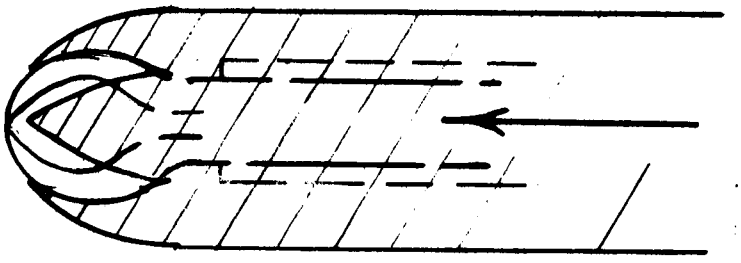

b.

Concentric tube with claw-like spring tips is forced beneath Lunar surface. Following insertion into Lunar surface, inner tube is forced through outer claws. Sample is then obtained.

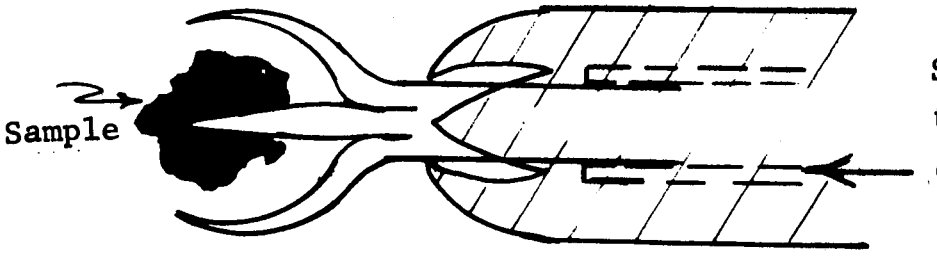

c.

Sleeve forces inner claw to close prior to removal of inner tube.

Fig. 74 Illustration of a Possible Lunar Exobiological Sampling Tool

a) Cutaway of Sampling Probe, b) and c) Operation of Sampling Probe

The assembly could be driven into the lunar surface, or might be dropped from a descending LEM. The inner tube would then be forced through the claw tip of the outer tube, expand, (like a drafting pencil) core or grab a specimen. The claw of the inner tube would be closed by the intermediate tube or sleeve and then be withdrawin to its original position. The inner tube and sleeve could then be withdrawn and used as a sample return container, or the sample could be transferred to another container. Once the outer tube has been inserted, it could be driven deeper and a series of replaceable inner tubes used to sample at each penetration increment. With a properly prepared tool, the contamination of the surface and the astronaut might be limited to the outer tube (shroud), and not be returned with the sample. Although such a tool will function best in a particulate, tuffaceous or scoraceous surface, its success in an unbrecciated massive rock would probably be inferior to a more conventional rock drill. Ecological sampling in massive rock may not be too promising under any circumstances.

The use of soft metals as lubricants might be particularly suitable for this tool, if the sample should also be sealed by the metal and not be subject to further exposure and contamination. The many anticipated vacuum welding problems (Ref. 55) would then be come an asset instead of a liability. The tool would also be applicable for use with a prelaunched protective shield.

To additionally assure that viable organisms introduced into the lunar surface do not contaminate the samples, the astronaut could be equipped with a thermal device to sterilize the area to be sampled. As the lunar surface is expected to have a low thermal conductivity this procedure would probably not degrade an ecology at depth.

The use of tracers in this area has largely been ignored, although potentially suitable tracer materials are available. It may be possible for the astronauts to ingest some harmless tracer material to be emitted with their sweat, breath, etc., thereby filling the space suit and LEM environments. An alternate approach would be to coat the interior of the LEM and the suit with tracer material. The advantage of an ingested tracer is that its emission rate will vary with the man's physical activity. Should the tracer be subsequently detected in lunar samples, the relative concentration of tracer material in different specimens would influence their exobiological significance, despite the possible absence of any other indication of life or proto-life.

The nature of the task lends itself to the use of such radioactive materials as tritiated water or carbon 14. Their maximum permissible total body burdens are respectively 2×10^3 microcuries and 400 microcuries (Ref. 56). The $H_2{}^3O$ (0.018 Mev β) and $C^{14}O_2$ (0.155 Mev) are both significantly greater than the solar induced ground state.

They are both weak β emitters with radioactive half lives that are respectively 12.4 years and 5600 years (Ref. 57). With a biological half life of the order of 8.5 days, which is longer than the first Apollo missions, a tritium tracer could be administered to the astronauts while still on earth.

V. CONCLUSIONS

A. Results of the Study

The work performed under this contract and the results achieved are summarized in Sec. I and II. One accomplishment has been the calculation, from existing data, of contamination by various processes. Another results has been the defining of areas in which existing data are inadequate.

The studies of contaminant composition (Sec. II.B.1) and of the far field molecular flux (Sec. IV.A) are valid independent of further discoveries about the lunar environment. Other results, for example, erosion distributions (Sec. IV.B and C), depend in detail on the structure of the lunar surface and can be continually improved as more knowledge of the surface becomes available (Sec. V.B). The Luna 9 photographs of the lunar surface became available near the end of this contract. They will permit a more realistic choice of surface models. These photographs indicate a porous, rocky, dust free, relatively firm surface possibly resembling a vesicular or semicompacted structure. It is premature to conclude that all areas of the moon are identical to the one in the photograph. Despite this, the photographs provide valuable guidelines to surface models (cf. Sec. V.B).

It was inevitable that the study would disclose areas of ignorance concerning contamination in the lunar environment. These areas include (cf. Sec. V.B) the nature and quantity of bacterial contaminants under Apollo conditions, chemical reactions in the lunar radiation environment, and adsorption and desorption of gas in the lunar environment.

Two recent publications are of importance to the study of contamination. They summarize conclusions reached at two conferences where eminent scientists met to consider the future scientific exploration of space. The conferences conducted by NASA (Ref. 40) and by the National Academy of Sciences (Ref. 58) provide guidelines against which our study can be judged.

A few examples, taken from Ref. 40, illustrate the importance attached by these scientists to the contamination of lunar samples.

On page 11 of Ref. 40, a group of scientists suggest the following specifications for LEM scientific equipment:

> "Sample containers should keep samples sterile and chemically clean. Stainless steel is acceptable. More studies should be completed relative to the use of teflon in the lunar environment."

They also specify an "aseptic sample collection tool" (cf. Sec. IV.I).

On the same page the importance of space suit leakage (cf. Sec. V.B) is mentioned:

> "Studies and tests should be started immediately to determine the amounts and effects of the outgassing of the astronauts' suits and the escape of the atmosphere from the LEM. Sterilization of the escaping atmosphere from the LEM should be considered. Analyses of the possible contaminants in the LEM fuel and the effects on sample collection should be undertaken."

Lunar atmospheric contamination is considered on page 13 of Ref. 40 where the group recommends that

> "Pressure, flux and mass measurements for determination of neutral and ionic constituents should be conducted. This is advantageous for early flights because of the uncontaminated state of the atmosphere."

On missions after Apollo, the group recommends on page 17 as part of the equipment:

> "Lunar Drills. The development of a 1-inch drill capable of penetrating to a depth of 3 meters in either rubble or solid rock is recommended. It should be operable from a roving vehicle. It is necessary for lunar het flow studies and for obtaining biological samples."

In view of the possibility for penetration of rocket exhaust gas and other contaminants into a porous lunar surface (Sec. V.B), the suggested requirement for a 3-meter drill might be reexamined.

B. Areas for Further Investigation

The photographs of the lunar surface recently transmitted to earth from Luna 9 will permit the recalculation of results presented in this report, using parameters that correspond to the lunar structure indicated in the photographs. It would be desirable to recompute the distributions of eroded material (Secs. IV.B.1 and IV.B.2), which were calculated for a dust model, using parameters representative of the resistance of vesicular or semicompacted surfaces to shearing stress produced by exhaust gas flow (cf., Sec. II.D.3). The photographs indicate a porous surface. Consequently, there may be considerable penetration of exhaust gas into the lunar surface. It has been suggested that a drill be used to obtain samples that are free of surface contamination (Sec. IV.I). It therefore would be advisable to investigate the depth to which contaminants can penetrate so that the drill can be designed to reach greater depths. Penetration of exhaust gas into the lunar surface will also affect subsurface temperature distributions (Sec. IV.H) and may affect atmospheric contamination (Sec. IV.E).

The area of bacterial contamination is important and will require much additional theoretical and experimental study to determine the type and amount of bacterial contaminants and organic debris that can be expected on the Apollo mission (Secs. II.B.3 and III.C). Our survey of this area demonstrates that existing data are inadequate. Much painstaking experimental testing involving specialized equipment and techniques is required.

Since bacteriological contaminants spread in the gas leaked from space suits or vented from the ascent stage, it would be desirable to know the distribution of gas from these sources. Space suit leakage is significant because of the intimate contact between the astronaut and the collected samples.

To determine the distribution of adsorbed exhaust gas on the lunar surface (Sec. IV.D) or the distributions of atmospheric contaminants, (Sec. IV.E) it is necessary to know the rates of adsorption and desorption of gas on the lunar surface (Sec. IV.F and G). Almost no reliable data are available on these processes under lunar environmental conditions. Experimental data are needed.

The results obtained for contamination of the lunar atmosphere (Sec. IV.E) could be improved by including more detailed information on adsorption and desorption coefficients and also by including more detailed treatment of surface temperature variation effects, molecular velocity distributions, solar wind variations, and other items not included in the present study.

The exhaust of the descent and ascent rockets may affect instrument packages (ALSEP, etc.) left on the lunar surface by the Apollo and subsequent missions. Such packages may be affected by heating resulting from contact with the ascent stage exhaust, by impacts from lunar surface material eroded by the ascent engine plume, and descent stage propellant leakage or explosion subsequent to launching of the ascent stage. It would be advisable to extend techniques developed during the current contract to the examination of such problems.

Chemical reactions on the lunar surface in the lunar radiation environment is an area requiring further experimental investigation. The chemical composition of the descent engine exhaust has been determined with respect to the principal constituents. However, as noted in Sec. II.B.1, additional information may be desired concerning the abundances of trace combustion products or the products originating from the phenolic ablative materials. These can be experimentally determined.

A number of devices for minimizing contamination are suggested in Sec. IV.I. The feasibility of the suggestions should be further explored.

The Apollo mission will not enter an uncontaminated environment. In addition to contamination from the mission itself, the moon will already have experienced contamination from Lunik, Surveyor and other missions. While the contamination effects of these missions will probably be small, it is not evident that they are all negligible. Pre-Apollo contamination effects on the Apollo mission should be investigated to make sure some significant aspects are not being overlooked.

C. The Apollo Scientific Program and Consequences of Cumulative Contamination

The following recommendation was made in the written report (Ref. 1) of the oral presentation on this contract, which was made at NASA/MSC on November 2, 1965. It is repeated here because the Principal Scientist feels it is of importance.

The strongest impression left by the oral presentation and subsequent conversations with people concerned with lunar experiments is that the problems of lunar contamination should be given greater weight in planning the Apollo mission scientific program. Many people concerned with programs which involve tool design, experiments, and sample collection techniques are aware of contamination

problems and are seeking ways to deal with them. However, people concerned with the over-all planning of the Apollo scientific mission should also be continually aware of the effects of cumulative contamination due to subsequent missions. This is vitally important because certain significant lunar experiments which may be performed on the Apollo mission may be impossible on later missions due to cumulative contamination. It is possible that the door to whole fields of scientific investigation may be forever closed after the first manned mission. Exobiological experiments immediately come to mind because this field has received considerable comment. Undoubtedly, investigation would disclose other areas in which the first Apollo mission may be the last chance to gather data. By contrast, it would be hard to suggest a geological experiment that would be seriously affected by the cumulative contamination of a great number of missions.

It is unlikely that the Apollo mission will be man's last visit to the moon. What is urgently needed is a survey to determine the important classes of experiments which must be performed at the earliest possible date in the course of man's exploration of the moon. Experts in various fields should be consulted in order to stimulate thinking in this area. It is already late, and efforts should begin as soon as possible.

The Apollo scientific program must always be subordinate to the overriding concern for mission safety. But within this limitation, the progressive closing out of important areas of research by cumulative contamination should be a prime factor in planning the scientific program.

VI. REFERENCES

1. Aronowitz, L. et al., Investigation of Lunar Surface Chemical Contamination by LEM Descent Engine and Associated Equipment, Grumman Research Department Memorandum RM-237, January 1966, interim report on Contract NAS 9-4860.

2. Design Reference Mission, Apollo Mission Planning Task Force - Vol. I: Mission Description Report No. LED 540-12, for Contract No. NAS 9-1100, October 1964.

3. Classified (Confidential) Addendum to this report.

4. Oman, R. A., Research in Gas Surface Interaction, 1964-65 - Part I: Numerical Calculations of Gas-Surface Interactions, Grumman Research Department Report RE-222, August 1965, Part I of final report on Contract No. NASw-1027.

5. Savage, F. A., and Breeding, R. E., E.M. #NA-SS-1053, Hamilton Standard Division of United Aircraft Co., November 6, 1965.

6. Singer, S. F., and Walker, E. H.,"Photoelectric Screening of Bodies in Interplanetary Space,"Icarus, Vol. 1, p. 7-12, May 1962.

7. Photochemistry in the Liquid and Solid States, ed. by Heidt, Livingston, Rabinowitch, and Daniels, John Wiley and Sons, New York, p. 21, 1960.

8. Kohn, H. W., and Taylor, E. H., J. Phys. Chem., Vol. 63, p. 966, 1959.

9. Halpern, J., Advances in Catalysis, Vol. XI, p. 301 ff., Academic Press, New York, 1959.

10. Singer, S. F., and Walker, E. H., "Electrostatic Dust Transport on the Lunar Surface," Icarus, Vol. 1, p. 112-120, September 1962.

11. Walker, E. H., "Comments on a P per by M. L. Coffman," Charging Grains of Dust," J. Geophys. Res., Vol. 69, p. 566-568, February 1, 1964.

12. Coekelbergs, R., Crucq, A., and Frennet, A., "Radiation Catalysis," Advances in Catalysis, Vol. 13, p. 55 ff., Academic Press, 1962.

13. Moulton, F. R., An Introduction to Celestial Mechanics, The MacMillan Co., 1959.

14. Roberts, L., "Exhaust Jet-Dust Layer Interaction During a Lunar Landing," Proceedings 13th International Astronautical Congress, Varna, Bulgaria, 1962.

15. Roberts, L., "The Action of a Hypersonic Jet on a Dust Layer," presented at IAS 31st Annual Meeting, New York, N.Y., January 1963, paper number 63-50.

16. Roberts, L., "The Interaction of a Rocket Exhaust with the Lunar Surface," presented at a Specialists Meeting on The Fluid Dynamics Aspects of Space Flight under sponsorship of the Fluid Dynamics Panel of the Advisory Group for Aeronautical Research and Development, Marseilles, France, April 20-24, 1964.

17. Bagnold, R. A., The Physics of Blown Sand and Desert Dunes, Methuen and Co., London, 1960.

18. Grossman, R. L., Characteristics of Particles Blown Away by Exhaust Jet Impingement on a Lunar Surface, Grumman Advanced Development Report No. ADR 04-04-62.3, December 1962.

19. Hoerner, S. F., Fluid Dynamic Drag, published by the Author (148 Busteed Drive, Midland Park, New Jersey), 1958.

20. Hsu, S. T., Engineering Heat Transfer, D. Van Nostrand Co., Inc., Princeton, N. J., 1963, p. 333.

21. Luzzi, T., Radiation from the LEM Landing Rocket Exhaust Gases, Grumman Research Department Memorandum RM-235, June 1964.

22. Carslaw, H., and Jaeger, J., Conduction of Heat in Solids, Oxford Press, 1959.

23. Wright, R. G., Lunar Characteristics Report, Grumman Aircraft Engineering Corporation Report No. LED-540-6, March 20, 1964.

24. Luzzi, T., A Review of the Physics of Gas Adsorption on Solid Surfaces, Grumman Research Department Report RE-185, October 1964.

25. Sidran, M., Adsorption and Desorption of LEM Exhaust Gases on the Lunar Surface, Grumman Research Department (in preparation).

26. Milford, S. N. and Pomilla, F. R., Variations in the Lunar Atmosphere, Grumman Research Department Report (in preparation).

27. Hinton, F. L. and Taeusch, D. R., "Variation of the Lunar Atmosphere with the Strength of the Solar Wind," J. Geophys. Res., Vol. 69, p. 1341, 1964.

28. Aller, L. H., The Abundance of the Elements, Interscience Publishers, New York, p. 192, 1961.

29. Hinterreger, H. E., "Interplanetary Ionization by Extreme Ultraviolet Radiation," Astrophys. J., Vol. 132, p. 801, 1960.

30. Gault, D. E., Shoemaker, E. M., and Moore, J. H., Spray Ejected from the Lunar Surface by Meteoroid Impact, NASA Tech. Note D-1767.

31. Gault, D. E. and Heitowit, E. D., The Partition of Energy for Hypervelocity Impact Craters Formed in Rock, NASA Ames Res. Ctr., Moffett Field, California.

32. Wehner, G. K., Kenknight, C. E., and Rosenberg, D., "Modification of the Lunar Surface by the Solar Wind Bombardment," Planet. Space Sci., Vol. 11, p. 1257, 1963.

33. Opik, E. J., "The Lunar Atmosphere," Planet. Space Sci., Vol. 9, p. 211, 1962.

34. Ingrao, H. C., Young, A. T., and Linsky, J. L., A Critical Analysis of Lunar Temperature Measurements in the Infrared, Scientific Report No. 6, NASA Res. Grant NsG 64-60, Harvard College Observatory, 1965.

35. Linsky, J. L., A Computer Program to Solve the Heat Conduction Equation in the Lunar Surface for Temperature-Dependent Thermal Properties, Scientific Report No. 7, NASA Res. Grant NsG 64-60, Harvard College Observatory, 1965.

36. Holland, J., Personal Communication, 1966.

37. Glaser, P., "Implications of High Vacuum on the Characteristics of the Lunar Surface," Twelfth National Vacuum Symposium, Am. Vacuum Soc., 29 September 1965.

38. Wechsler, A. E. and Glaser, P. E., "Pressure Effects on Postulated Lunar Materials," Icarus, Vol. 4, p. 335, 1965.

39. Wechsler, A. E. and Simon, J., Unpublished work at ADL, Inc. under Contract NAS8-20076, 1966.

40. NASA 1965 Summer Conference on Lunar Exploration and Science, Falmouth, Mass., NASA SP-88, July 19-31, 1965.

41. Hall, L. B. and Bruch, C. W., "Procedures Necessary for the Prevention of Planetary Contamination," Life Sciences and Space Research, edit. by M. Florkin, John Wiley and Sons, Inc., New York, 1965.

42. Fox, S. W., "How Did Life Begin," Science, Vol. 132, July 1960.

43. Fox, S. W., "The Chemical Problem of Spontaneous Generation," J. Chem. Educ., Vol. 34, October 1957.

44. Miller, S. L., "Production of Some Organic Compounds Under Possible Primitive Earth Conditions," J. Am. Chem. Soc., Vol. 77, May 1955.

45. Fox, S. W., Havada, K., and Vegotsky, A., "Thermal Polymerization of Amino Acids and a Theory of Biochemical Origins," Experientia, Vol. 15, November 1959.

46. Fox, S. W. et al., "Chemical Synthesis of Proteinoids," Part 1, Conference on Nutrition in Space and Related Waste Problems, NASA SP-70, April 27-30, 1964.

47. Sinyan, Y. Y., "The Possibility of Physico Chemical Synthesis of Carbohydrates in a Space Ship Cabin," Problems of Space Biology, Vol. 3, edit. by N. M. Sisakyan and V. I. Yazdovsky, trans. Joint Publ. Res. Service, JPRS-25287, 29 June 1964.

48. Gall, L. S. and Riely, P. E., "Determination of Aerobic Microflora of Human Feces," Republic Aviation Corporation, Final Rept. on Air Force Contract AF33(615)-1748, Rept., AMRL-TR-64-107, October 1964.

49. Pilgrim, A. J., Fosberg, T. M. and Anderson, J. H., "Manned Environmental System Assessment," Proc. of the XV Internat. Astronautical Congress, Warsaw, 1964, Vol. IV.

50. Helvey, W. M. et al., Effects of Prolonged Exposure to Pure Oxygen on Human Performance, Republic Aviation Corporation, RAC 393-1, Final Rept. on Contract NASr-92, 30 November 1962.

51. Riely, P. E., Geib, D., and Shovenstein, D., "Determination of the Indigenous Microflora of Men in Controlled Environments," Republic Aviation Div., Fairchild Hiller Corporation/Aerospace Medical Research Labs, Wright-Patterson Air Force Base, Ohio, AMRL-TR-65 - Final Report AF Contract AF33(615)-1814.

52. Parin, V. V., Volynkin, Y. M., and Vassilyev, P. V., "Manned Space Flight - Some Scientific Results," Life Sciences and Space Research, edit. by M. Florkin, John Wiley and Sons, Inc., New York, 1965.

53. Moyer, J. E. and Lewis, Y. Z., Studies of the Two Man Space Cabin Simulator: Interchange of Oral and Intenstinal Bacteria," School of Aerospace Medicine, Brooks AFB, Texas, SAM-TDR-64-3, March 1964.

54. Imshenetsky, A. A. and Lysenko, "Ultra-High Vacuum and Micro-Organisms," Life Sciences and Space Research, edit. by M. Florkin, John Wiley and Sons, Inc., New York, 1965.

55. Penn, S. H., "Wildcatting on the Moon," presented at the VII Symposium on Rock Mechanics, Penn. State University, University Park, Pa., June 16, 1965.

56. National Bureau of Standards Handbook No. 69, U. S. Department of Commerce, June 5, 1959.

57. American Institute of Physics Handbook, edit. by D. E. Gray, McGraw-Hill Book Co., New York, 1957.

58. Space Research Directions for the Future, Part One, Space Sciences Board, National Academy of Sciences, Washington, D.C., December 1965.